AN EVALUATION OF SCALING METHODS FOR EARTHQUAKE RESPONSE SPECTRA

by

JAMES M. NAU

and

WILLIAM J. HALL

A Report on a Research Project Sponsored by the

NATIONAL SCIENCE FOUNDATION

Research Grant Nos. ENV 77-07190 and PFR 80-02582

UNIVERSITY OF ILLINOIS

Urbana, Illinois

May 1982

50272-101

REPORT DOCUMENTATION PAGE	1. REPORT NO. UILU-ENG-82-2007	2.	3. Recipient's Accession No.

4. Title and Subtitle

AN EVALUATION OF SCALING METHODS FOR EARTHQUAKE RESPONSE SPECTRA

5. Report Date: May 1982

6.

7. Author(s)

J. M. Nau and W. J. Hall

8. Performing Organization Rept. No. SRS 499

9. Performing Organization Name and Address

University of Illinois at Urbana-Champaign
Department of Civil Engineering
208 N. Romine Street
Urbana, Illinois 61801

10. Project/Task/Work Unit No.

11. Contract(C) or Grant(G) No.
(C) ENV 77-07190
(G) PFR 80-02582

12. Sponsoring Organization Name and Address

National Science Foundation
Washington, D.C. 20550

13. Type of Report & Period Covered

14.

15. Supplementary Notes

16. Abstract (Limit: 200 words)

In this study, scaling methods are evaluated with the purpose of reducing the dispersion encountered in normalized spectral ordinates. The scaling factors considered comprise two major groups, one based on ground motion data and the other, directly on response quantities. Within the group based on ground motion values are the integrals of the squared acceleration, velocity, and displacement, and those quantities derived therefrom, namely the root-square, mean-square, and root-mean-square motions. Included within the group based on response quantities are the spectrum intensity and the mean Fourier amplitude.

The scaling parameters were evaluated using a set of twelve representative earthquake recordings. Response spectra for elastic, elastoplastic, and bilinear hysteretic systems for wide ranges of damping and ductility were used in the statistical study. The results show that a three-parameter system of spectrum intensities, computed within low, medium, and high frequency regions, may afford a better means of scaling earthquake response spectra.

17. Document Analysis a. Descriptors

Earthquake Resistant Design, Seismic, Response Spectra, Scaling Methods, Statistical Analysis, Dynamic Response, Inelastic Systems, Damping, Ductility

b. Identifiers/Open-Ended Terms

c. COSATI Field/Group 13M

18. Availability Statement	19. Security Class (This Report)	21. No. of Pages
Release Unlimited	UNCLASSIFIED	349
	20. Security Class (This Page) UNCLASSIFIED	22. Price

ACKNOWLEGEMENT

This report was prepared as a doctoral dissertation by Mr. James M. Nau and was submitted to the Graduate College of the University of Illinois at Urbana-Champaign in partial fulfillment of the requirements for the degree of Doctor of Philosophy in Civil Engineering. The thesis was completed under the supervision of Professor William J. Hall.

The investigation was a part of a research program sponsored by the National Science Foundation under Grants ENV 77-07190, Engineering Design For Natural Hazards and PFR 80-02582, Earthquake Engineering Design Investigations. Any opinions, findings, and conclusions or recommendations expressed in this publication are those of the authors and do not necessarily reflect the views of the National Science Foundation.

The numerical results presented in this report were obtained with the use of the CDC Cyber 175 and IBM 4341 computers; most of the figures were prepared using the Zeta 1453B plotting device. These facilities are supported by the Computing Services Office (CSO) of the University of Illinois. Partial computer service funding was provided by the Research Board of the Graduate College of the University of Illinois.

The authors wish to thank Professors A. R. Robinson, D. A. W. Pecknold, and R. E. Miller for their constructive comments throughout the study. The authors are also grateful for the assistance provided by the CSO Systems Consulting staff.

ABSTRACT

AN EVALUATION OF SCALING METHODS
FOR EARTHQUAKE RESPONSE SPECTRA

James Michael Nau, Ph.D.
Department of Civil Engineering
University of Illinois at Urbana-Champaign, 1982

In current practice, design response spectra are scaled or normalized by the three peak ground motion values -- displacement in the low, velocity in the intermediate, and acceleration in the high range of frequencies. In this study, alternative scaling factors are evaluated with the purpose of reducing the dispersion encountered in normalized spectral ordinates. The scaling factors fall into two major groups, one based on ground motion data, and the other, directly on response quantities. Within the group based on ground motion values are the integrals of the squared acceleration, velocity, and displacement, and those quantities derived therefrom, the root-square, mean-square, and root-mean-square motions. Included within the group based on response quantities are the spectrum intensity and the mean Fourier amplitude.

The foregoing scaling parameters have been evaluated statistically using a set of twelve representative earthquake recordings. Response spectra for elastic, elastoplastic, and bilinear hysteretic systems for wide ranges of damping and ductility have been used in the statistical study. The results show that a three parameter system of spectrum intensities, computed within low, medium, and high frequency regions, may afford a better means of scaling earthquake response spectra. Reductions in dispersion ranging from 20 percent in the velocity region to 45 percent in the displacement and acceleration regions may be realized if elastic

spectra are normalized by the spectrum intensities rather than the peak ground motions. The spectrum intensities also afford reductions in scatter for normalized inelastic spectra, for low to moderate displacement ductilities.

As a prelude to the investigation regarding the dispersion characteristics of normalized spectra, an efficient algorithm was developed for the computation of inelastic response spectra. The method is based upon the exact solution of the equations of motion and permits the computation of dynamic response in a simple, arithmetic manner. Compared with Newmark's beta method, the procedure provides a two- to threefold savings in computation time.

TABLE OF CONTENTS

Page

LIST OF TABLES

LIST OF FIGURES

CHAPTER 1

INTRODUCTION

1.1 Background and Motivation

In earthquake-resistant design practice, two methods are commonly employed to determine design forces and to verify seismic performance. The first method, direct step-by-step integration of the equations of motion, may be justified in particular cases. However, several such analyses are often required to encompass the range of possible structural models, material properties, and variabilities in ground motion. Because of the high cost of inelastic time-history computations, such methods may not be feasible, especially in preliminary design, for the vast majority of structures. The second method, the modal analysis-design spectrum approach, is particularly attractive for its simplicity. Although strictly applicable to linear elastic structures, approximate modal methods which account for hysteretic behavior of structural elements have been developed. Gulkan and Sozen (19) incorporate the effects of inelastic energy dissipation to enable the evaluation of the design force for a single-degree-of-freedom system using the linear design response spectrum. Iwan and Gates (17, 35, 36) propose a closely related approach. In these methods, equivalent linear system parameters (period and damping) are computed for the hysteretic system and the inelastic response is estimated from the linear response spectrum. An extension to the multi-degree-of-freedom case, the "substitute-structure" method, has been reported by Shibata and Sozen (73, 74). In this technique, the design forces are estimated from linear elastic modal analysis of a fictitious

is characterized by estimates of the expected peak values of ground acceleration, velocity, and displacement. The corresponding design spectra are constructed by amplifying these ground motion maxima by appropriate factors determined from the previously mentioned statistical studies. In the roughly ten years since the development of these design procedures, two important observations have been made. First, from the statistical studies themselves, it has been noted that the dispersion or scatter in the data is large. For example, coefficients of variation exceeding 50 percent have resulted when spectra are normalized or scaled by peak ground motion values. Secondly, from observations following actual earthquakes, it has been noted that levels of damage are inconsistent with large ground motion maxima. That is, greater levels of damage might have been expected had the peak instrumental ground motions been known beforehand. Of course, these peak parameters convey little or no information regarding the earthquake duration and frequency content, two important elements affecting the damage. The conclusion is that ground motion maxima, alone, are poor indicators of earthquake damage potential or earthquake strength.

The objective of this study is to evaluate the current practice of scaling earthquake response spectra by the three peak ground motions. Other investigators have suggested such studies (40), and, in fact, Cornell, Banon, and Shakal (11) have reported results in which response spectra were scaled by mean Fourier amplitudes of acceleration. In this study, alternative scaling techniques are investigated in greater detail than heretofore considered.

1.2 Objectives of Study

The primary objective of this study is to investigate alternative methods for scaling earthquake response spectra. The approach, simply stated, is to statistically evaluate normalizing factors which have been proposed over the years, with the goal of reducing (ideally, minimizing) the dispersion or scatter encountered in current scaling methods. It must be pointed out that the purpose is not to recommend a new or radically different procedure for establishing design spectra. Rather, the goal is to formulate a basis, within the general framework of current practice, upon which further research can lead to improved methods for specifying the earthquake hazard and the corresponding design response spectra.

Two additional objectives of this study may be identified. The first is to examine and compare several numerical procedures for computing earthquake response spectra. Although this investigation is not intended to be comprehensive, the findings show that considerable savings in computational effort may be realized when advantage is taken of the piecewise-linear character of both the earthquake ground motion and the load-deformation functions commonly employed in the modeling of hysteretic behavior. The second objective is to assess the influence of damping and inelastic material model parameters on mean spectra. As in previous studies (35, 36, 69), the goals are to determine the effect of viscous damping when combined with inelastic action and to examine the sensitivity of response to varying levels of strain-hardening in the bilinear hysteretic load-deformation model. The results of this comparative phase of the study may prove useful in preliminary design, when the details concerning the load-deformation characteristics of structural elements have not yet

been precisely evaluated.

1.3 Organization

This introductory chapter has set forth some of the evidence supporting the design spectrum approach in earthquake-resistant design. In addition, the technique presently used to construct design spectra was briefly described. Together, these presentations provided the background and enabled the formulation of the objectives for the research task reported in this study.

Chapter 2 begins with an overview of response spectrum concepts with emphasis on the interpretation of the response quantities summarized in spectra computed from strong-motion earthquake records. An account of current approaches employed to characterize the earthquake hazard, wherefrom design spectra are constructed, is presented.

In Chapter 3, the properties of the single-degree-of-freedom systems and the actual earthquake recordings used in the statistical study are described. Also included in Chapter 3 is a detailed description of the numerical procedure used to compute response spectra. Briefly, this technique is based upon the exact solution of the equations of motion and permits the evaluation of response in an efficient, arithmetical manner. Other details regarding spectral calculation, including computation of response from ground motions with nonzero initial conditions and the development of spectra for preselected levels of displacement ductility, are discussed. The spectra for elastic, elastoplastic, and bilinear systems, computed from the ensemble of twelve earthquake records, are presented in Chapter 3. An examination of these spectra provides some insight into the effects of damping and inelastic behavior,

and how these effects differ for ground motions of varying characteristics.

Chapter 4 contains a description of the two groups of normalizing or scaling factors proposed by numerous investigators as improved measures of earthquake strength. The parameters based on ground motion data include the integrals of the squared motions and the closely related root-square, mean-square, and root-mean-square values of acceleration, velocity, and displacement. Those based directly on response quantities include Housner's spectrum intensity and the mean Fourier amplitude. Chapter 4 closes with an outline of the statistical procedure used to evaluate the various scaling parameters.

Chapter 5 begins with a comparison of mean normalized spectra to determine the general influence of damping and strain-hardening on seismic response. The major purpose of Chapter 5, however, is to describe the results of the statistical evaluation of the scaling methods described in Chapter 4. The results show that the average dispersion in elastic spectra may be minimized by normalizing by the spectrum intensity, computed over appropriately selected frequency intervals. In addition, the spectrum intensity reduces the scatter, compared with that associated with scaling by ground motion maxima, in inelastic spectra for low to moderate ductilities.

Finally, Chapter 6 presents a summary and the significant conclusions of this study. Also, a critical review of this research effort is presented so that the results and conclusions may be perceived in proper scope. This critical appraisal enables the suggestion of topics for further study.

1.4 Notation

The notation and symbols used in this study are defined where they appear in the text. For ease of reference, however, a list of the most important symbols follows:

A = design ground acceleration; also used as a subscript which denotes the acceleration region of the response spectrum

a = ground acceleration

$\hat{a}$ = acceleration of prefixed ground motion pulse

$\bar{a}$ = modified ground acceleration

$a_{11},\ldots,a_{22}$ = elements of matrix [A]

$[A],[B]$ = matrices relating response quantities at time t_{i+1} to those at time t_i

a_j,b_j = variables used to define pseudovelocity in the jth frequency interval

b_j,c_j,d_j = coefficients in the influence functions for the prefixed ground motion pulse, $j = 1,2,3$

$b_{11},\ldots,b_{22}$ = elements of matrix [B]

C = constant in coefficients b_j, c_j, and d_j

C_1,C_2 = constants of integration

COV = coefficient of variation

c = damping constant for the single-degree-of-freedom system

c_{cr} = critical damping

c_β = constant in the expression for the frequency ensemble work

D = design ground displacement; also used as a subscript which denotes the displacement region of the response spectrum

d = ground displacement

$\hat{d}$ = displacement of prefixed ground motion pulse

E_a,E_v,E_d = integral of the squared ground acceleration, velocity, and displacement, respectively

E_m = energy per unit mass absorbed by the single-degree-of-freedom system

E_{max} = maximum energy absorbed by the single-degree-of-freedom system

$F(\omega)$ = Fourier spectrum of ground acceleration

$\overline{FS}$ = mean Fourier amplitude

f = undamped natural frequency for the single-degree-of-freedom system

f_ℓ = lower frequency limit for spectral calculations from records with nonzero initial motions

f_s = starting frequency within each logarithmic cycle

g_j = influence functions for the prefixed ground motion pulse, $j = 1,2,3$

H = duration of the prefixed ground motion pulse

h = normalized integral of the squared ground acceleration

i = subscript denoting ith quantity; also used as a discrete time coordinate for the prefixed ground motion pulse

j = an index

k = spring stiffness of the linear elastic single-degree-of-freedom system; initial and unloading stiffness of elastoplastic and bilinear hysteretic systems

M_L = local or Richter magnitude

MMI = Modified Mercalli Intensity

m_b = body-wave magnitude

m = mass of the single-degree-of-freedom system

N = number of equal time steps into which the prefixed ground motion pulse is divided

n = an index; also used to denote the number of earthquake records

o = subscript denoting initial values of ground acceleration, velocity, and displacement

p = subscript denoting peak values of ground acceleration, velocity, and displacement

P_a, P_v, P_d = mean-square ground acceleration, velocity, and displacement, respectively

R = resistance or spring force in the single-degree-of-freedom system

R_y, R_{max} = yield and maximum resistance or spring force, respectively, in the single-degree-of-freedom system

rms = subscript denoting root-mean-square values of ground acceleration, velocity, and displacement

rs = subscript denoting root-square values of ground acceleration, velocity, and displacement

S_d = spectral displacement

S_v = pseudo-spectral velocity

S_a = pseudo-spectral acceleration

$\bar{S}_v$ = mean pseudo-spectral velocity

$\tilde{S}_d, \tilde{S}_v, \tilde{S}_a$ = ordinates of mean pseudovelocity spectra

SI = spectrum intensity

s = set remaining after an excursion of yielding

T = undamped natural period for the single-degree-of-freedom system

t = time

t_5, t_{95} = time for buildup of 5 and 95 percent, respectively, of the integral of the squared ground acceleration

t_f = total duration of the earthquake ground motion

$u, \dot{u}, \ddot{u}$ = relative displacement, velocity, and acceleration, respectively, of the single-degree-of-freedom system

u_e = maximum displacement of the elastic single-degree-of-freedom system

$u_{max}, \dot{u}_{max}$ = maximum relative displacement and velocity, respectively, of the single-degree-of-freedom system

u_y = initial yield displacement of the single-degree-of-freedom system

u_{yp}, u_{yn} = current positive and negative yield displacements, respectively, of the single-degree-of-freedom system

u_{unl} = relative displacement at the instant of unloading for the single-degree-of-freedom system

V = design ground velocity; also used as a subscript which denotes the velocity region of the response spectrum

v = ground velocity

$\hat{v}$ = velocity of prefixed ground motion pulse

W_F = frequency ensemble work

W_T = period ensemble work

$x, \dot{x}, \ddot{x}$ = absolute displacement, velocity, and acceleration, respectively, of the single-degree-of-freedom system

$\ddot{x}_{max}$ = maximum absolute acceleration of the single-degree-of-freedom system

z = denotes ground acceleration, velocity, or displacement

α = ratio of strain-hardening stiffness to initial elastic stiffness for the bilinear hysteretic single-degree-of-freedom system

β = fraction of critical damping for the single-degree-of-freedom system

β_2 = equivalent fraction of critical damping associated with the strain-hardening branch of the bilinear hysteretic force-deformation model

Δ = prefix denoting an incremental quantity

μ = displacement ductility

Σ = denotes summation

σ = standard deviation

τ = time coordinate for the prefixed ground motion pulse; also used as a dummy variable of integration

ϕ = spectral reduction or deamplification factor

ψ = spectral scaling factor

ω = undamped circular natural frequency of the single-degree-of-freedom system

ω_D = damped circular natural frequency of the single-degree-of-freedom system

ω_2 = equivalent circular frequency associated with the strain-hardening branch of the bilinear hysteretic force-deformation model

$|\ |$ = denotes the absolute value of a quantity

$[\ ]$ = denotes a matrix quantity

$\{\ \}$ = denotes a vector quantity

CHAPTER 2

REVIEW OF CURRENT PRACTICE

2.1 Introduction

In this chapter, a review of response spectrum concepts and the guidelines currently used to construct seismic design spectra are presented. An important aspect associated with the development of earthquake design spectra is the selection of the maximum ground motions expected at the site under consideration. The techniques and considerations employed in estimating these ground motions are briefly described.

2.2 Response Spectrum Concepts

The single-degree-of-freedom system shown in Fig. 2.1 consists of a concentrated mass connected to the ground by a weightless spring and damper. The absolute displacement of the mass is x and that of the ground is d. Hence, the relative displacement of the mass with respect to the ground is

$$u = x - d \tag{2.1}$$

The mass of the system is denoted by m, the damping constant is c, and the resistance is designated as R(u), since the restoring force is a function of the relative displacement u. The resistance function may be linearly elastic, for which

$$R(u) = ku \tag{2.2}$$

where k is the stiffness of the spring element. Many systems, however, behave nonlinearly during moderately intense earthquake excitation. These nonlinear systems may behave elastically, but the majority of

structures of practical importance are hysteretic. That is, significant energy dissipation occurs in the regions of plastic deformation. Hysteretic behavior may be approximated for analytical purposes by a variety of resistance functions, several of which are described in Chapter 3.

The single-degree-of-freedom system is characterized by its circular natural frequency, defined as

$$\omega = \sqrt{k/m} \tag{2.3}$$

This parameter corresponds to the frequency of small amplitude oscillations for the undamped system in free vibration. The circular natural frequency is related to the frequency f and period T as follows:

$$\omega = 2\pi f = \frac{2\pi}{T} \tag{2.4}$$

For the inelastic system, the natural frequency and period are defined as those computed using the initial elastic stiffness.

Energy dissipation within the linear range of response is modeled by viscous damping in which the restoring force is assumed to be proportional to the relative velocity $\dot{u}$. The damping constant is most often expressed as a fraction or percentage of critical, the smallest damping for which no oscillations occur in free vibration (10). The critical damping is

$$c_{cr} = 2\omega m \tag{2.5}$$

Hence, the damping constant may be expressed as

$$c = 2\beta\omega m \tag{2.6}$$

where β is the fraction of critical damping.

With the foregoing definitions, the equation of motion for the single-degree-of-freedom system is

$$\ddot{u} + 2\beta\omega\dot{u} + \frac{R(u)}{m} = -a(t) \tag{2.7}$$

where a(t) is the ground acceleration. For the linear elastic system, i.e. for R(u) = ku, the relative displacement u(t), the relative velocity $\dot{u}(t)$, and the absolute acceleration $\ddot{x}(t)$ may be expressed as (48):

$$\left.\begin{aligned} u(t) &= -\frac{1}{\omega_D}\int_0^t a(\tau)e^{-\beta\omega(t-\tau)}\sin\omega_D(t-\tau)d\tau \\ \dot{u}(t) &= -\int_0^t a(\tau)e^{-\beta\omega(t-\tau)}\cos\omega_D(t-\tau)d\tau - \beta\omega u(t) \\ \ddot{x}(t) &= \ddot{u}(t) + a(t) = -2\beta\omega\dot{u}(t) - \omega^2 u(t) \end{aligned}\right\} \tag{2.8}$$

where τ is a dummy variable of integration and ω_D is the damped circular natural frequency given by

$$\omega_D = \omega\sqrt{1-\beta^2} \tag{2.9}$$

The maximum response quantities, $|u_{max}|$, $|\dot{u}_{max}|$, and $|\ddot{x}_{max}|$ are of particular interest. These maximum values may be summarized in the form of response spectra in which a particular maximum response quantity is plotted versus frequency, for a given damping value. Accordingly, three types of spectra may be constructed -- relative displacement spectra, relative velocity spectra, and absolute acceleration spectra. However, by defining the pseudovelocity and pseudoacceleration, all three spectral quantities may be conveniently displayed on a four-way logarithmic plot. These response values are

$$\left.\begin{aligned} S_d &= |u_{max}| \\ S_v &= \omega S_d \\ S_a &= \omega S_v = \omega^2 S_d \end{aligned}\right\} \qquad (2.10)$$

where S_d denotes the spectral displacement, and S_v and S_a are the pseudovelocity and pseudoacceleration, respectively. With these definitions the tripartite spectrum features the pseudovelocity ordinates plotted versus frequency. The displacement and pseudoacceleration axes intersect the frequency axis at angles of 45 degrees.

The spectral displacement S_d is the true maximum relative displacement for the single-degree-of-freedom system. A comparison of Eqs. 2.10 and 2.8 reveals that the pseudovelocity S_v and pseudoacceleration S_a are not true spectral quantities; hence, the prefix "pseudo" is used. However, the pseudovelocity is approximately equal to the maximum relative velocity for systems with intermediate frequencies. The pseudovelocity differs substantially from the true spectral velocity for low and high frequency systems. For example, Fig. 2.2 compares these velocity quantities for elastic systems with 5 percent damping subjected to the S16E component of the Pacoima Dam record of Feb. 9, 1971. It is clear from this figure that within a region of frequencies extending from about 0.5 to about 5 cps or higher, the pseudovelocity closely approximates the true spectral velocity. The pseudovelocity is of practical importance since it provides an estimate of the maximum energy absorbed by the linear elastic system,

$$E_{max} = \frac{1}{2} k S_d^2 = \frac{1}{2} m(\omega S_d)^2 = \frac{1}{2} m S_v^2 \qquad (2.11)$$

The pseudoacceleration for undamped systems is precisely equal to the true spectral acceleration. For damped systems, the true spectral acceleration is closely approximated by the pseudoacceleration, except for very low frequencies. This conclusion is clear from Fig. 2.3 in which the acceleration quantities are compared for elastic systems with 5 percent damping. As in Fig. 2.2, the spectra in Fig. 2.3 were computed from the Pacoima Dam record. The pseudoacceleration, when multiplied by the mass of the single-degree-of-freedom system, gives, precisely, the maximum force in the spring,

$$R_{max} = kS_d = m\omega^2 S_d = mS_a \tag{2.12}$$

For elastic systems, then, a complete representation of the important response quantities is portrayed in the form of tripartite spectra. Henceforth, these spectra are referred to simply as "response spectra" or as "pseudovelocity spectra."

The design of inelastic systems involves the estimation of the yield resistance or yield deformation so that the maximum inelastic displacement is limited to a prescribed level. Therefore, it is advantageous to define the response spectra for inelastic systems so that this information can be readily determined. Accordingly, the yield level u_y required to limit the maximum displacement to a specified multiple of the yield level itself is plotted on the displacement axis of the tripartite grid. Spectra of this type are referred to as inelastic yield spectra, which are developed for various levels of displacement ductility, defined as

$$\mu = \left| \frac{u_{max}}{u_y} \right| \tag{2.13}$$

For consistency with the elastic spectrum, the pseudovelocity and pseudoacceleration are, respectively,

$$\left.\begin{aligned} S_{v\mu} &= \omega u_y \\ S_{a\mu} &= \omega S_{v\mu} = \omega^2 u_y \end{aligned}\right\} \qquad (2.14)$$

where the subscript μ has been added to distinguish the inelastic quantities from the corresponding elastic values. Note that if the yield deformation for the elastic system is considered to be equal to its maximum displacement, the elastic spectrum corresponds to the yield spectrum for a ductility of unity.

Two other types of spectra, derived from the yield spectra, may be constructed for the inelastic system. These are the inelastic acceleration and total deformation spectra. From the inelastic yield spectrum, the yield resistance required to limit the maximum displacement to a given ductility is

$$R_y = m\omega^2 u_y = mS_{a\mu} \qquad (2.15)$$

For the elastoplastic system, the yield resistance is equal to the maximum force in the spring. However, for the bilinear system, or for others with strain-hardening, the maximum resistance is

$$R_{max} = mS_{a\mu}[1+\alpha(\mu-1)] \qquad (2.16)$$

where α is the ratio of the strain-hardening stiffness to the initial elastic stiffness. Hence, to estimate these maximum forces directly, the inelastic acceleration spectrum may be constructed, in which the value of

R_{max}/m is plotted on the acceleration axis. For this type of spectrum, the displacement and velocity axes are meaningless. However, for the elastoplastic system, the inelastic yield and acceleration spectra are identical. If one is interested in total displacements, the total deformation spectrum features the values of μu_y plotted on the displacement axis. For these spectra, the velocity and acceleration axes are of no significance. Since the information contained in the inelastic acceleration and total deformation spectra is derivable from the yield spectrum, there is no reason to explicitly consider these spectra in this study. However, for the elastoplastic system, it is often convenient to show both the yield (or acceleration) spectrum and the total deformation spectrum on the same grid.

2.3 Construction of Design Spectra

Analytical tools are available for evaluating the response of a system to a specified earthquake ground motion. However, because of the uncertainties and variabilities associated with the expected ground motions, several time-history analyses employing a family of representative ground motions may be required to assure structural integrity and overall seismic adequacy. In addition, the high cost of time-history computations, particularly for complex multi-degree-of-freedom systems, requires that simpler methods be employed to specify the seismic design loading. Accordingly, the spectrum approach has evolved, in which the earthquake environment is characterized in the form of a smoothed design response spectrum. The design spectrum does not represent the response to be expected from any single earthquake event. Instead, the spectrum

represents a smoothed statistical summary of the response obtained from a large family of motions.

The development of seismic design spectra consists of the following basic steps:

1. Definition of the earthquake hazard in terms of the expected maximum ground motions affecting the site under consideration.
2. Amplification of the maximum ground motions to obtain the elastic design spectrum.
3. Deamplification of the elastic spectrum to determine the inelastic yield spectrum.

The present discussion deals with the mechanics of constructing the design spectra, i.e. steps 2 and 3 above. The specification of the earthquake hazard in step 1 is treated separately, in the next section.

Guidelines for constructing earthquake design spectra were developed by Blume (5) and Newmark (51). These studies were unified to form the approach summarized in Refs. 13 and 52. The procedure developed in the foregoing studies was refined in a later investigation by Hall, Mohraz, and Newmark (20), in which a larger sample of earthquake motions was considered. These requirements, summarized by Newmark and Hall (59), form the basis for the guidelines presented herein.

The general procedure for constructing elastic and inelastic design spectra is illustrated in Fig. 2.4. To develop the elastic spectrum, the three design ground motions are plotted as straight lines, parallel to the corresponding axes on the tripartite grid. In Fig. 2.4 the design displacement, velocity, and acceleration are denoted by D, V, and A, respectively. The spectral bounds are then determined by multiplying

the maximum ground motions by appropriate amplification factors which depend upon the damping and the cumulative probability level. The probability function which best describes the range of values is the logarithmic normal distribution (59). Equations for the amplification factors for the median (50 percentile cumulative probability) and the median plus one standard deviation (84.1 percentile cumulative probability) are shown in Table 2.1. Listed in Table 2.2 are numerical values for the amplification factors for a range of damping values from 0.5 to 20 percent of critical. Generally, the 84.1 percentile amplification values are adopted for design use.

The amplified ground motions define the elastic spectrum between 0.1 and 8 cps. For frequencies above 33 cps, the design spectrum is obtained by multiplying the maximum ground acceleration by unity. That is, for rigid systems, the spectral acceleration is identical to the maximum ground acceleration. Between 8 and 33 cps, the design spectrum is obtained by drawing a straight line between the spectral values at these two frequencies. For flexible systems, i.e. those with frequencies less than about 0.03 cps, the spectral ordinates correspond to the peak ground displacement. For these very flexible systems, the mass remains motionless during excitation; therefore, the maximum relative displacement corresponds to the peak ground displacement. The spectrum between 0.03 and 0.1 cps is obtained by drawing a straight line between the spectral values at these frequencies. Thus, the elastic design spectrum consists of amplified displacement, velocity, and acceleration regions between 0.1 and 8 cps. Below 0.1 cps and above 8 cps, the spectrum begins its respective transition to the maximum ground displacement and maximum

ground acceleration. At frequencies below 0.03 cps the spectrum corresponds to the peak ground displacement; above 33 cps, the spectrum is defined by the maximum ground acceleration.

The inelastic yield spectrum is constructed by reducing or deamplifying the elastic spectrum, as shown in the lower sketch of Fig. 2.4. For frequencies below 0.03 cps, the elastic spectrum is deamplified by $1/\mu$, where μ is the design ductility. Similarly, in the amplified displacement and velocity regions, the elastic spectrum is reduced by the factor,

$$\phi_D = \phi_V = \frac{1}{\mu} \tag{2.17}$$

This reduction factor results from the observation that for low and intermediate frequencies, the maximum displacements for the elastic and inelastic systems are approximately equal. In the acceleration-amplified region, the deamplification factor corresponds to that which is obtained from equating the energy absorbed by the inelastic system to that for an elastic system of the same frequency (50). This reduction factor is

$$\phi_A = \frac{1}{\sqrt{2\mu-1}} \tag{2.18}$$

Above 33 cps, spectral reductions are small; hence, for conservatism, the inelastic design spectrum is assumed to correspond to the elastic design spectrum without deamplification. The design spectrum constructed by deamplifying the elastic spectrum in accordance with the foregoing rules corresponds to the yield or acceleration spectrum for the elasto-plastic system. The total deformation spectrum is readily obtained by

multiplying all ordinates of the yield spectrum by the displacement ductility μ. In the displacement and velocity regions, of course, the total deformation spectrum corresponds to the elastic spectrum.

The procedure outlined above for the construction of inelastic spectra applies strictly to cases where the resistance function may be approximated as elastoplastic (59). Note, however, that the spectral reduction factors are independent of damping, which implies that damping has the same effect on both elastic and inelastic response. In a recent study by Riddell and Newmark (67), the simplified procedures for constructing inelastic yield spectra were investigated. In that study, reduction or deamplification factors for elastoplastic systems with 2, 5, and 10 percent damping were derived. These results are shown in Fig. 2.5. From this figure it is clear that in the displacement region, the reduction factor $1/\mu$ is conservative for all damping and ductility. In the velocity and acceleration regions, however, the adequacy of the simplified rules depends upon both the damping and ductility. Generally, the greater the damping, the smaller the ductility must be for the simplified rules to provide conservative results. In the velocity region, the deamplification $1/\mu$ is conservative for systems with 2, 5, and 10 percent damping if the design ductility is less than 6, 3, and 2, respectively. In the acceleration region, the old rule corresponds closely to the computed reduction factors for systems with 5 percent damping; for 2 percent damping the factor $1/\sqrt{2\mu-1}$ is conservative for all ductilities. However, for 10 percent damping, the old rule is unconservative for all ductilities, although for μ less than about 2, the differences are small. Finally, it is worthy of note that the deamplification factors increase with

damping in all three spectral regions. This result indicates that damping is less effective in limiting inelastic response, compared with its influence on elastic systems.

Riddell and Newmark (67) also develop spectral deamplification factors for bilinear and stiffness degrading systems. These results, together with those shown in Fig. 2.5, permit the designer to explicitly account for damping and the type of material nonlinearity when constructing inelastic design spectra.

2.4 Selection of the Earthquake Hazard

Earthquake-resistant design requires the evaluation of the earthquake hazard and the selection of structural resistances. These determinations require the consideration of the consequences of structural failure in terms of loss of life and the economics associated with repair or replacement. Furthermore, the various design parameters must be evaluated in a consistent manner; otherwise, the design may become uneconomical or even unsafe. If extreme conditions are assumed throughout the design process, unreasonably severe and costly design requirements may result. More importantly, such excessive requirements may alter the behavior of the system in such a way that the structure has a reduced capacity for other design conditions. In other words, earthquake design requirements are but one of possibly several criteria upon which the design must be based. Overattention to earthquake loading may result in unsatisfactory performance under other design conditions.

The earthquake hazard is generally established in the form of the expected peak ground motions at the site under consideration. In the

following paragraphs, a brief account of the procedures currently used to estimate these motions is presented. It must be realized that the process of establishing the design motions requires consideration of a large body of geological, seismological, and geotechnical information. Accordingly, the discussion here is not intended to be comprehensive; only the essential features associated with the selection of the design ground motions are presented. State-of-the-art reviews of the procedures and considerations required to determine appropriate design motions are available, as for example in Ref. 22.

Two methods are generally employed to determine the design ground motions (53). First, in cases where an extensive history of earthquake activity exists and geological investigations are practical, estimates can be made of the possible magnitude and location of future earthquakes. In many instances, such earthquakes may occur along well-defined faults. Estimates of the ground motion intensities at the site may then be obtained. These estimates are generally made from attenuation formulas, developed from available observational data. Many such formulas have been proposed over the years, and they may take a variety of forms involving the numerous parameters affecting the attenuation characteristics of ground motion. Idriss (34) provides a comprehensive summary of the important empirically derived attenuation relationships. Most of these relationships provide estimates of the peak ground motions from earthquake magnitude and source-to-site distance.

The second procedure for developing the design ground motion is used when the occurrence of earthquakes in the particular region is not associated with well-defined geological features or when insufficient

seismic data is available. For these cases, relationships have been developed in which the ground motions, generally acceleration or velocity, are expressed in terms of a qualitative measure of the intensity of the motion, e.g. the Modified Mercalli Intensity (MMI). However, the MMI is a subjective measure of observed damage caused by an earthquake and as such, is not readily subject to mathematical manipulation. In addition, the MMI depends upon the type and age of the structure, properties of the building materials, methods of construction, and the like. Therefore, one might expect some change in damage assessment over the years, as the quality of materials and design and construction practices improved. Despite these shortcomings, in many cases, particularly in the central and eastern sections of the United States, Modified Mercalli Intensity data is all that is available.

In many instances, only the peak ground acceleration at the site is estimated. In these cases, statistically derived relationships between the peak ground motions are used. For example, Newmark and Hall (59) recommend that, lacking other specific information, a V/A ratio of 48 in./sec/g be used for competent soil conditions; for rock sites, a V/A ratio of 36 in./sec/g is suggested. In addition, to ensure that the spectrum contains an adequately broad frequency content, AD/V^2 should be equal to about 6.

The peak ground motions estimated from the foregoing procedures require further consideration. First, it has been documented that structures located near the earthquake source may experience large amplitude, high frequency components of acceleration. However, the levels of damage observed within many of these structures are not as

great as would have been expected from the recorded ground motions. Notable examples of such occurrences are summarized by Newmark (56). Reports of damage caused by the Parkfield earthquake of June 27, 1966, the Bear Valley earthquake of Sept. 4, 1972, and the Ancona, Italy events of June 1972 are generally inconsistent with the severity of the recorded motions as characterized by the peak acceleration levels. The instrumental peak acceleration recorded on the abutment of the Pacoima Dam during the San Fernando earthquake of Feb. 9, 1971 was nearly 1.2 g. Yet, very minor damage to the dam or to nearby structures was observed.

The observation that structural damage need not be consistent with maximum instrumental readings has led to the use of effective ground accelerations in the construction of design spectra (54, 56, 59). The specification of a ground acceleration for design which is less than the expected maximum value is based, in part, upon the reasoning that a single peak of intense, short duration motion may contribute less to the cumulative damage of a structure than several or many cycles of somewhat less severe ground shaking (62). In fact, Newmark (54) has suggested that the effective ground acceleration may be only one-third to one-half of the expected instrumental reading for structures located in the near vicinity of the surface expression of a fault or at the epicenter.

Selection of appropriate effective ground accelerations is especially important when dealing with structures whose fundamental natural frequency falls in the acceleration-amplified region of the response spectrum. In this frequency region, about 2 to 8 cps, the

spectral amplitude is directly proportional to the maximum ground acceleration. If the ground motion contains a significant level of high frequency energy, the spectral amplitudes may be overestimated. Accordingly, Page et al. (62) employed filtering techniques to remove high frequency components from near-field records to arrive at effective ground acceleration levels for use in design for some segments of the trans-Alaska pipeline. At the present time, however, the procedures for estimating the effective ground motions, including the use of filtering techniques, are not based on definitive methods; judgment and experience regarding structural response are required.

A consideration related to the effective acceleration concept applies to structures with relatively large foundations. It has been observed from actual measurements that these structures respond with less intensity than smaller structures, or than would be implied from free-field motions. This observation is particularly evident in the near-field, where the motions may include significant high frequency components. The high frequency accelerations appear to be filtered by the structure, thereby reducing the large amplitudes. Newmark, Hall, and Morgan (57) suggest that the accelerations imparted to a structure approach an average of the free-field excitation over some wave passage or transit time. The transit time is related to the longest plan dimension of the building, or the mean or geometric mean of the dimension, and the shear wave velocity. At greater distances from the earthquake source, the high frequency ground motions attenuate; hence, structural filtering effects diminish.

From the preceding discussion it is apparent that the estimation of appropriate design ground motions requires the consideration of many factors, some of which are, at the present time, poorly understood. For example, while the rationale for basing the design spectrum on effective motions is clear, the methods involved in the evaluation of these quantities are vague. As additional recorded and observational data accumulate, new and improved methods for specifying the earthquake hazard and the corresponding design spectra will undoubtedly evolve. A goal of this study is to provide some insight into these same areas, via an examination of the correlation between response spectra and various measures of earthquake strength.

CHAPTER 3

RESPONSE OF SINGLE-DEGREE-OF-FREEDOM SYSTEMS TO EARTHQUAKE MOTIONS

3.1 Introduction

This chapter contains a description of the properties of the single-degree-of-freedom systems and the earthquake ground motions used in the statistical evaluation of alternative scaling methods. Also included in this chapter is a discussion of the numerical procedure employed in the computation of response spectra. Although many numerical techniques are available, the method described herein is particularly advantageous for its simplicity and accuracy, but above all, for its efficiency. Several details regarding spectral calculations, for example, the treatment of records with nonzero initial motions and the development of inelastic spectra for specified levels of displacement ductility, are set forth. The chapter closes with the presentation of the spectra computed from the selected ensemble of strong-motion earthquake records. Comparison of these spectra permits some insight into the influence of damping and material nonlinearity on the response to specific ground motions.

3.2 Systems under Study

Two structure-related quantities for the single-degree-of-freedom systems under study require definition. These parameters, damping and the load-deformation model, are described in this section.

Energy dissipation within the linear elastic range of response arises primarily from various sources of damping. For analytical convenience, damping is generally approximated as velocity-dependent

or viscous. Damping values are most commonly specified as percentages of critical damping which is defined as the smallest value for which no oscillations about the equilibrium position occur in free response (10). Values of damping vary over a wide range and depend upon a number of important factors such as the structural material, the types of connections between structural elements, the amplitude of the response, and for most structures, the degree of deterioration accumulated through previous loadings. For example, the damping associated with a cracked concrete beam may be several times that for a similar, uncracked beam. It is evident that the selection of appropriate damping values requires a great deal of judgment. Even in cases where measurements of damping are made, the damping varies with the method employed for its calculation, e.g., from free-vibration tests and the logarithmic decrement approach or from steady-state, power bandwidth methods. Furthermore, tests conducted to experimentally verify damping values are most commonly conducted at low amplitudes. Although generally conservative, the levels of damping determined from such tests may not be representative of the higher values expected during excitation of greater intensity.

Newmark (58) has summarized from a variety of sources the levels of damping shown in Table 3.1. Newmark points out that for each entry, the lower value in the pair is essentially a lower bound and is therefore conservative for design use. The upper value is approximately the average and may thus be more appropriate for design purposes. Other recommended damping values may be found in the literature and in current design codes and regulations, as for example, in Ref. 12. Damping values corresponding to 2, 5, and 10 percent of critical, representative of those shown in

Table 3.1, are selected for use in this study.

Most structures behave inelastically, at least to some degree, when subjected to earthquakes of moderate and higher intensities. Many investigators have evaluated these inelastic effects for the most common structural elements and assemblages fabricated of steel, reinforced and prestressed concrete, and masonry. Riddell and Newmark (67) present a comprehensive review of the important experimental findings and discuss the various analytical load-deformation models which have been proposed to predict the hysteretic response of structures. On the basis of this review, Riddell and Newmark employed three load-deformation models in their statistical study of inelastic response spectra. These models, the elastoplastic, bilinear, and stiffness degrading resistance functions, are shown in Fig. 3.1. The stiffness degrading model is composed of an initial bilinear spine; loading progresses either on a strain-hardening branch or towards the farthest point attained in the previous inelastic cycle. It should also be mentioned that the rules governing the stiffness degrading model employed by Newmark and Riddell were developed to avoid inconsistencies associated with small amplitude and incomplete hysteresis loops (68). A strain-hardening stiffness of 3 percent of the initial stiffness, as shown in Fig. 3.1, was selected as a representative value for the bilinear and degrading models.

Mean inelastic yield spectra, taken from the study by Riddell and Newmark (67), are shown in Figs. 3.2 through 3.4. These spectra, computed from a group of 10 strong-motion earthquake records, provide an indication of the influence of the load-deformation model on mean response. As concluded by Riddell and Newmark (67) and Riddell (69), the ordinates

of the mean spectra are not significantly different for the various nonlinear models. In Figs. 3.2 and 3.3, differences in mean response primarily occur in the intermediate range of frequencies for large displacement ductilities. Minor differences are evident in the low and high ranges of frequency, corresponding to those regions below about 0.1 cps and above 10 cps. Perhaps most important are the results in Fig. 3.4 which indicate surprisingly little difference in the mean spectra, for all frequencies and ductilities, for the bilinear and stiffness degrading models. Considering the apparent gross differences in the simple bilinear and the more complex stiffness degrading model, one might have expected, a priori, greater differences in mean response.

Other investigators have reached similar conclusions regarding the effect of the nonlinear model on mean response. Iwan and Gates (35) and Iwan (36), for example, performed a statistical study employing the broad range of hysteretic models shown in Fig. 3.5. The systems in Fig. 3.5 are shown for the case of cyclic loading with monotonically increasing amplitude. The six digit code for five of the systems contains the values for the parameters which control the ratio of the various slopes and the locations of points of slope change. Also included is the simple bilinear hysteretic model (BLH). The purpose of the studies by Iwan and Gates was to determine linear values of damping and period to enable the estimation of inelastic response from the linear elastic response spectrum. Optimal parameters which minimize the error between the true inelastic response and that approximated from the elastic spectrum are developed. The differences in the optimum linear parameters, even for moderate to large ductilities, are small, despite the widely varying characteristics

of hysteretic behavior. Iwan and Gates (35) conclude therefrom that it may not be necessary to know the precise details of the load-deformation relationship in order to make reasonably accurate estimates of response.

The preceding discussion does not, and should not, imply that there are no systematic differences in the time-histories of response for individual cases. Insofar as peak response estimates are concerned, however, the evidence does indicate that the type and details of the hysteretic models are of secondary importance. Accordingly, the elasto-plastic and bilinear hysteretic load-deformation models are selected to approximate inelastic behavior for the single-degree-of-freedom systems considered in this study. Note that the elastoplastic system is actually a special form of bilinear hysteresis in which the strain-hardening stiffness is zero.

Two additional reasons for the selection of the bilinear model are noteworthy. First, the bilinear system is the simplest which can be used to approximate inelastic behavior. Since nonlinear action is known and in fact is expected to occur in structures subjected to moderately severe earthquakes, any study of response spectra should at least include a crude model for hysteretic effects. Secondly, the objective of this study is not to evaluate the influence of a wide variety of hysteretic models. Rather, the purpose is to employ a class of spectra, representative of conditions encountered in practice, in a study devoted to the evaluation of methods used to derive design response spectra.

For the bilinear system, three values for the strain-hardening stiffness, 2, 5, and 10 percent of the initial elastic stiffness, are chosen for use in this study. These levels of strain-hardening cover

the realistically broad range which might be encountered in practice and enable the evaluation of the sensitivity of response to one common variable of hysteretic behavior. An intermediate, constant value of damping, 5 percent of critical, is used in all bilinear systems. For the elastoplastic model, damping values corresponding to 2, 5, and 10 percent of critical are employed. Thus, six different combinations of damping and inelasticity are considered. For each of these cases, the levels of displacement ductility for which response spectra are computed encompass the range of values recommended for design by Newmark (58): the ductilities generally appropriate are on the order of 1 to 1.5 for light equipment; from 1.2 to 2 for massive equipment; from 1.5 to 3 for piping systems; from 1.5 to 2.5 for reinforced concrete structures loaded largely in shear or compression; from 2 to 5 for concrete in flexure; from 2.5 to 10 for steel loaded primarily in tension or flexure; and from 1.5 to 3 for steel members in compression, with the lower value corresponding to those elements which buckle at or below the yield levels of axial stress. On this basis, ductilities corresponding to 1, i.e., the linearly elastic case, 1.5, 2, 3, 5, and 10 are chosen.

3.3 Ground Motions

An ensemble of twelve earthquake accelerograms, recorded from actual past events, are chosen for use in this study. Pertinent earthquake data and recording site information are given in Tables 3.2 and 3.3. As the data in these tables reveals, the records encompass a broad range of the various parameters, including the geographical location, magnitude, maximum intensity, focal depth, epicentral distance, and recording site

soil conditions. There are several common features, however. All records are taken from instruments housed in instrument shelters at ground level or in basements of relatively small buildings. Accordingly, approximately free-field conditions prevail. In addition, each record contains a peak ground acceleration exceeding 0.15 g. Beyond these similarities, no additional attempts have been made to categorize the records selected for this study. In fact, the rather broad range of characteristics was desired to cover those which might be expected in practice. The results of this investigation are intended to be generally applicable and not restricted to a particular class of earthquake events or records from those events. However, it must be pointed out that seven of the twelve records are from California earthquakes. Hence, the results of this study will be biased, at least to some degree, inasmuch as the faulting and other tectonic processes are necessarily related for those events.

The ground motions used in this study are shown in Figs. 3.6 through 3.17. A casual examination of these records reveals their widely varying characteristics. Compare, for example, the impulsive-type motions of Cholame-Shandon, Gilroy, and Bucarest to those of El Centro, Taft, and Santiago. The differences in duration of strong shaking are readily apparent, as are the relative amplitudes of the acceleration peaks comprising the records. Other specific record data, including initial and maximum ground motions, are listed in Table 3.4.

The records selected for this study were obtained in digitized form, for a uniform time interval, from magnetic tapes available from the National Geophysical and Solar-Terrestrial Data Center in Boulder, Colorado. All records have been "corrected" using the procedure developed at the

California Institute of Technology, the details of which are summarized in Refs. 32, 75, and 81. The adjustments involve baseline corrections of long period errors (79) and instrument corrections of high frequency errors (80). One feature of this procedure is that it provides estimates of the initial ground displacement, velocity, and acceleration. Physically, the ground must be in motion when recording begins, since a small level of excitation is required to trigger the recording instrument. The initial ground motions for the records used in this study are summarized in Table 3.4. A difficulty arises when response spectra are computed from records with nonzero initial motions. The details of this problem and one method of treatment are described later in this chapter. It is sufficient to note here that the remedy involves the short, low-amplitude acceleration pulse added at the beginning of each record shown in Figs. 3.6 through 3.17.

Another characteristic of the Caltech processing methods is that the ground velocities and displacements differ slightly from those derived from direct integration of the corrected accelerogram. The velocities and displacements shown in Figs. 3.6 through 3.17 are determined directly from the corrected accelerograms assuming that the acceleration varies linearly between successive digitized points. That is,

$$a(t) = a_i + \frac{\Delta a_i}{\Delta t_i}(t-t_i) \quad , \quad t_i \leq t \leq t_{i+1} \tag{3.1}$$

where

$$\left.\begin{aligned} \Delta a_i &= a_{i+1} - a_i \\ \Delta t_i &= t_{i+1} - t_i \end{aligned}\right\} \tag{3.2}$$

In these expressions a_i and a_{i+1} correspond to the ground accelerations at times t_i and t_{i+1}, respectively. Successive integrations of Eq. 3.1 give the ground velocity and displacement,

$$v(t) = v_i + a_i(t-t_i) + \frac{1}{2}\frac{\Delta a_i}{\Delta t_i}(t-t_i)^2 \quad , \quad t_i \leq t \leq t_{i+1} \tag{3.3}$$

$$d(t) = d_i + v_i(t-t_i) + \frac{1}{2}a_i(t-t_i)^2 + \frac{1}{6}\frac{\Delta a_i}{\Delta t_i}(t-t_i)^3 \quad , \quad t_i \leq t \leq t_{i+1} \tag{3.4}$$

where v_i and d_i are the ground velocity and displacement, respectively, at time t_i. Evaluating Eqs. 3.3 and 3.4 at $t = t_{i+1}$ gives the recursion equations for the velocity and displacement,

$$v_{i+1} = v_i + \frac{1}{2}\Delta t_i(a_i+a_{i+1}) \tag{3.5}$$

$$d_{i+1} = d_i + v_i\Delta t_i + \frac{(\Delta t_i)^2}{6}(2a_i+a_{i+1}) \tag{3.6}$$

The velocity and displacement time-histories shown in Figs. 3.6 through 3.17 were evaluated by repeated application of Eqs. 3.5 and 3.6. The velocities published by Caltech are in very close agreement with those computed from Eq. 3.5. In fact, to the scale used in Figs. 3.6 through 3.17, negligible differences can be detected in these velocities. However, greater differences are evident in the displacement time-histories. For example, the published Caltech displacements for the Adak, Alaska record and those computed directly from the corrected accelerogram by means of Eqs. 3.5 and 3.6 are compared in Fig. 3.18. Also, the ground displacement maxima and the times of these maxima are compared in Table 3.5; for the Adak, Alaska record, the difference in the peak ground displacement is nearly 40 percent.

The reason for the discrepancies shown in Fig. 3.18 and Table 3.5 is that the Caltech correction procedures introduce long period components (longer than about 16 sec) in the integrated velocity and displacement time-histories. These long period "errors" arise entirely from the accelerogram data processing methods (75). Hence, to arrive at the "corrected" velocities, i.e. those published by Caltech, the accelerogram is integrated and high-pass filtered to remove the low frequency components. Actually, the high-pass filtering is accomplished by subtracting the low-pass filtered signal from the original signal (32). Similarly, the "corrected" velocities are integrated and high-pass filtered to arrive at the "corrected" displacements. Since in this study the velocities are not filtered prior to integration, the "errors" are integrated resulting in greater observed differences in the displacement time-histories.

It must be pointed out that for the purposes of this study, the foregoing differences in the ground displacements are unimportant. It is true, however, that the low frequency asymptote for the elastic pseudovelocity spectrum is the peak ground displacement computed directly from the corrected record via Eqs. 3.5 and 3.6.

3.4 Method for Response Computation

As described in Chapter 2, inelastic response spectra are commonly presented in the form of inelastic yield spectra and are displayed on tripartite grids. In these spectra, the initial yield level u_y required to limit the maximum relative displacement u_{max} to a specified multiple of the yield level is plotted on the displacement axis. In other words, inelastic yield spectra are generally plotted for specific levels of

displacement ductility, $\mu = |u_{max}/u_y|$. Accordingly, the process of developing inelastic spectra from strong-motion earthquake records is iterative: the initial yield level is adjusted, and the response computations are repeated, until the target ductility is obtained to within some prescribed accuracy. It is apparent, therefore, that a large number of computations may be required to develop the desired spectra, and in the interest of economy, the numerical integration technique must be efficient.

A number of efficient methods are available for the computation of earthquake response spectra. An exact technique for linearly elastic systems has been reported by Nigam and Jennings (60, 61). In this method, the equation of motion is solved analytically within each successive time step assuming the ground acceleration varies linearly between digitized points. Gates (17) and Iwan and Gates (35) have extended this approach to a class of bilinear and stiffness degrading systems; however, few details regarding the application of the method are presented. Accordingly, the purposes of this section are to 1) review the exact method for linearly elastic systems; 2) extend this method to the bilinear hysteretic and elastoplastic systems used in this study; and 3) examine the accuracy and efficiency of the extended method by comparison with Newmark's algorithm (45).

3.4.1 Linearly Elastic Systems

The analytical method described in this section has been reported by Nigam and Jennings (60, 61). However, the technique was originally developed by W. D. Iwan in an unpublished study at the California Institute of Technology.

The equation of motion for the response of the linearly elastic single-degree-of-freedom system subjected to base excitation is

$$\ddot{u} + 2\beta\omega\dot{u} + \omega^2 u = -a_i - \frac{\Delta a_i}{\Delta t_i}(t-t_i) \quad , \quad t_i \leq t \leq t_{i+1} \tag{3.7}$$

where the ground acceleration, a(t), has been replaced by its piecewise-linear approximation given in Eq. 3.1. In Eq. 3.7, u, $\dot{u}$, and $\ddot{u}$ are the relative displacement, velocity, and acceleration, respectively; β, the fraction of critical damping; and ω, the undamped circular natural frequency. The solutions for the relative displacement, u, and velocity, $\dot{u}$, are

$$u(t) = e^{-\beta\omega(t-t_i)}\left[C_1\cos\omega_D(t-t_i) + C_2\sin\omega_D(t-t_i)\right] - \frac{1}{\omega^2}\frac{\Delta a_i}{\Delta t_i}(t-t_i) + \frac{2\beta}{\omega^3}\frac{\Delta a_i}{\Delta t_i} - \frac{a_i}{\omega^2} \tag{3.8}$$

and

$$\dot{u}(t) = e^{-\beta\omega(t-t_i)}\left[(C_2\omega_D - \beta\omega C_1)\cos\omega_D(t-t_i) - (C_1\omega_D + \beta\omega C_2)\sin\omega_D(t-t_i)\right] - \frac{1}{\omega^2}\frac{\Delta a_i}{\Delta t_i} \tag{3.9}$$

In these expressions ω_D is the damped circular natural frequency, $\omega_D = \omega\sqrt{1-\beta^2}$, and C_1 and C_2 are constants. These constants are evaluated by defining

$$\left.\begin{aligned} u(t=t_i) &= u_i \\ \dot{u}(t=t_i) &= \dot{u}_i \end{aligned}\right\} \tag{3.10}$$

Thus, C_1 and C_2 are

$$\left.\begin{aligned} C_1 &= u_i + \frac{a_i}{\omega^2} - \frac{2\beta}{\omega^3}\frac{\Delta a_i}{\Delta t_i} \\ C_2 &= \frac{1}{\omega_D}\left(\dot{u}_i + \beta\omega u_i + \frac{\beta}{\omega} a_i + \frac{1-2\beta^2}{\omega^2}\frac{\Delta a_i}{\Delta t_i} \right) \end{aligned}\right\} \qquad (3.11)$$

The relative displacement and velocity at the end of the time step, u_{i+1} and $\dot{u}_{i+1}$, may be determined by substituting Eq. 3.11 into Eqs. 3.8 and 3.9 and setting $t = t_{i+1}$. The resulting recursion formulas for u_{i+1} and $\dot{u}_{i+1}$ may be conveniently expressed in matrix form as,

$$\begin{Bmatrix} u_{i+1} \\ \dot{u}_{i+1} \end{Bmatrix} = [A(\beta,\omega,\Delta t_i)] \begin{Bmatrix} u_i \\ \dot{u}_i \end{Bmatrix} + [B(\beta,\omega,\Delta t_i)] \begin{Bmatrix} a_i \\ a_{i+1} \end{Bmatrix} \qquad (3.12)$$

where

$$[A(\beta,\omega,\Delta t_i)] = \begin{bmatrix} a_{11} & a_{12} \\ a_{21} & a_{22} \end{bmatrix}$$

and

$$[B(\beta,\omega,\Delta t_i)] = \begin{bmatrix} b_{11} & b_{12} \\ b_{21} & b_{22} \end{bmatrix} \qquad (3.13)$$

The elements of matrices [A] and [B] are functions of β, ω, and Δt_i and are given by Nigam and Jennings (60, 61). After simplifying elements b_{21} and b_{22}, the coefficients of [A] and [B] are:

$$
\left.
\begin{aligned}
a_{11} &= e^{-\beta\omega\Delta t_i}\left(\cos\omega_D\Delta t_i + \frac{\beta}{\sqrt{1-\beta^2}} \sin\omega_D\Delta t_i \right) \\
a_{12} &= \frac{e^{-\beta\omega\Delta t_i}}{\omega_D} \sin\omega_D\Delta t_i \\
a_{21} &= -\frac{\omega}{\sqrt{1-\beta^2}} e^{-\beta\omega\Delta t_i} \sin\omega_D\Delta t_i \\
a_{22} &= e^{-\beta\omega\Delta t_i}\left(\cos\omega_D\Delta t_i - \frac{\beta}{\sqrt{1-\beta^2}} \sin\omega_D\Delta t_i \right)
\end{aligned}
\right\} \qquad (3.14a)
$$

and

$$
\left.
\begin{aligned}
b_{11} &= e^{-\beta\omega\Delta t_i}\left[\left(\frac{2\beta^2-1}{\omega^2\Delta t_i} + \frac{\beta}{\omega} \right) \frac{\sin\omega_D\Delta t_i}{\omega_D} + \left(\frac{2\beta}{\omega^3\Delta t_i} + \frac{1}{\omega^2} \right) \cos\omega_D\Delta t_i \right] - \frac{2\beta}{\omega^3\Delta t_i} \\
b_{12} &= -e^{-\beta\omega\Delta t_i}\left[\left(\frac{2\beta^2-1}{\omega^2\Delta t_i} \right) \frac{\sin\omega_D\Delta t_i}{\omega_D} + \frac{2\beta}{\omega^3\Delta t_i} \cos\omega_D\Delta t_i \right] - \frac{1}{\omega^2} + \frac{2\beta}{\omega^3\Delta t_i} \\
b_{21} &= -\frac{1}{\omega^2\Delta t_i}\left(a_{11}-1 \right) - a_{12} \\
b_{22} &= -b_{21} - a_{12}
\end{aligned}
\right\} \qquad (3.14b)
$$

Note that if the record is digitized at equal time intervals, the coefficients of [A] and [B] are constant for a given frequency. Hence, given the initial conditions for the single-degree-of-freedom system, usually $u(0) = \dot{u}(0) = 0$, response computations proceed rapidly by applying the recursion relationships defined by Eq. 3.12. Monitoring the response quantities as computation proceeds enables the determination of the

maximum relative displacement, i.e. the spectral displacement. The calculations are repeated for a family of frequencies for each selected damping value. Thereby, an entire set of elastic response spectra is developed for the given earthquake record.

The procedure described above can, of course, be applied to accelerograms digitized at unequal time intervals. However, the evaluation of matrices [A] and [B] at each step of integration, i.e. for each Δt_i, increases the computation time considerably. Experience has shown that this increase in computation time may be 100 percent or more. To maintain computational efficiency for records digitized at unequal time intervals, Nigam and Jennings (60, 61) recommend an approximate method involving time coordinate rounding. However, with the development of uniform processing and correction procedures, records are routinely digitized at equal time steps of 0.01 or 0.02 sec. Hence, it is unnecessary, insofar as the discussion here is concerned, to consider the treatment of records digitized at unequal time intervals.

The time step used in the response computations is selected as the smaller of the digitized interval of the earthquake accelerogram or some fraction of the period of free vibration, for example T/10. For systems whose natural period governs the selection of Δt_i, i.e. for high frequencies, Δt_i must be chosen so that an integral number of time steps comprises the digitized interval of the accelerogram. This restriction on Δt_i preserves uniform time intervals and guarantees that response quantities will be computed at times corresponding to those of the given earthquake record. For example, suppose that the response of a system with $T = 0.12$ sec is to be determined. In addition, assume that the earthquake

accelerogram is digitized at intervals of 0.02 sec. If the time step is not to exceed, say, T/10 or the digitized interval, Δt_i must be selected as 0.01 sec, providing two time steps between successive digitized values of acceleration.

Aside from the uncertainties associated with the recording and processing of the accelerogram itself, errors in spectral calculations result from approximations employed in the numerical integration technique used for response computation. In this sense, the method described herein is exact. However, error is introduced by discretization. That is, the true maximum displacement or velocity, i.e. the spectral quantities, will not, in general, occur at one of the discrete times at which computations are made. The maximum error results when the true maximum falls midway between two consecutive time points, as depicted in Fig. 3.19. If the response within the time step is approximated by a sinusoid of frequency equal to the natural frequency of the single-degree-of-freedom system (60, 61), the maximum error is

$$\text{maximum error, \%} = \left(1 - \cos \frac{\pi \Delta t_i}{T} \right) \times 100 \qquad (3.15)$$

Note that the true spectral quantities are greater than those computed at the discrete time points. By appropriately selecting the time step, however, the maximum error in the spectral ordinates may be controlled. For example, the expression above gives 4.9 percent error for $\Delta t_i = T/10$, 1.2 percent for T/20, and 0.3 percent for T/40. Thus, a time step corresponding to $\Delta t_i = T/20$ is generally adequate and is used in this study for the computation of elastic spectra.

3.4.2 Bilinear Hysteretic Systems

The bilinear hysteretic load-deformation model is shown in Fig. 3.20. In this figure, u_y represents the initial yield level; u_{yp} and u_{yn} are the current positive and negative yield levels; s, the current set remaining after an excursion of yielding; k, the initial elastic and unloading stiffness; and α, the ratio of the strain-hardening stiffness to the elastic stiffness. Initially, of course, $s = 0$, $u_{yp} = u_y$, and $u_{yn} = -u_y$. Note that kinematic hardening for the bilinear system is shown, in which the current positive and negative yield levels are separated by a region of linearly elastic deformation of magnitude $2u_y$.

Consider first the linear elastic response which follows unloading. For this case, the equation of motion for $t_i \leq t \leq t_{i+1}$ is

$$\ddot{u} + 2\beta\omega\dot{u} + \omega^2(u-s) = -a_i - \frac{\Delta a_i}{\Delta t_i}(t-t_i) \tag{3.16}$$

where all symbols are as previously defined. This equation may be more conveniently expressed as

$$\ddot{u} + 2\beta\omega\dot{u} + \omega^2 u = -\bar{a}_i - \frac{\Delta \bar{a}_i}{\Delta t_i}(t-t_i) \tag{3.17}$$

where

$$\left.\begin{aligned} \bar{a}_i &= a_i - \omega^2 s \\ \bar{a}_{i+1} &= a_{i+1} - \omega^2 s \end{aligned}\right\} \tag{3.18}$$

The notation $\Delta\bar{a}_i$ in Eq. 3.17 is used for convenience since $\Delta\bar{a}_i \equiv \Delta a_i$ from Eq. 3.2. The solution for Eq. 3.17 is given by Eq. 3.12 with the

substitution of $\bar{a}_i$ and $\bar{a}_{i+1}$ for a_i and a_{i+1},

$$\begin{Bmatrix} u_{i+1} \\ \dot{u}_{i+1} \end{Bmatrix} = [A(\beta,\omega,\Delta t_i)] \begin{Bmatrix} u_i \\ \dot{u}_i \end{Bmatrix} + [B(\beta,\omega,\Delta t_i)] \begin{Bmatrix} \bar{a}_i \\ \bar{a}_{i+1} \end{Bmatrix} \tag{3.19}$$

in which the coefficients of matrices [A] and [B] are defined by Eqs. 3.14.

The set s required in Eq. 3.18 is computed at the instant of unloading. Following an excursion of positive yielding, the set is given by $s = (1-\alpha) \times (u_{unl}-u_y)$; following an excursion of negative yielding, $s = (1-\alpha)(u_{unl}+u_y)$. In these equations, u_{unl} is the relative displacement computed at the instant of unloading. At the same time, the current yield levels are updated. For example, following a positive yield excursion, $u_{yp} = u_{unl}$ and $u_{yn} = u_{unl} - 2u_y$.

Now consider excursions of loading beyond the current yield levels for the bilinear system. With reference to Fig. 3.20, the equation of motion for relative displacements greater than the current positive yield level u_{yp} is

$$\ddot{u} + 2\beta\omega\dot{u} + \omega^2(u_{yp}-s) + \alpha\omega^2(u-u_{yp}) = -a_i - \frac{\Delta a_i}{\Delta t_i}(t-t_i) \tag{3.20}$$

This differential equation applies for $u > u_{yp}$ until unloading is detected, when the product $\dot{u}_i \times \dot{u}_{i+1} < 0$. Simplifying Eq. 3.20 gives

$$\ddot{u} + 2\beta_2\omega_2\dot{u} + \omega_2^2 u = -\bar{a}_i - \frac{\Delta\bar{a}_i}{\Delta t_i}(t-t_i) \tag{3.21}$$

in which

$$\left.\begin{aligned} \beta_2 &= \frac{\beta}{\sqrt{\alpha}} \\ \omega_2 &= \omega\sqrt{\alpha} \end{aligned}\right\} \tag{3.22}$$

and

$$\left.\begin{aligned} \bar{a}_i &= a_i + \omega^2 u_y(1-\alpha) \\ \bar{a}_{i+1} &= a_{i+1} + \omega^2 u_y(1-\alpha) \end{aligned}\right\} \tag{3.23}$$

Note that β_2 and ω_2, equivalent properties associated with the strain-hardening branch of the force-deformation model, are defined only for $\alpha > 0$. For an excursion of negative yielding, for $u < u_{yn}$, Eq. 3.21 applies with the modification,

$$\left.\begin{aligned} \bar{a}_i &= a_i - \omega^2 u_y(1-\alpha) \\ \bar{a}_{i+1} &= a_{i+1} - \omega^2 u_y(1-\alpha) \end{aligned}\right\} \tag{3.24}$$

The character of the solution of Eq. 3.21 may be underdamped ($\beta_2 < 1$), critically damped ($\beta_2 = 1$), or overdamped ($\beta_2 > 1$). However, for the majority of bilinear systems of practical interest, the response is underdamped. For example, for the bilinear systems considered in this study, in which $\beta = 0.05$ and $\alpha = 0.02$, 0.05, and 0.10, the largest value of β_2 is $0.05/\sqrt{0.02}$ or 0.35. Thus, the solution as expressed by Eq. 3.19 holds with the substitution of β_2 and ω_2 for β and ω in the elements of [A] and [B] given in Eqs. 3.14.

3.4.3 Elastoplastic Systems

The discussion regarding the linearly elastic portions of the response for the bilinear system also applies to the elastoplastic system. For yield excursions, however, the equation of motion for the elastoplastic system is

$$\ddot{u} + 2\beta\omega\dot{u} = -\bar{a}_i - \frac{\Delta\bar{a}_i}{\Delta t_i}(t-t_i) \tag{3.25}$$

where $\bar{a}_i$ and $\bar{a}_{i+1}$ are computed, with $\alpha = 0$, in accordance with either Eq. 3.23 for positive yielding or Eq. 3.24 for negative yielding. The solution for Eq. 3.25 may also be expressed by Eq. 3.19 in which the elements of matrices [A] and [B] are:

$$\left.\begin{aligned} a_{11} &= 1 \\ a_{12} &= \frac{1}{2\beta\omega}\left(1-e^{-2\beta\omega\Delta t_i}\right) \\ a_{21} &= 0 \\ a_{22} &= e^{-2\beta\omega\Delta t_i} \end{aligned}\right\} \tag{3.26a}$$

$$\left.\begin{aligned} b_{11} &= \frac{1}{4\beta^2\omega^2}\left[\left(1-e^{-2\beta\omega\Delta t_i}\right)\left(1+\frac{1}{2\beta\omega\Delta t_i}\right) - \beta\omega\Delta t_i - 1\right] \\ b_{12} &= \frac{1}{4\beta^2\omega^2}\left[-\frac{1}{2\beta\omega\Delta t_i}\left(1-e^{-2\beta\omega\Delta t_i}\right) - \beta\omega\Delta t_i + 1\right] \\ b_{21} &= \frac{1}{4\beta^2\omega^2\Delta t_i}\left[e^{-2\beta\omega\Delta t_i}\left(1+2\beta\omega\Delta t_i\right) - 1\right] \\ b_{22} &= \frac{1}{4\beta^2\omega^2\Delta t_i}\left[1-e^{-2\beta\omega\Delta t_i} - 2\beta\omega\Delta t_i\right] \end{aligned}\right\} \tag{3.26b}$$

For the special case of no viscous damping ($\beta = 0$), the coefficients of [A] and [B] are:

$$\left.\begin{aligned} a_{11} &= 1 \\ a_{12} &= \Delta t_i \\ a_{21} &= 0 \\ a_{22} &= 1 \end{aligned}\right\} \qquad (3.27a)$$

$$\left.\begin{aligned} b_{11} &= -\frac{1}{3}(\Delta t_i)^2 \\ b_{12} &= -\frac{1}{6}(\Delta t_i)^2 \\ b_{21} &= -\frac{1}{2}(\Delta t_i) \\ b_{22} &= -\frac{1}{2}(\Delta t_i) \end{aligned}\right\} \qquad (3.27b)$$

The coefficients in Eqs. 3.27 may be obtained from those in Eqs. 3.26 by taking the limit as β approaches zero.

3.4.4 Notes for a Computational Algorithm

To maintain satisfactory accuracy in the response computations for the bilinear hysteretic and elastoplastic systems, the points at which the character of the solution changes - at yielding and unloading - must be detected reasonably precisely. This may be accomplished conveniently as follows. Before response computations begin, matrices [A] and [B] are evaluated and stored for the time interval Δt_i and for one or several fractional time steps. The fractional time steps may be selected, for example, as $\Delta t_i/10$, $\Delta t_i/100$, and $\Delta t_i/1000$. Note that two sets of matrices

[A] and [B] corresponding to the linear elastic and strain-hardening branches of the load-deformation model are required. When yielding or unloading is detected within a time step Δt_i, the first (largest) fractional time step and corresponding [A] and [B] are used to locate the time subinterval during which yielding or unloading occurs. Once this subinterval is determined, the second fractional time step is employed to further refine the subinterval during which yielding or unloading takes place. The foregoing scheme is repeated until the smallest fractional time step is used or until the response quantities at yielding or unloading are determined to within some prescribed accuracy. It is important to note that the fractional time intervals are used progressively, as described above, to refine the previously determined time subinterval during which a change in response behavior is detected. Because the computations in Eq. 3.19 are solely arithmetic and the required matrices [A] and [B] have been computed beforehand and stored, the method of fractional time stepping to detect yielding and unloading is efficient.

For the computation of inelastic spectra in this study, the basic time step $\Delta t_i = T/10$ and three fractional time steps, $\Delta t_i/10$, $\Delta t_i/100$, and $\Delta t_i/1000$, are used. Experience with undamped elastoplastic systems, however, has shown that satisfactory accuracy is generally obtained using $\Delta t_i = T/10$ and one fractional time step, $\Delta t_i/10$. For this choice, response maxima differed from those using the three fractional time step scheme by about 0.2 percent. The computation times using three fractional time steps ranged from 3 to 8 percent greater than those using one fractional time step; hence, economy is not significantly compromised when several

the basic time step was $\Delta t_i = T/10$. Three fractional time steps, $\Delta t_i/10$, $\Delta t_i/100$, and $\Delta t_i/1000$, were used to detect yielding and unloading. For Newmark's method, two sets of computations were made, one using a time step of T/10; the other, T/20. Fractional time stepping to detect yielding and unloading was not employed in Newmark's method. Note that for T/10, the time step used in the calculations for frequencies less than 5 cps corresponds to the digitized interval of the accelerogram, or 0.02 sec. For T/20, the digitized interval governs for frequencies less than 2.5 cps. Accordingly, for Newmark's method the computation times for the two low frequency regions are the same, to two significant figures, as shown in Table 3.6. Note, however, that the computation time for the exact method for each of these low frequency regions is about 1 sec, or 40 percent less than that for Newmark's method. For high frequencies, the exact method provides significantly greater savings, and a comparison of total computation times shows a two- to threefold savings for the exact method.

To compare the accuracies of the methods, consider the selected relative displacement maxima summarized in Table 3.7. Newmark's method gives maximum displacements to within about 7 percent for a time step of T/10, and 2 percent for T/20, compared with those obtained from the exact method.

3.5 Records with Nonzero Initial Motions

As mentioned in Section 3.3, the Caltech accelerogram processing procedures provide estimates of the ground motions at the instant at which the instrument is triggered and recording begins. These initial

motions may be expressed as $a(0) = a_o$, $v(0) = v_o$, and $d(0) = d_o$, where $a(t)$, $v(t)$, and $d(t)$ are, respectively, the ground acceleration, velocity, and displacement. The time coordinate t, of course, is measured from the instant at which recording commences. A difficulty arises when response computations are made for systems subjected to base excitation with nonzero initial conditions. Namely, the initial conditions for the single-degree-of-freedom oscillator are not known. To clarify this point, consider the initial conditions for the relative displacement and velocity given by

$$\left.\begin{aligned} u(0) &= x(0) - d_o \\ \dot{u}(0) &= \dot{x}(0) - v_o \end{aligned}\right\} \tag{3.29}$$

where $x(t)$ and $\dot{x}(t)$ are the absolute displacement and velocity of the mass, respectively. It is apparent that the absolute motions, $x(0)$ and $\dot{x}(0)$, depend upon the ground motions not recorded, i.e. those before the instrument is triggered. Hence, with $x(0)$ and $\dot{x}(0)$ unknown, $u(0)$ and $\dot{u}(0)$ are unknown.

In spite of the foregoing problem, at-rest initial conditions are commonly assumed. However, an inconsistency arises when considering very flexible systems, i.e. for $\omega \to 0$. With $u(0) = \dot{u}(0) = 0$, Eqs. 3.29 give $x(0) = d_o$ and $\dot{x}(0) = v_o$. For the infinitely flexible system, these initial conditions are obviously incorrect since the mass of the system must remain motionless for all time. Hence, the proper initial conditions for the very low frequency systems result from $x(t) = \dot{x}(t) = 0$, from which $u(0) = -d_o$ and $\dot{u}(0) = -v_o$. However, for very high frequency

systems, i.e. for $\omega \to \infty$ there is no relative motion between the mass and the ground, and the initial conditions are precisely $u(0) = \dot{u}(0) = 0$. In view of these limiting cases, it is clear that one set of initial conditions does not apply for all frequencies. Accordingly, one early approach for treating records with nonzero initial motions was to change initial conditions for the oscillator at some intermediate frequency. Pecknold and Riddell (64) and Nelson (44) briefly considered this approach; the results, however, were unsatisfactory. In addition, Nelson (44) points out the arbitrariness of the selection of the intermediate frequency at which the initial conditions are altered.

Pecknold and Riddell (63, 64) were the first investigators to propose a successful method of treating the problems encountered in response computations from records with nonzero initial motions. In this method, a short acceleration pulse is added at the beginning of the earthquake record. For this prefixed pulse, let $\hat{a}$, $\hat{v}$, and $\hat{d}$ denote, respectively, the pulse acceleration, velocity, and displacement. Also, assume that the pulse acts from $0 \leq \tau \leq H$, or $-H \leq t \leq 0$. The prefixed acceleration pulse consists of the superposition of three influence functions which were derived by minimizing $\int_0^H \dot{\hat{a}}^2 \, d\tau$ subject to the constraints $\int_0^H \hat{a}(\tau) d\tau = v_o$ and $\int_0^H \hat{v}(\tau) d\tau = d_o$. The prefixed pulse is piecewise linear so that conventional integration methods, as described in Section 3.3, yield the velocity v_o and displacement d_o at the end of the pulse. The ordinates of the prefixed acceleration pulse are given by

$$\hat{a}_i = a_o g_1(i) + \frac{v_o}{H} g_2(i) + \frac{d_o}{H^2} g_3(i) \qquad (3.30)$$

where $\hat{a}_i = a(i\Delta\tau)$. The pulse is divided into N ($N \geq 3$) intervals such that $\Delta\tau = H/N$. The influence functions $g_1(i)$, $g_2(i)$, and $g_3(i)$ are cubic polynomials in the discrete variable i and are given by

$$g_j(i) = b_j\left(\frac{i}{N}\right) + c_j\left(\frac{i}{N}\right)^2 + d_j\left(\frac{i}{N}\right)^3 \tag{3.31}$$

in which j = 1,2,3 and i = 1,2,..., N. The coefficients b_j, c_j, and d_j depend upon the number of intervals N and are given by

$$\left.\begin{aligned} b_1 &= \frac{(N^2+1)(3N^2+4)}{C}, \quad c_1 = \frac{-12N^2(N^2+1)}{C}, \quad d_1 = \frac{10N^4}{C} \\ b_2 &= \frac{-24N^2(N^2+1)}{C}, \quad c_2 = \frac{12N^2(7N^2+2)}{C}, \quad d_2 = \frac{-60N^4}{C} \\ b_3 &= \frac{60N^4}{C}, \quad c_3 = \frac{-180N^4}{C}, \quad d_3 = \frac{120N^4}{C} \end{aligned}\right\} \tag{3.32}$$

in which $C = (N^2-1)(N^2-4)$.

To show the influence of at-rest initial conditions on the elastic response spectra computed from records with nonzero initial motions, consider the following example. Undamped elastic spectra were computed, assuming at-rest initial conditions, for the two accelerograms of the Melendy Ranch record shown in Figs. 3.21 and 3.22. In Fig. 3.21 the Melendy Ranch record is shown without a prefixed pulse; the initial ground velocity and displacement are clearly evident in this record. In Fig. 3.22, the record has been shifted in time to accommodate a 2-second prefixed pulse. Note that Fig. 3.22 is identical to Fig. 3.8 and is repeated here for ease of reference. The undamped spectra computed from these records are shown in Fig. 3.23. It is clear from this figure that

the correct asymptotic behavior at low frequencies is achieved only for the spectrum computed from the record with the prefixed pulse. That is, at low frequencies, the spectral displacement approaches the peak ground displacement, d_p, in this case 1.28 in. In fact, it can be shown (63) that the low frequency asymptote for spectra computed from records with nonzero initial motions corresponds to a constant pseudovelocity equal in magnitude to the initial ground velocity, v_o. This behavior is clearly evident in Fig. 3.23 for the spectrum computed from the Melendy Ranch record with no prefixed pulse, for which $|v_o| = 1.17$ in./sec. In addition, note in Fig. 3.23 that the significant differences between the spectra extend up to a frequency of about 0.5 cps. Above about 2 cps, the spectra are identical, consistent with the previous discussion regarding the initial conditions for high frequency systems. Pecknold and Riddell (63) estimate that the frequency below which spectral ordinates may be in error is $f_\ell = v_o/(2\pi d_p)$, which for the Melendy Ranch record is 0.15 cps. It is evident from Fig. 3.23 that the spectral errors may extend to a frequency several times the value given by the expression above.

In this study, a prefixed acceleration pulse was added to each record, as shown in Figs. 3.6 through 3.17. The ordinates of each pulse were computed in accordance with Eq. 3.30, where the initial ground motions are as given in Table 3.4. For each record, a pulse duration of 2 seconds was selected so that the amplitude of the pulse is small. The number of intervals was chosen, for convenience, so that the time step for the pulse matched the digitized interval of the remainder of the record.

3.6 Yield Spectra for Specified Levels of Displacement Ductility

Inelastic yield spectra are generally presented for selected levels of displacement ductility. That is, the initial yield level which limits the maximum relative displacement to a specified multiple of the yield level itself is plotted on the displacement axis. To construct yield spectra, computations are made for several trial yield levels, for each frequency and damping value. The yield level corresponding to a given target ductility is then estimated by interpolation. Response computations are repeated using the latest estimate for the yield level, until the target ductility is attained to within some prescribed accuracy. In this study, the interpolation is performed assuming a locally linear variation between $\log(u_y)$ and $\log(\mu)$. Convergence is achieved when the computed ductility is within about 1 percent of the target value.

The variation of ductility with yield level for several cases is shown in Figs. 3.24 and 3.25 for the Pacoima Dam record. In these figures, u_e is the maximum relative displacement for an elastic system with the indicated frequency and damping value. Hence, the ordinates are the values by which the elastic spectral displacements must be reduced to provide the corresponding ductilities. Although the results presented in Figs. 3.24 and 3.25 apply only to the specific earthquake record, several features of the data are generally applicable to all records used in this study.

First, note that for very low frequencies, i.e. $f = 0.03$ cps, the ductility increases uniformly with decreasing yield level. Note also that for all ductilities, the reduction factor, u_y/u_e, is independent of damping and strain-hardening, and corresponds very closely to $1/\mu$.

For high frequencies, for example 7 cps, the ductility again increases uniformly, although more rapidly than for the very low frequencies, as the yield level decreases. For ductilities less than about 2, the reduction factor is roughly $1/\sqrt{2\mu-1}$ for all levels of damping and strain-hardening. It is clear, however, that for high frequency systems with moderate to large ductility, damping and strain-hardening influence the reduction factor. Specifically, for a given reduction factor, the ductility increases with damping, indicating that the effectiveness of damping in reducing response amplitude diminishes as the level of the inelastic response increases. On the other hand, the effect of strain-hardening on high frequency systems follows the logical trend: increasing the level of strain-hardening decreases the ductility for the same spectral reduction factor.

The smooth variation of ductility with yield level for the high frequency systems is indeed advantageous. For these systems, response computations are relatively more costly since a small time step is required. However, economy is generally maintained because the smooth variation of μ with u_y enables rapid convergence for each target ductility.

For the intermediate frequencies, the variation of ductility with yield level may be very irregular. Note, in addition, that the ductility need not be a single-valued function of the yield level. For example, for elastoplastic systems with f = 4 cps, a ductility of 10 is obtained for three different yield levels. Also, for a frequency of 0.65 cps, a range of yield levels will result in a ductility of 2 for elastoplastic systems with 5 percent damping. It should be noted that for such cases, the yield level used in the inelastic spectrum corresponds to that which

the trial and interpolation procedure (described earlier) finds first. For some frequencies, strain-hardening tends to diminish the irregularities, as for example f = 2.6 cps and f = 4 cps. However, for f = 0.15 cps and f = 0.65 cps, strain-hardening has little effect.

3.7 Frequencies and Durations for Spectral Calculations

Important savings in spectral computations may be achieved by limiting both the number of frequencies and the duration of the excitation. However, the shape and other features of the spectra should not be masked by considering too few frequencies or insufficient duration. The general effects of frequency density on earthquake spectra are shown in Figs. 3.26 through 3.29. In these figures, elastic spectra computed from the Pacoima Dam record for increasing damping values are presented. A total of 79 frequencies between 0.035 and 35 cps were used, with 26 frequencies in each logarithmic cycle. In each figure, the solid curve connects each of the 79 spectral ordinates; the dashed curve joins every other point. Hence, the dashed spectra correspond to those in which 13 frequencies are used in each logarithmic cycle, providing a total of 40 spectral values. It is clear that for the undamped case, several significant spectral ordinates are missed if coarse frequency intervals are used; however, when 2 percent damping is introduced, the essential spectral features are satisfactorily maintained. As the damping increases, the differences in the spectra diminish. These results are expected, of course, since damping has a general smoothing effect on earthquake response spectra.

In this study, in which spectra for 2, 5, and 10 percent damping are considered, spectral computations are made for 40 frequencies between 0.035 and 35 cps, with 13 in each logarithmic cycle. These frequencies

are computed from

$$f_i = f_s \times 10^{(i/13)} \quad , \quad i = 1,2,\ldots,13 \qquad (3.33)$$

where f_s is the starting frequency for each logarithmic cycle, namely f_s = 0.035, 0.35, and 3.5 cps. For convenience, this same set of 40 frequencies is used for all records.

Since response spectra contain the peak response values, the duration of the ground motion must be sufficient to enable the evaluation of these true maxima. Too short a duration will generally result in unconservative estimates of maximum response. The earthquake durations used for the response computations performed in this study are summarized in Table 3.8. To determine these durations, elastic spectra were first computed using the total duration for each record, as shown in Figs. 3.6 through 3.17. For each frequency, the time of maximum relative displacement was noted. It was observed, as expected, that for each frequency, the latest time of maximum response occurred for the least damping, 2 percent of critical. It was also noted that the latest time for maximum response decreased as the frequency increased. That is, for higher frequencies, the maximum relative displacement occurred earlier than for low frequency systems. Again, this result is anticipated since for low frequency (long period) systems, the ground motion behaves essentially as an impulse; therefore, peak response occurs in free vibration after the strong ground motion ceases. For high frequency systems, however, the maximum relative displacement generally occurs closely after the peak ground acceleration.

The foregoing observations enabled the selection of the frequency ranges and corresponding durations, as summarized in Table 3.8. Where

possible, the chosen duration corresponds to a time roughly 50 percent greater than that at which the latest response maximum was observed for elastic systems with 2 percent damping. Calculations for elastoplastic systems for several cases revealed that this criterion for selecting the duration for inelastic response computations is generally satisfactory. Exceptions arise, of course, in those cases where peak response occurs very late or during free vibration as, for example, in the Taft and Adak, Alaska records. For these situations, and for the others noted in Table 3.8, the entire record is employed. In all cases, however, response computations are continued for one full period of free vibration following the ground motion.

Finally, it should be noted that the durations shown in Table 3.8 are not rounded values; this is because the durations correspond to times at which the ground velocities are zero. These points were selected so that the ground was at rest at the end of the earthquake.

3.8 Presentation and Discussion of Results

Response spectra computed from the group of twelve earthquake accelerograms are presented in Figs. 3.30 through 3.89. Elastic spectra for 0, 2, 5, 10, and 20 percent damping are shown in Figs. 3.30 through 3.41. Note that those for zero and 20 percent damping are shown for comparative purposes only and are not used in subsequent statistical processing. Figures 3.42 through 3.53 contain elastoplastic yield spectra for 5 percent damping; Figs. 3.54 through 3.65 show bilinear yield spectra for 5 percent damping and 5 percent strain-hardening. In the interest of brevity, the yield spectra for elastoplastic systems with 2 and 10

percent damping and those for bilinear systems with 2 and 10 percent strain-hardening are not shown. The yield spectra presented, however, are representative of those computed for the broad range of conditions considered in this study.

In the paragraphs which follow, features of the various spectra are described. Several observations, for example, are made concerning the influence of damping and strain-hardening on inelastic yield spectra. These effects are shown for each record in the spectra of Figs. 3.66 through 3.89. Figures 3.66 through 3.77 contain elastoplastic spectra for 2, 5, and 10 percent damping for ductilites of 1 (elastic), 3 and 10. Figures 3.78 through 3.89 compare elastoplastic and bilinear yield spectra for 10 percent strain-hardening for these same ductilities. While qualitative trends may be noted by considering the spectra for individual records, specific conclusions may only be reliably obtained by examining mean spectra. The presentation of mean spectra, however, and the quantitative assessment of the factors affecting mean response are deferred to Chapter 5.

The elastic spectra in Figs. 3.30 through 3.41 exemplify the characteristics of the records used in this study. The spectra for the El Centro, Taft, and Santiago records, for example, are broad in terms of their frequency content. In contrast are those spectra for the short duration, impulsive-type motions of the Gilroy and Bucarest records. These latter spectra are characterized by large spectral amplitudes over narrow frequency ranges. Note also that damping has relatively greater effect in decreasing response for the broadband spectra. For example, the separation between the elastic spectra for El Centro, Taft, or Santiago is clearly greater than that for Gilroy or Bucarest.

Riddell and Newmark (67) and Riddell (69) have previously commented on the effects of damping when combined with inelastic action. The results of this study are in general agreement with those of Riddell and Newmark and may be summarized as follows:

1. For low frequencies (less than about 0.07 cps for most records), spectral ordinates are independent of damping for all ductilities.
2. For high frequencies (greater than about 20 cps), the effectiveness of damping increases as the ductility increases.
3. For the intermediate range of frequencies, the influence of damping in reducing response amplitudes diminishes as the level of inelastic response increases.

The foregoing trends are generally evident from an examination of the elastoplastic spectra shown in Figs. 3.66 through 3.77. However, there are noteworthy exceptions. For example, for intermediate frequencies, the spectra for several records indicate that damping may be least effective in reducing response for moderate ductility. The differences between the three spectra for $\mu = 3$ for Pacoima, El Centro, Taft, and Kilauea appear to be, on the average, less than those for $\mu = 10$. These differences are perhaps most noticeable in the Kilauea, Hawaii spectra for frequencies between about 0.5 and 5 cps. On the other hand, several spectra reveal that damping has approximately the same effect for all ductilities. The Gilroy and Bucarest spectra, for example, show that response is reduced essentially by the same amount, for $\mu = 1$, 3, and 10, as damping increases.

The general influence of strain-hardening on yield spectra may be assessed from Figs. 3.78 through 3.89. It is reasonable to expect that

a system with strain-hardening would require a lower yield level to attain the same ductility as that for the same system in which yielding is perfectly plastic. With minor exceptions, this trend is apparent in all spectra. Note, however, for low frequency systems, the yield level is insensitive to the amount of strain-hardening; the only exception arises in the Taft spectra for $\mu = 10$. For most spectra, strain-hardening has relatively little effect for moderate ductility, i.e. $\mu = 3$. This observation is particularly evident in the spectra computed from the Cholame-Shandon, Melendy Ranch, Gilroy, and Bucarest records. In cases where strain-hardening does influence the spectra for moderate ductility, the differences occur primarily for intermediate frequencies. As the level of inelastic response increases, the effects of strain-hardening, of course, become more pronounced. Finally, it is worth noting that strain-hardening tends to smooth yield spectra, especially for large μ. This effect is shown, for example, in the Bonds Corner, El Centro, and Kilauea spectra where strain-hardening depresses the local peaks in the elasto-plastic spectra for $\mu = 10$.

CHAPTER 4

SPECTRAL SCALING FACTORS

4.1 Introduction

In this chapter, the parameters which are evaluated as normalizing factors for earthquake response spectra are described. These scaling parameters are used to normalize both elastic and inelastic spectra, since in current practice inelastic design spectra are derived directly from elastic spectra. Proposed by various investigators as potential descriptors of earthquake intensity, the normalizing factors considered in this study comprise two major groups. The first group contains those quantities determined from the recorded ground motions. Within this group are the peak values of ground acceleration, velocity, and displacement which presently serve as spectral scaling factors. The other factors within this category are derived from the integrals of the squared ground motions and include the root-square, mean-square, and root-mean-square acceleration, velocity, and displacement. The second group of scaling factors is based directly on response-related quantities and includes Housner's spectrum intensity and the mean Fourier amplitude. The chapter closes with a brief summary of the statistical procedure used to evaluate the dispersion characteristics of the normalized spectra.

4.2 Scaling Factors Based on Ground Motion Quantities

The peak ground acceleration, velocity, and displacement are currently used as spectral scaling factors. Although not descriptive of the intensity of the entire ground motion time-histories, the peak displacement and acceleration are indicators of structural response for

low and high frequency elastic systems. As described in Chapter 2, the maximum response of an elastic single-degree-of-freedom system may be characterized as displacement-amplified for low frequencies and acceleration-amplified for high frequencies. The peak ground velocity, when plotted as a constant pseudovelocity on the elastic spectrum, indicates an intermediate frequency region of velocity amplification. Hence, the peak ground motions do, in fact, possess physical appeal. They may be thought of as "static" response quantities; the dynamic response may be interpreted as some magnified "static" response. This concept, of course, is analogous to that employed in elementary dynamics in which the amplitude of the response to harmonic excitation is expressed in a convenient nondimensional form.

Recognizing that instrumental peak values do not portray the overall intensity of the ground motion, Arias (2) and Housner and Jennings (31) proposed a measure of earthquake strength based upon the energy available for damage. It is possible to draw some general conclusions about the energy input to structures by first considering the linearly elastic oscillator. For this system, the vibrational energy is dissipated by viscous damping. Arias (2) defined the intensity of the ground motion as the sum of the energies dissipated, per unit mass, by a population of structures of all natural frequencies,

$$W_F = \int_0^\infty E_m d\omega \tag{4.1}$$

In this expression, E_m is the energy dissipated per unit mass for an elastic system with frequency ω. Housner and Jennings (31) termed the

intensity given by Eq. 4.1 as the "frequency ensemble work."

To evaluate the energy dissipated by viscous damping, consider the equation of motion for the elastic single-degree-of-freedom system,

$$\ddot{u} + 2\beta\omega\dot{u} + \omega^2 u = -a(t) \tag{4.2}$$

This equation indicates that the system subjected to base acceleration a(t) is equivalent to the same system with a fixed base and an applied force per unit mass of -a(t). Multiplying each term of Eq. 4.2 by an increment of displacement, $\dot{u}\,dt$, and integrating from t = 0 to t = ∞ gives the work done, per unit mass, by each of the constituent forces. The result is

$$\frac{1}{2}\dot{u}^2\Big|_0^\infty + 2\beta\omega\int_0^\infty \dot{u}^2 dt + \frac{1}{2}\omega^2 u^2\Big|_0^\infty = -\int_0^\infty a(t)\dot{u}\,dt \tag{4.3}$$

Since the oscillator is initially at rest, $u(0) = \dot{u}(0) = 0$. If $\beta > 0$, the motions eventually damp out; hence, $u(\infty) = \dot{u}(\infty) = 0$. Thus, the energy dissipated per unit mass is

$$E_m = 2\beta\omega\int_0^\infty \dot{u}^2 dt = -\int_0^\infty a(t)\dot{u}\,dt \tag{4.4}$$

Note that the energy dissipated by viscous damping is equivalent to the work done by the applied forces, i.e. the inertia forces, during the excitation. Of course, for the undamped oscillator energy is not dissipated; the work done by the applied forces is retained within the system in the form of kinetic and potential energies. At any time, t, for the undamped system,

$$E_m(t) = \frac{1}{2}\dot{u}^2(t) + \frac{1}{2}\omega^2 u^2(t) = -\int_0^t a(\tau)\dot{u}\, d\tau \qquad (4.5)$$

where τ is a dummy variable of integration.

In view of the foregoing discussion, the Arias intensity or the frequency ensemble work may be interpreted as the work done by the applied forces, per unit mass, for structures of all natural frequencies; therefore,

$$W_F = -\int_0^\infty \left(\int_0^\infty a(t)\dot{u}\, dt \right) d\omega \qquad (4.6)$$

Employing the solution for $\dot{u}(t)$ in the form of a Duhamel integral, Arias (2) and Housner and Jennings (31) show that the intensity may be simplified to yield

$$W_F = \frac{\cos^{-1}\beta}{\sqrt{1-\beta^2}} \int_0^{t_f} a^2(t)dt \qquad (4.7)$$

where t_f is the total duration of the earthquake. For the undamped system, the Arias intensity or the frequency ensemble work is

$$W_F = \frac{\pi}{2}\int_0^{t_f} a^2(t)dt \qquad (4.8)$$

The coefficient $c_\beta = \cos^{-1}\beta/\sqrt{1-\beta^2}$ in Eq. 4.7 decreases, and hence W_F decreases, as β increases. This results from the fact that $\dot{u}$ is smaller for the damped system; consequently, the power input is less (31). However, for the range of damping values of practical importance, the decrease in c_β is small. For example, for $\beta = 10\%$, $c_\beta = 1.48$, only 6 percent less

than for the undamped case for which $c_\beta = \pi/2 = 1.57$. Hence, the intensity parameter W_F may be considered constant for the range of damping values used in this study, i.e. for 2 to 10 percent of critical. If the work per unit mass given by Eq. 4.4 is integrated with respect to the undamped period T, rather than the frequency ω, the "period ensemble work" (31) results which, for the undamped oscillator is

$$W_T = \pi^2 \int_0^{t_f} v^2(t)dt \tag{4.9}$$

The frequency and period ensemble works, defined by Eqs. 4.8 and 4.9, describe the energy input capabilities of the ground motion and were derived strictly for the linearly elastic system. Arias (2), however, points out that for simple elastoplastic systems, the intensity computed by integrating the energy dissipated by hysteresis correlates well with that obtained from viscously damped linear models. Similarly, Housner and Jennings (31) postulate that the frequency ensemble work is insensitive to the mechanism by which energy is dissipated and hence may apply to hysteretic structures. This reasoning, in part, is reflected by the insensitivity of W_F to large changes in damping for the linear system. Therefore, for this study the integrals of the squared ground motions (as well as the other scaling parameters described herein) are employed as normalizing factors for inelastic and elastic spectra. These scaling factors are given by

$$\left.\begin{aligned} E_a &= \int_0^{t_f} a^2(t)\ dt \\ E_v &= \int_0^{t_f} v^2(t)\ dt \\ E_d &= \int_0^{t_f} d^2(t)\ dt \end{aligned}\right\} \tag{4.10}$$

where, as before, t_f is the total duration of the earthquake. Although the integral of the squared ground displacement apparently has no physical meaning in terms of the energy dissipating characteristics of the single-degree-of-freedom system, this scaling factor is included because several other displacement-related quantities are derived therefrom. The parameters E_a and E_v are proportional to the frequency and period ensemble works of Eqs. 4.8 and 4.9. Note, however, that the constants have been eliminated. These constants are immaterial since dispersion is characterized by the dimensionless coefficient of variation (see Section 4.4).

The remaining scale factors comprising the group based upon ground motion quantities are related to those given in Eqs. 4.10 and may be summarized as follows:

1. The root-square ground motions,

$$\left.\begin{aligned} a_{rs} &= \sqrt{E_a} \\ v_{rs} &= \sqrt{E_v} \\ d_{rs} &= \sqrt{E_d} \end{aligned}\right\} \qquad (4.11)$$

2. The mean-square ground motions,

$$\left.\begin{aligned} P_a &= \frac{1}{t_{95}-t_5}\int_{t_5}^{t_{95}} a^2(t)dt \\ P_v &= \frac{1}{t_{95}-t_5}\int_{t_5}^{t_{95}} v^2(t)dt \\ P_d &= \frac{1}{t_{95}-t_5}\int_{t_5}^{t_{95}} d^2(t)dt \end{aligned}\right\} \qquad (4.12)$$

where t_{95}-t_5 denotes the significant or strong-motion duration, defined later.

3. The root-mean-square (rms) ground motions,

$$\left.\begin{aligned} a_{rms} &= \sqrt{P_a} \\ v_{rms} &= \sqrt{P_v} \\ d_{rms} &= \sqrt{P_d} \end{aligned}\right\} \qquad (4.13)$$

The root-square ground motions given by Eqs. 4.11 were mentioned by Housner (27) as "measures of overall effectiveness." The mean-square and root-mean-square motions defined in Eqs. 4.12 and 4.13 are often encountered in random vibration theory (78). However, some physical reasoning may be offered for their use as earthquake intensity or strength parameters. Housner (30) proposed that a measure of seismic destructiveness might be given by the rate of energy input to structures. Since the integral of the squared ground acceleration is proportional to the total input energy (per unit mass), Housner argues that the average rate of buildup of this integral should provide an indication of earthquake severity. This quantity corresponds, then, to the mean-square acceleration, termed by Housner (30) as the "earthquake power."

The root-mean-square ground motions have been offered as potential measures of earthquake strength (26, 27, 28, 33). In their development of artificial accelerograms, Housner and Jennings (26) proposed scaling the pseudoearthquakes by rms acceleration to provide records typifying those of past events. Studies have also indicated that structural

response may be related to the ground motion intensity as measured by the rms acceleration. Housner (28), for example, points out that failure, i.e. collapse, of simple yielding structures depends upon the duration and the rms acceleration. These findings, originally obtained by Husid (33), were based upon the response of one-story elastoplastic frames with gravity effects.

The duration used to compute the mean-square and rms ground motions requires consideration. First, it should be pointed out that the duration used to compute these quantities need not be related to that employed in the spectral calculations. As described in Chapter 3, the durations for spectral computations were selected by observing the times of peak response displacement. These times of response maxima need not be indicative of the duration of strong shaking, since, for example, many low and intermediate frequency systems attain their maximum response in free vibration, after the strong ground motion ceases.

No single interpretation of strong-motion duration is widely accepted for use in engineering practice. Bolt (6), for example, proposes the "bracketed duration" as the time between the first and last acceleration values exceeding an arbitrary level, say 0.05 or 0.10 g. The definition of significant duration adopted in this study, however, is that offered by Trifunac and Brady (83) and by Dobry, et al. (15). Donovan (16) proposed a similar definition somewhat earlier. In this definition, the duration is based upon the buildup of available seismic energy, i.e. the integral of the squared ground acceleration. The significant duration is taken as the interval between the times at which 5 percent and 95 percent of the seismic energy is attained.

In Eqs. 4.12 these times are denoted as t_5 and t_{95}, respectively. The same duration, $t_{95}-t_5$, is used to compute the mean-square and rms ground velocity and displacement.

To visualize the basis for the foregoing definition of significant duration, consider the example shown in Fig. 4.1. In this figure, the recorded ground acceleration and computed rms acceleration are presented for the El Centro record without the Pecknold-Riddell prefixed pulse. The rms acceleration at time t is,

$$a_{rms} = \left[\frac{1}{t} \int_0^t a^2(t)dt \right]^{\frac{1}{2}} \tag{4.14}$$

The center plot in Fig. 4.1 is a nondimensional representation of the accumulation of the integral of the squared ground acceleration, given by

$$h(t) = \frac{\int_0^t a^2(t)dt}{\int_0^{t_f} a^2(t)dt} \tag{4.15}$$

That is, the value of the integral at time t has been normalized by the final value, at $t = t_f$. Hence, h(t) is the fraction of the total value of the integral attained up to time t. Plots of this type were first proposed by Husid, as described by Idriss (34), to study the growth in the level of shaking with time. Several important features, generally applicable to all accelerograms, are observed in the Husid plot of Fig. 4.1. First, note that h(t) initially builds slowly because of the weak

motion contained in the very early phase of ground shaking. After this period of weak motion, h(t) builds rapidly; as the acceleration levels decrease following the peak value, the seismic energy accumulates more slowly. After a sufficiently long time, very little additional seismic energy is developed. For the El Centro record shown in Fig. 4.1, for example, very little energy is contained in the record after about 26 seconds. Hence, an intermediate portion of the record comprises the significant or strong-motion contribution. For definitiveness, but arbitrarily (83), the first 5 percent and the last 5 percent are deleted from the Husid plot. The remaining 90 percent is defined as the significant or strong-motion portion as depicted in Fig. 4.1.

Removal of the initial 5 percent of the motion is desirable since the artificial prefixed pulse has been added to each accelerogram, as described in Chapter 3. However, the addition of the prefixed pulse has a negligible effect on the mean-square and rms ground motions computed from Eqs. 4.12 and 4.13. For example, the ground acceleration, Husid plot, and rms acceleration for the El Centro record with the prefixed pulse are shown in Fig. 4.2. The record in Fig. 4.2 has been shifted by 2 seconds to accommodate the prefixed pulse, the amplitudes of which are small compared with the accelerations of the actual ground motion. At any time, then, the integral of the squared acceleration for the record with the pulse corresponds to that which was developed 2 seconds earlier in the record without the pulse. Thus, the rms acceleration is less, at each time point, for the record with the prefixed pulse. However, note that t_5 and t_{95} shown in Fig. 4.2 are simply shifted by 2 seconds. Therefore, the significant duration, $t_{95}-t_5$, is the same as

that for the record with no prefixed pulse. Since the contributions of of the squared pulse motions are quite small, the mean-square and rms quantities computed from Eqs. 4.12 and 4.13 are the same as those computed for the record without the prefixed pulse.

The integrals of the squared ground motion required in Eqs. 4.10 through 4.13 may be determined by squaring Eqs. 3.1, 3.3, and 3.4 and integrating from $t = t_i$ to $t = t_{i+1}$. The value of the integrals at time t_{i+1} may be expressed as,

$$\int_0^{t_{i+1}} z^2(t)dt = \int_0^{t_i} z^2(t)dt + \int_{t_i}^{t_{i+1}} z^2(t)dt \tag{4.16}$$

where z denotes the ground acceleration, velocity, or displacement. The recursion formulas are,

$$\left.\begin{aligned}
&\int_{t_i}^{t_{i+1}} a^2(t)dt = \frac{\Delta t_i}{3}\left(a_i^2+a_i a_{i+1}+a_{i+1}^2\right)\\
&\int_{t_i}^{t_{i+1}} v^2(t)dt = \Delta t_i v_i^2 + \frac{(\Delta t_i)^2}{3} v_i(2a_i+a_{i+1}) +\\
&\qquad + \frac{(\Delta t_i)^3}{60}\left(8a_i^2+9a_i a_{i+1}+3a_{i+1}^2\right)\\
&\int_{t_i}^{t_{i+1}} d^2(t)dt = \Delta t_i d_i^2 + (\Delta t_i)^2 d_i v_i +\\
&\qquad + \frac{(\Delta t_i)^3}{12}\left[4v_i^2 + d_i(3a_i+a_{i+1})\right] +\\
&\qquad + \frac{(\Delta t_i)^4}{60} v_i(11a_i+4a_{i+1}) +
\end{aligned}\right\} \tag{4.17}$$

$$+\frac{(\Delta t_i)^5}{1260}(33a_i^2+25a_ia_{i+1}+5a_{i+1}^2)\Bigg]\sim$$

The values of the ground motion parameters described in this section are listed in Tables 4.1 through 4.5 for the records used in this study.

4.3 Scaling Factors Based on Response Quantities

In this study, two parameters derived directly from the response of elastic single-degree-of-freedom systems are used as scaling factors for earthquake spectra. These quantities are the spectrum intensity proposed by Housner (23) and the mean Fourier amplitude, previously used by Cornell et al. (11) as a normalizing factor for elastic spectra.

Since the maximum spring force for the linearly elastic system is directly proportional to the pseudovelocity, S_v, Housner (23) argues that the spectrum itself is a measure of the severity of the earthquake. Housner proceeds to define the spectrum intensity (23, p. 24):

> In using the spectrum as a measure of the intensity of an earthquake, that is, as a measure of the capability of the earthquake to produce stresses, allowances must be made for the fact that in a city the periods of vibration of the structures will cover a wide range. If the significant range of periods is taken to be from 0.1 seconds to 2.5 seconds, the average value of S_v over this range is a measure of the intensity of the earthquake. It is a measure of the intensity in the sense that if a city contained a large number of structures having a uniform distribution of periods ranging from 0.1 to 2.5 seconds, and the city were subjected to different earthquakes, then on the average the ratios of the maximum stresses produced would be proportional to the average values of S_v for the different earthquakes. It is thus seen that this measure of the intensity is an average measure for a range of periods.
>
> Since measures of earthquake intensities are useful only for comparing different earthquakes, it makes no difference whether the average value of S_v is used or whether the area under the curve is used. Accordingly the spectrum intensity of an earthquake

is defined to be the area under the spectrum curve between the periods 0.1 and 2.5 seconds.

Since the stresses in a structure produced by an earthquake depend upon the amount of damping present, it is informative to measure the spectrum intensities of earthquakes for various amounts of damping. The undamped intensity is the area under the spectrum curve computed for zero damping (β=0%); the 0.2 damped intensity is the area under the spectrum curve computed for 0.2 critical damping (β=20%), etc.

Hence, the spectrum intensity is defined as

$$SI(\beta,T_1\text{-}T_2) = \int_{T_1}^{T_2} S_v(\beta,T)dT \tag{4.18}$$

where T_1 = 0.1 sec and T_2 = 2.5 sec. Alternatively, the spectrum intensity may be expressed as

$$SI(\beta,f_1\text{-}f_2) = \int_{f_1}^{f_2} \frac{S_v(\beta,f)}{f^2}\,df \tag{4.19}$$

where f_1 = 0.4 cps and f_2 = 10 cps. This latter form is used to compute the spectrum intensities in this study. For these calculations, the pseudovelocity is assumed to vary linearly, in the log-log domain, between spectral points. That is, within the jth interval,

$$S_v(\beta,f) = b_j f^{a_j}, \quad f_j \leq f \leq f_{j+1} \tag{4.20}$$

where a_j and b_j are computed within each frequency interval from

$$\left.\begin{aligned} a_j &= \frac{\log(S_{v_{j+1}}/S_{v_j})}{\log(f_{j+1}/f_j)} \\ b_j &= S_{v_j} f_j^{-a_j} \end{aligned}\right\} \tag{4.21}$$

The spectrum intensity is the sum of the areas within each frequency interval; hence,

$$SI(\beta,f_1-f_2) = \sum_{j=j_{f_1}}^{j=j_{f_2}} \left\{ \frac{b_j}{a_j-1} \left[f_{j+1}^{(a_j-1)} - f_j^{(a_j-1)} \right] \right\} \qquad (4.22)$$

where j_{f_1} and j_{f_2} correspond to the indices of the frequency limits over which the spectrum intensity is computed. The spectrum intensities between 0.4 and 10 cps for the earthquake records used in this study are shown in Table 4.6.

Housner (24) indicates that the undamped spectrum intensity is a measure of both the magnitude of the accelerations and the duration of the ground motion. On the other hand, in Ref. 23 Housner notes that to associate the spectrum intensity with observed damage, it must be recognized that buildings have appreciable amounts of damping. Therefore, it may be more reliable to take the 20 percent damped, rather than the undamped, spectrum intensities as indicators of damage. The ability of the spectrum intensity to adequately describe earthquake damage potential was questioned, however, by Housner himself following the Parkfield earthquake of June 27, 1966. In Ref. 29, Housner notes that the ordinates of the pseudovelocity spectra, and hence the spectrum intensities, are about 50 percent greater for the Cholame-Shandon No. 2 record of the Parkfield earthquake than those for the El Centro shock of May 18, 1940. (Compare the spectra of Figs. 3.31 and 3.35 and the spectrum intensities in Table 4.6). However, the damage caused by the Parkfield earthquake was minor

compared with that which resulted from the El Centro shock. Housner concludes from these observations that as indicators of earthquake damage potential, neither the elastic pseudovelocity nor the spectrum intensities are as reliable as originally thought. Despite this apparent negative evidence, the spectrum intensity is indeed a measure of intensity of ground shaking; it need not, however, relate directly to damage (29).

In this study, the spectrum intensities for all levels of damping are evaluated as potential spectral scaling factors. In addition, it should be noted that the frequency region over which the spectrum intensity is computed, i.e. 0.4 to 10 cps, is rather arbitrarily selected. As will be described in Chapter 5, spectrum intensities computed from other frequency regions are investigated as normalizing factors for response spectra.

Cornell et al. (11) have used the amplitudes of the Fourier spectrum of the ground acceleration as scaling factors for elastic spectra. In Cornell's study, normalizing factors were determined by averaging the Fourier amplitudes within three frequency regions corresponding to the low frequency "displacement" region, the intermediate "velocity" region, and the high frequency "acceleration" region. The dispersion in the elastic spectra normalized by these mean Fourier amplitudes was compared with that observed in the spectra normalized by the peak ground motions. The detailed findings of Cornell's study are deferred to Chapter 5 so that they may be compared with those obtained in this investigation. However, it is noted here that significant reductions in scatter, especially for small damping, resulted when the spectra were normalized by the mean Fourier amplitudes.

It is instructive to investigate the physical interpretation of the Fourier spectrum of the ground acceleration and to determine its relationship to the pseudovelocity spectrum. The Fourier spectrum of the ground acceleration is given in Ref. 10 as,

$$F(\omega) = \int_{-\infty}^{+\infty} a(\tau)e^{-i\omega\tau}\, d\tau \tag{4.23}$$

where τ is a dummy variable of integration. Note that $e^{-i\omega\tau} = \cos\omega\tau - i\sin\omega\tau$ and that $a(\tau) \neq 0$ only for $0 \leq \tau \leq t_f$; hence, the Fourier spectrum becomes

$$F(\omega) = \int_0^{t_f} a(\tau)\cos\omega\tau d\tau - i\int_0^{t_f} a(\tau)\sin\omega\tau d\tau \tag{4.24}$$

for which the amplitude is

$$|F(\omega)| = \left\{ \left[\int_0^{t_f} a(\tau)\cos\omega\tau d\tau\right]^2 + \left[\int_0^{t_f} a(\tau)\sin\omega\tau d\tau\right]^2 \right\}^{\frac{1}{2}} \tag{4.25}$$

Now, for an undamped single-degree-of-freedom oscillator, consider the work done by the inertia forces developed by the ground acceleration from $t = 0$ to $t = t_f$. This work is obtained by evaluating Eq. 4.5 at $t = t_f$ and is

$$E_m(t_f) = \frac{1}{2}\dot{u}^2(t_f) + \frac{1}{2}\omega^2 u^2(t_f) \tag{4.26}$$

where E_m is the work per unit mass. The solutions for $u(t_f)$ and $\dot{u}(t_f)$ may be expressed by the Duhamel integral and its time derivative.

The square root of twice the energy per unit mass at $t = t_f$ is

$$\sqrt{2E_m(t_f)} = \left\{ \left[\int_0^{t_f} a(\tau)\cos\omega(t-\tau)d\tau \right]^2 + \left[\int_0^{t_f} a(\tau)\sin\omega(t-\tau)d\tau \right]^2 \right\}^{\frac{1}{2}} \tag{4.27}$$

which upon simplification yields

$$\sqrt{2E_m(t_f)} = \left\{ \left[\int_0^{t_f} a(\tau)\cos\omega\tau d\tau \right]^2 + \left[\int_0^{t_f} a(\tau)\sin\omega\tau d\tau \right]^2 \right\}^{\frac{1}{2}} \tag{4.28}$$

Note that Eq. 4.25 is identical to Eq. 4.28. That is,

$$|F(\omega)| = \sqrt{2E_m(t_f)} \tag{4.29}$$

Thus, the Fourier amplitude may be interpreted as a measure of the total energy, at the end of the earthquake, within an undamped single-degree-of-freedom system. Furthermore, the Fourier amplitude has the dimensions of velocity and is, in fact, the maximum velocity attained by the undamped single-degree-of-freedom oscillator during free vibration, for $t \geq t_f$. Because the spectral velocity, namely the maximum velocity, may occur at time $t < t_f$, it is apparent that $S_v(\omega) \geq |F(\omega)|$ for each frequency ω. In other words, the Fourier amplitude spectrum is bounded by the pseudo-velocity spectrum.

In the spectral calculations, $u(t_f)$ and $\dot{u}(t_f)$ are evaluated; hence, the Fourier amplitude for each frequency may be computed from

$$|F(\omega)| = [\dot{u}^2(t_f) + \omega^2 u^2(t_f)]^{\frac{1}{2}} \tag{4.30}$$

This expression for the Fourier amplitude results from the substitution of Eq. 4.26 into Eq. 4.29. The Fourier amplitude spectra and for comparison, the undamped pseudovelocity spectra, are shown in Figs. 4.3 through 4.14 for the records used in this study. Note in these figures that the velocity axis is linear rather than logarithmic so that the differences between the spectra are more apparent. It should also be mentioned, as indicated in Chapter 3, that the frequency intervals used to compute the undamped spectra are rather large. Nevertheless, these spectra are used to compute mean Fourier amplitudes within selected frequency regions,

$$\overline{FS}(f_1\text{-}f_2) = \frac{1}{f_2-f_1}\int_{f_1}^{f_2} |F(f)|\,df \qquad (4.31)$$

As for the pseudovelocity, the Fourier amplitude is assumed to vary linearly, in the log-log domain, between spectral values. The frequency regions used to compute mean Fourier amplitudes are identified in Chapter 5; however, it is noted here that these frequency regions are appropriately selected to provide the least dispersion in the normalized spectra.

4.4 Procedure for Statistical Analysis

The parameters described previously in this chapter are evaluated as normalizing factors for earthquake response spectra. This evaluation is accomplished by comparing the variations in the sets of normalized spectra. The goal, of course, is to identify those factors which produce the least scatter or dispersion in the normalized spectra. In the following paragraphs, the measure of dispersion and the details associated with its

calculation are summarized.

At each spectral frequency, the mean normalized pseudovelocity is computed from

$$\bar{S}_v = \frac{1}{n} \sum_{i=1}^{n} \frac{S_{v_i}}{\psi_i} \tag{4.32}$$

where ψ_i is the normalizing factor for the ith record and n is the number of earthquake records. The variance is the average squared deviation from the mean, defined by

$$\sigma^2 = \frac{1}{n-1} \sum_{i=1}^{n} \left(\frac{S_{v_i}}{\psi_i} - \bar{S}_v \right)^2 \tag{4.33}$$

The standard deviation is the square root of the variance,

$$\sigma = \left[\frac{1}{n-1} \sum_{i=1}^{n} \left(\frac{S_{v_i}}{\psi_i} - \bar{S}_v \right)^2 \right]^{1/2} \tag{4.34}$$

The standard deviation is more effectively computed by expanding Eq. 4.34,

$$\sigma = \left\{ \frac{1}{n-1} \left[\sum_{i=1}^{n} \left(\frac{S_{v_i}}{\psi_i} \right)^2 - n\bar{S}_v^2 \right] \right\}^{1/2} \tag{4.35}$$

This latter expression for the standard deviation gives improved accuracy since the number of subtractions is reduced (to only one) and is postponed until the final step in the calculation (41).

Note that Eqs. 4.33 and 4.34 define the so-called unbiased variance and standard deviation. These unbiased values result when the divisor

(n-1) is used instead of n. Of course, for a large number of observations, the differences between the biased and unbiased quantities diminish. In any case, it should be recognized that only (n-1) of the deviations from the mean are independent (41). That is, (n-1) of the deviations determine the nth, since their sum is zero. It should be noted, however, that for the purposes of this comparative study, whether the biased or unbiased values are used is immaterial.

The variance and standard deviation are measures of absolute variation. Namely, they provide the actual variation present in a set of data, and therefore depend upon the scale of measurement. To compare the variation or dispersion in several sets of data, i.e. for the various sets of normalized spectra considered in this study, it is desirable to use a measure of relative variation. For this purpose, the coefficient of variation is employed, which is defined as

$$COV = \frac{\sigma}{\bar{S}_v} \tag{4.36}$$

Note that the dimensionless COV gives the standard deviation as a fraction of the mean, and hence is independent of the scale of measurement. For example, if each observation in a set of data is multiplied by a constant k, the sample mean and standard deviation are, respectively, $k\bar{x}$ and $k\sigma$. The COV, however, is unaffected. It is clear then, that constants, for example those in Eqs. 4.8 and 4.9, may be eliminated from spectral normalizing factors.

CHAPTER 5

STATISTICAL EVALUATION OF SCALING METHODS

5.1 Introduction

This chapter begins with a brief description of the characteristics of the mean inelastic yield spectra computed in this study. The statistics associated with the spectra normalized by the peak ground acceleration, velocity, and displacement are presented and compared with those of previous studies. In Chapter 3, the effects of damping and strain-hardening on spectra obtained from individual ground motions were examined. A comparison of average spectra, however, permits a more general assessment of the influence of these two structure-related parameters.

The major objective of this chapter is to evaluate the spectral scaling parameters described in Chapter 4. The goal is to determine which of the scaling factors provide less dispersion than that obtained when the spectra are normalized by the peak ground motions. The results show that the most promising alternative scaling procedure is a three-parameter system of spectrum intensities. Namely, three spectrum intensities, the areas under the elastic pseudovelocity spectrum within three ranges of frequency, constitute a set of normalizing factors which reduces the scatter compared with that encountered in current spectral scaling practice. These spectrum intensities significantly reduce the scatter for linearly elastic systems. When the same intensities are used to normalize inelastic spectra, reductions in dispersion are realized for low to moderate ductilities.

5.2 Characteristics of Mean Normalized Inelastic Spectra

The inelastic yield spectra considered in this study are normalized by the peak ground motions, averaged, and compared. The purpose is to quantify the effects of damping for the elastoplastic system and to assess the influence of the level of strain-hardening for the bilinear hysteretic system. The details of the procedure used for comparison and the results of the evaluation are outlined in the following sections.

5.2.1 Computation of Mean Spectral Ordinates

The mean spectral ordinates are computed from the average of the spectra normalized by the corresponding peak ground motion. For example, the mean spectral displacement is determined from the average of the spectra normalized by the peak ground displacement. The mean spectral ordinates are associated with the frequency regions of constant ground motion amplification and are evaluated in a manner illustrated in Figs. 5.1 through 5.3. In these figures, the dashed lines represent those of best fit. Note from Figs. 5.1 through 5.3 that the amplified spectral region is taken from 0.071 cps to 8.5 cps. Below 0.071 cps and above 8.5 cps, the spectra begin their respective transitions to the peak ground displacement, 1 inch in Fig. 5.1, and the peak ground acceleration, 1 g in Fig. 5.3.

In the mean spectra shown in Figs. 5.1 through 5.3, the displacement, velocity, and acceleration regions are, respectively, 0.071-0.54 cps, 0.51-3.7 cps, and 2.2-8.5 cps. Note that the frequencies separating these regions do not coincide; namely, the frequency intervals, especially the velocity and acceleration regions, overlap. This results

from the fact that a particular frequency region is determined from the mean of the spectra normalized by the corresponding peak ground motion. Since the ratio of the maximum ground motions for each record are different, the shapes of the mean spectra are not identical. Accordingly, the frequency limits determined from the mean of the spectra normalized by the various ground motions need not agree.

The lines of best fit for the mean spectra are computed in an iterative fashion. First, estimates of the frequencies defining the mid-frequency region, f_2 and f_3 in Fig. 5.4, are made. The average spectral ordinates within the three frequency regions are

$$\tilde{S}_d = \frac{\int_{f_1}^{f_2} \bar{S}_v(f)df}{\pi(f_2^2 - f_1^2)} \tag{5.1}$$

$$\tilde{S}_v = \frac{\int_{f_2}^{f_3} \bar{S}_v(f)df}{f_3 - f_2} \tag{5.2}$$

$$\tilde{S}_a = \frac{2\pi \int_{f_3}^{f_4} \bar{S}_v(f)df}{\ln\left(\frac{f_4}{f_3}\right)} \tag{5.3}$$

where $\bar{S}_v$ is the mean normalized pseudovelocity, at each frequency, computed in accordance with Eq. 4.32. To perform the required integrations, it is assumed that log $(\bar{S}_v)$ varies linearly with log (f). The frequencies f_2 and f_3 may now be determined from

$$f_2 = \frac{\tilde{S}_v}{2\pi \tilde{S}_d} \quad \text{and} \quad f_3 = \frac{\tilde{S}_a}{2\pi \tilde{S}_v} \tag{5.4}$$

If the computed frequencies f_2 and f_3 do not agree with those assumed, the calculations are repeated using the computed values. This iterative procedure is repeated until the assumed and computed frequencies agree to within some prescribed accuracy, taken in this study as 0.1 percent. For this tolerance, generally no more than six cycles are required for convergence.

The method outlined above was employed to determine the mean spectral ordinates illustrated in Figs. 5.1 through 5.3 and summarized in Table 5.1. The coefficient of variation is determined in an analogous fashion from the mean + 1σ spectra. For comparison, the corresponding statistics evaluated in two previous studies are also shown in Table 5.1. It should be noted that the differences between the various quantities listed in Table 5.1 result from the limited number and choice of records used in the cited statistical studies. In this study 12 earthquake components are used; Riddell and Newmark (67) employed 10 components of ground motion. In Ref. 51, both horizontal components of 14 records were used. Hence, in this latter study, the sample size was 28. The variabilities in the data of Table 5.1 primarily reflect the characteristics of the chosen groups of accelerograms. Nevertheless, the maximum difference between any two corresponding mean spectral ordinates is about 15 percent.

5.2.2 Effect of Damping on Mean Spectra

The mean elastoplastic yield spectra normalized by peak ground displacement, velocity, and acceleration are shown in Figs. 5.5 through

5.10. An examination of these figures provides an assessment of the influence of damping when combined with hysteretic behavior. These effects may be summarized as follows:

1. For very flexible systems, the mean response is independent of damping for all levels of displacement ductility.
2. For high frequency systems, damping is somewhat effective in reducing response, particularly for large displacement ductilities.
3. For a broad intermediate range of frequencies, the influence of damping decreases as the level of inelastic response increases. This characteristic is apparent from Figs. 5.5 through 5.10 by observing that the differences between the spectra within each group decrease as the displacement ductility increases. However, note from Figs. 5.6 and 5.8 that the influence of damping for $\mu = 10$ is slightly greater than that for $\mu = 3$. Specifically, from Fig. 5.6 an increase in damping from 2 to 10 percent decreases the mean displacement ordinate by 16 percent for $\mu = 3$. For $\mu = 10$, however, the mean displacement ordinate decreases by 19 percent when damping is increased from 2 to 10 percent. Similar observations are apparent in Fig. 5.8 for the mean velocity ordinate for ductilities of 3 and 10.

The spectral reduction factors, the ratios of the mean inelastic ordinates to the corresponding mean elastic values, are shown in Table 5.2. For comparison, the results of Riddell and Newmark (67) are also shown in Table 5.2. Note that within all three spectral regions, the reduction factors increase, for a given ductility, as the damping

increases. This observation indicates that damping becomes less important, compared with its influence on elastic systems, as the level of inelastic response increases. It is also noteworthy that the spectral reduction factors increase relatively more rapidly with damping in the acceleration and velocity regions than in the displacement region. This result shows that damping has greater effect in reducing response for systems of intermediate and high frequency. For example, for a ductility of 3, the reductions in the mean displacement, velocity, and acceleration ordinates are, respectively, 16, 21, and 24 percent, for an increase in damping from 2 to 10 percent. Thus, in an average sense, the effectiveness of damping in reducing response increases as the frequency of the system increases.

5.2.3 Effect of Strain-Hardening on Mean Spectra

The effects of varying levels of strain-hardening on average response are exemplified by the mean normalized spectra shown in Figs. 5.11 through 5.19 and by the spectral reduction factors presented in Table 5.3. From the mean spectra, the general influence of strain-hardening is as expected: strain-hardening decreases the yield level required for the system to attain a given displacement ductility. Note, however, that the influence of strain-hardening is small for low levels of inelastic response. As the displacement ductility increases, of course, strain-hardening has proportionately greater effect in reducing response.

The influence of strain-hardening also varies with the frequency of the system. For very flexible systems, i.e. for frequencies less than about 0.07 cps, mean spectral values are independent of the level

of strain-hardening. As the frequency of the single-degree-of-freedom system increases, the effect of strain-hardening increases. However, strain-hardening has relatively little effect, even for large ductilities, in the low frequency region of the spectrum, extending from about 0.1 to 0.5 cps. This observation is readily apparent from Figs. 5.11 through 5.13 and from the data in Table 5.3. For each ductility, the spectral reduction factor ϕ_D decreases only slightly as the level of strain-hardening increases. Only for large ductilities, i.e. for $\mu = 5$ and 10 is any important change in ϕ_D observed. In the velocity and acceleration regions, i.e. for systems of intermediate and high frequency, strain-hardening has a more pronounced influence on mean response. For example, for a ductility of 10, ϕ_V and ϕ_A decreases by 21 and 23 percent, respectively, as the strain-hardening increases from 0 to 0.10. In the displacement region, the largest decrease in ϕ_D is 12 percent for $\mu = 5$.

The foregoing observations provide useful information for design. In particular, mean response, especially for low to moderate ductilities, is relatively insensitive to rather large changes in strain-hardening. Of course, this conclusion does not imply that there are no differences in the response of individual systems subjected to specific earthquake motions. However, for reasonably accurate estimates of response, it may not be necessary to know the precise details, e.g. the level of strain-hardening, associated with the hysteretic material model. This conclusion, of course, coincides with that reached by previous investigators (35, 36, 40, 67).

5.3 Dispersion Characteristics of Spectra Normalized by Peak Ground Motions

As described in Chapter 4, normalizing response spectra by the peak ground motions has physical appeal. Namely, the maximum dynamic response to earthquake excitation may generally be perceived as an amplified peak ground motion. However, an examination of the dispersion characteristics of response spectra provides an additional motivation for current scaling practice. When normalized by the peak ground motions, three distinct frequency regions arise in which the coefficient of variation is a minimum. These frequency regions are clearly identified in Figs. 5.20 through 5.23, in which the coefficients of variation are plotted versus frequency for elastoplastic yield spectra with 5 percent damping. Normalization by the peak ground displacement, d_p, provides the least coefficient of variation for low frequencies. Below the transition frequency of 0.071 cps, the coefficient of variation decreases rapidly. This results from the fact that for very flexible systems, the response is directly related to the peak ground displacement -- for elastic and inelastic systems, $S_d = d_p$. Hence, for systems of infinite flexibility, the COV = 0 for spectra normalized by d_p. For spectra normalized by the peak ground velocity, v_p, the coefficient of variation is a minimum within an intermediate range of frequencies, as illustrated in Figs. 5.20 through 5.23. The least coefficient of variation for high frequencies results for spectra normalized by the peak ground acceleration, a_p. A rapid decrease in the coefficient of variation for spectra normalized by a_p is observed for frequencies greater than the spectral transition frequency of 8.5 cps. For elastic spectra normalized by a_p, the coefficient of variation

approaches zero for rigid systems, since for these systems, $S_a = a_p$.

The frequency regions defined by the minimum coefficients of variation are shown in Tables 5.4 and 5.5 for the entire set of inelastic spectra considered in this study. Several features of these frequency regions are noteworthy. First, the frequecy regions defined by the minimum coefficients of variation do not precisely correspond to those of constant spectral amplification. For example, as shown in Figs. 5.1 through 5.3, the regions of constant displacement, velocity, and acceleration amplification for elastic spectra with 5 percent damping are, respectively, 0.071-0.54 cps, 0.51-3.7 cps, and 2.2-8.5 cps. From Table 5.4 the corresponding frequency regions in which the coefficients of variation are a minimum are 0.071-0.20 cps, 0.20-2.0 cps, and 2.0-8.5 cps. For the comparative evaluation of the alternative normalizing parameters, the frequency regions defined by the minimum coefficients of variation are used. In all subsequent references to the displacement, velocity, and acceleration regions, the frequency ranges summarized in Tables 5.4 and 5.5 are implied. The second feature of these frequency regions is that they are not substantially affected by viscous damping and the level of strain-hardening. Note, however, that the magnitude of the maximum inelastic response does influence the frequency regions. As the displacement ductility increases, the displacement and velocity regions broaden at the expense of the acceleration region.

It is apparent from the data plotted in Figs. 5.20 through 5.23 that within each frequency region, the coefficient of variation fluctuates. For example, in Fig. 5.20, the coefficient of variation in the displacement region varies between about 0.35 and 0.50. So that

the effects of damping and strain-hardening on the dispersion characteristics of normalized spectra may be quantified, the coefficients of variation are averaged within each frequency region. These results are summarized in Tables 5.6 and 5.7. The data in Table 5.6 indicates that within any spectral region, the average coefficient of variation decreases with damping, for a given ductility. The only exception is in the acceleration region for a ductility of 10, where the average coefficient of variation increases slightly from 0.26 for 5 percent damping to 0.28 for 10 percent damping. It is also clear that, for any damping value, the average coefficient of variation decreases as the level of the inelastic response increases. Again, an exception is noted in the acceleration region where the average coefficient of variation increases for ductilities of 5 and 10. Generally, then, both damping and inelastic action tend to decrease the average coefficients of variation, i.e. the scatter, for spectra normalized by the peak ground motions. This conclusion arises from the fact that both of these energy dissipative mechanisms have a smoothing effect on response spectra. Local spectral irregularities diminish as damping and hysteretic energy losses increase; accordingly, the dispersion in normalized response ordinates decreases.

The same general influence, but to a somewhat lesser extent, is apparent as the level of strain-hardening increases for the bilinear hysteretic system. Of course, for small levels of inelastic response, i.e. for low ductilities, the effects of strain-hardening on the average coefficients of variation are small. However, the average coefficients of variation in Table 5.7 indicate that for most cases, increases in strain-hardening decrease the dispersion. This effect is most pronounced

for large ductilities in the displacement region. In the velocity and acceleration regions, the decreases in the average coefficients of variation are generally smaller. In the acceleration region, however, for a ductility of 5, the average coefficient of variation decreases by 25 percent for an increase in strain-hardening of 10 percent. On the other hand, note that in the velocity region, the average coefficient of variation increases slightly for a ductility of 10, as strain-hardening increases.

5.4 Evaluation of Scale Factors Based on Ground Motion Quantities

The dispersion characteristics of elastoplastic yield spectra normalized by the factors computed from the ground motions are shown in Figs. 5.24 through 5.35. These results, for elastoplastic systems with 5 percent damping and ductilities of 1 (elastic), 2, 5, and 10, are typical of those for the entire set of spectra considered in this study. The graphical presentation of the results provides a convenient visual means for evaluating those scaling parameters derived from ground motion data.

For the displacement-related factors, note that for all ductilities, E_d, the integral of the squared ground displacement, and P_d, the mean-square ground displacement, are particularly poor normalizing parameters. However, for elastic systems, i.e. for $\mu = 1$, the root-square displacement d_{rs} provides some reduction in scatter within the displacement region. It is interesting to note that within the displacement region, normalizing by peak displacement d_p produces a local maximum coefficient of variation of about 0.50 between 0.8 and 0.9 cps. Within this same range of frequencies, normalizing by d_{rs} produces a minimum coefficient of variation of

about 0.25. Hence, for elastic spectra, normalizing by the root-square displacement decreases the scatter or dispersion compared with that observed in spectra normalized by peak displacement. As the level of inelastic response increases, however, the improvement afforded by the root-square displacement diminishes. This trend is readily discernible from Fig. 5.25 in which the coefficients of variation for a ductility of 2 are shown. For ductilities greater than about 3 to 5 the peak ground displacement provides the least dispersion within the entire displacement region. It is also worthy to note that the root-mean-square displacement d_{rms} does not improve the dispersion characteristics. However, normalizing by d_{rms} results in coefficients of variation comparable to, for the most part, those obtained from scaling by d_{rs} and d_p.

The normalizing factors based on ground velocity are compared in Figs. 5.28 through 5.31. Again, it is apparent that E_v and P_v are poor spectral normalizing factors, as evidenced by their large coefficients of variation. As was the case for the displacements, the coefficients of variation for v_p, v_{rs}, and v_{rms} are comparable within the velocity region. However, with only minor exceptions, none of the velocity-related scaling factors provide less scatter than that obtained by normalizing by the peak ground velocity. This conclusion applies for both elastic and inelastic systems for all ductilities. The same results are noted for the acceleration-related factors compared in Figs. 5.32 through 5.35. Of these parameters, the root-square acceleration a_{rs} provides only minor reductions in scatter within limited ranges of frequency.

On the basis of the foregoing evaluation, it is concluded that, at least for the ensemble of earthquake accelerograms considered in this study, the normalizing factors based upon ground motion data do not constitute promising alternatives to the peak motions. As previously noted, however, the root-square displacement does potentially provide some improvement as a normalizing parameter for elastic spectra in the low frequency region.

5.5 Evaluation of Scale Factors Based on Response Quantities

The response-related normalizing factors which are investigated in this study include Housner's spectrum intensity and the mean Fourier amplitude. Since the spectrum intensity and Fourier amplitude are closely related to the pseudovelocity spectrum, it is likely that these parameters may provide the most promising alternative spectral scaling factors. The evaluation of these normalizing factors begins by considering elastic spectra.

5.5.1 Elastic Spectra Normalized by Spectrum Intensity and Mean Fourier Amplitude

The spectrum intensity, described in detail in Chapter 4, is defined as the area beneath the elastic pseudovelocity spectrum between two frequencies. In Housner's original definition, the frequency limits are 0.4 and 10 cps, which encompass those of most buildings and facilities located within a typical municipality. When elastic spectra are normalized by the spectrum intensities (summarized in Table 4.6), the dispersion characteristics shown in Fig. 5.36 are obtained. The coefficients of variation for elastic spectra with 5 percent damping are shown in Fig. 5.36 and are typical of those for the range of damping values considered

in this study. The solid curve in Fig. 5.36 represents the coefficients of variation which result from normalization by undamped spectrum intensity. The remaining curves display the coefficients of variation obtained by normalizing the spectra by 2, 5, and 10 percent damped spectrum intensities. The velocity region denoted in Fig. 5.36 corresponds to that obtained from normalization by the peak ground velocity. This frequency region, as shown in Table 5.4, extends from 0.2 to 2 cps.

Two features of the results presented in Fig. 5.36 are important. First, the trends of the curves are identical to those obtained from normalization by the peak ground velocity. That is, the coefficients of variation are a minimum within an intermediate region of frequencies; for low and high frequencies, the coefficients of variation increase sharply. This similarity in the behavior of the coefficients of variation for the spectrum intensity and peak velocity provides a clue that a three-parameter definition of spectrum intensity may exist as a potential alternative normalizing scheme. The second feature of the data shown in Fig. 5.36 is that as long as the spectra are normalized by damped spectrum intensities, the coefficients of variation within the velocity region are insensitive to the level of damping.

To investigate the effects of the frequency limits within which the spectrum intensity is computed, consider the results shown in Fig. 5.37. In this figure, the coefficients of variation for elastic spectra with 5 percent damping normalized by spectrum intensity between 0.2 and 2 cps are presented. Note from Fig. 5.37 that again, the coefficients of variation are a minimum within a central region of frequency. The least coefficients of variation occur in the range extending from about 0.2 to

0.7 cps. Also, as previously observed in Fig. 5.36, the coefficients of variation in the velocity region are insensitive to damping provided that damped spectrum intensities are used. Based on this observation, 2 percent damped spectrum intensities are employed for further study.

A comparison of the coefficients of variation for elastic spectra with 5 percent damping normalized by the peak ground velocity and the 2 percent spectrum intensities is shown in Fig. 5.38. It is clear from this figure that varying the frequency limits within which the spectrum intensity is computed affects the coefficient of variation. Furthermore, note that SI(2%, 0.2-2 cps) provides less scatter than v_p for frequencies up to about 0.7 cps, while SI(2%, 0.4-10 cps) results in smaller coefficients of variation for frequencies greater than 0.7 cps. Note that the improvement afforded by SI(2%, 0.4-10 cps) extends beyond 2 cps, up to about 3 cps.

The potential of low frequency and high frequency-based spectrum intensities are shown in Figs. 5.39 through 5.42. In Fig. 5.39, the coefficients of variation for elastic spectra normalized by spectrum intensities computed between 0.071 and 0.20 cps are shown. Note that these frequency limits correspond to those defining the displacement region for elastic spectra with 5 percent damping. The coefficients of variation for the spectra normalized by peak ground displacement and SI(2%, 0.071-0.20 cps) are compared in Fig. 5.40. Figures 5.41 and 5.42 contain similar data for elastic spectra normalized by peak ground acceleration and spectrum intensity between 2 and 8.5 cps. An examination of Figs. 5.38, 5.40, and 5.42 shows that a three-parameter set of 2 percent damped spectrum intensities may indeed provide a better means for

the average coefficients of variation decrease with damping within the displacement and velocity regions. In the acceleration region, a constant average coefficient of variation of 0.24 results. However, when the spectra are normalized by the peak ground motions, the average coefficients of variation decrease markedly with increased damping. Hence, the reductions in the average coefficients of variation, shown in the right-hand column of Table 5.10, decrease with damping. Nevertheless, the results reveal that, on the average, normalization by the 2 percent damped spectrum intensities does, in fact, decrease the dispersion in elastic spectra. The improvement in the velocity region, however, is roughly half of that observed in the displacement and acceleration regions.

The dispersion characteristics of elastic spectra with 5 percent damping normalized by the three-parameter system of spectrum intensities are depicted graphically in Figs. 5.46 through 5.49. In Fig. 5.46, the three frequency regions arise in which the corresponding coefficients of variation are a minimum. Note, however, that the frequency separating the velocity and acceleration regions has shifted from 2 cps (Fig. 5.20) to about 3 cps. The coefficients of variation obtained from normalization by the spectrum intensities and by the peak ground motions are compared directly in Figs. 5.47 through 5.49. The displacement, velocity, and acceleration regions denoted in these figures correspond to those obtained from normalizing by the peak ground motions. The reduction in the coefficients of variation over the entire displacement region is clearly evident in Fig. 5.47. However, in Fig. 5.48 the coefficients of variation for normalization by the spectrum intensity are greater than those for v_p between about 0.2 and 0.5 cps. For frequencies extending from 0.5 to

about 3 cps, normalizing by SI(2%, 0.50-3.5 cps) results in smaller coefficients of variation. On the average, the coefficient of variation is reduced by 18 percent in the region from 0.2 to 2 cps. Similar results are apparent in the acceleration region where, for frequencies greater than 3 cps, normalizing by SI(2%, 5.4-35 cps) provides significant reductions in the coefficient of variation. For frequencies between 2 and 3 cps, the peak ground acceleration affords smaller dispersion.

Because the frequency separating the velocity and acceleration regions shifts when the spectra are normalized by the spectrum intensities, it is perhaps more appropriate to compare the results in the manner shown in Fig. 5.50. In this figure, the lower bounds for the coefficients of variation obtained from both normalizing schemes are plotted. In each plot, the solid line represents the least coefficients of variation obtained from normalization by the peak ground motions. Likewise, the dashed line represents the least coefficients of variation arising from normalization by the three spectrum intensities. The center plot in Fig. 5.50, for example, contains the lowermost coefficients of variation obtained from Figs. 5.20 and 5.46. It is discernible from Fig. 5.50 that scaling elastic spectra by the three spectrum intensities defined by Eq. 5.5 and summarized in Table 5.9 provides, on the whole, less dispersion in normalized spectral ordinates. As the damping increases, the reduction in dispersion decreases, as previously mentioned in the discussion regarding the average coefficients of variation in Table 5.10.

The second scaling factor based on the response of single-degree-of-freedom systems is the Fourier amplitude. In a manner analogous to that for the spectrum intensities, a three-parameter system of mean Fourier

amplitudes is evaluated as an alternative normalizing procedure. The frequency limits for computing the mean Fourier amplitudes which minimize the average coefficients of variation in the three spectral regions are shown in Table 5.11. It is clear that, as for the spectrum intensities, the frequency limits for the mean Fourier amplitudes are insensitive to damping. Accordingly, the mean Fourier amplitudes which minimize the average coefficients of variation for elastic spectra with 5 percent damping are selected:

$$\left.\begin{aligned} \overline{FS}_d &= \overline{FS}(0.035 - 0.31 \text{ cps}) \\ \overline{FS}_v &= \overline{FS}(0.28 - 1.3 \text{ cps}) \\ \overline{FS}_a &= \overline{FS}(1.4 - 19 \text{ cps}) \end{aligned}\right\} \qquad (5.6)$$

These mean Fourier amplitudes are listed in Table 5.12 for the earthquake ground motions considered in this study. In Table 5.13 the average coefficients of variation for elastic spectra normalized by the mean Fourier amplitudes and the peak ground motions are compared. For spectra with 2 percent damping, the mean Fourier amplitudes produce moderate reductions in the average dispersion. However, as the damping increases, the mean Fourier amplitudes generate larger scatter than that arising from normalization by the peak ground motions. This trend is particularly evident in the acceleration region, where the average coefficients of variation for spectra normalized by the mean Fourier amplitude increase with damping.

A graphical comparison of the coefficients of variation versus frequency for elastic spectra normalized by the peak ground motions and the mean Fourier amplitudes is shown in Fig. 5.51. It is clear that as the damping increases, the reductions in dispersion obtained from normalization by the mean Fourier amplitudes decrease. This decrease

is most noticeable for frequencies greater than about 2 cps. However, for small damping, the mean Fourier amplitudes provide, on the average, somewhat less dispersion.

Similar results were previously obtained by Cornell, Banon, and Shakal (11). In their study of response prediction alternatives, mean Fourier amplitudes were used to scale elastic spectra for 0, 2, and 10 percent damping. Both horizontal components of 70 sets of records from Western U.S. strong-motion earthquakes were used. Hence, the total sample size was 140. No more than 7 records from a single earthquake were included to avoid biasing the results. All motions were recorded in the basements of buildings or in free-field locations.

The results of Cornell's study for 2 and 10 percent damping are shown in Fig. 5.52. In this figure, $\overline{FS}(0.3)$, $\overline{FS}(1.0)$ and $\overline{FS}(4.0)$ denote average Fourier amplitudes within three frequency regions corresponding to 0.2-0.4 cps, 0.4-2 cps, and 2-6 cps, respectively. It is interesting to note that the coefficients of variation in Fig. 5.52 do not fluctuate with frequency as irregularly as those determined in this study, presented in Figs. 5.20 and 5.51. It should also be noted that the frequency regions of minimum coefficient of variation identifiable in Fig. 5.52 do not precisely correspond to those determined from this study. For example, Fig. 5.52 indicates that the frequency separating the displacement and velocity regions is between 0.4 and 0.5 cps, compared with 0.2 cps from Fig. 5.20. Of course, one possible explanation for these observations is that the number of ground motions used in this study is small. In addition, it is likely that the results presented by Cornell *et al.* (11) have been smoothed.

Despite the foregoing differences, the trends of the results shown in Fig. 5.52 parallel those obtained from this study. Specifically, the largest reductions in the coefficients of variation are observed in the low frequency displacement region. As the frequency and damping increase, the reductions in dispersion which result from normalization by the mean Fourier amplitudes decrease. These trends correspond to those discernible in Fig. 5.51 and those noted in the average coefficients of variation summarized in Table 5.13. However, a comparison of the data in Tables 5.10 and 5.13 and an examination of the coefficients of variation versus frequency plotted in Figs. 5.50 and 5.51 show that the 2 percent damped spectrum intensities outperform the mean Fourier amplitudes as normalizing parameters for elastic spectra.

5.5.2 Inelastic Yield Spectra Normalized by Spectrum Intensity and Mean Fourier Amplitude

In current practice, inelastic seismic design spectra are derived directly from elastic spectra. Accordingly, the 2 percent damped spectrum intensities and the mean Fourier amplitudes used to normalize elastic spectra are evaluated as alternative scaling factors for the inelastic spectra considered in this study. Typical results of this evaluation are summarized in Figs. 5.53 through 5.56, which show the coefficients of variation for elastoplastic systems with 5 percent damping. In Figs. 5.53 and 5.54 the coefficients of variation obtained from normalizing the elastoplastic yield spectra by the peak ground motions and the spectrum intensities defined by Eq. 5.5 are compared. A similar comparison for spectra normalized by the mean Fourier amplitudes given by Eq. 5.6 is shown in Figs. 5.55 and 5.56. These results indicate that

as the level of inelastic response increases, both scaling methods produce progressively larger coefficients of variation compared with those obtained from normalization by the peak ground motions. This trend is particularly evident for high frequencies, between about 3 and 10 cps. It is clear, however, that on the average, normalizing inelastic spectra by 2 percent damped spectrum intensities provides smaller coefficients of variation than those which result from normalization by the mean Fourier amplitudes. This conclusion, noted previously for elastic systems, holds for all displacement ductilities, for all inelastic spectra considered in this study.

The results obtained from normalizing the elastoplastic and bilinear yield spectra by the 2 percent damped spectrum intensities are summarized in Figs. 5.57 through 5.59. In these figures, the percent reductions in the average coefficients of variation for spectra normalized by the spectrum intensities, compared with those obtained from normalization by the peak ground motions, are plotted versus displacement ductility. The displacement, velocity, and acceleration regions denoted in Figs. 5.57 through 5.59 correspond to those listed in Tables 5.4 and 5.5.

Several of the trends observed in Figs. 5.57 through 5.59 have previously been noted. Specifically, the reductions in the average coefficients of variation in each spectral region decrease with damping and ductility for elastoplastic systems. A similar trend is noted as the level of strain-hardening increases for the bilinear system. However, in the displacement region, reductions in dispersion are evident for ductilities up to about 3 for all damping and strain-hardening. Although the decreases in the average coefficients of variation are

smaller in the velocity region, reductions are apparent for ductilities up to about 4 to 5. In the acceleration region, the improvement afforded by the 2 percent spectrum intensity decays rapidly as the magnitude of the inelastic response increases. These observations indicate that the spectral scaling factors which provide an improved method of normalization for elastic systems need not afford the same improvement for hysteretic systems. This conclusion lends support to those previous investigators (3, 4) who question the validity of predicing inelastic response from elastic response.

5.6 Concluding Remarks

In this chapter, alternative spectral normalizing factors proposed by several previous investigators have been evaluated. The goal was to determine which, if any, of the normalizing parameters reduce the dispersion observed in elastic and inelastic spectra normalized by the peak ground motions. With the exception of the root-square displacement, none of the parameters based upon ground motion data reduce the scatter. The root-square displacement provides moderate reductions in the coefficients of variation for low frequency elastic systems. Those parameters based more directly on the response quantities, the spectrum intensity and the Fourier amplitude, are effective in reducing the dispersion in normalized elastic spectra and in inelastic spectra for low ductility. A three-parameter system of spectrum intensities, computed within appropriately selected frequency regions from the 2 percent damped elastic pseudovelocity spectrum, offers the most promising alternative scaling method. This result is not surprising since the spectrum intensity is

determined directly from the pseudovelocity spectrum itself. Hence, the spectrum intensity bears a closer relationship, than does the mean Fourier amplitude, to the data being normalized.

CHAPTER 6

SUMMARY AND CONCLUSIONS

6.1 Summary

The primary objective of this study was to evaluate the current practice of normalizing earthquake response spectra by the peak ground motions. In this evaluation, alternative normalizing factors were investigated to determine which, if any, of the various parameters provide less dispersion than that which results from normalization by the maximum ground displacement, velocity, and acceleration. The goal was not to develop a new or radically different procedure for establishing design spectra. Rather, the purpose was to formulate a basis, within the general framework of present methods, upon which further research can lead to improved procedures for specifying the earthquake hazard and the corresponding design response spectra.

The normalizing factors considered in this study were categorized into two groups, one based on ground motion data and the other, on response-related quantities. The parameters within the group based on recorded ground motions were the integrals of the squared ground motions, and the root-square, mean-square, and root-mean-square motions. Those in the response-related category included the spectrum intensity and the amplitudes of the Fourier spectrum of the ground acceleration. A three-parameter system of spectrum intensities, computed from the 2 percent damped elastic pseudovelocity spectrum, was developed. The spectrum intensities were determined within low, intermediate, and high ranges of frequency, appropriately selected to provide the least average

dispersion in the corresponding frequency regions of the elastic spectra. A similar set of three mean Fourier amplitudes was derived.

In the statistical analysis, spectra for elastic and inelastic systems, computed from an ensemble of 12 earthquake accelerograms, were considered. The group of ground motions was selected to encompass a wide variety of conditions such as geographical location, earthquake magnitude, epicentral distance, and amplitude and duration of strong shaking. The response spectra, computed for displacement ductilities of 1 (elastic), 1.5, 2, 3, 5, and 10, included those for elastoplastic systems with 2, 5, and 10 percent damping. Bilinear systems with 5 percent damping and 2, 5, and 10 percent strain-hardening were also considered.

In current practice, inelastic design spectra are developed by reducing the elastic spectra by factors which are independent of damping. Thus, it is tacitly assumed that damping has an equal influence on elastic and inelastic response. Previous studies, however, have shown that the simplified rules for constructing inelastic spectra may overestimate the effects of damping for intermediate and high frequency systems. In addition, the simplified rules were developed specifically for cases where the load-deformation characteristics may be modeled as elastic-perfectly plastic. Hence, another objective of this study was to compare the inelastic spectra to evaluate the influence of damping when combined with hysteretic behavior and to determine the sensitivity of response to varying levels of strain-hardening for the bilinear system. The purpose was to provide additional data so that the designer

may explicitly account for these structure-related parameters in deriving inelastic design spectra.

In an early, independent phase of this study, an algorithm for the computation of response spectra for elastoplastic and bilinear hysteretic systems was formulated. The method, an extension of that proposed by previous investigators for elastic systems, takes advantage of the piecewise-linear character of the earthquake accelerogram and the load-deformation law for the single-degree-of-freedom system. Accordingly, the equation of motion may be solved exactly within each successive time step. To assess its performance, this exact method of computation was compared with Newmark's beta method.

6.2 Conclusions

The significant conclusions obtained from this study may be summarized for each of the stated objectives:

1. Alternative Scaling Methods

   a) For elastic spectra, the root-square displacement offers moderate reductions in scatter compared with that which results from normalization by the peak ground displacement. In the low frequency region, between 0.07 and 0.2 cps, the root-square displacement provides, on the average, about a 30 percent decrease in the coefficient of variation for the normalized spectra. Unlike the displacement region, in the velocity and acceleration regions none of the alternative ground motion parameters provide less dispersion than that which results from normalization by the corresponding peak ground motion.

b) For all inelastic spectra, none of the normalizing factors based on ground motion data provide noteworthy reductions in scatter compared with that obtained from normalization by the peak ground motions.

c) The spectrum intensities and mean Fourier amplitudes provide, on the average, less dispersion in normalized elastic spectra than that which results from normalization by the peak ground motions. For elastic spectra with 2 percent damping, the spectrum intensities provide about 40 percent less scatter in the displacement and acceleration regions. In the intermediate frequency or velocity region, normalizing by the corresponding spectrum intensity reduces the dispersion by 20 percent. These reductions in average dispersion decrease with damping, particularly in the displacement and acceleration regions. For 10 percent damped spectra, the reductions are about 20 percent in each spectral region.

The mean Fourier amplitudes decrease the average dispersion in elastic spectra with small damping. For elastic spectra with 2 percent damping, the mean Fourier amplitudes provide 15 to 20 percent less scatter in the normalized spectra. The improvement afforded by the mean Fourier amplitudes diminishes rapidly with damping, especially in the high frequency or acceleration region of the spectra. For 5 and 10 percent damped spectra, normalization by the associated mean Fourier amplitude actually increases the dispersion compared with that obtained from the peak acceleration.

d) The spectrum intensities outperform the mean Fourier amplitudes as normalizing factors for the inelastic spectra. The reductions in average scatter produced by the spectrum intensities decrease with damping, strain-hardening, and level of inelastic response. However, in the displacement region, reductions in average dispersion are apparent for all damping and strain-hardening for ductilities up to about 3. Although the reductions are smaller in the velocity region, the corresponding spectrum intensity decreases the scatter for systems with ductilities less than about 4. The improvement afforded by the spectrum intensity in the acceleration region decays rapidly with damping and ductility. For damping less than 5 percent of critical and for ductilities less than about 1.7, the spectrum intensity reduces the scatter in the normalized spectral ordinates.

2. Effects of Damping and Strain-Hardening on Mean Response

a) Damping

For flexible systems, i.e. those with frequencies less than about 0.07 cps, mean response is independent of damping for all ductilities. For high frequency systems, damping is somewhat effective in decreasing response amplitudes for inelastic systems; this influence is most appreciable for large displacement ductilities. For a broad intermediate range of frequencies, between about 0.1 and 10 cps, the effectiveness of damping, with only minor exception, decreases as the level of inelastic

response increases. Spectral reduction factors for elasto-plastic systems with 2, 5, and 10 percent damping were derived to permit explicit consideration of damping when combined with hysteretic behavior.

b) Strain-Hardening

An examination of average bilinear yield spectra indicates that strain-hardening decreases the yield level or the yield resistance required for a system to attain a given ductility. However, for low to moderate ductilities, i.e. for those less than about 2 or 3, mean response is relatively insensitive, for all frequencies, to increases in strain-hardening of up to 10 percent. In addition, for flexible systems, mean response is independent of the level of strain-hardening, for all ductilities. For intermediate and high frequency systems, the effect of strain-hardening becomes more pronounced, particularly as the displacement ductility increases.

Since strain-hardening decreases the required yield resistance for a given ductility, the use of elastoplastic design spectra is generally conservative. For the same frequency, any level of strain-hardening tends to decrease the ductility demand. Hence, if elastoplastic design spectra are used for systems with unrecognized strain-hardening, the actual ductility will be less than expected. Nevertheless, spectral reduction factors which explicitly reflect the effects of varying levels of strain-hardening have been derived in this study.

3. Computation of Inelastic Response Spectra

The analytical method developed in this study permits the computation of dynamic response in an efficient, arithmetical manner. Compared with Newmark's beta method, the exact technique results in a two- to threefold savings in computation time. Although developed in this study for the computation of elasto-plastic and bilinear response, the procedure may readily be extended for other load-deformation models, provided the restoring force is piecewise-linear.

6.3 Critical Overview and Recommendations for Further Study

One obvious shortcoming of this study is that a relatively small sample of earthquake ground motions was considered. Furthermore, seven of the twelve accelerograms were from California events. Because of the limited number and choice of records, the results of this study are necessarily biased. However, the accelerograms employed do cover a wide variety of conditions such as earthquake magnitude, focal depth, epicentral distance, recording site geology, and amplitude and duration of the recorded motions. Therefore, it is believed that this study lays the foundation upon which further research may provide additional insight into the characterization of the earthquake hazard, wherefrom seismic design spectra may be derived.

Several specific areas of further research are recommended. First, comprehensive studies involving larger samples of motions, perhaps appropriately categorized, are required before alternative spectral scaling parameters may be proposed for general design use. Twelve earthquake

records are too few to enable the formulation of an improved design method. However, the results of this study indicate that several spectral normalizing factors may be eliminated as viable response prediction alternatives. These parameters include, with the possible exception of the root-square displacement, all of those alternative normalizing factors computed from ground motion data. Hence, further investigations may concentrate on those normalizing factors determined from response-related quantities, i.e. the spectrum intensities and the mean Fourier amplitudes.

The successful implementation of a spectrum intensity or Fourier amplitude-based design approach requires additional research. Studies must be made to provide the designer with a method for predicting the spectrum intensities or mean Fourier amplitudes. Such investigations might involve the regression of the alternative spectral scaling factors on earthquake magnitude and source-to-site distance. In this study of attenuation characteristics, an evaluation of the uncertainties associated with the prediction scheme should be made. Before the peak ground motions are replaced as descriptors of the earthquake hazard, it must be verified that the alternative parameters -- the spectrum intensities, mean Fourier amplitudes, or any others -- can be predicted as reliably.

TABLES

Table 2.1 Equations for Elastic Spectrum Amplification Factors for Horizontal Motion. After Newmark and Hall (59)

Quantity	Cumulative Probability, Percent	
Acceleration		$4.38 - 1.04\ln\beta$
Velocity	84.1 (One Sigma)	$3.38 - 0.67\ln\beta$
Displacement		$2.73 - 0.45\ln\beta$
Acceleration		$3.21 - 0.68\ln\beta$
Velocity	50 (Median)	$2.31 - 0.41\ln\beta$
Displacement		$1.82 - 0.27\ln\beta$

Table 2.2 Elastic Spectrum Amplification Factors for Horizontal Motion. After Newmark and Hall (59)

Damping, Percent of Critical	Cumulative Probability, Percent					
	84.1 (One Sigma)			50 (Median)		
	Accel.	Vel.	Displ.	Accel.	Vel.	Displ.
0.5	5.10	3.84	3.04	3.68	2.59	2.01
1	4.38	3.38	2.73	3.21	2.31	1.82
2	3.66	2.92	2.42	2.74	2.03	1.63
3	3.24	2.64	2.24	2.46	1.86	1.52
5	2.71	2.30	2.01	2.12	1.65	1.39
7	2.36	2.08	1.85	1.89	1.51	1.29
10	1.99	1.84	1.69	1.64	1.37	1.20
20	1.26	1.37	1.38	1.17	1.08	1.01

Table 3.1 Recommended Damping Values.
After Newmark (58)

Stress Level	Type and Condition of Structure	Percentage Critical Damping
Working stress, no more than about 1/2 yield point	a. Vital piping	1 to 2
	b. Welded steel, prestressed concrete, well reinforced concrete (only slight cracking)	2 to 3
	c. Reinforced concrete with considerable cracking	3 to 5
	d. Bolted and/or riveted steel, wood structures with nailed or bolted joints	5 to 7
At or just below yield point	a. Vital piping	2 to 3
	b. Welded steel, prestressed concrete (without complete loss in prestress)	5 to 7
	c. Prestressed concrete with no prestress left	7 to 10
	d. Reinforced concrete	7 to 10
	e. Bolted and/or riveted steel, wood structures with bolted joints	10 to 15
	f. Wood structures with nailed joints	15 to 20

Table 3.2 Earthquake Data

Earthquake	Date and Time	Epicenter Coordinates	Magnitude M_L*	Maximum MMI	Focal Depth (km)	Record and Component Used in this Study
San Fernando, Calif.	Feb. 9, 1971 0600 PST (76)	34.40°N 118.40°W (43)	6.4 (76)	XI (43)	8 (43)	Pacoima Dam, S16E
Parkfield, Calif.	June 27, 1966 2026 PST (76)	35.95°N 120.50°W (43)	5.6 (76)	VII (43)	8.6 (9)	Cholame-Shandon No. 2, N65E
Bear Valley, Calif.	Sept. 4, 1972 1104 PDT (8)	36.64°N 121.29°W (8)	4.7 (8)	VI (8)	2 (8)	Melendy Ranch, N29W
Coyote Lake, Calif.	Aug. 6, 1979 1005 PDT (38)	37.10°N 121.50°W (72)	5.9 (38)	VII (38)	9.6 (38)	Gilroy Array No. 6, 230 Deg.
Imperial Valley, Calif.	Oct. 15, 1979 1616 PDT (39)	32.64°N 115.33°W (39)	6.6 (39)	IX (65)	12 (65)	Bonds Corner, 230 Deg.
Imperial Valley, Calif.	May 18, 1940 2037 PST (76)	32.73°N 115.50°W (43)	6.7 (76)	X (43)	16 (9)	El Centro, S00E
Kern County, Calif.	July 21, 1952 0453 PST (76)	35.00°N 119.01°W (43)	7.7 (76)	XI (43)	16 (9)	Taft-Lincoln School Tunnel, S69E
Andreanof Island, Alaska	May 1, 1971 2008 AST (70)	51.4°N 177.2°W (70)	7.0 (70)	VI (70)	43 (70)	Adak, Alaska U.S. Naval Station, West
Kilauea, Hawaii	Apr. 26, 1973 2026 GMT (37)	19.93°N 155.10°W (37)	6.3 (37)	VIII (37)	50 (37)	Hawaii National Park, Namakani Paio Camp., S30W
Managua, Nicaragua	Dec. 23, 1972 0629 GMT (8)	12.4°N 86.1°W (8)	6.2 (8)	IX (8)	5 (14)	ESSO Refinery, South
Bucarest, Rumania	Mar. 4, 1977 1922 GMT (7)	45.87°N 26.75°E (71)	7.1** (71)	IX (7)	110 (71)	Building Research Institute, S-N
Off Central Chile Coast	July 8, 1971 2303 local (70)	32.5°S 71.2°W (70)	7.5 (70)	X (70)	58 (70)	Univ. of Chile, Santiago Engineering Bldg, N10W

Notes: * Richter or Local Magnitude, M_L

** Body-wave Magnitude, m_b

Numbers in parentheses identify entries in the List of References.

Table 3.3 Recording Site Data

Record, Component	U.S.G.S. Station No. and Coordinates	Epicentral Dist. (km)	Recording Site Geology	Instrument Location, Structure
Pacoima Dam, S16E	#279 34.334°N 118.396°W (87)	9.1 (9)	highly jointed diorite gneiss (82)	abutment of concrete dam, instr. shltr. (87)
Cholame-Shandon No. 2, N65E	#1013 35.731°N 120.286°W (87)	31.9 (9)	alluvium, 45 m; sandstone (87)	ground level, instr. shltr. (87)
Melendy Ranch, N29W	#1211 36.59°N 121.19°W (87)	8 (43)	30 ft alluvium; weathered siltstone to 200 ft (18)	ground level, 1-story bldg. (87)
Gilroy Array No. 6, 230 Deg.	#1413 37.026°N 121.484°W (87)	10 (66)	rock (87)	ground level, 1-story bldg. (87)
Bonds Corner, 230 Deg.	#5054 32.693°N 115.338°W (87)	6 (38)	alluvium (87)	ground level, 1-story bldg. (87)
El Centro, S00E	#117 32.794°N 115.549°W (87)	9.3 (9)	alluvium, more than 300 m (87)	ground level, 2-story bldg. (87)
Taft, S69E	#1095 35.15°N 119.46°W (87)	43 (9)	alluvium (87)	tunnel, 1-story bldg. (87)
Adak, Alaska, West	#2701 51.88°N 176.58°W (87)	70 (70)	basalt (87)	ground level, instr. shltr. (87)
Kilauea, Hawaii, S30W	#2801 19.43°N 155.30°W (87)	59 (43)	(not available)	ground level, 1-story bldg. (87)
Managua, South	#3501 12.14°N 86.32°W (87)	6 (14)	alluvium, about 1000 m (84)	ground level, 1-story bldg. (87)
Bucarest, S-N	* 44.44°N 26.15°E (43)	166 (71)	10 m loess; sandy deposits to 44 m (7)	basement, 1-story bldg. (71)
Santiago, N10W	#4400 33.47°S 70.67°W (87)	120 (70)	alluvium, about 250 m (67)	basement, 3-story bldg. (87)

Notes: * Not a U.S. Geological Survey Station.

Numbers in parentheses identify entries in the List of References.

Table 3.4 Ground Motion Data

Record, Component	Initial Ground Motions			Ground Motion Maxima					
	Accel., in./sec^2	Vel., in./sec	Displ., in.	Accel., g	Time, sec	Vel., in./sec	Time, sec	Displ., in.	Time, sec
Pacoima Dam, S16E	3.05	-0.484	-0.167	1.17	9.74	44.6	5.04	-16.5	9.78
Cholame-Shandon No. 2, N65E	-5.01	0.830	0.620	0.489	5.74	30.7	6.46	-10.3	6.18
Melendy Ranch, N29W	5.19	-1.17	-0.0935	-0.516	3.76	5.41	3.72	1.28	3.78
Gilroy Array No. 6, 230 Deg.	2.26	0.209	-0.187	-0.417	4.88	17.3	4.73	-3.85	4.51
Bonds Corner, 230 Deg.	0.287	-1.74	0.514	0.786	8.79	17.4	9.60	-5.72	9.37
El Centro, S00E	0.548	1.84	-0.850	-0.348	4.12	-13.2	4.18	-4.87	10.58
Taft, S69E	2.45	0.0655	0.0245	-0.179	5.70	6.98	5.56	-4.09	51.14
Adak, Alaska, West	3.18	0.595	0.576	-0.186	8.14	3.15	8.32	2.88	12.92
Kilauea, Hawaii, S30W	-0.441	0.114	-0.0370	0.159	9.24	-2.65	8.56	-0.466	8.72
Managua, South	-1.93	0.179	0.201	0.324	8.08	-11.9	7.96	2.60	7.50
Bucarest, S-N	-2.22	0.586	-0.439	0.206	5.26	29.6	5.70	-7.85	5.24
Santiago, N10W	-1.71	-1.31	0.658	-0.159	19.06	9.13	19.70	4.79	23.76

Note: Times of maxima are for records with a 2-second prefixed pulse.

Table 3.5 Comparison of Ground Displacement Maxima

Record, Component	This Study		Caltech	
	Displ., in.	Time, sec	Displ., in.	Time, sec
Pacoima Dam, S16E	-16.5	9.78	-14.8	9.78
Cholame-Shandon No. 2, N65E	-10.3	6.18	-10.4	6.18
Melendy Ranch, N29W	1.28	3.78	1.06	3.78
Gilroy Array No. 6, 230 Deg.	-3.85	4.51	-3.68	4.51
Bonds Corner, 230 Deg.	-5.72	9.37	-5.76	9.37
El Centro, S00E	-4.87	10.58	-4.29	10.58
Taft, S69E	-4.09	51.14	3.60	46.12
Adak, Alaska, West	2.88	12.92	-2.09	7.16
Kilauea, Hawaii, S30W	-0.466	8.72	-0.449	8.72
Managua, South	2.60	7.50	-2.49	8.44
Bucarest, S-N	-7.85	5.24	7.90	6.20
Santiago, N10W	4.79	23.76	-4.05	17.30

Note: Times of maxima are for records with a 2-second prefixed pulse.

Table 3.6 Comparison of Computation Times on the CDC Cyber 175 for the Exact Method and Newmark's Method: Elasto-plastic Systems with 5% Damping Subjected to the Pacoima Dam Record of Feb. 9, 1971, Component S16E

	Computation Times, in seconds		
		Newmark's Method	
Case	Exact, Δt_i = T/10	Δt_i = T/10	Δt_i = T/20
13 freqs., 0.035 - 0.293 cps	1.0	1.6	1.6
13 freqs., 0.35 - 2.93 cps	1.1	1.6	1.6
14 freqs., 3.5 - 35 cps	2.0	5.8	9.2
Total	4.1	9.0	12.4

Table 3.7 Comparison of Response Maxima for the Exact Method and Newmark's Method: Elastoplastic Systems with 5% Damping Subjected to the Pacoima Dam Record of Feb. 9, 1971, Component S16E

Frequency, in cps	Initial Yield Level u_y, in inches	Maximum Relative Displacement, in inches		
		Exact,	Newmark's Method	
		Δt_i = T/10	Δt_i = T/10	Δt_i = T/20
0.03500	3.134	15.66	15.65	15.65
0.05954	2.838	14.17	14.16	14.16
0.1013	2.948	-14.74	-14.74	-14.74
0.1723	4.246	-21.31	-21.31	-21.31
0.2932	5.593	-27.83	-27.81	-27.81
0.4988	3.705	-18.54	-18.53	-18.53
0.8486	2.518	-12.64	-12.63	-12.63
1.444	1.412	-7.126	-7.112	-7.112
2.456	0.6952	3.474	3.444	3.444
2.932	0.4824	2.400	2.468	2.414
3.500	0.5494	-2.744	-2.671	-2.736
4.178	0.4026	-2.015	-1.941	-2.001
4.988	0.3178	-1.594	-1.573	-1.579
5.954	0.2360	-1.181	-1.197	-1.194
8.486	0.1256	-0.6303	-0.6757	-0.6433
10.13	0.08622	-0.4313	-0.4495	-0.4386
14.44	0.03713	-0.1847	-0.1962	-0.1871
20.57	0.02027	-0.1022	-0.1058	-0.1034
35.00	0.007109	-0.03555	-0.03488	-0.03541

Note: For frequencies above the dashed lines, the time step used in the computations corresponds to the digitized interval of the input accelerogram, 0.02 sec.

Table 3.8 Ground Motion Durations for Computing Inelastic Response Spectra

Record, Component	Frequencies, cps	Latest time of max. displ.,[1] sec	Duration,[2] sec
Pacoima Dam, S16E	all	13.08	18.20
Cholame-Shandon No. 2, N65E	$f \leq 2.06$	21.94	29.92
	$f > 2.06$	6.87	16.74
Melendy Ranch, N29W	all	9.82	14.98
Gilroy Array No. 6, 230 Deg.	all	6.80	10.46
Bonds Corner, 230 Deg.	$f \leq 2.06$	21.00	29.75
	$f > 2.06$	9.41	18.48
El Centro, S00E	$f \leq 0.246$	42.54	55.42[3]
	$0.246 < f \leq 2.06$	16.66	29.60
	$f > 2.06$	7.00	15.87
Taft, S69E	$f \leq 0.246$	57.05	55.39[3]
	$f > 0.246$	13.20	39.20
Adak, Alaska, West	all	27.01	25.83[3]
Kilauea, Hawaii, S30W	all	22.86	34.55[3]
Managua, South	all	14.74	24.95
Bucarest, S-N	all	11.70	18.02[3]
Santiago, N10W	$f \leq 2.06$	49.08	51.94[3]
	$f > 2.06$	19.86	37.79

Notes:
1. For frequencies within the indicated range, the latest time of maximum relative displacement for elastic systems with 2% damping.
2. All durations are for records with a 2-second prefixed pulse.
3. Corresponds to the duration of entire record.

Table 4.1 Peak Ground Motions

Record, Component	Peak Ground Motions		
	Accel. (g)	Vel. (in./sec)	Displ. (in.)
Pacoima Dam, S16E	1.17	44.6	16.5
Cholame-Shandon No. 2, N65E	0.489	30.7	10.3
Melendy Ranch, N29W	0.516	5.41	1.28
Gilroy Array No. 6, 230 Deg.	0.417	17.3	3.85
Bonds Corner, 230 Deg.	0.786	17.4	5.72
El Centro, S00E	0.348	13.2	4.87
Taft, S69E	0.179	6.98	4.09
Adak, Alaska, West	0.186	3.15	2.88
Kilauea, Hawaii, S30W	0.159	2.65	0.466
Managua, South	0.324	11.9	2.60
Bucarest, S-N	0.206	29.6	7.85
Santiago, N10W	0.159	9.13	4.79

Table 4.2 Integrals of Squared Ground Motion

Record, Component	Integrals of Squared Ground Motion: Accel., ($in.^2/sec^3/1000$)	Vel., ($in.^2/sec/100$)	Displ., ($in.^2$-sec/100)
Pacoima Dam, S16E	76.9	14.7	8.80
Cholame-Shandon No. 2, N65E	17.3	5.31	1.25
Melendy Ranch, N29W	5.55	0.140	0.0163
Gilroy Array No. 6, 230 Deg.	7.46	1.16	0.0614
Bonds Corner, 230 Deg.	57.4	5.11	0.585
El Centro, S00E	16.8	3.35	2.19
Taft, S69E	5.54	1.37	1.35
Adak, Alaska, West	2.81	0.181	0.453
Kilauea, Hawaii, S30W	2.58	0.0811	0.00290
Managua, South	18.7	1.36	0.209
Bucarest, S-N	7.87	6.29	0.838
Santiago, N10W	3.55	0.906	2.25

Table 4.3 Root-Square Ground Motions

Record, Component	Root-Square Ground Motions		
	Accel., $(in./sec^{3/2})$	Vel., $(in./sec^{1/2})$	Displ., $(in.-sec^{1/2})$
Pacoima Dam, S16E	277	38.4	29.7
Cholame-Shandon No. 2, N65E	132	23.0	11.2
Melendy Ranch, N29W	74.5	3.75	1.28
Gilroy Array No. 6, 230 Deg.	86.4	10.8	2.48
Bonds Corner, 230 Deg.	240	22.6	7.65
El Centro, S00E	130	18.3	14.8
Taft, S69E	74.4	11.7	11.6
Adak, Alaska, West	53.0	4.25	6.73
Kilauea, Hawaii, S30W	50.8	2.85	0.539
Managua, South	137	11.7	4.57
Bucarest, S-N	88.7	25.1	9.16
Santiago, N10W	59.6	9.52	15.0

Table 4.4 Mean-Square Ground Motions

Record, Component	t_5 (sec)	t_{95} (sec)	Mean-Square Ground Motions Accel., ($in.^2/sec^4/1000$)	Vel., ($in.^2/sec^2/10$)	Displ., ($in.^2/10$)
Pacoima Dam, S16E	4.71	11.75	9.84	19.2	7.54
Cholame-Shandon No. 2, N65E	5.28	12.24	2.24	6.76	1.46
Melendy Ranch, N29W	3.49	5.98	2.01	0.320	0.0272
Gilroy Array No. 6, 230 Deg.	4.02	7.23	2.09	3.42	0.155
Bonds Corner, 230 Deg.	4.98	14.77	5.28	4.06	0.432
El Centro, S00E	3.67	28.15	0.618	1.08	0.586
Taft, S69E	5.65	34.68	0.172	0.215	0.108
Adak, Alaska, West	5.37	16.10	0.236	0.124	0.325
Kilauea, Hawaii, S30W	8.25	19.13	0.213	0.0604	0.00174
Managua, South	4.39	12.69	2.03	1.46	0.158
Bucarest, S-N	5.02	12.47	0.951	7.29	0.991
Santiago, N10W	11.08	39.52	0.112	0.262	0.646

Table 4.5 Root-Mean-Square Ground Motions

Record, Component	Root-Mean-Square Ground Motions		
	Accel. (g)	Vel. (in./sec)	Displ. (in.)
Pacoima Dam, S16E	0.257	13.8	8.69
Cholame-Shandon No. 2, N65E	0.123	8.22	3.82
Melendy Ranch, N29W	0.116	1.79	0.521
Gilroy Array No. 6, 230 Deg.	0.118	5.85	1.24
Bonds Corner, 230 Deg.	0.188	6.37	2.08
El Centro, S00E	0.0644	3.28	2.42
Taft, S69E	0.0339	1.47	1.04
Adak, Alaska, West	0.0398	1.12	1.80
Kilauea, Hawaii, S30W	0.0378	0.777	0.132
Managua, South	0.117	3.82	1.26
Bucarest, S-N	0.0799	8.54	3.15
Santiago, N10W	0.0274	1.62	2.54

Table 4.6 Spectrum Intensities

Record, Component	Spectrum Intensity, 0.4-10 cps, in. β=0%	β=2%	β=5%	β=10%	β=20%
Pacoima Dam, S16E	203	164	137	116	91.1
Cholame-Shandon No. 2, N65E	140	110	93.9	79.3	61.7
Melendy Ranch, N29W	21.1	16.3	13.9	11.9	9.63
Gilroy Array No. 6, 230 Deg.	72.4	60.2	53.9	47.4	39.4
Bonds Corner, 230 Deg.	136	94.4	71.7	55.9	42.0
El Centro, S00E	111	68.2	53.0	42.4	31.8
Taft, S69E	51.3	33.0	26.0	19.5	14.9
Adak, Alaska, West	17.8	11.2	9.04	7.21	5.45
Kilauea, Hawaii, S30W	17.8	10.9	8.63	6.71	5.07
Managua, South	70.6	52.1	42.9	34.0	24.7
Bucarest, S-N	139	113	96.9	81.2	62.5
Santiago, N10W	40.7	24.3	18.3	14.7	11.0

Table 5.1 Statistics for Mean Elastic Spectra

Damping, percent	Spectral Region	This Study		Ref. 67		Ref. 51	
		Mean	COV	Mean	COV	Mean	COV
2	Displ.	1.56	0.38	1.69	0.49	1.68	0.49
	Vel.	1.83	0.54	2.03	0.42	2.06	0.45
	Accel.	2.73	0.38	3.08	0.24	2.76	0.32
5	Displ.	1.37	0.33	1.47	0.43	1.40	0.46
	Vel.	1.46	0.49	1.55	0.39	1.66	0.40
	Accel.	2.12	0.35	2.28	0.22	2.11	0.23
10	Displ.	1.19	0.35	1.23	0.39	1.15	0.41
	Vel.	1.15	0.43	1.20	0.36	1.34	0.35
	Accel.	1.65	0.29	1.78	0.18	1.65	0.22

Table 5.2 Spectral Reduction Factors for Elastoplastic Systems

	Displacement Region, ϕ_D					
	β = 2%		β = 5%		β = 10%	
Ductility	This Study	Ref. 67	This Study	Ref. 67	This Study	Ref. 67
1	1.00	1.00	1.00	1.00	1.00	1.00
1.5	0.60	0.59	0.61	0.60	0.62	0.63
2	0.42	0.43	0.42	0.45	0.44	0.47
3	0.27	0.28	0.28	0.30	0.30	0.31
5	0.16	0.16	0.17	0.17	0.17	0.18
10	0.073	0.076	0.076	0.080	0.078	0.084
	Velocity Region, ϕ_V					
	β = 2%		β = 5%		β = 10%	
Ductility	This Study	Ref. 67	This Study	Ref. 67	This Study	Ref. 67
1	1.00	1.00	1.00	1.00	1.00	1.00
1.5	0.60	0.56	0.62	0.62	0.67	0.65
2	0.42	0.40	0.47	0.46	0.51	0.51
3	0.29	0.28	0.33	0.33	0.36	0.37
5	0.19	0.19	0.22	0.23	0.24	0.26
10	0.12	0.12	0.14	0.14	0.15	0.17
	Acceleration Region, ϕ_A					
	β = 2%		β = 5%		β = 10%	
Ductility	This Study	Ref. 67	This Study	Ref. 67	This Study	Ref. 67
1	1.00	1.00	1.00	1.00	1.00	1.00
1.5	0.62	0.64	0.66	0.69	0.71	0.72
2	0.49	0.51	0.54	0.58	0.59	0.61
3	0.37	0.39	0.42	0.46	0.47	0.49
5	0.28	0.29	0.33	0.34	0.37	0.38
10	0.22	0.21	0.26	0.26	0.30	0.28

Table 5.3 Spectral Reduction Factors for Bilinear Systems with 5% Damping

	Displacement Region, ϕ_D			
Ductility	$\alpha = 0$	$\alpha = 0.02$	$\alpha = 0.05$	$\alpha = 0.10$
1	1.00	1.00	1.00	1.00
1.5	0.61	0.61	0.61	0.61
2	0.42	0.42	0.42	0.42
3	0.28	0.28	0.27	0.27
5	0.17	0.16	0.16	0.15
10	0.076	0.071	0.070	0.072

	Velocity Region, ϕ_V			
Ductility	$\alpha = 0$	$\alpha = 0.02$	$\alpha = 0.05$	$\alpha = 0.10$
1	1.00	1.00	1.00	1.00
1.5	0.62	0.62	0.61	0.61
2	0.47	0.46	0.46	0.44
3	0.33	0.31	0.30	0.29
5	0.22	0.21	0.20	0.19
10	0.14	0.12	0.11	0.11

	Acceleration Region, ϕ_A			
Ductility	$\alpha = 0$	$\alpha = 0.02$	$\alpha = 0.05$	$\alpha = 0.10$
1	1.00	1.00	1.00	1.00
1.5	0.66	0.66	0.65	0.64
2	0.54	0.53	0.52	0.50
3	0.42	0.41	0.39	0.37
5	0.33	0.31	0.29	0.28
10	0.26	0.23	0.22	0.20

Table 5.4 Frequency Regions in which the Coefficient of Variation is a Minimum: Elastoplastic Spectra Normalized by Peak Ground Motions

Damping, percent	Ductility	Displacement	Velocity	Acceleration
2	1	0.071-0.20	0.20-2.0	2.0-8.5
	1.5	0.071-0.23	0.23-2.0	2.0-8.5
	2	0.071-0.24	0.24-2.5	2.5-8.5
	3	0.071-0.29	0.29-2.6	2.6-8.5
	5	0.071-0.34	0.34-3.4	3.4-8.5
	10	0.071-0.41	0.41-4.5	4.5-8.5
5	1	0.071-0.20	0.20-2.0	2.0-8.5
	1.5	0.071-0.22	0.22-2.0	2.0-8.5
	2	0.071-0.24	0.24-2.5	2.5-8.5
	3	0.071-0.29	0.29-2.6	2.6-8.5
	5	0.071-0.34	0.34-3.6	3.6-8.5
	10	0.071-0.43	0.43-4.6	4.6-8.5
10	1	0.071-0.20	0.20-2.0	2.0-8.5
	1.5	0.071-0.21	0.21-2.3	2.3-8.5
	2	0.071-0.24	0.24-2.6	2.6-8.5
	3	0.071-0.29	0.29-2.6	2.6-8.5
	5	0.071-0.34	0.34-3.9	3.9-8.5
	10	0.071-0.43	0.43-4.7	4.7-8.5

Table 5.5 Frequency Regions in which the Coefficient of Variation is a Minimum: Bilinear Spectra with 5% Damping Normalized by Peak Ground Motions

Strain-Hardening, percent	Ductility	Displacement	Velocity	Acceleration
0	1	0.071-0.20	0.20-2.0	2.0-8.5
	1.5	0.071-0.22	0.22-2.0	2.0-8.5
	2	0.071-0.24	0.24-2.5	2.5-8.5
	3	0.071-0.29	0.29-2.6	2.6-8.5
	5	0.071-0.34	0.34-3.6	3.6-8.5
	10	0.071-0.43	0.43-4.6	4.6-8.5
2	1	0.071-0.20	0.20-2.0	2.0-8.5
	1.5	0.071-0.22	0.22-2.0	2.0-8.5
	2	0.071-0.24	0.24-2.6	2.6-8.5
	3	0.071-0.30	0.30-2.6	2.6-8.5
	5	0.071-0.34	0.34-3.8	3.8-8.5
	10	0.071-0.43	0.43-5.5	5.5-8.5
5	1	0.071-0.20	0.20-2.0	2.0-8.5
	1.5	0.071-0.22	0.22-2.1	2.1-8.5
	2	0.071-0.24	0.24-2.7	2.7-8.5
	3	0.071-0.30	0.30-3.1	3.1-8.5
	5	0.071-0.33	0.33-3.7	3.7-8.5
	10	0.071-0.38	0.38-5.4	5.4-8.5
10	1	0.071-0.20	0.20-2.0	2.0-8.5
	1.5	0.071-0.22	0.22-2.1	2.1-8.5
	2	0.071-0.24	0.24-2.7	2.7-8.5
	3	0.071-0.24	0.24-3.1	3.1-8.5
	5	0.071-0.29	0.29-3.6	3.6-8.5
	10	0.071-0.35	0.35-5.0	5.0-8.5

Table 5.6 Average Coefficients of Variation for Elastoplastic Spectra Normalized by Peak Ground Motions

	Average COV, Displacement Region		
Ductility	β = 2%	β = 5%	β = 10%
1	0.48	0.41	0.34
1.5	0.41	0.37	0.32
2	0.37	0.35	0.32
3	0.36	0.34	0.31
5	0.35	0.34	0.34
10	0.33	0.33	0.29

	Average COV, Velocity Region		
Ductility	β = 2%	β = 5%	β = 10%
1	0.45	0.40	0.36
1.5	0.43	0.39	0.36
2	0.39	0.37	0.35
3	0.36	0.35	0.33
5	0.34	0.33	0.31
10	0.30	0.28	0.26

	Average COV, Acceleration Region		
Ductility	β = 2%	β = 5%	β = 10%
1	0.41	0.37	0.31
1.5	0.35	0.31	0.24
2	0.30	0.25	0.20
3	0.25	0.22	0.20
5	0.25	0.24	0.22
10	0.26	0.26	0.28

Table 5.7 Average Coefficients of Variation for Bilinear Spectra with 5% Damping Normalized by Peak Ground Motions

	Average COV, Displacement Region			
Ductility	$\alpha = 0$	$\alpha = 0.02$	$\alpha = 0.05$	$\alpha = 0.10$
1	0.41	0.41	0.41	0.41
1.5	0.37	0.37	0.37	0.37
2	0.35	0.35	0.34	0.33
3	0.34	0.33	0.32	0.30
5	0.34	0.33	0.29	0.24
10	0.33	0.27	0.21	0.20

	Average COV, Velocity Region			
Ductility	$\alpha = 0$	$\alpha = 0.02$	$\alpha = 0.05$	$\alpha = 0.10$
1	0.40	0.40	0.40	0.40
1.5	0.39	0.39	0.39	0.39
2	0.37	0.36	0.35	0.36
3	0.35	0.34	0.33	0.33
5	0.33	0.32	0.31	0.32
10	0.28	0.28	0.29	0.31

	Average COV, Acceleration Region			
Ductility	$\alpha = 0$	$\alpha = 0.02$	$\alpha = 0.05$	$\alpha = 0.10$
1	0.37	0.37	0.37	0.37
1.5	0.31	0.30	0.29	0.29
2	0.25	0.25	0.24	0.24
3	0.22	0.21	0.19	0.18
5	0.24	0.22	0.19	0.18
10	0.26	0.25	0.25	0.25

Table 5.8 Minimization of Average Coefficient of Variation for Elastic Spectra Normalized by 2% Spectrum Intensity

	Displacement Region, 0.071-0.20 cps	
Damping, percent	Freq. Limits for 2% SI, cps	Average COV
2	0.080-0.20	0.27(0.28)
5	0.080-0.24	0.25
10	0.085-0.28	0.24(0.25)

	Velocity Region, 0.20-2.0 cps	
Damping, percent	Freq. Limits for 2% SI, cps	Average COV
2	0.58-2.9	0.36(0.36)
5	0.50-3.5	0.33
10	0.46-3.5	0.30(0.30)

	Acceleration Region, 2.0-8.5 cps	
Damping, percent	Freq. Limits for 2% SI, cps	Average COV
2	3.8-35	0.23(0.24)
5	5.4-35	0.24
10	6.0-35	0.24(0.24)

( ) = Average COV for frequency limits from 5% spectra.

Table 5.9 Spectrum Intensities

Record, Component	Spectrum Intensities for 2% Damping, in.		
	0.080-0.24 cps	0.50-3.5 cps	5.4-35 cps
Pacoima Dam, S16E	224	131	2.44
Cholame-Shandon No. 2, N65E	90.0	85.1	0.688
Melendy Ranch, N29W	8.00	9.17	1.38
Gilroy Array No. 6, 230 Deg.	30.0	50.3	0.637
Bonds Corner, 230 Deg.	71.3	76.9	2.17
El Centro, S00E	90.2	51.4	0.842
Taft, S69E	77.9	26.3	0.374
Adak, Alaska, West	31.1	8.85	0.527
Kilauea, Hawaii, S30W	4.09	8.69	0.681
Managua, South	33.0	42.5	0.892
Bucarest, S-N	73.1	77.5	0.269
Santiago, N10W	64.5	18.5	0.427

Table 5.10 Comparison of Average Coefficients of Variation for Elastic Spectra Normalized by 2% Spectrum Intensity and Peak Ground Motions

Damping, percent	Displacement Region, 0.071-0.20 cps: Avg. COV for Spectra Scaled By: 2% SI(0.08-0.24)	Peak Displ.	Reduction, percent
2	0.28	0.48	+42
5	0.25	0.41	+39
10	0.25	0.34	+26

Damping, percent	Velocity Region, 0.20-2.0 cps: Avg. COV for Spectra Scaled By: 2% SI(0.50-3.5)	Peak Vel.	Reduction, percent
2	0.36	0.45	+20
5	0.33	0.40	+18
10	0.30	0.36	+17

Damping, percent	Acceleration Region, 2.0-8.5 cps: Avg. COV for Spectra Scaled By: 2% SI(5.4-35)	Peak Accel.	Reduction, percent
2	0.24	0.41	+41
5	0.24	0.37	+35
10	0.24	0.31	+23

Table 5.11 Minimization of Average Coefficient of Variation for Elastic Spectra Normalized by Mean Fourier Amplitude

	Displacement Region, 0.071-0.20 cps	
Damping, percent	Freq. Limits for $\overline{FS}$, cps	Average COV
2	0.035-0.30	0.37(0.38)
5	0.035-0.31	0.35
10	0.035-0.33	0.34(0.35)
	Velocity Region, 0.20-2.0 cps	
Damping, percent	Freq. Limits for $\overline{FS}$, cps	Average COV
2	0.28-1.3	0.39(0.39)
5	0.28-1.3	0.37
10	0.25-1.3	0.34(0.34)
	Acceleration Region, 2.0-8.5 cps	
Damping, percent	Freq. Limits for $\overline{FS}$, cps	Average COV
2	1.6-19	0.35(0.35)
5	1.4-19	0.39
10	1.3-18	0.42(0.42)

( ) = Average COV for frequency limits from 5% spectra.

Table 5.12 Mean Fourier Amplitudes

	Mean Fourier Amplitude, in./sec		
	0.035-0.31 cps	0.28-1.3 cps	1.4-19 cps
Pacoima Dam, S16E	27.4	77.1	21.6
Cholame-Shandon No. 2, N65E	16.0	43.7	7.05
Melendy Ranch, N29W	1.59	5.68	8.07
Gilroy Array No. 6, 230 Deg.	2.70	32.7	6.68
Bonds Corner, 230 Deg.	9.08	45.8	20.4
El Centro, S00E	11.2	41.8	10.9
Taft, S69E	8.53	18.2	5.86
Adak, Alaska, West	2.88	5.25	6.74
Kilauea, Hawaii, S30W	0.479	5.15	6.85
Managua, South	5.50	18.7	13.1
Bucarest, S-N	8.43	44.3	3.17
Santiago, N10W	7.64	12.6	6.51

Table 5.13 Comparison of Average Coefficients of Variation for Elastic Spectra Normalized by Mean Fourier Amplitudes and Peak Ground Motions

	Displacement Region, 0.071-0.20 cps		
Damping, percent	Avg. COV for Spectra Scaled By: $\overline{FS}$(0.035-0.31)	Peak Displ.	Reduction, percent
2	0.38	0.48	+21
5	0.35	0.41	+15
10	0.35	0.34	-3

	Velocity Region, 0.20-2.0 cps		
Damping, percent	Avg. COV for Spectra Scaled By: $\overline{FS}$(0.28-1.3)	Peak Vel.	Reduction, percent
2	0.39	0.45	+13
5	0.37	0.40	+8
10	0.34	0.36	+6

	Acceleration Region, 2.0-8.5 cps		
Damping, percent	Avg. COV for Spectra Scaled By: $\overline{FS}$(1.4-19)	Peak Accel.	Reduction, percent
2	0.35	0.41	+15
5	0.39	0.37	-5
10	0.42	0.31	-35

FIGURES

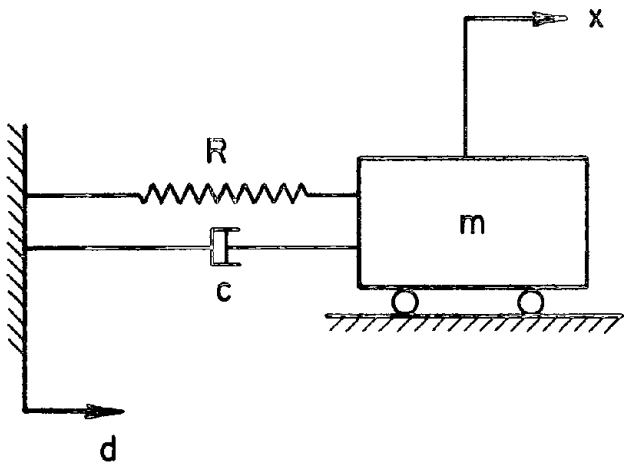

$$u = x - d$$

$$R = R(u)$$

$$c = 2\omega m\beta$$

Fig. 2.1 Single-Degree-of-Freedom System

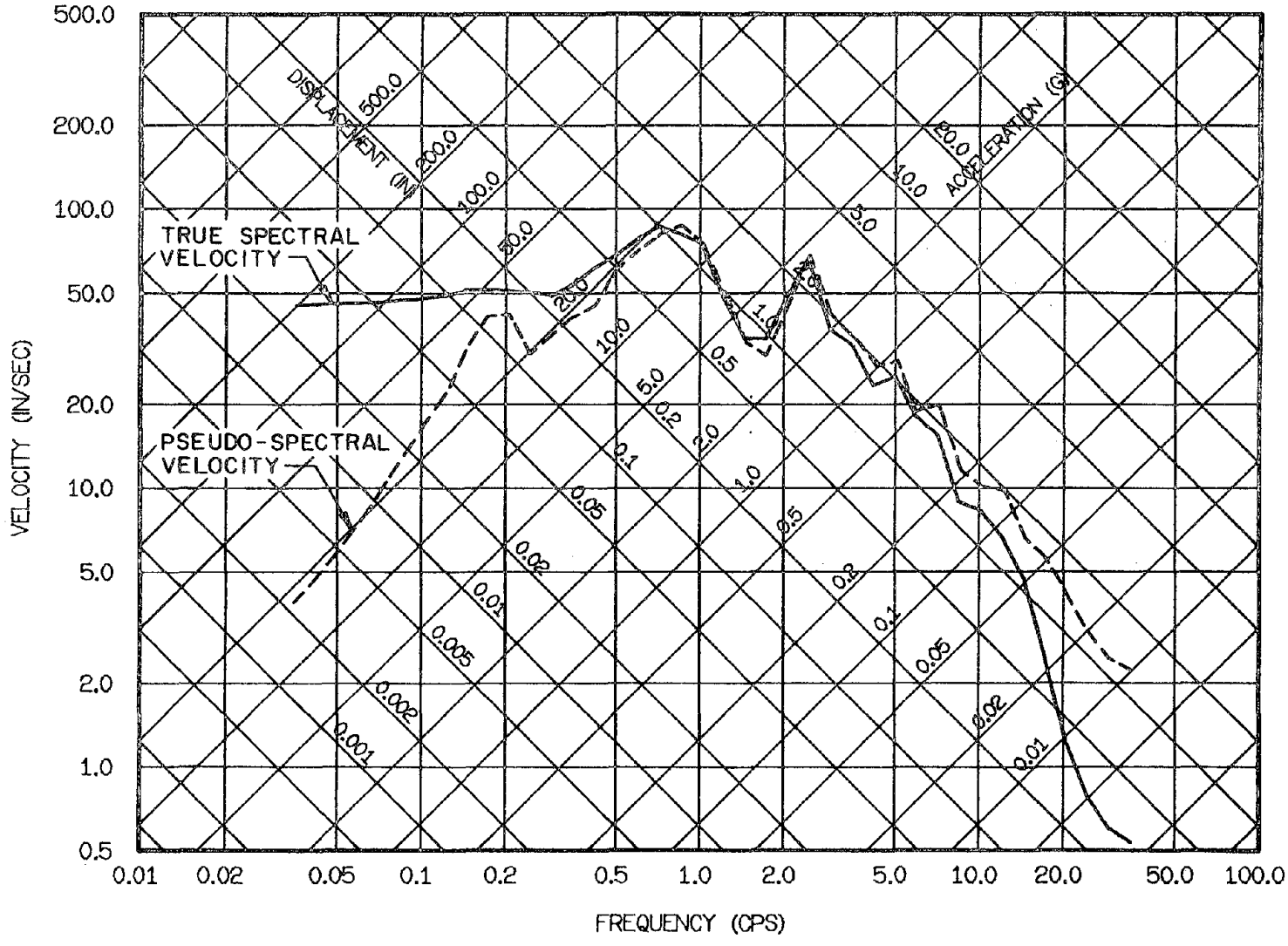

Fig. 2.2 Comparison of True and Pseudo-Spectral Velocities: Elastic Systems with 5% Damping Subjected to the Pacoima Dam Record of Feb. 9, 1971, Component S16E

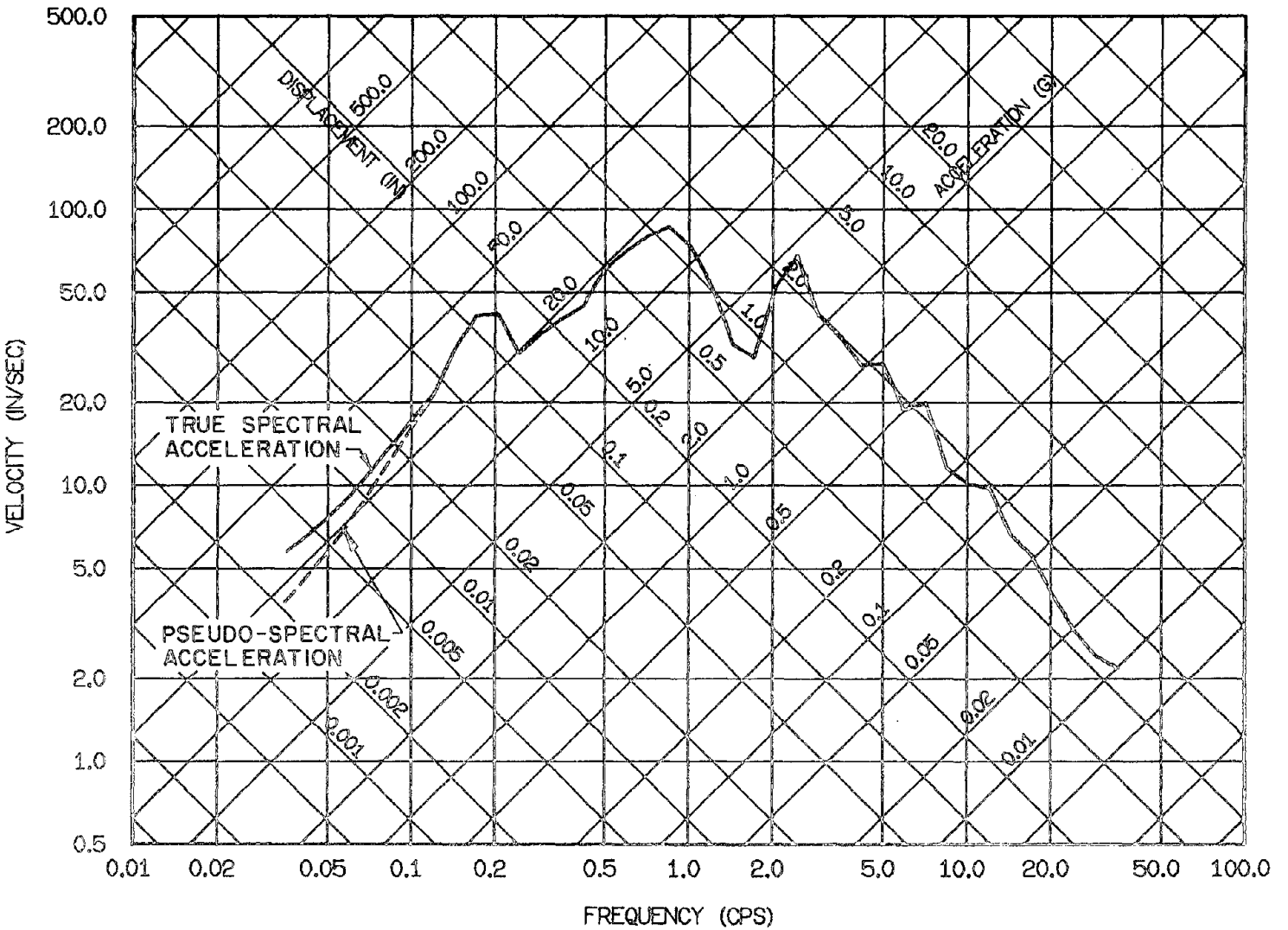

Fig. 2.3 Comparison of True and Pseudo-Spectral Accelerations: Elastic Systems with 5% Damping Subjected to the Pacoima Dam Record of Feb. 9, 1971, Component S16E

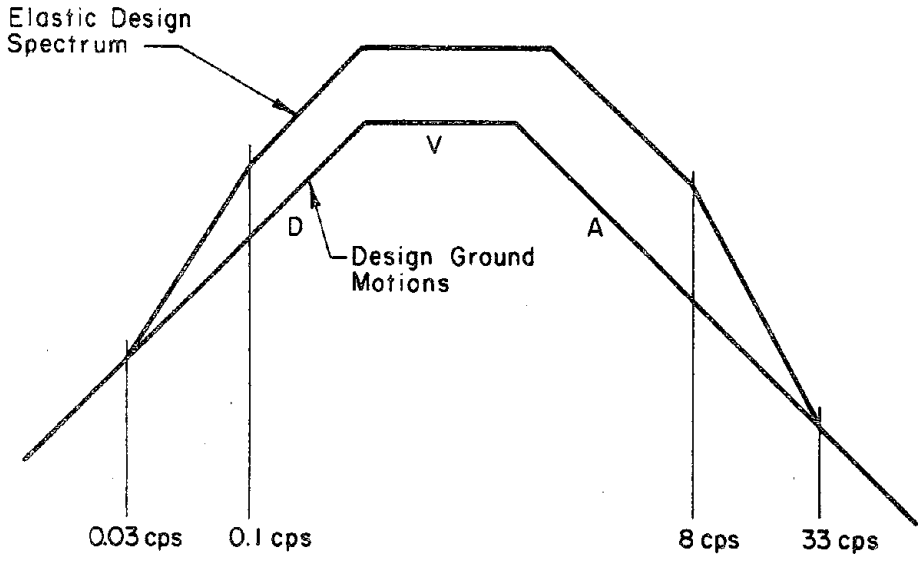

Construction of Elastic Design Spectrum

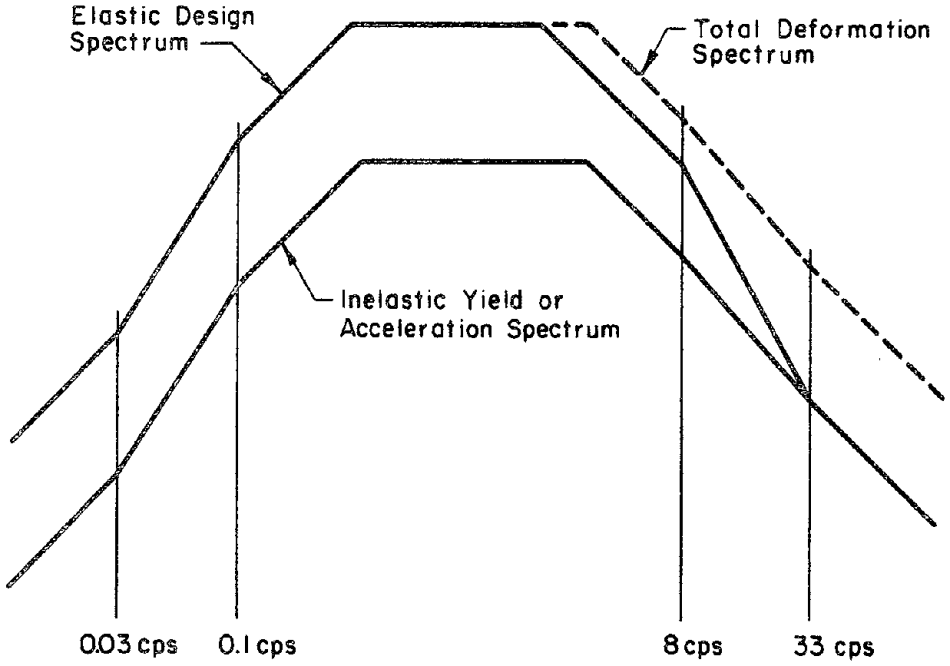

Construction of Inelastic Design Spectra

Fig. 2.4 Construction of Design Spectra

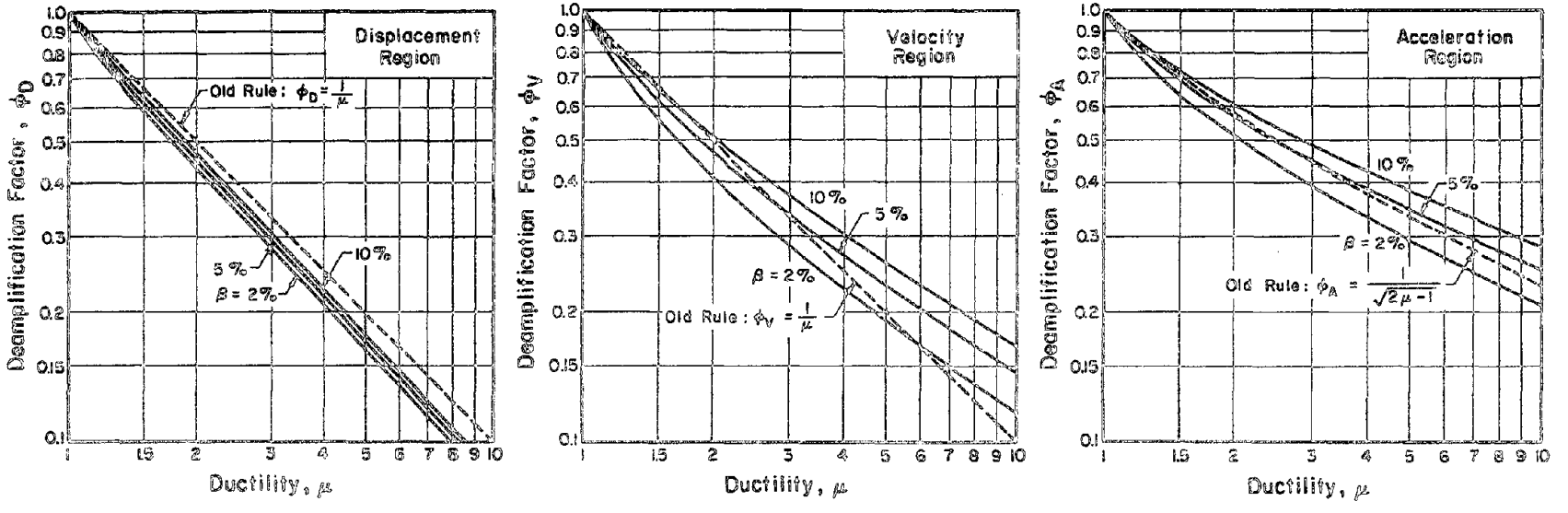

Fig. 2.5 Deamplification Factors for Elastoplastic Spectra. After Riddell and Newmark (67)

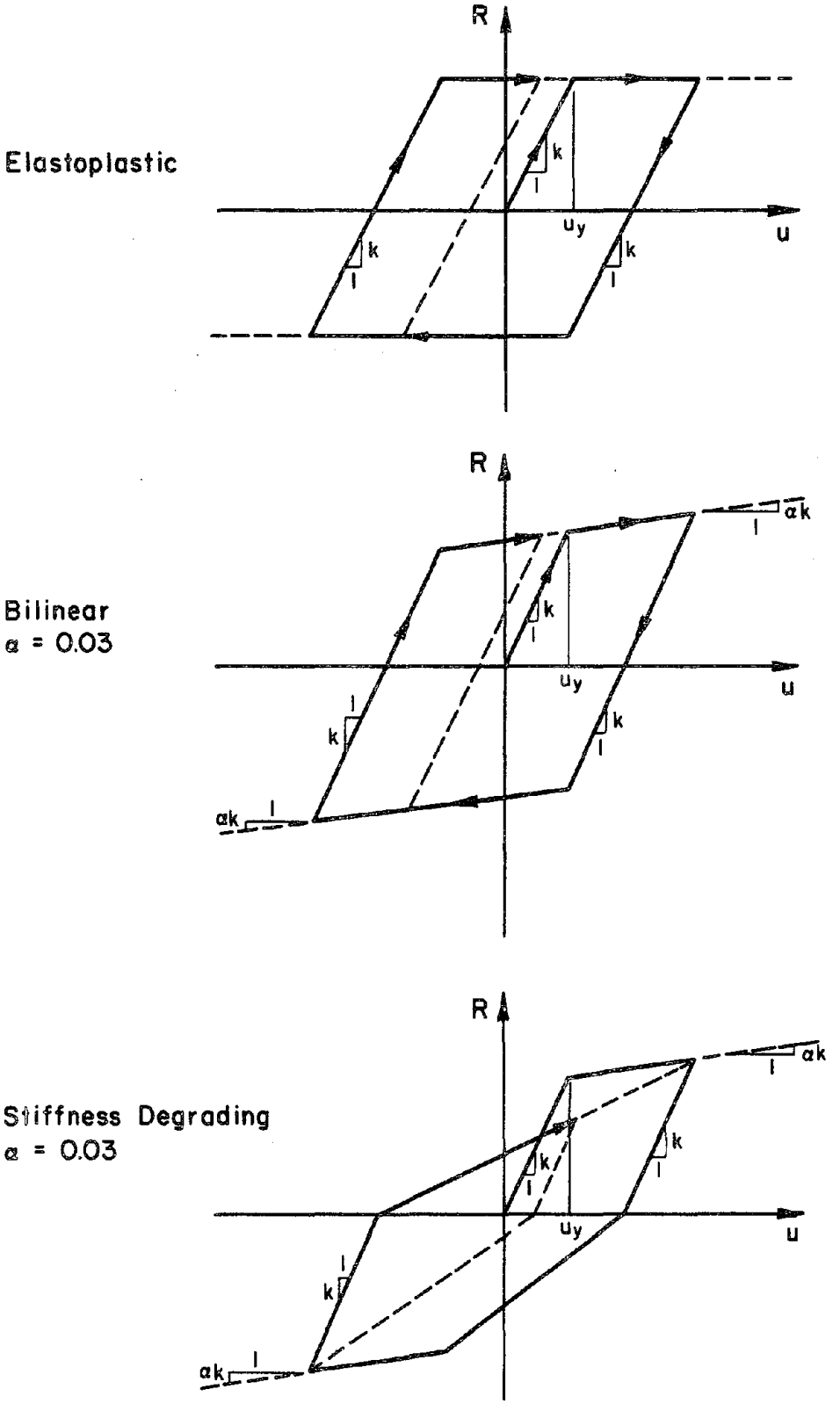

Fig. 3.1 Nonlinear Models used by Riddell and Newmark (67)

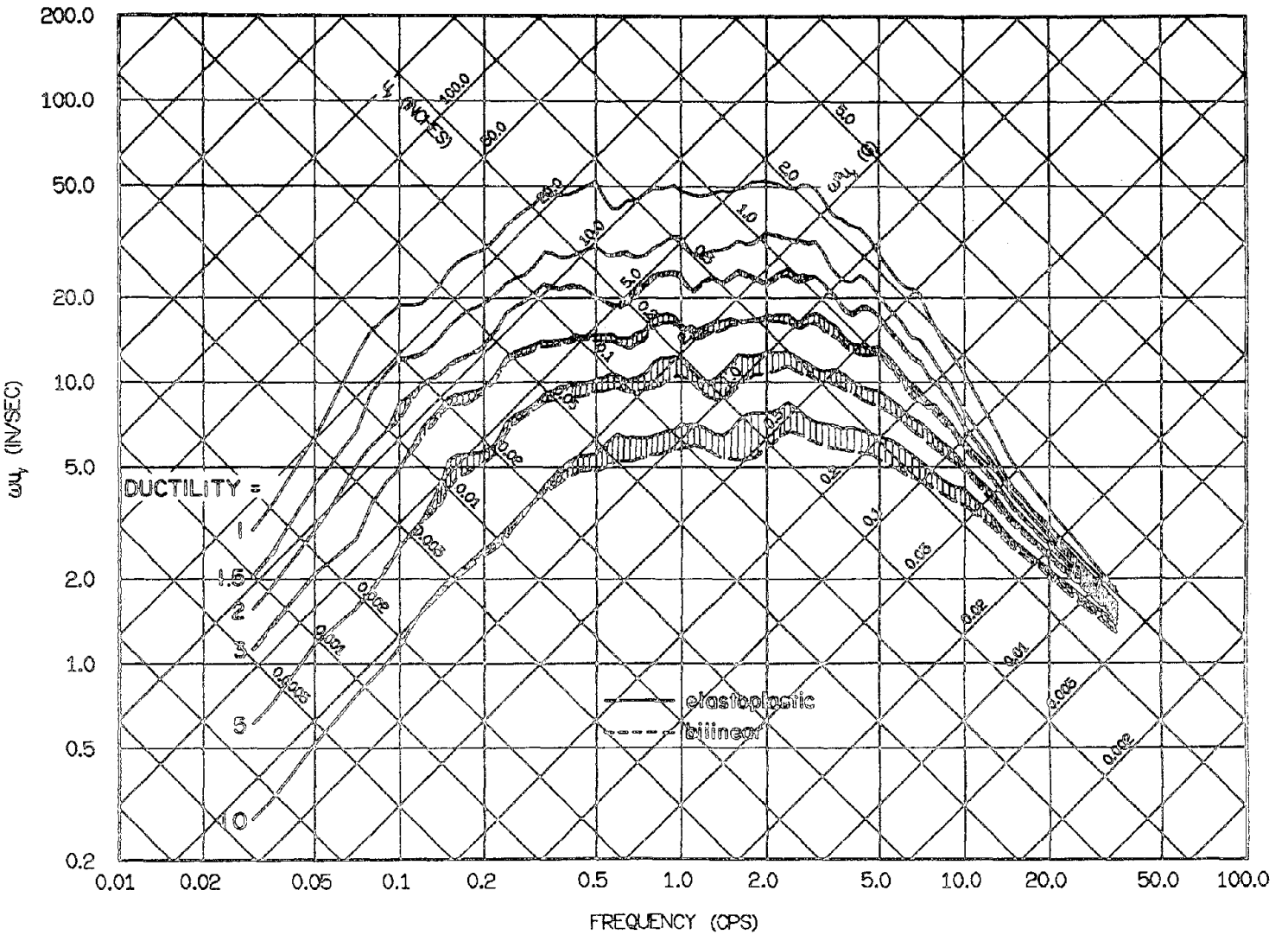

Fig. 3.2 Comparison of Mean Inelastic Yield Spectra Normalized by Peak Ground Acceleration: Elastoplastic and Bilinear Systems with 5% Damping. After Riddell and Newmark (67)

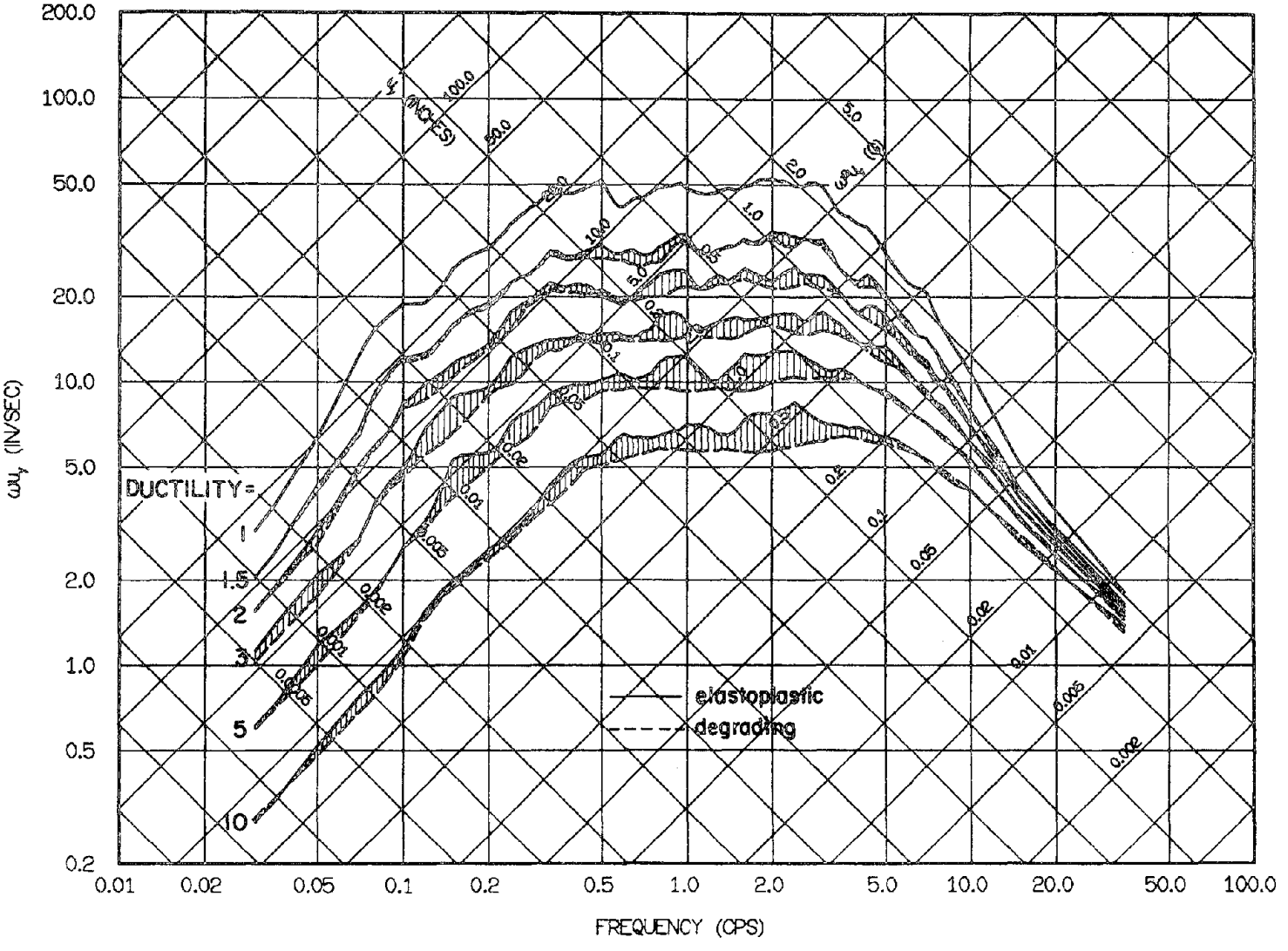

Fig. 3.3 Comparison of Mean Inelastic Yield Spectra Normalized by Peak Ground Acceleration: Elastoplastic and Stiffness Degrading Systems with 5% Damping. After Riddell and Newmark (67)

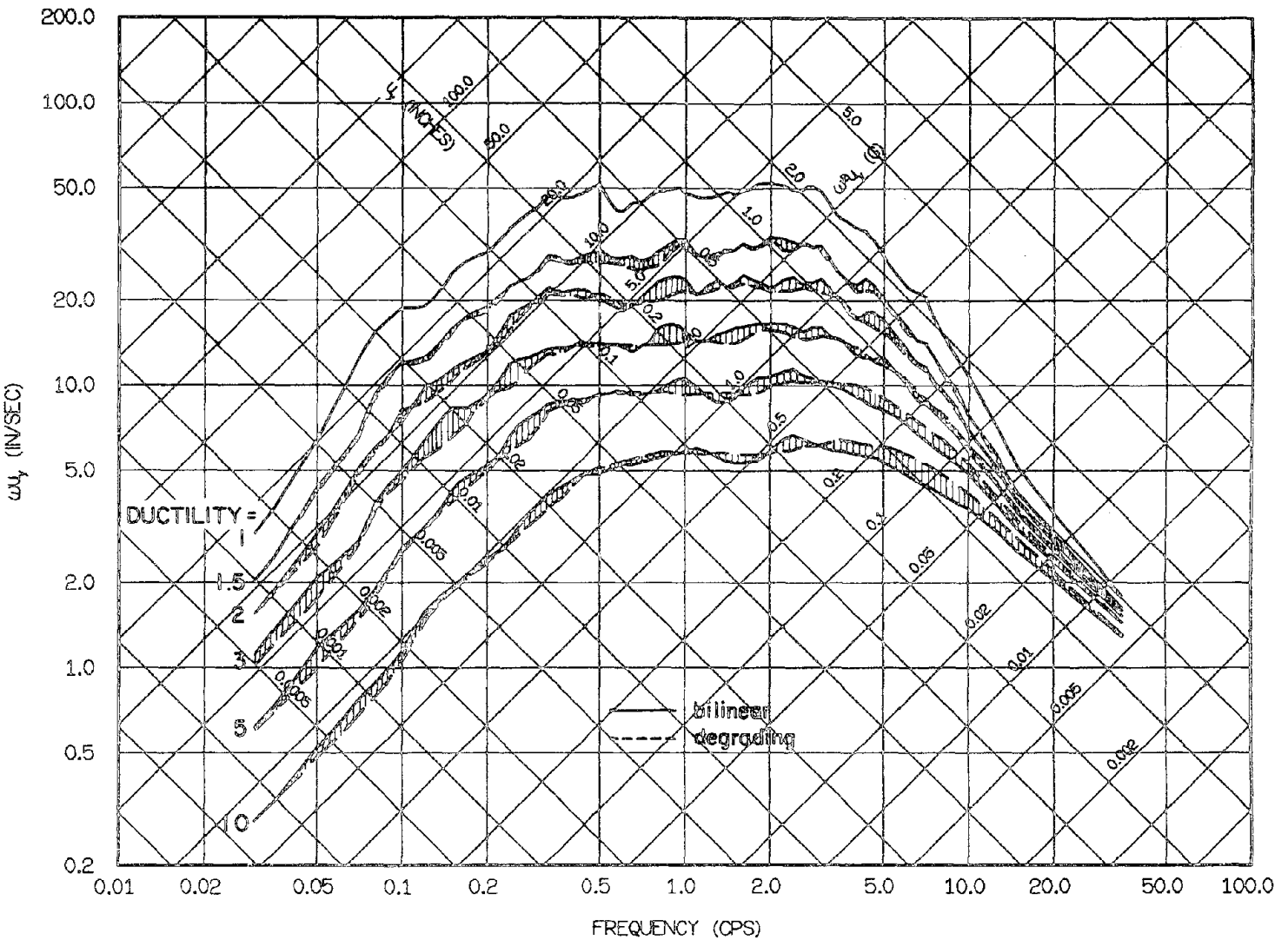

Fig. 3.4 Comparison of Mean Inelastic Yield Spectra Normalized by Peak Ground Acceleration: Bilinear and Stiffness Degrading Systems with 5% Damping. After Riddell and Newmark (67)

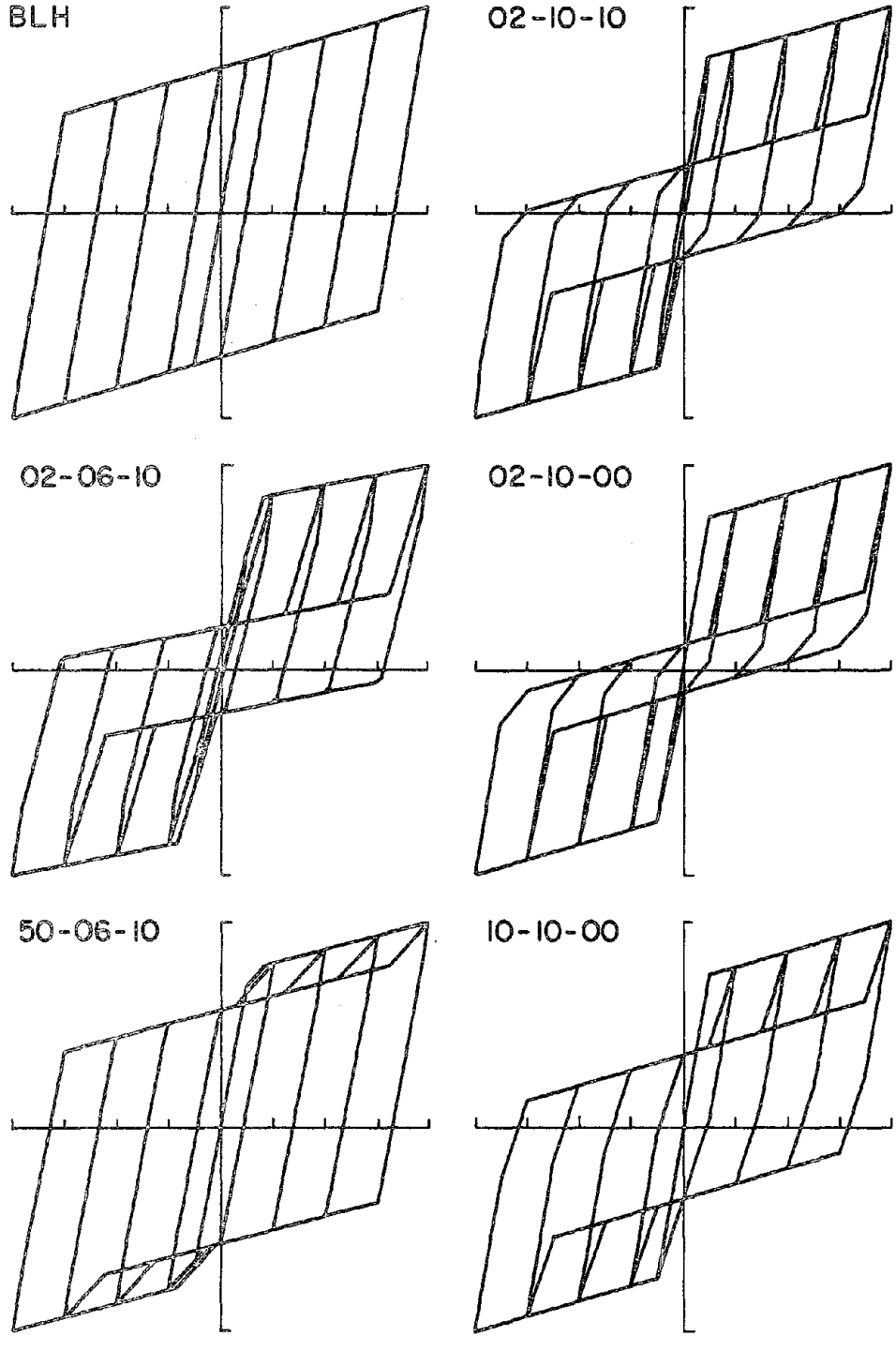

Fig. 3.5 Nonlinear Models used by Iwan and Gates (35, 36)

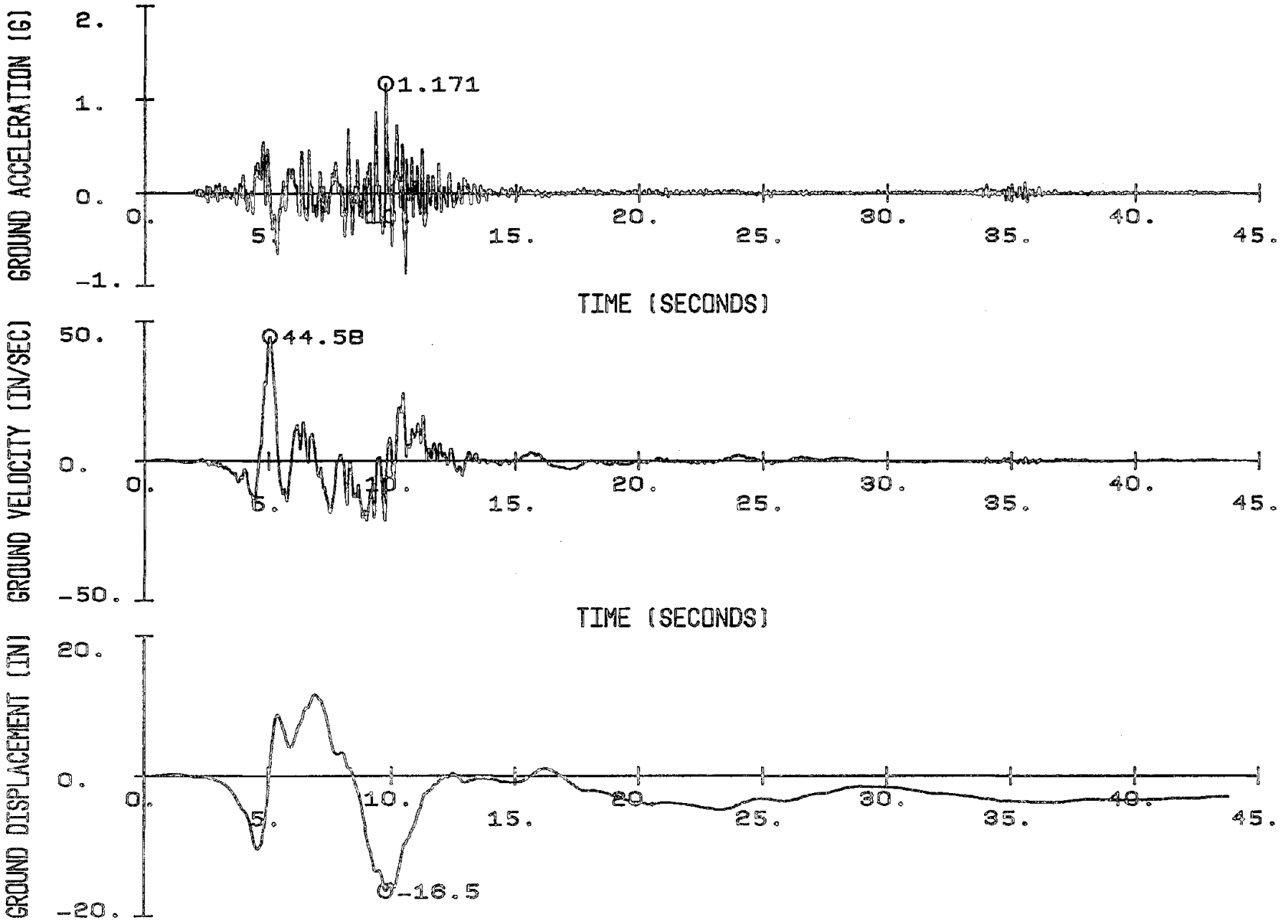

Fig. 3.6 Ground Motions for the Pacoima Dam Record of Feb. 9, 1971, Component S16E

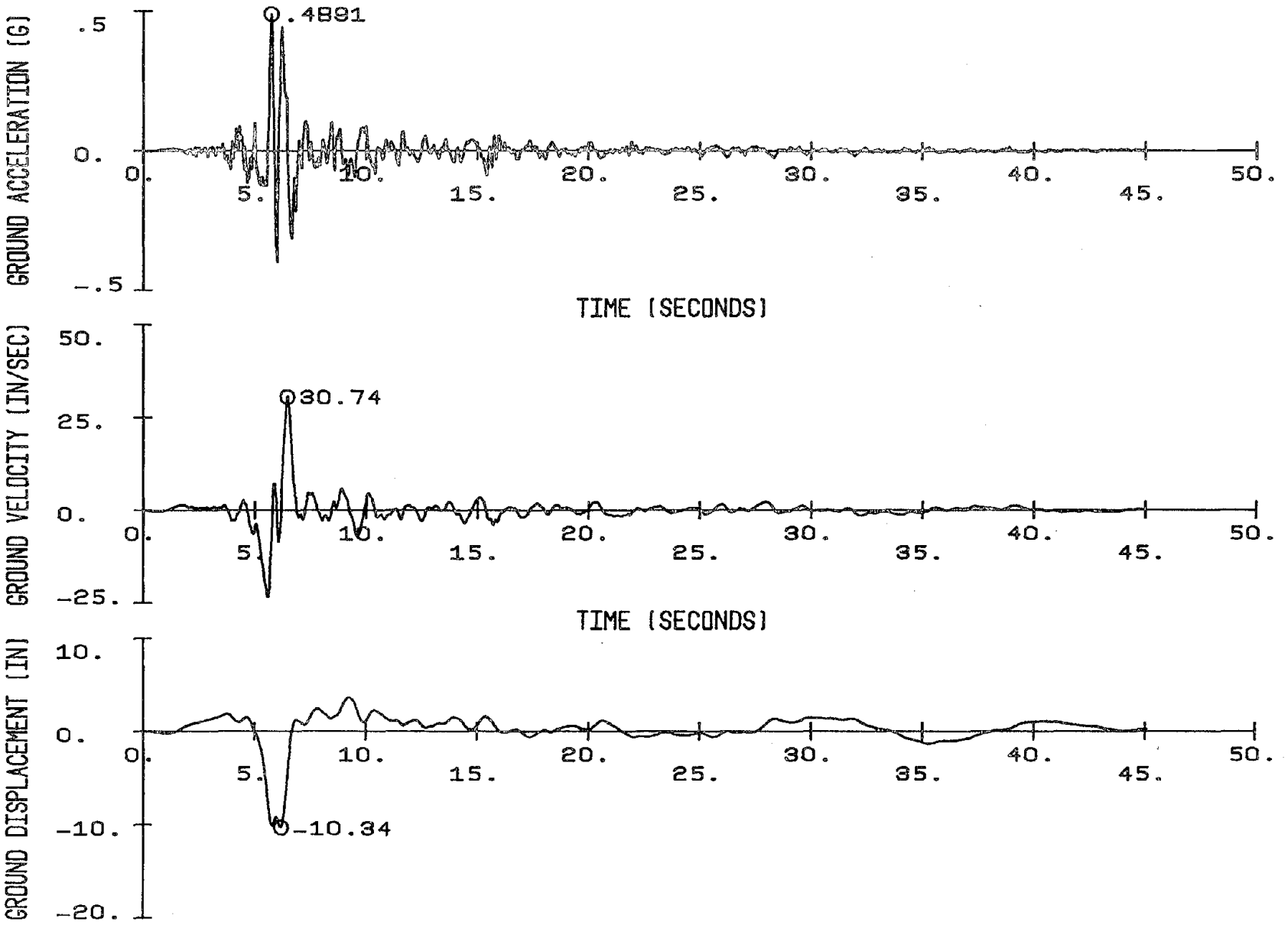

Fig. 3.7 Ground Motions for the Cholame-Shandon No. 2 Record of June 27, 1966, Component N65E

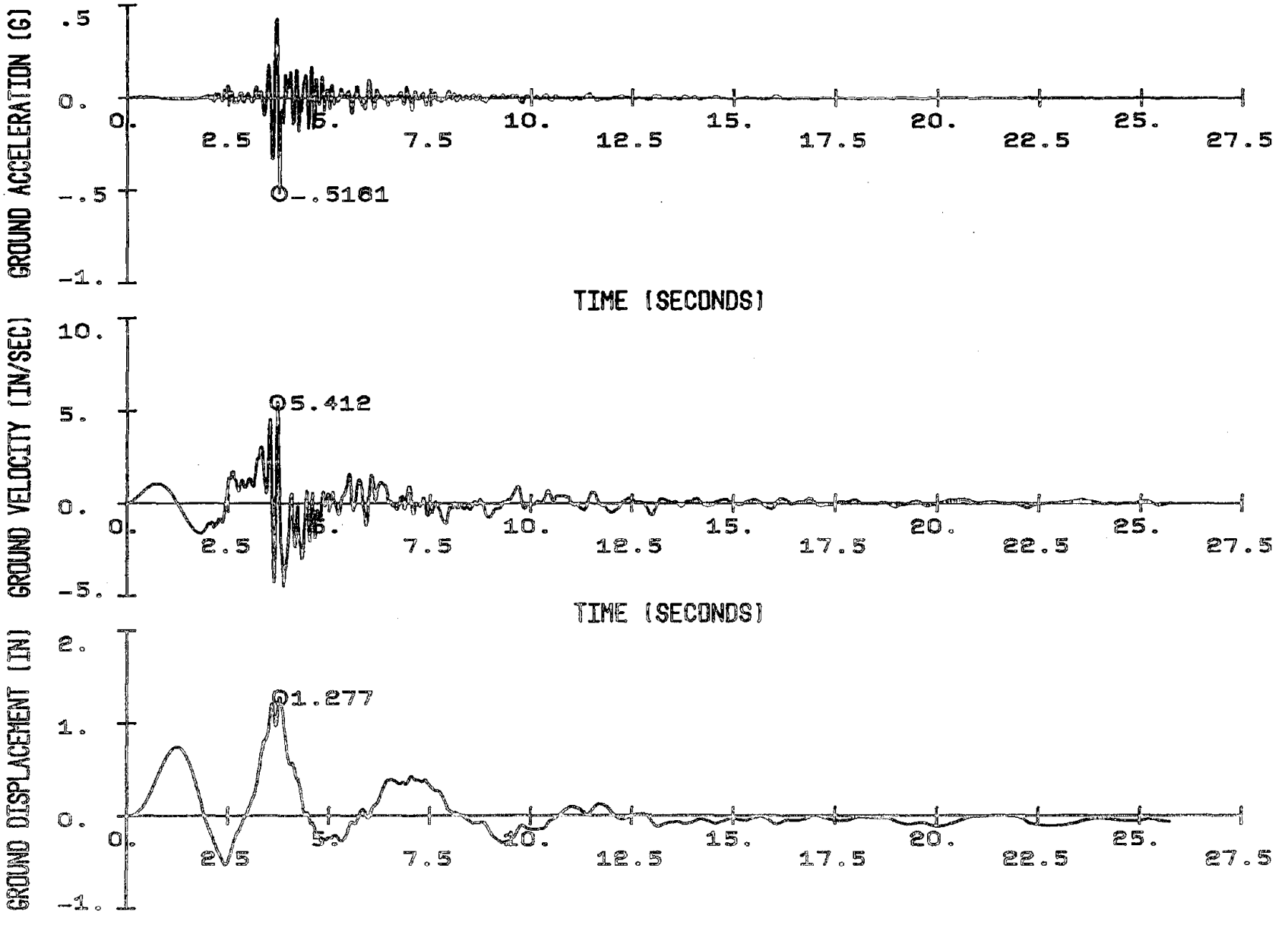

Fig. 3.8 Ground Motions for the Melendy Ranch Record of Sept. 4, 1972, Component N29W

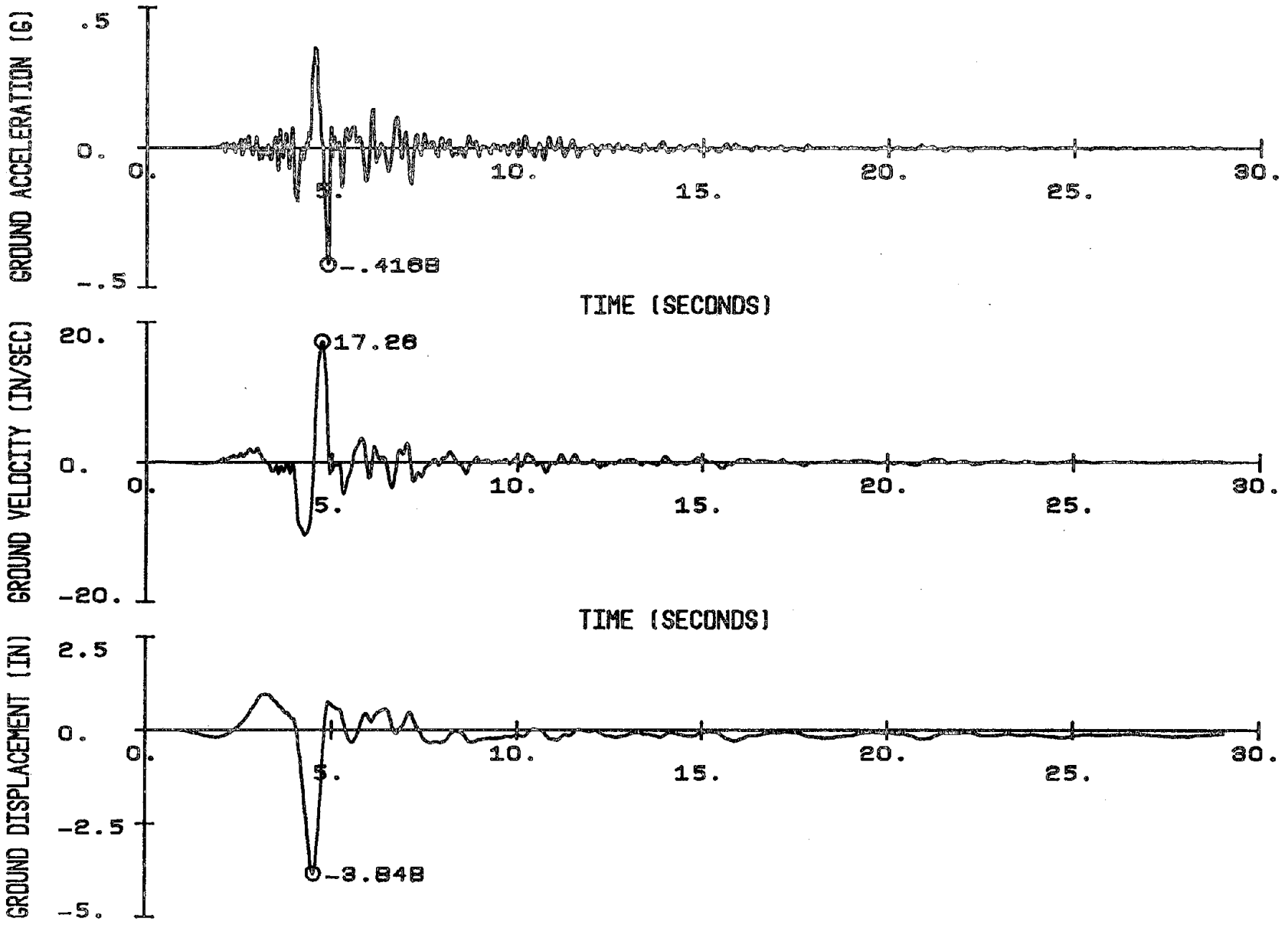

Fig. 3.9 Ground Motions for the Gilroy Array No. 6 Record of Aug. 6, 1979, Component 230 Deg

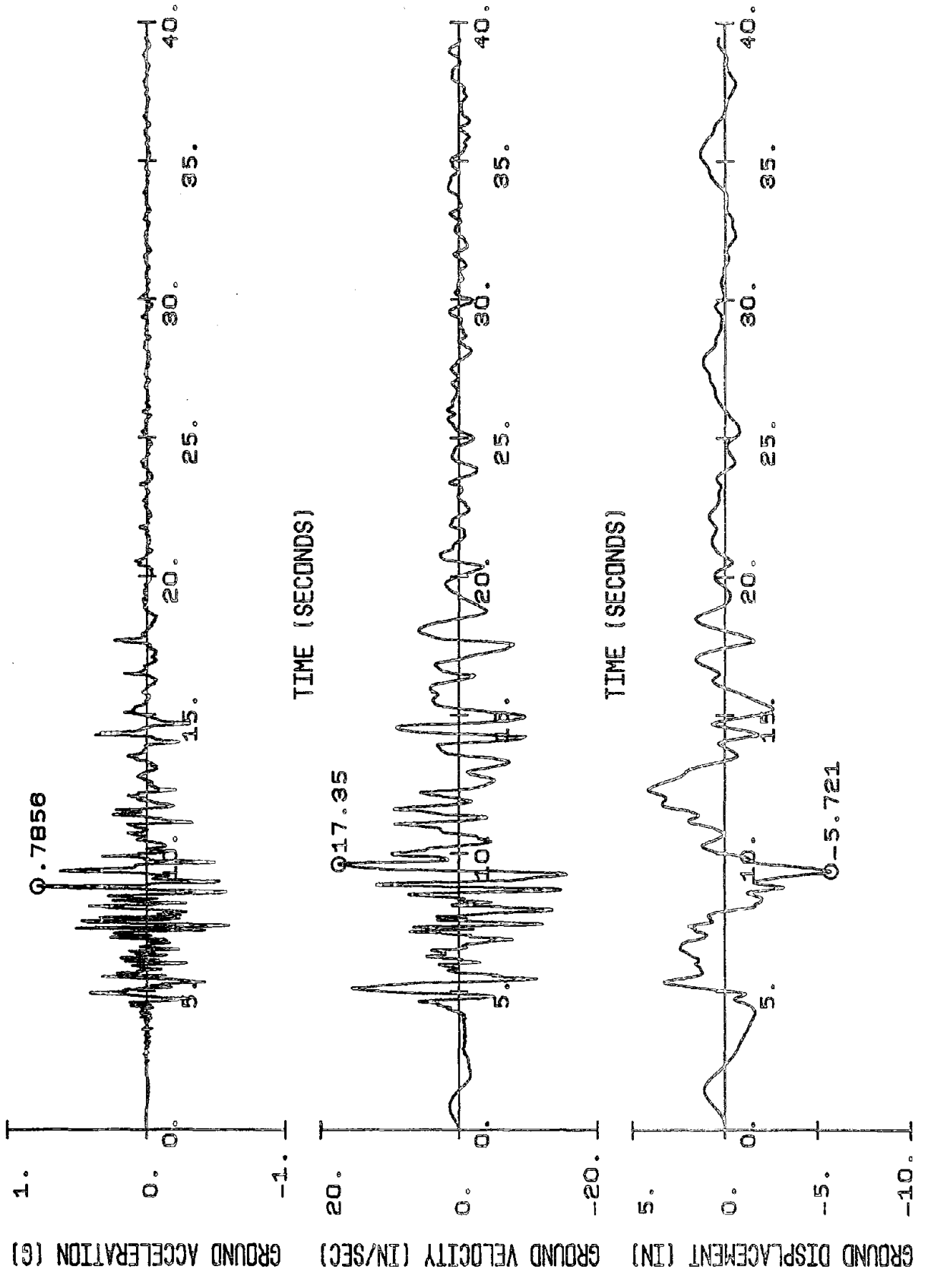

Fig. 3.10 Ground Motions for the Bonds Corner Record of Oct. 15, 1979, Component 230 Deg

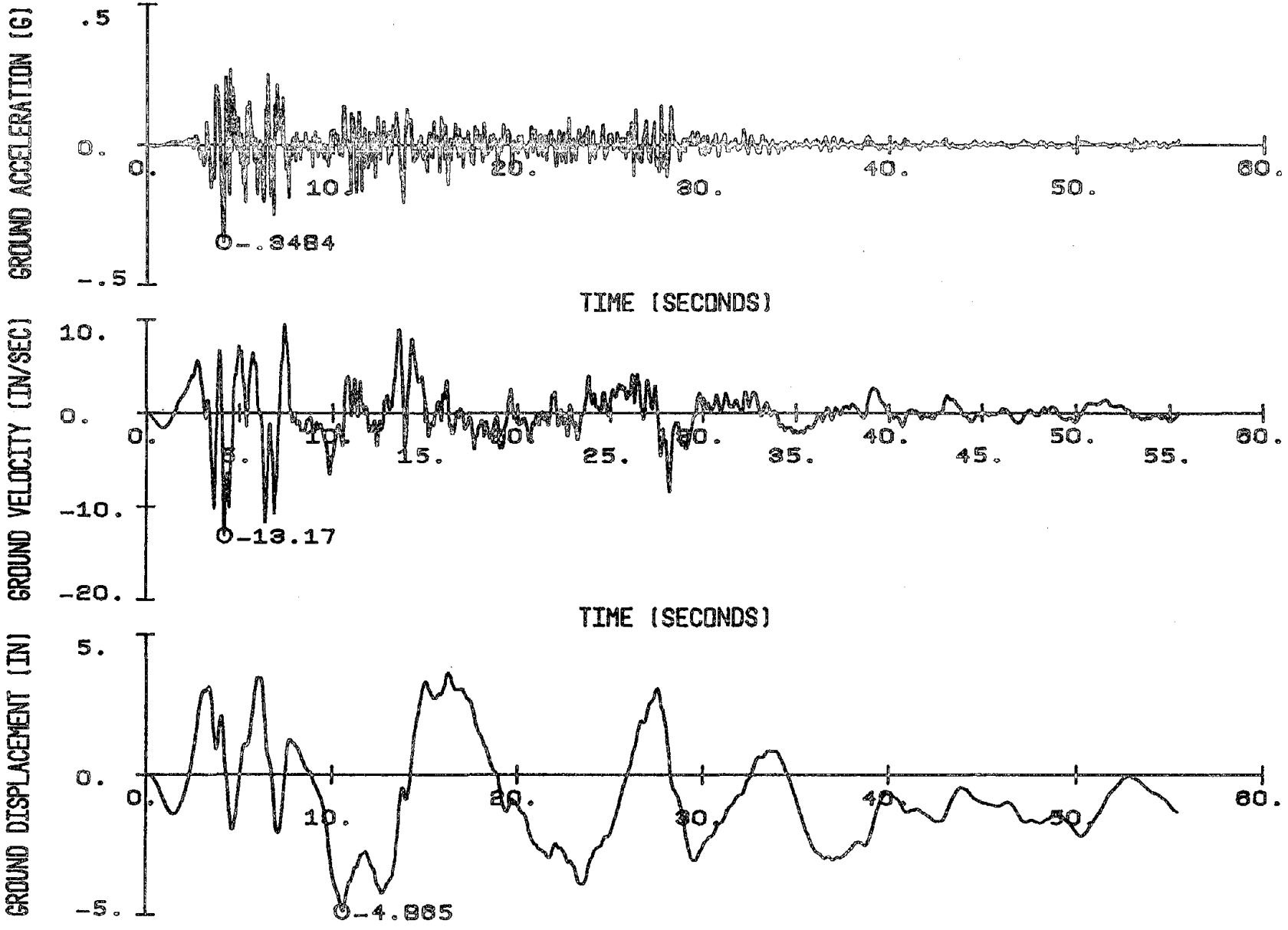

Fig. 3.11 Ground Motions for the El Centro Record of May 18, 1940, Component S00E

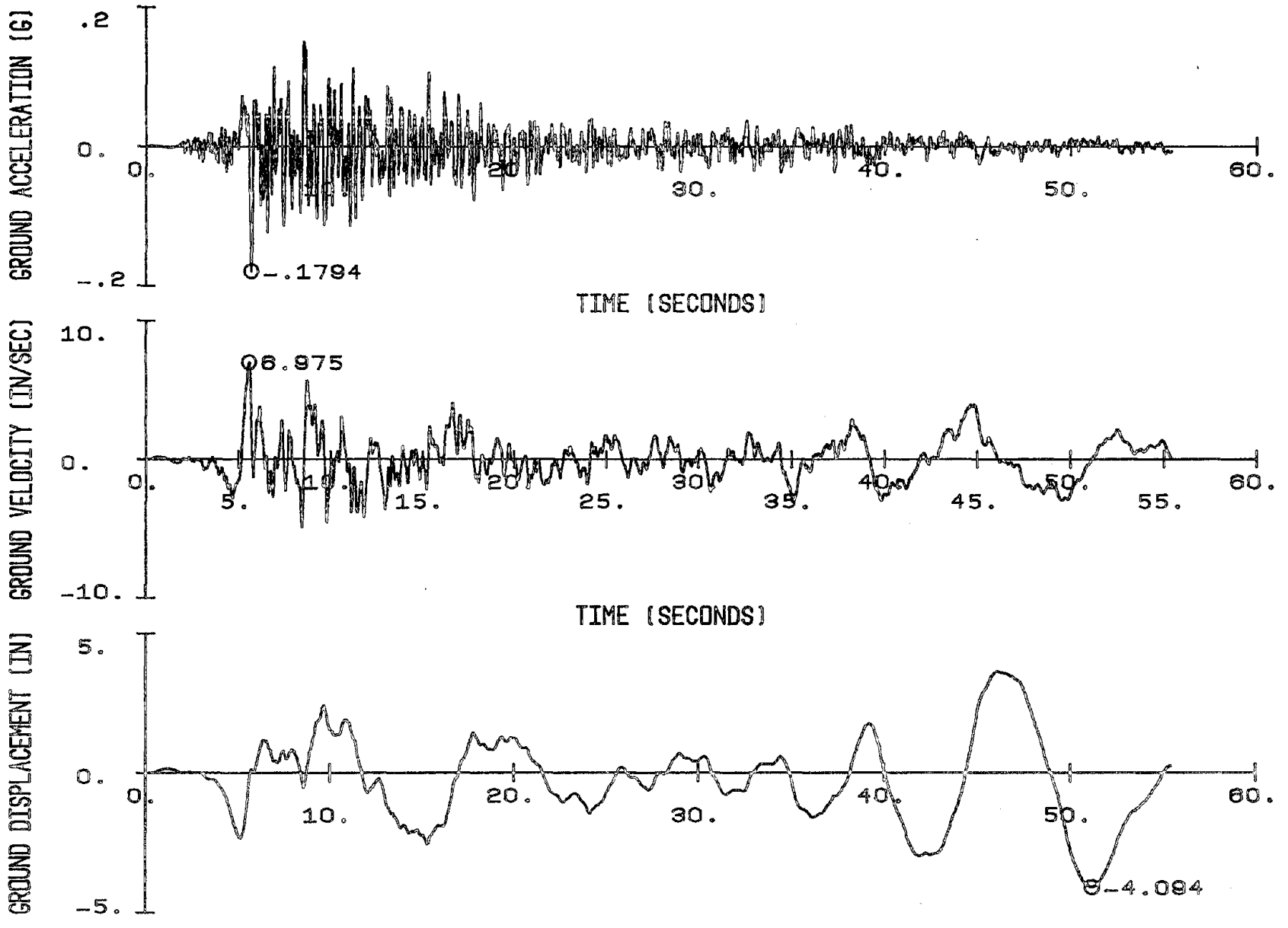

Fig. 3.12 Ground Motions for the Taft Record of July 21, 1952, Component S69E

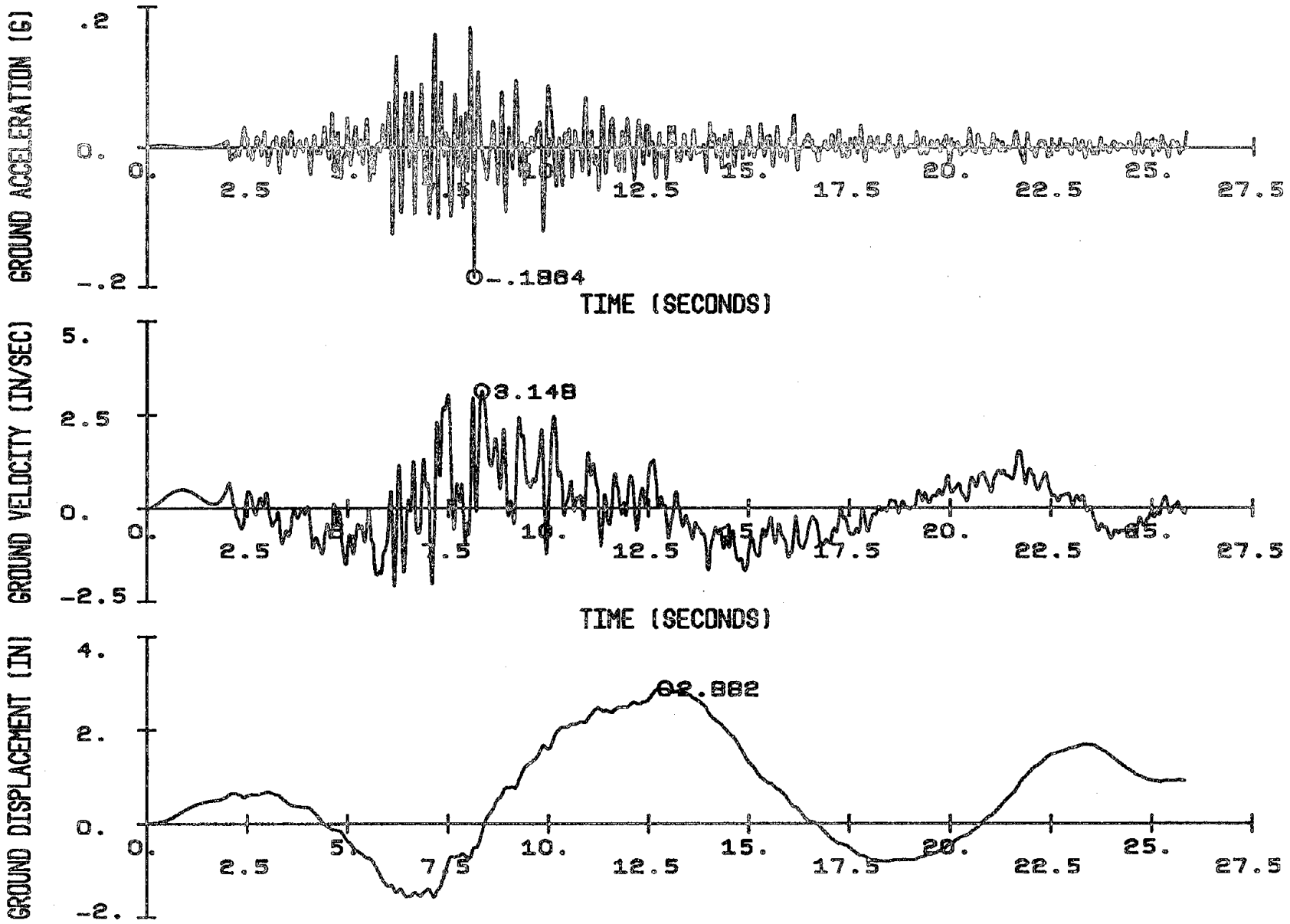

Fig. 3.13 Ground Motions for the Adak, Alaska Record of May 1, 1971, Component West

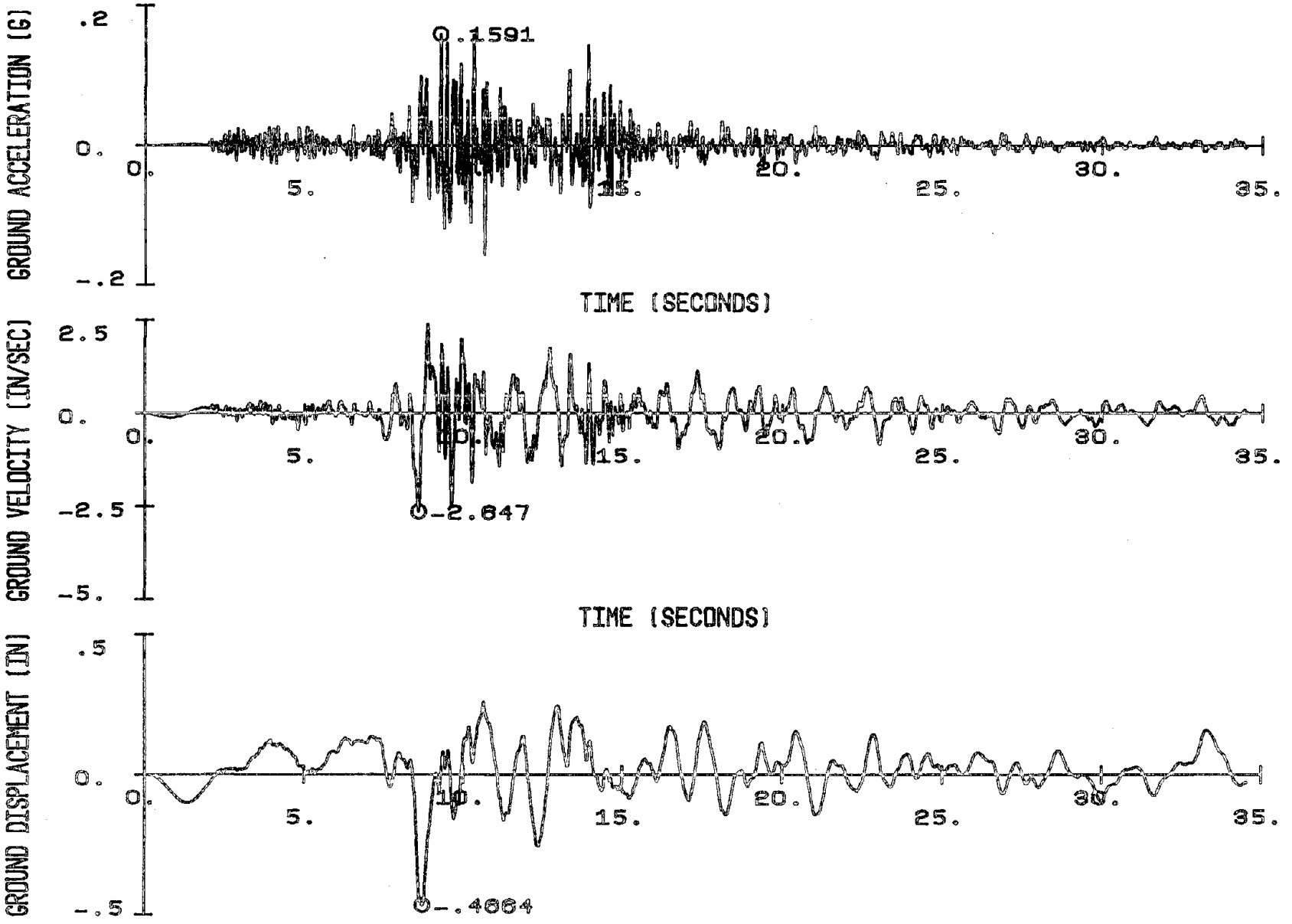

Fig. 3.14 Ground Motions for the Kilauea, Hawaii Record of April 26, 1973, Component S30W

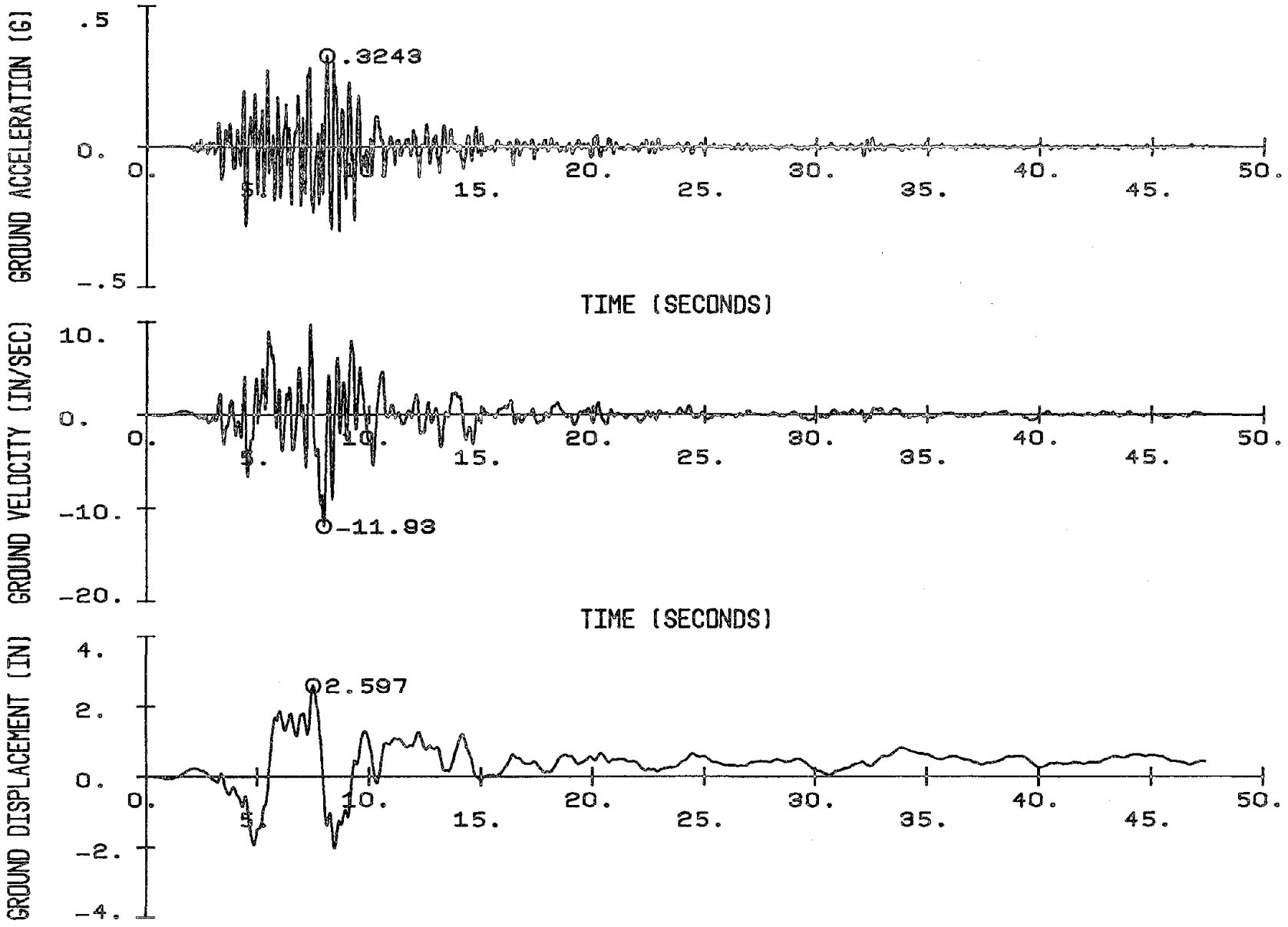

Fig. 3.15 Ground Motions for the Managua, Nicaragua Record of Dec. 23, 1972, Component South

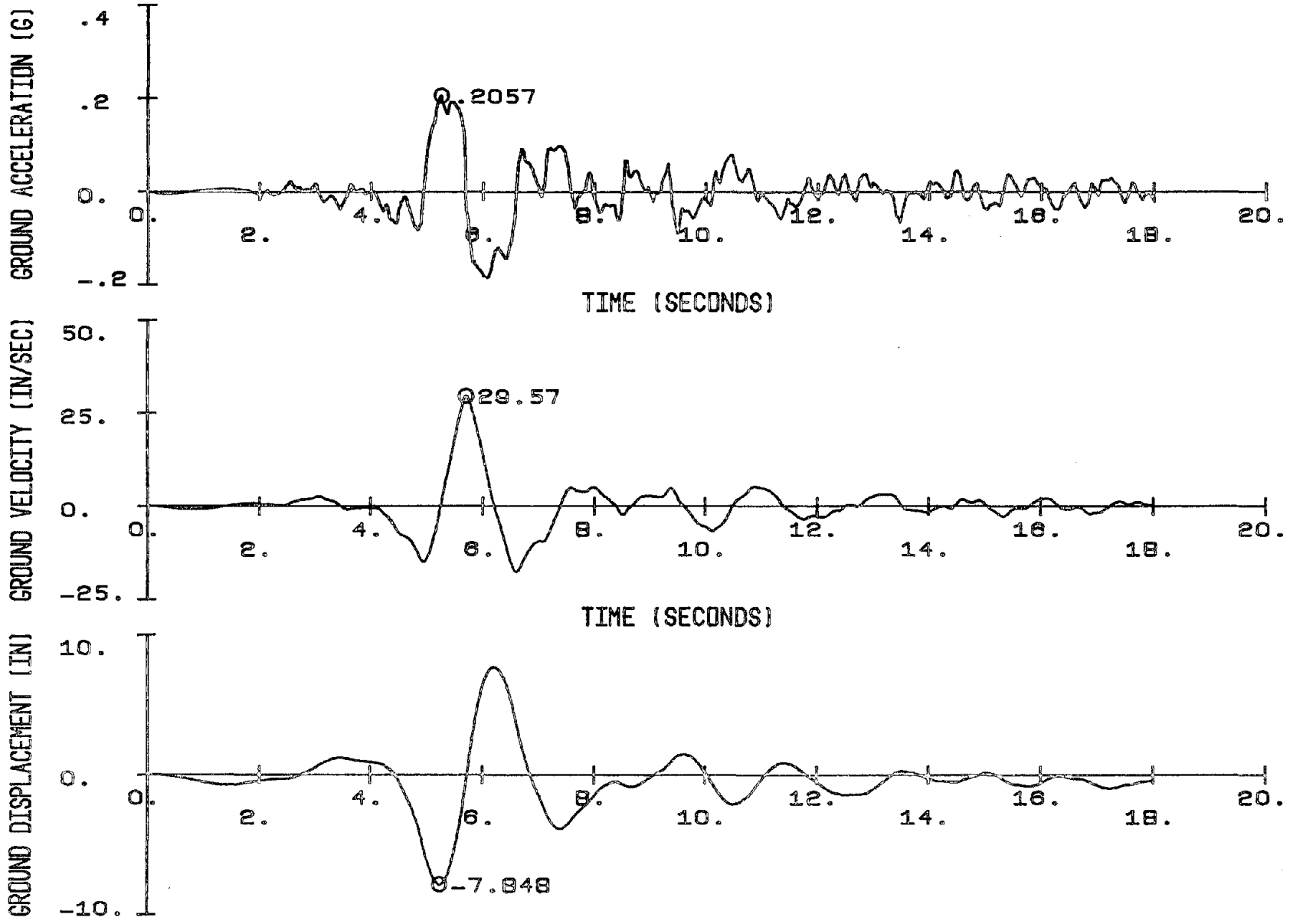

Fig. 3.16 Ground Motions for the Bucarest, Rumania Record of Mar. 4, 1977, Component S-N

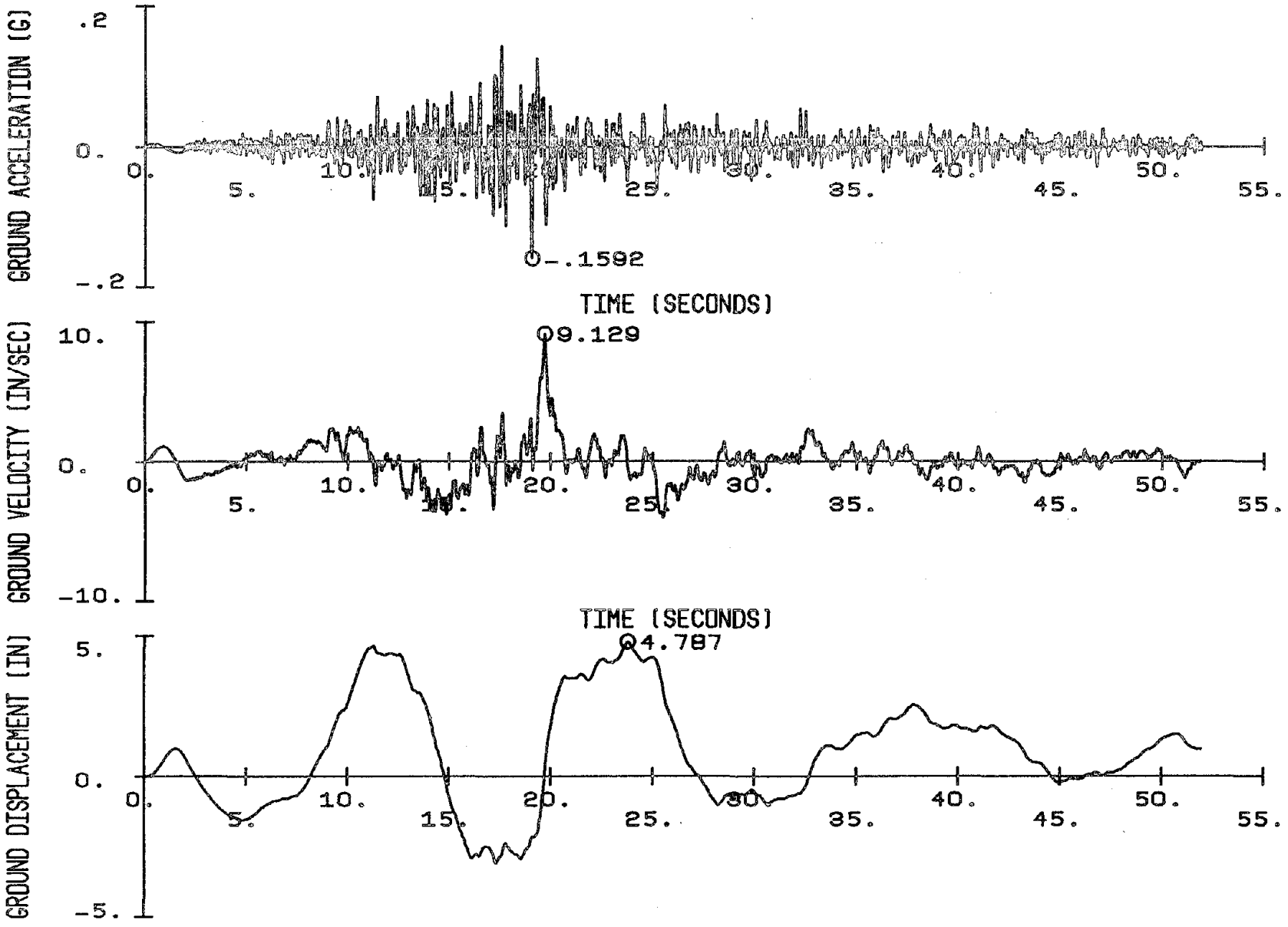

Fig. 3.17 Ground Motions for the Santiago, Chile Record of July 8, 1971, Component N10W

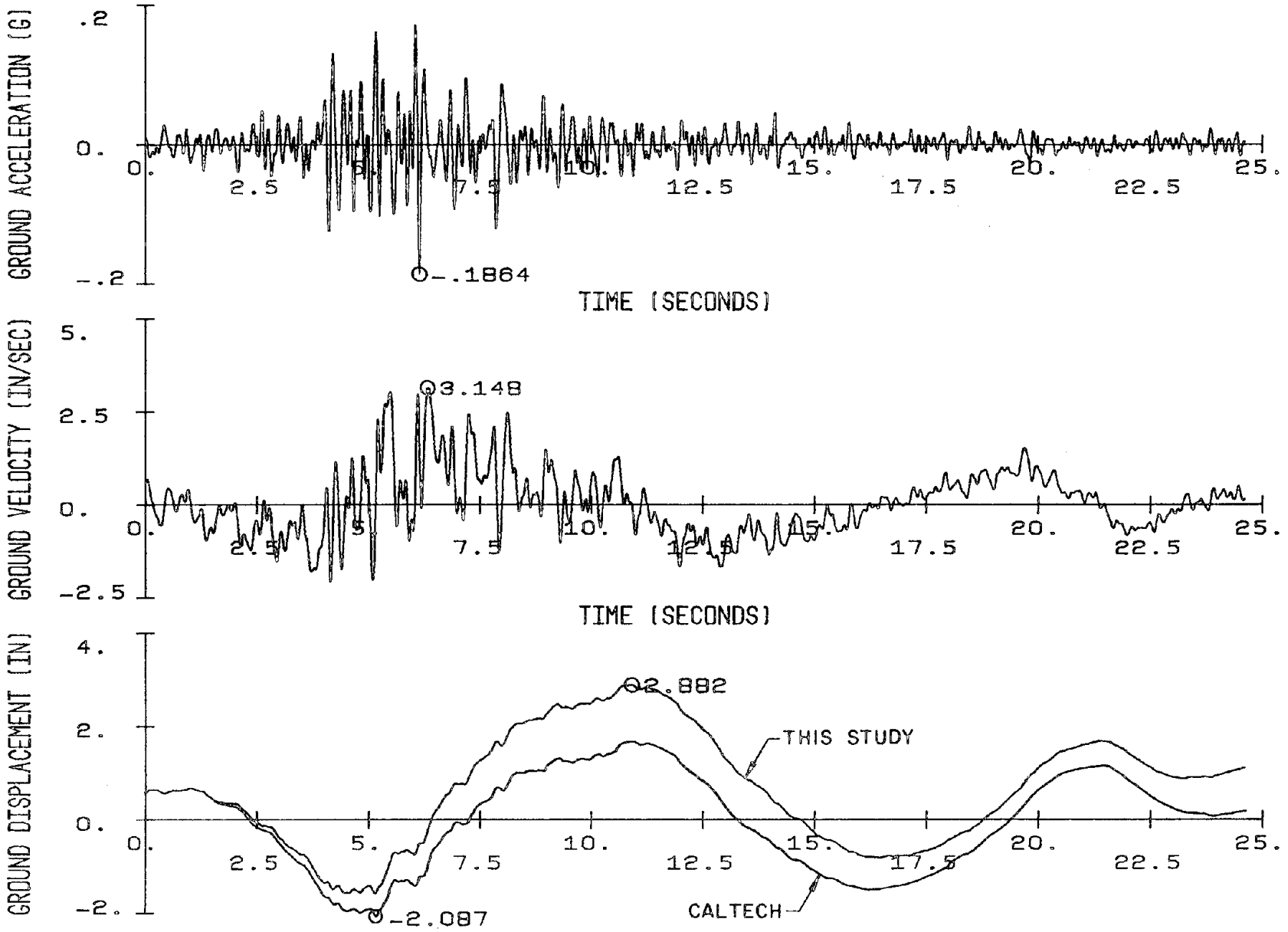

Fig. 3.18 Ground Motions for the Adak, Alaska Record: Comparison of Displacement Time-Histories

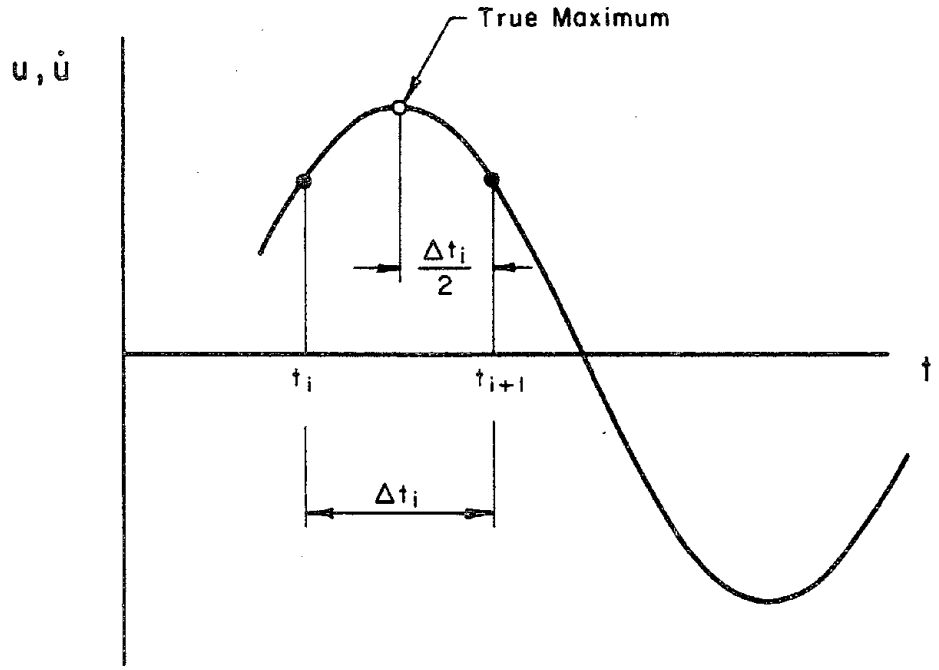

Fig. 3.19 Maximum Discretization Error.
After Nigam and Jennings (60, 61)

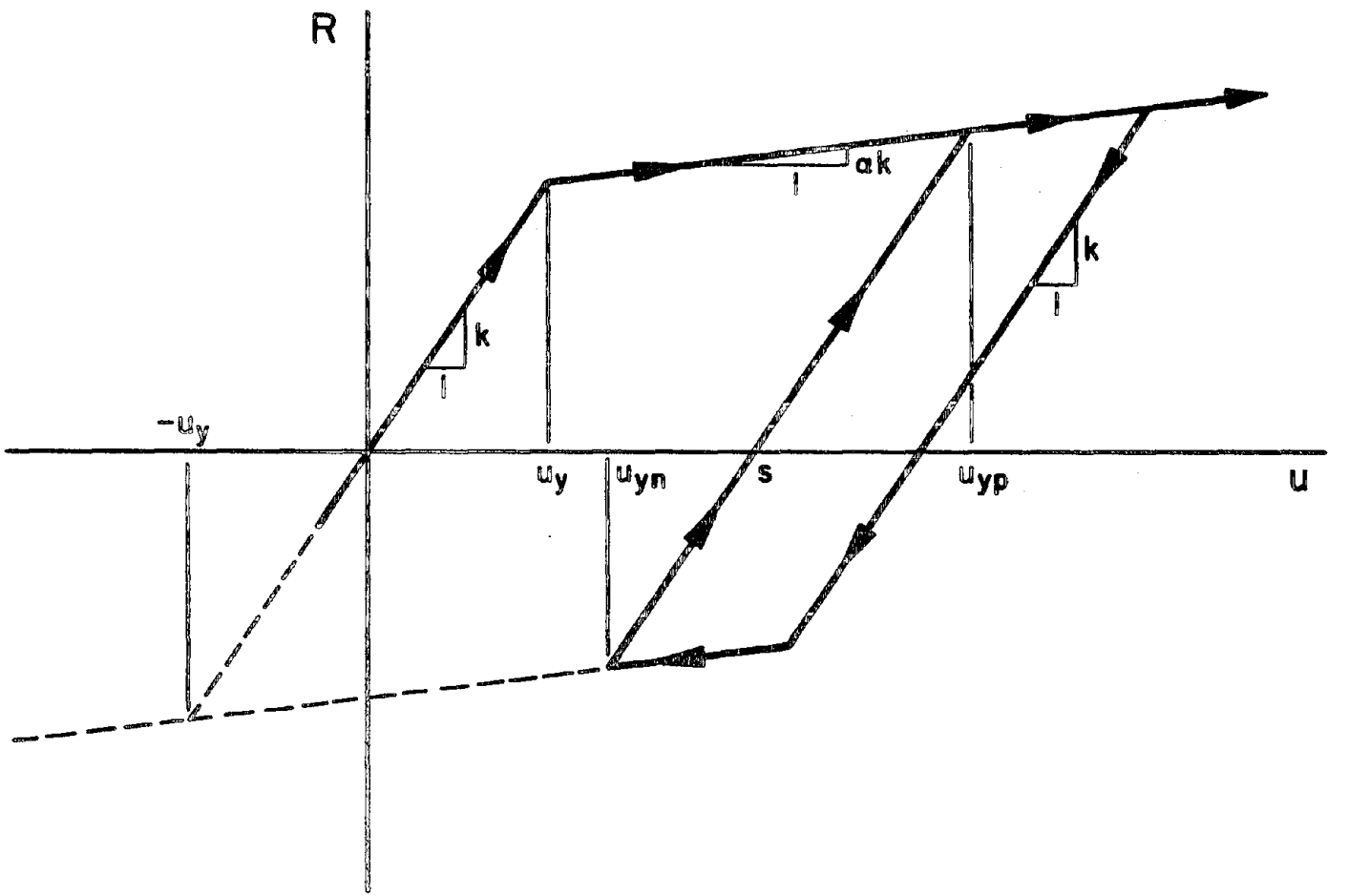

Fig. 3.20 Bilinear Hysteretic Load-Deformation Model

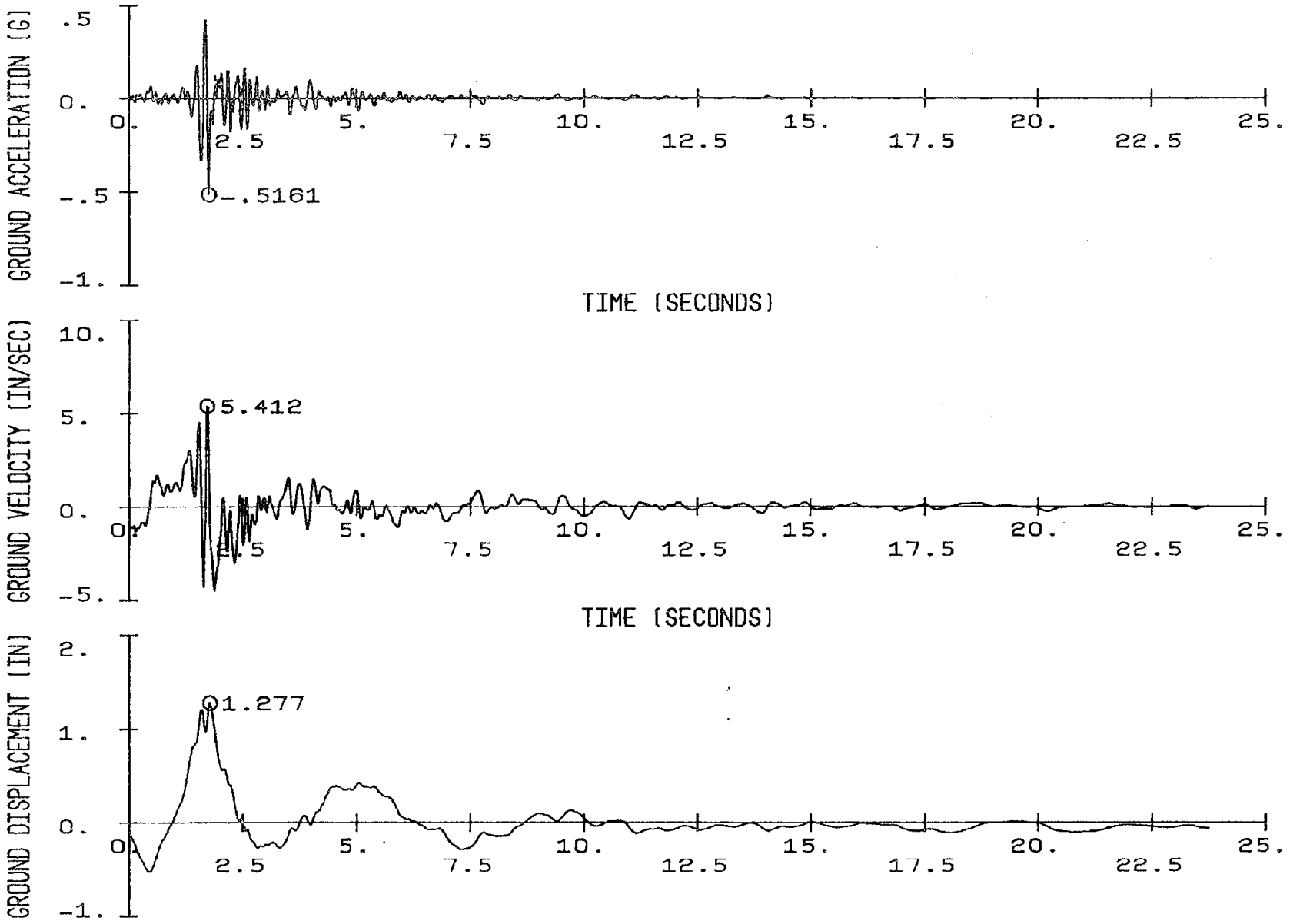

Fig. 3.21 Ground Motions for the Melendy Ranch Record of Sept. 4, 1972, Component N29W: Without Prefixed Pulse

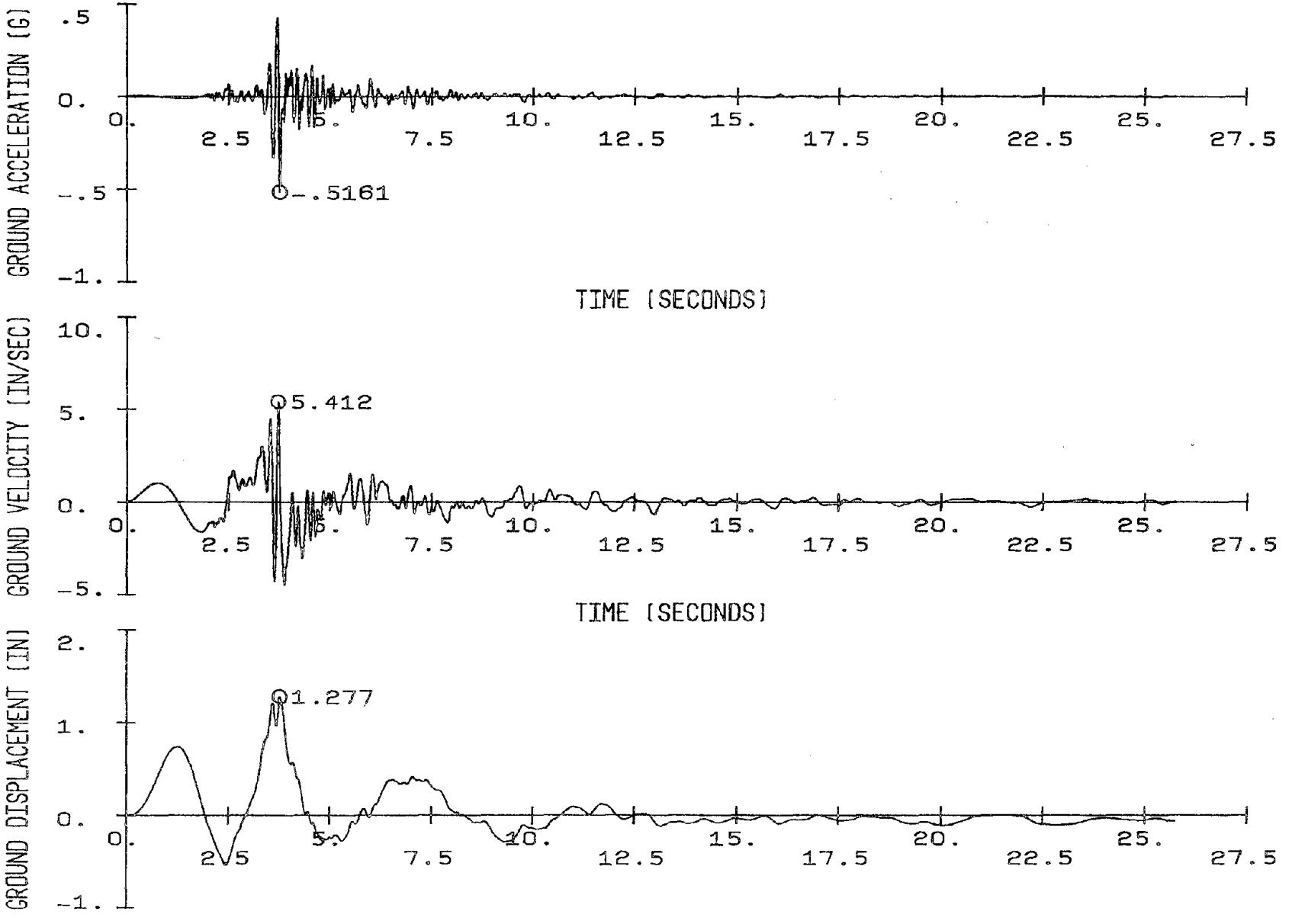

Fig. 3.22 Ground Motions for the Melendy Ranch Record of Sept. 4, 1972, Component N29W: With Prefixed Pulse

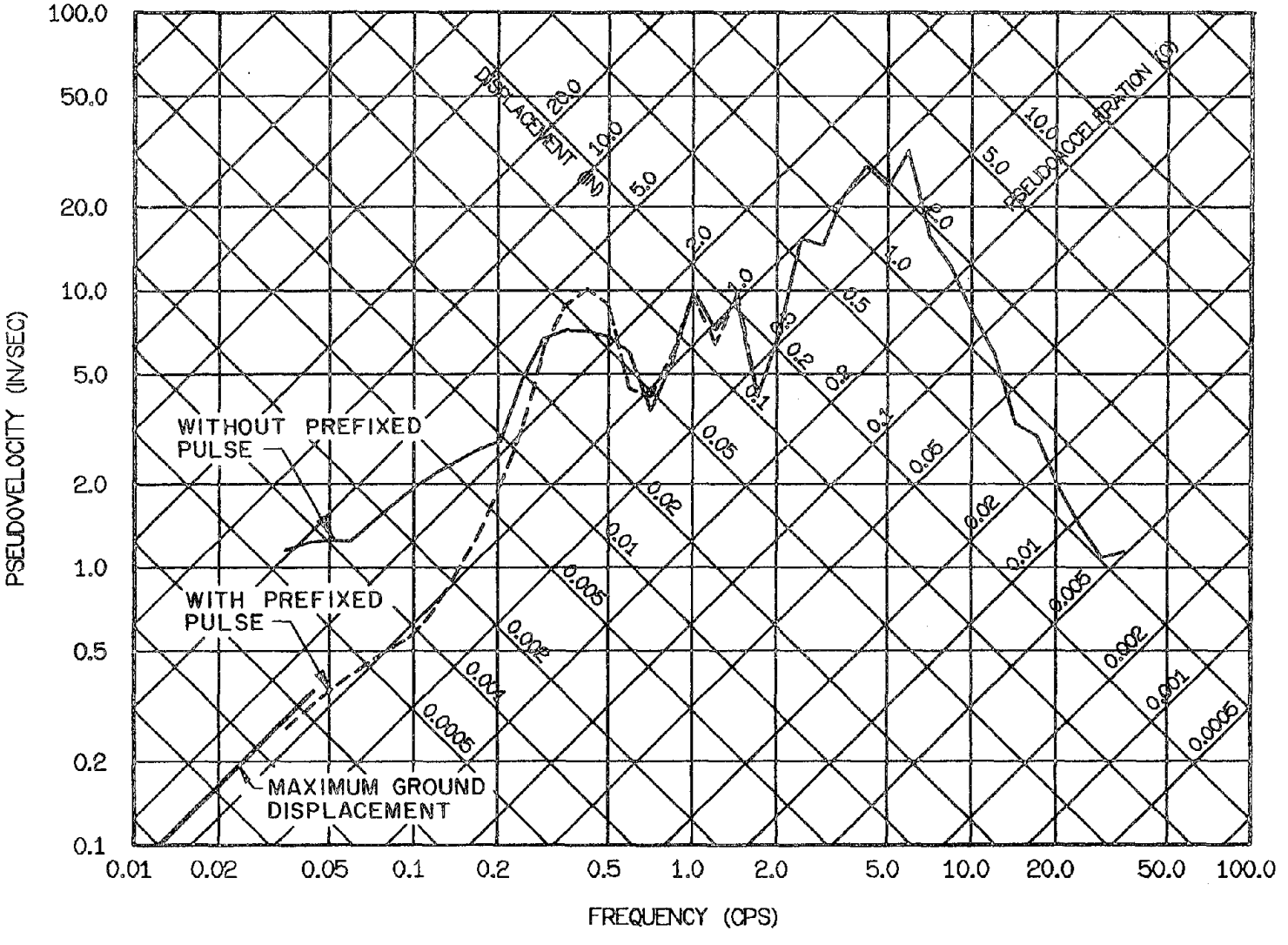

Fig. 3.23 Undamped Elastic Spectra for the Melendy Ranch Record of Sept. 4, 1972, Component N29W

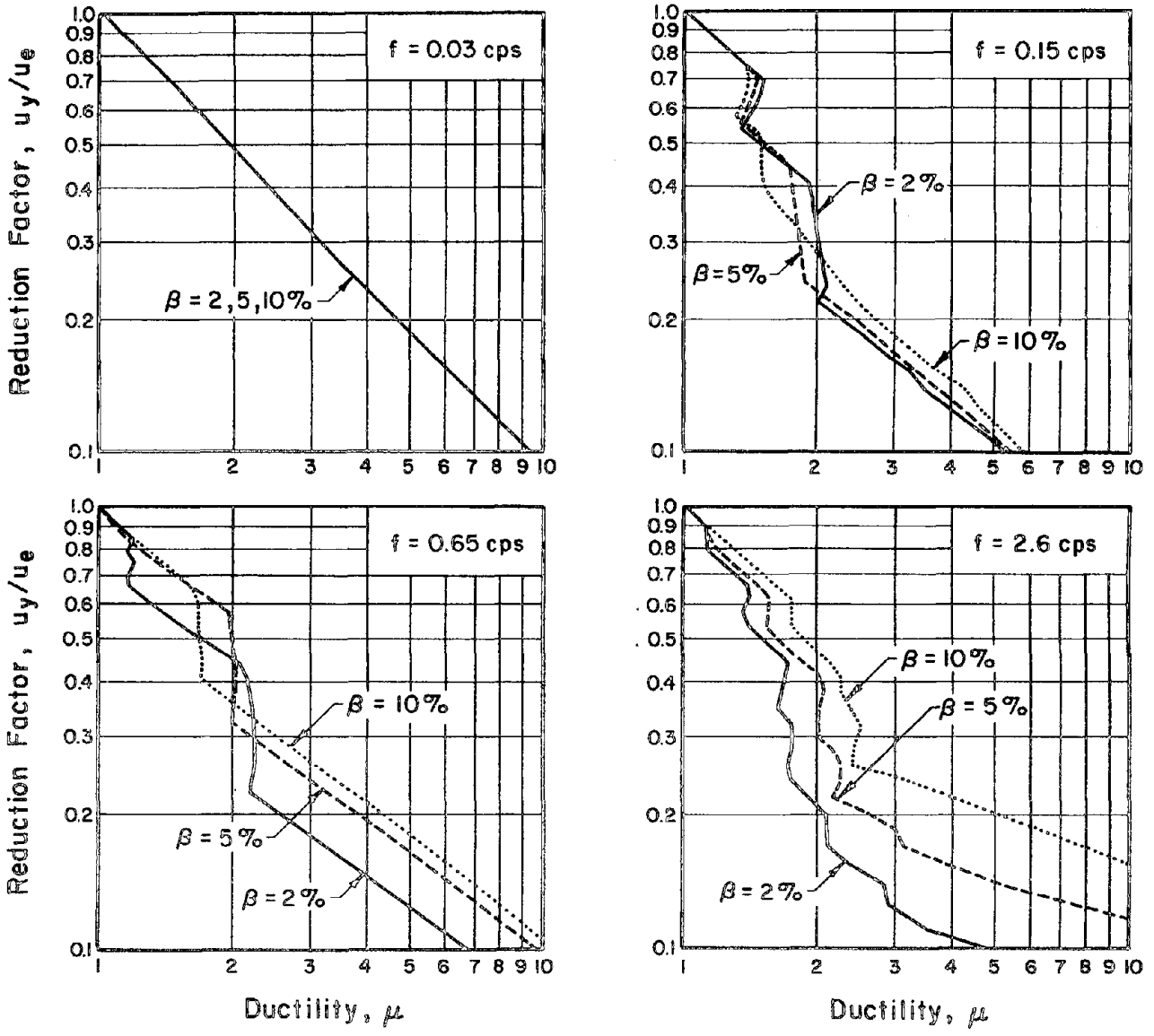

Fig. 3.24a Variation of Ductility with Yield Level for Elastoplastic Systems Subjected to the Pacoima Dam Record of Feb. 9, 1971, Component S16E

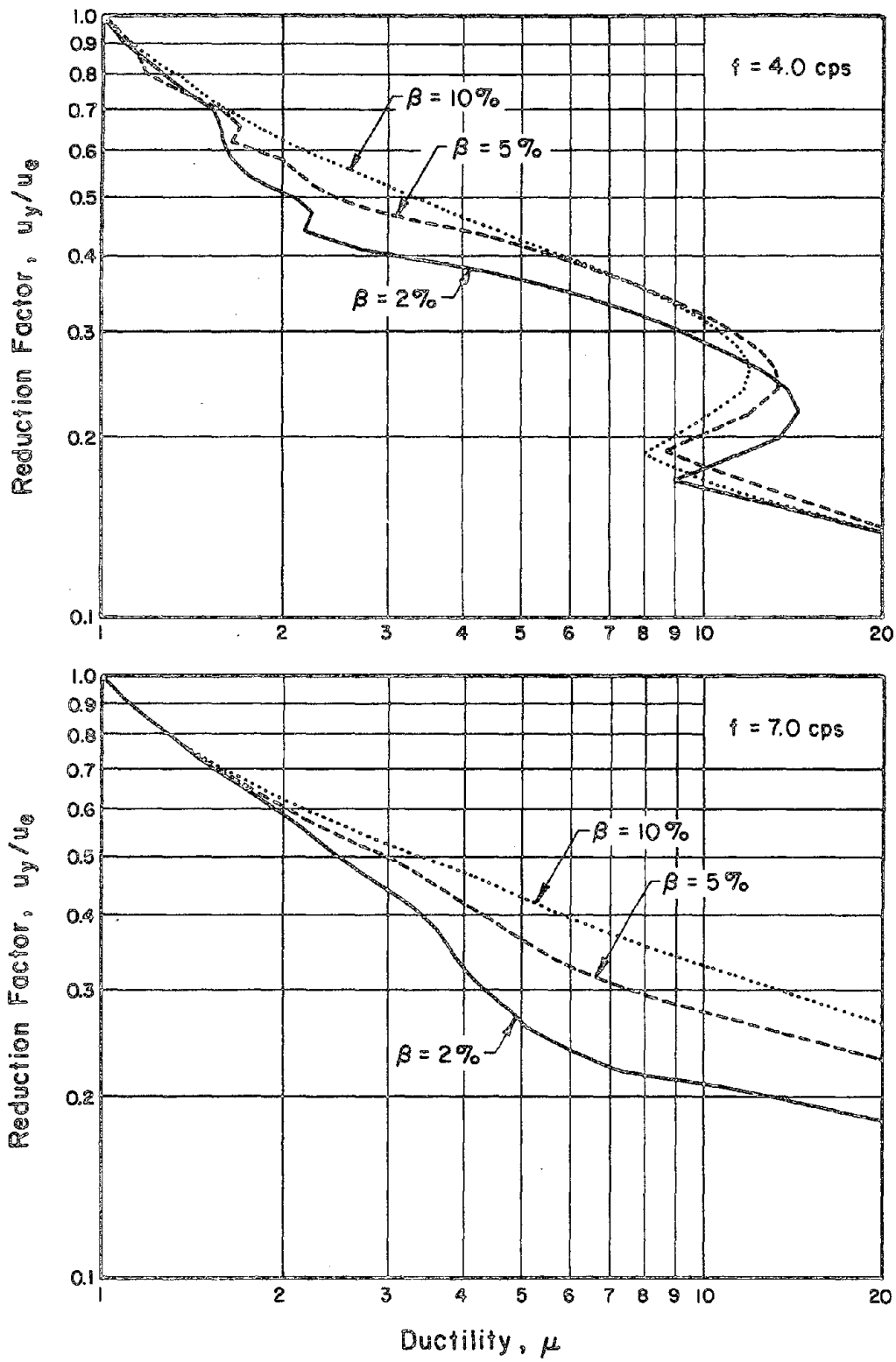

Fig. 3.24b Variation of Ductility with Yield Level for Elastoplastic Systems Subjected to the Pacoima Dam Record of Feb. 9, 1971, Component S16E

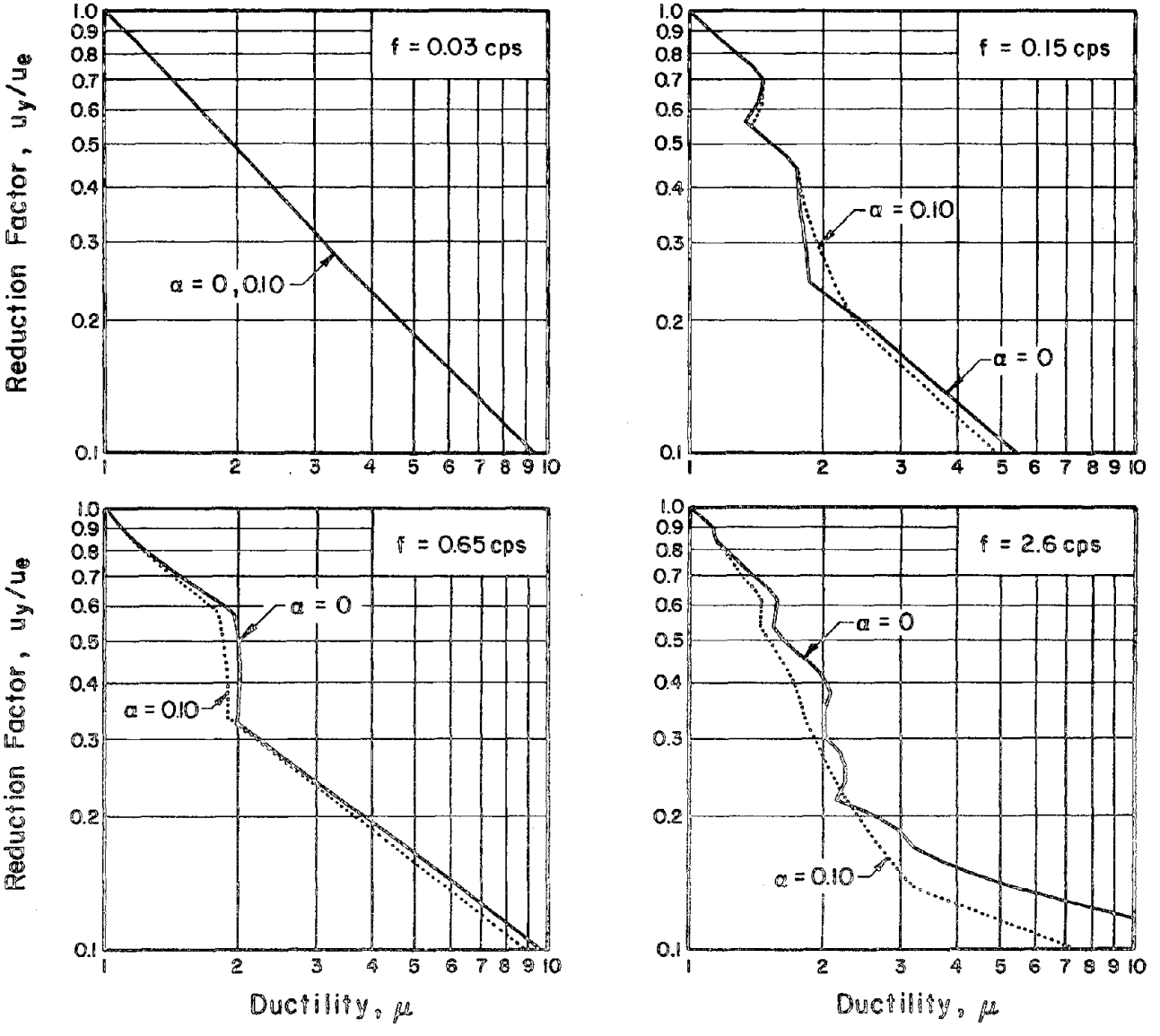

Fig. 3.25a Variation of Ductility with Yield Level for Bilinear Hysteretic Systems with 5% Damping Subjected to the Pacoima Dam Record of Feb. 9, 1971, Component S16E

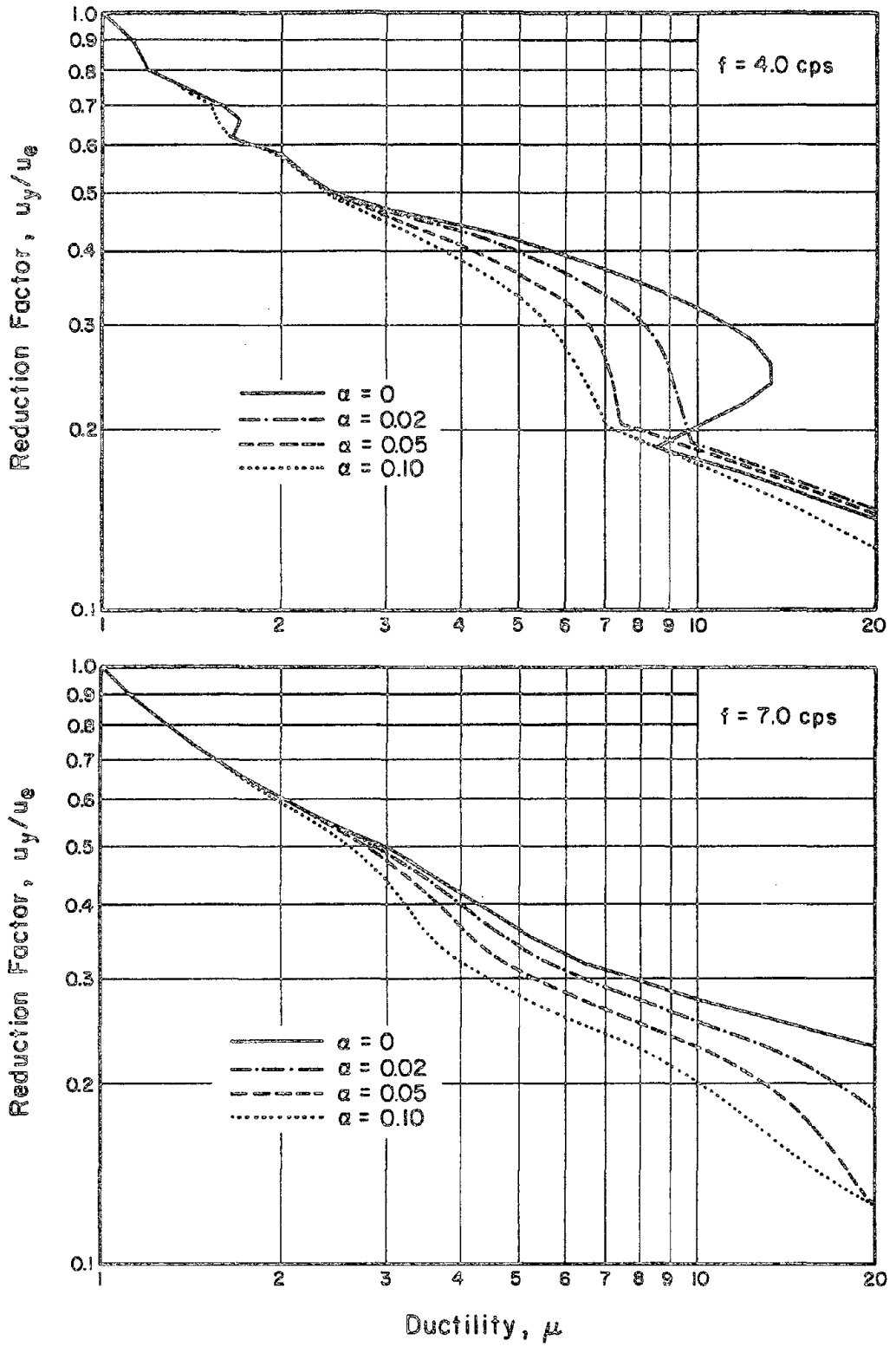

Fig. 3.25b Variation of Ductility with Yield Level for Bilinear Hysteretic Systems with 5% Damping Subjected to the Pacoima Dam Record of Feb. 9, 1971, Component S16E

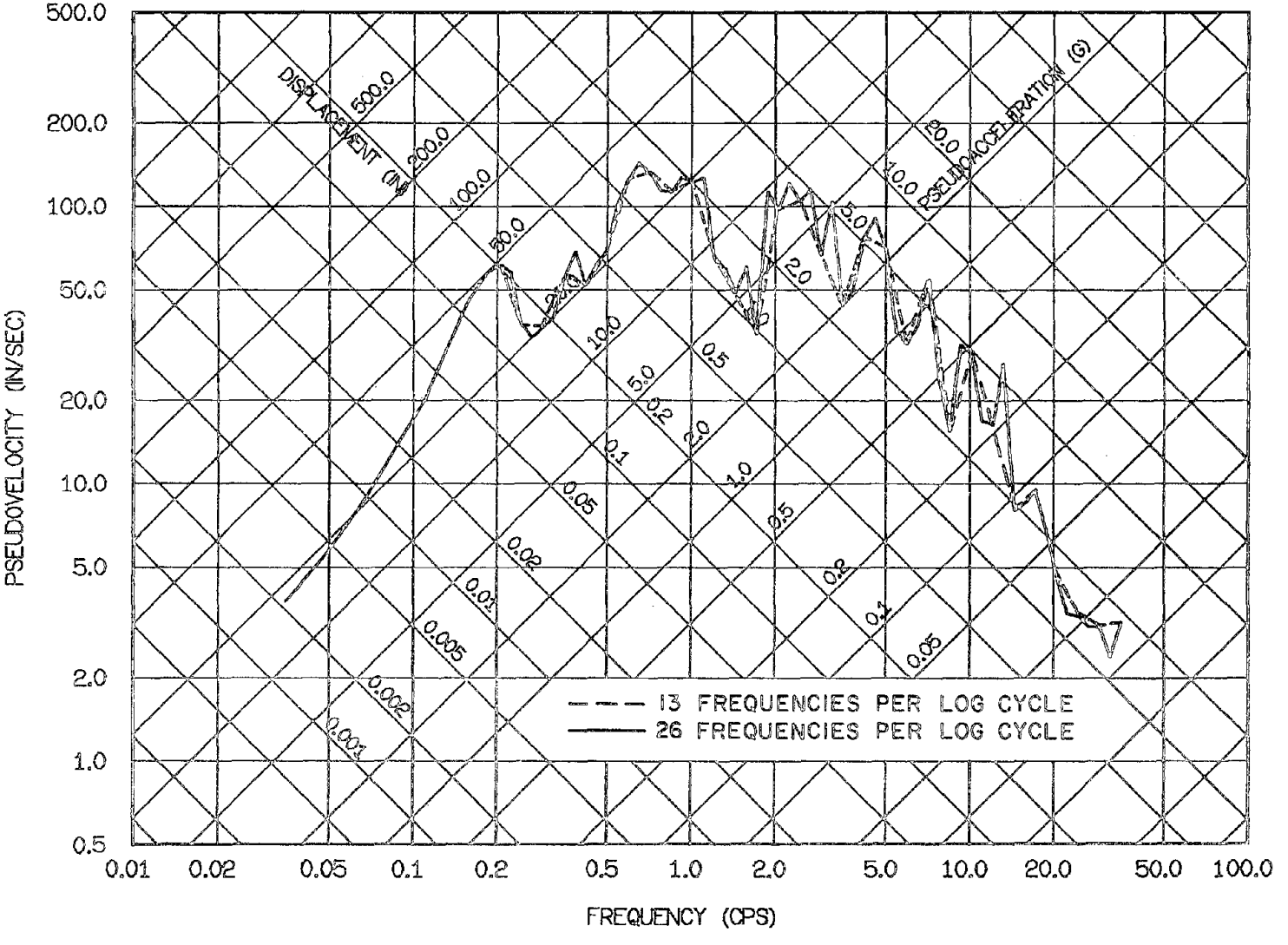

Fig. 3.26 Effect of Frequency Density on Elastic Spectra for the Pacoima Dam Record of Feb. 9, 1971, Component S16E: 0% Damping

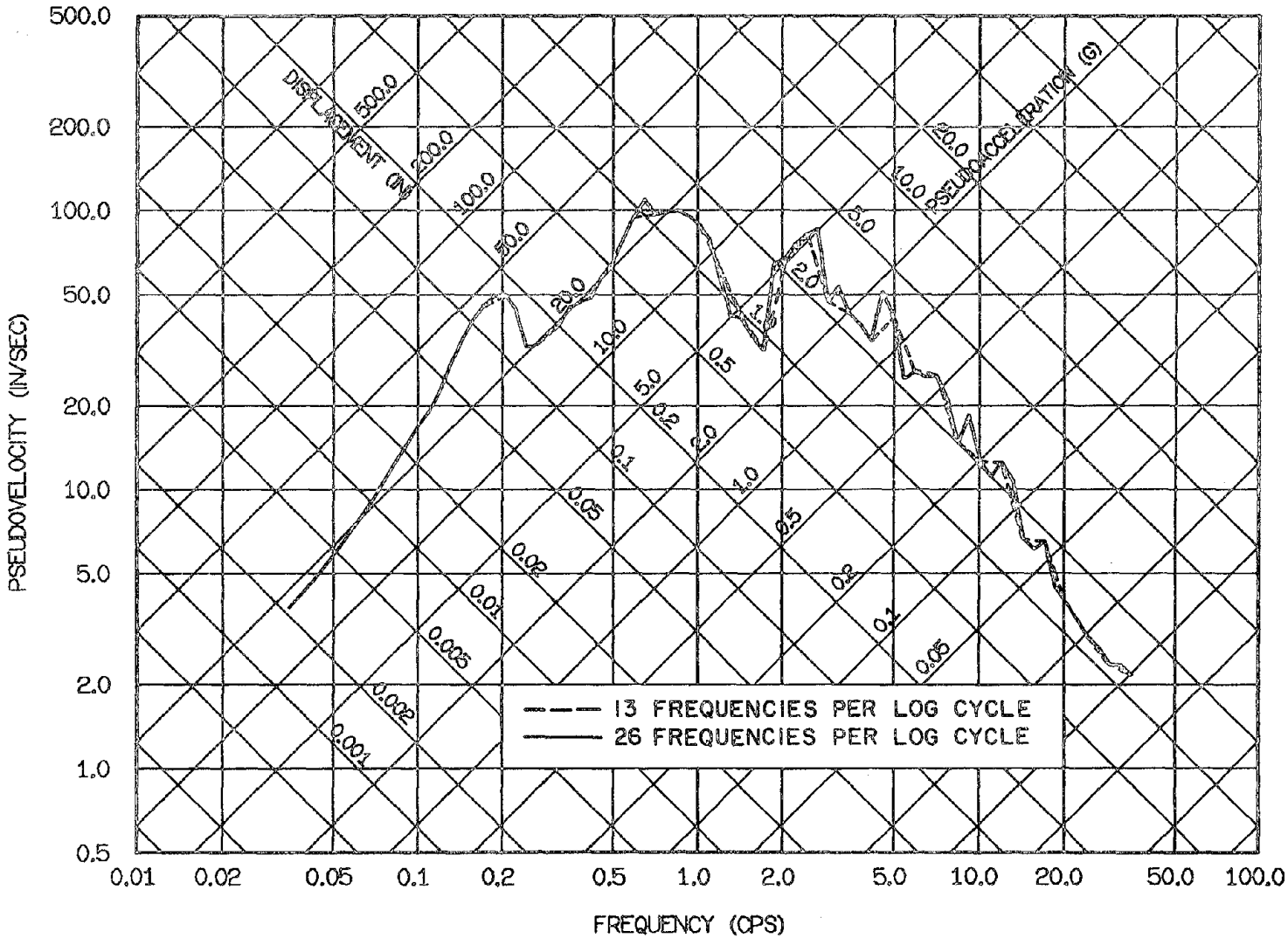

Fig. 3.27 Effect of Frequency Density on Elastic Spectra for the Pacoima Dam Record of Feb. 9, 1971, Component S16E: 2% Damping

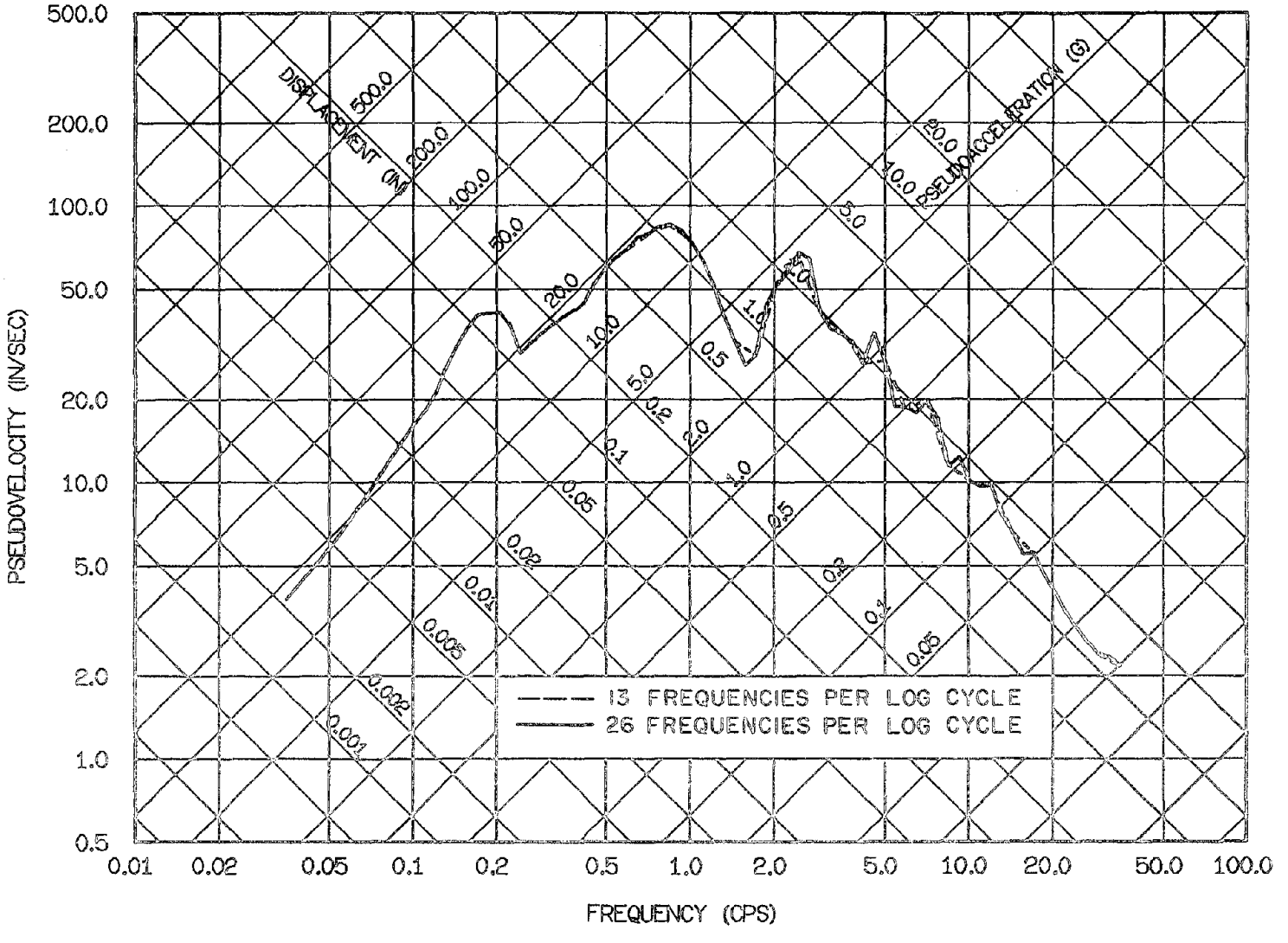

Fig. 3.28 Effect of Frequency Density on Elastic Spectra for the Pacoima Dam Record of Feb. 9, 1971, Component S16E: 5% Damping

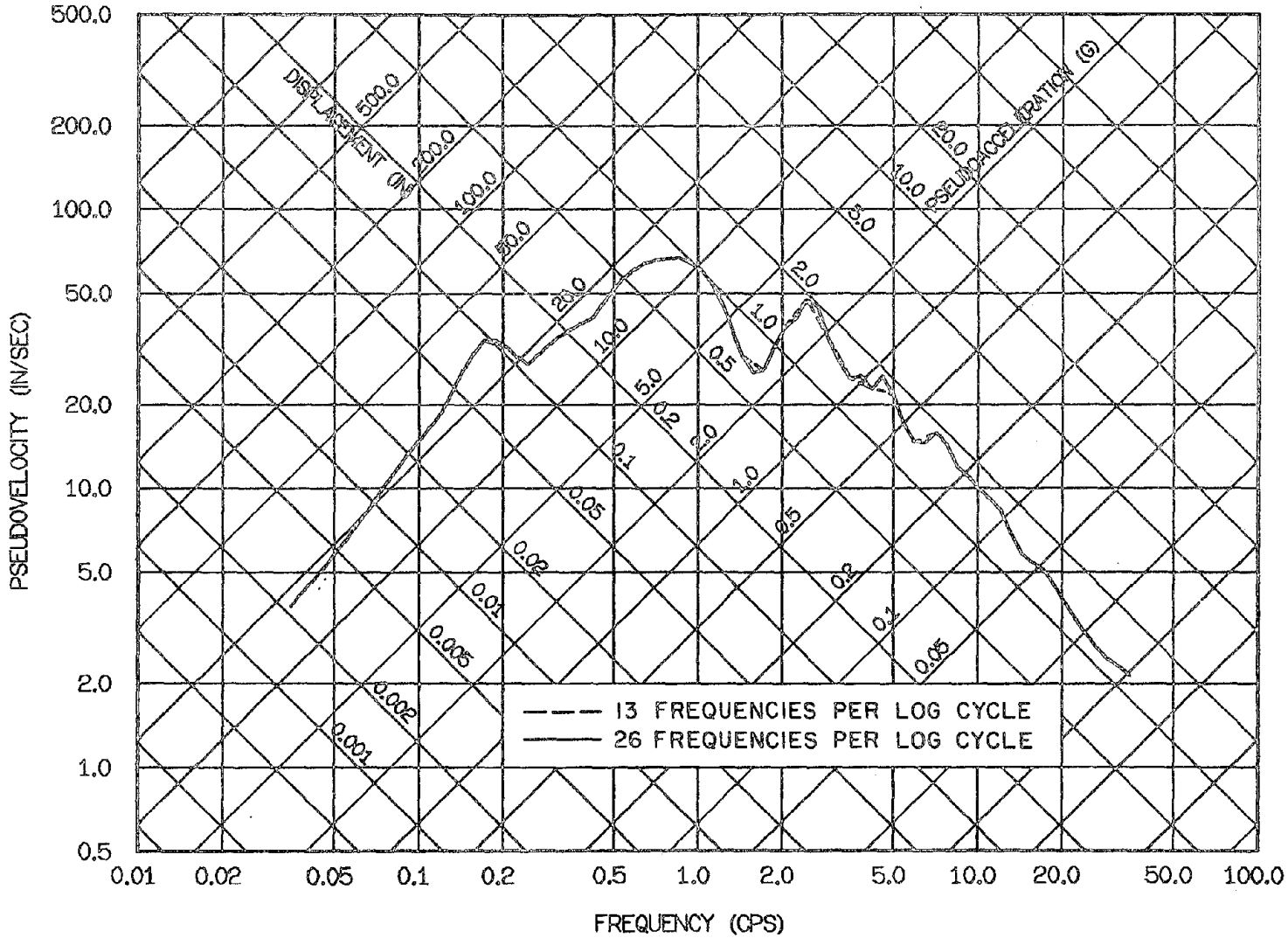

Fig. 3.29 Effect of Frequency Density on Elastic Spectra for the Pacoima Dam Record of Feb. 9, 1971, Component S16E: 10% Damping

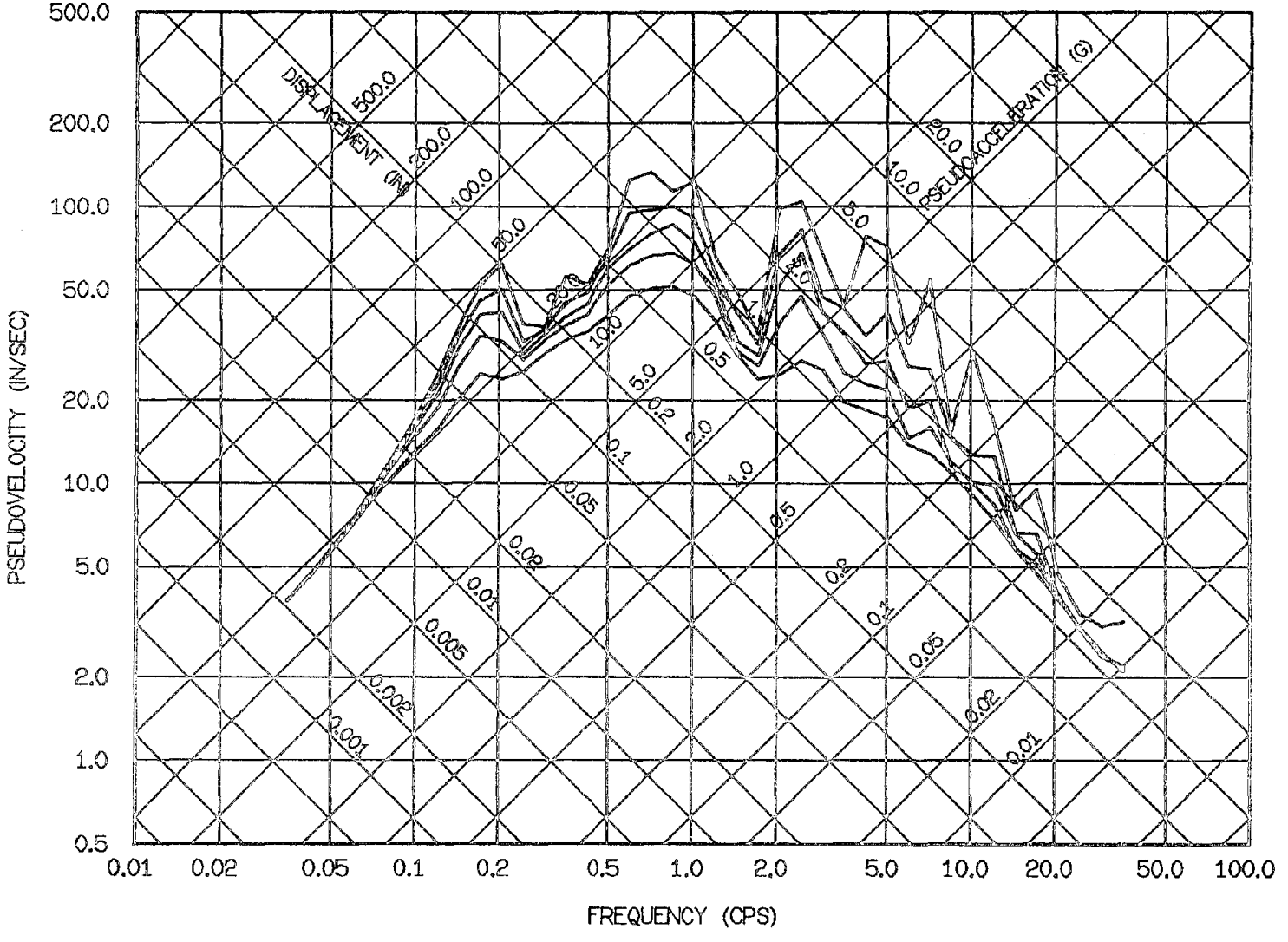

Fig. 3.30 Elastic Spectra for the Pacoima Dam Record of Feb. 9, 1971, Component S16E: 0, 2, 5, 10, and 20% Damping

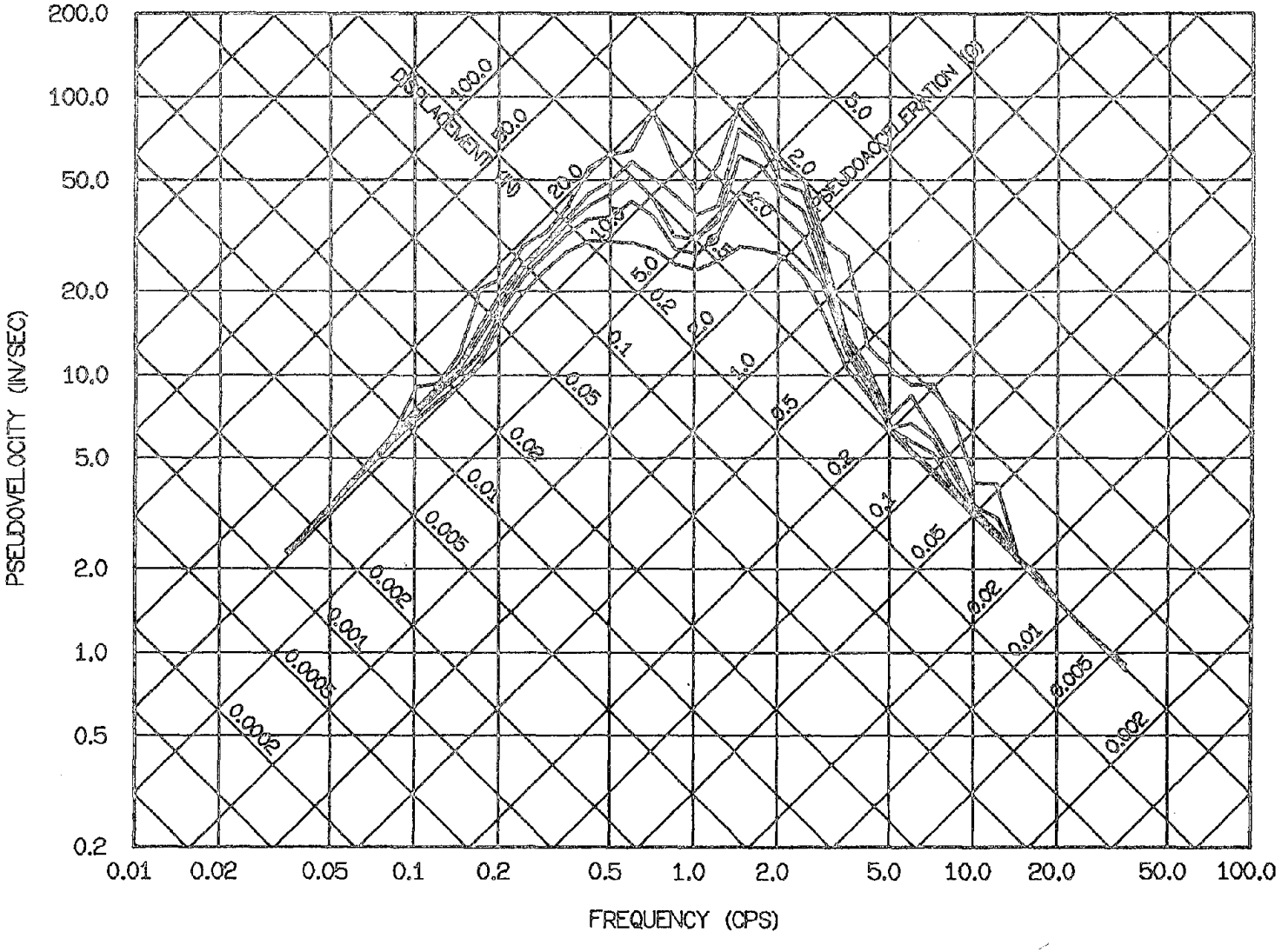

Fig. 3.31 Elastic Spectra for the Cholame-Shandon No. 2 Record of June 27, 1966, Component N65E: 0, 2, 5, 10, and 20% Damping

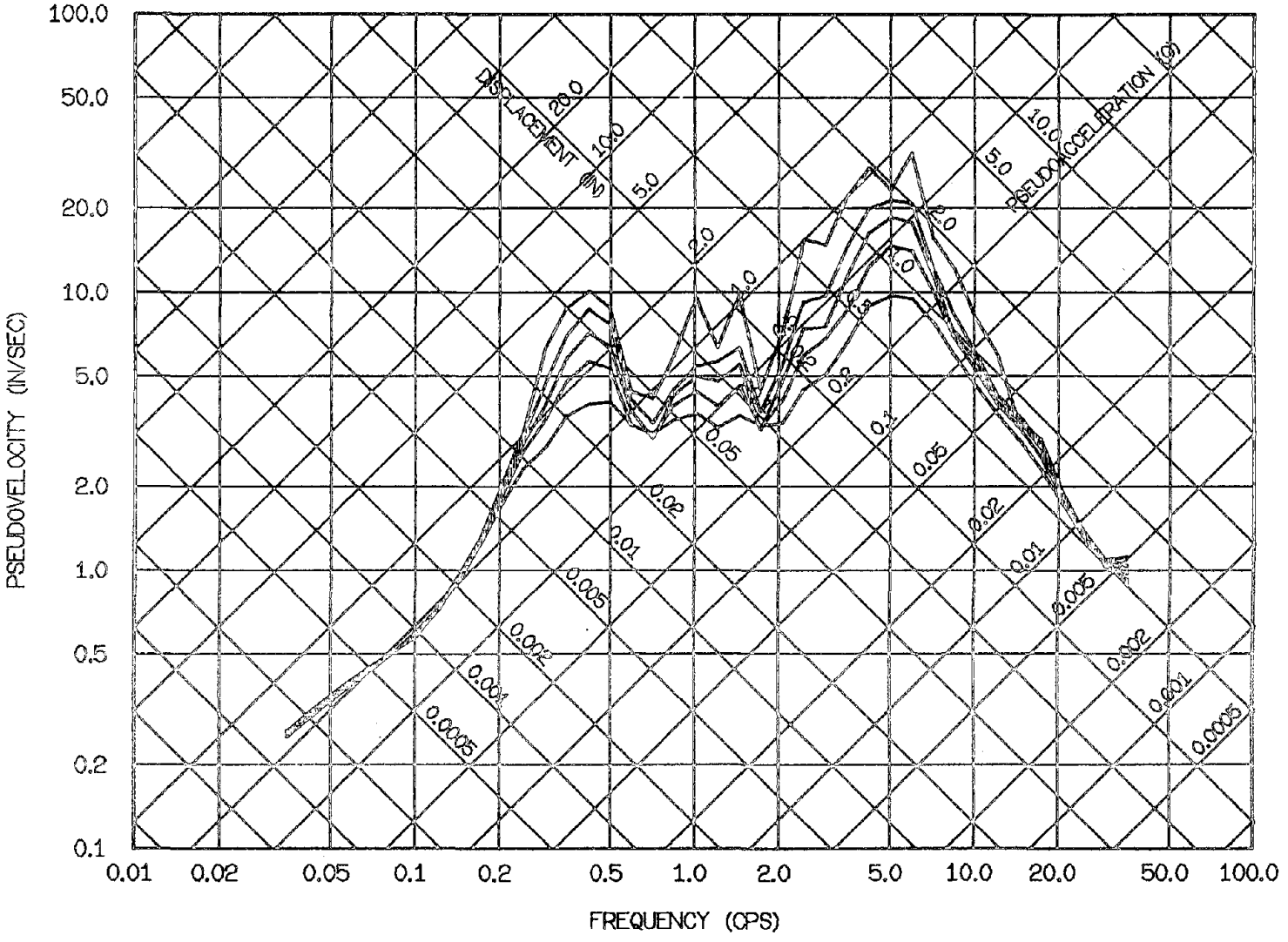

Fig. 3.32 Elastic Spectra for the Melendy Ranch Record of Sept. 4, 1972, Component N29W: 0, 2, 5, 10, and 20% Damping

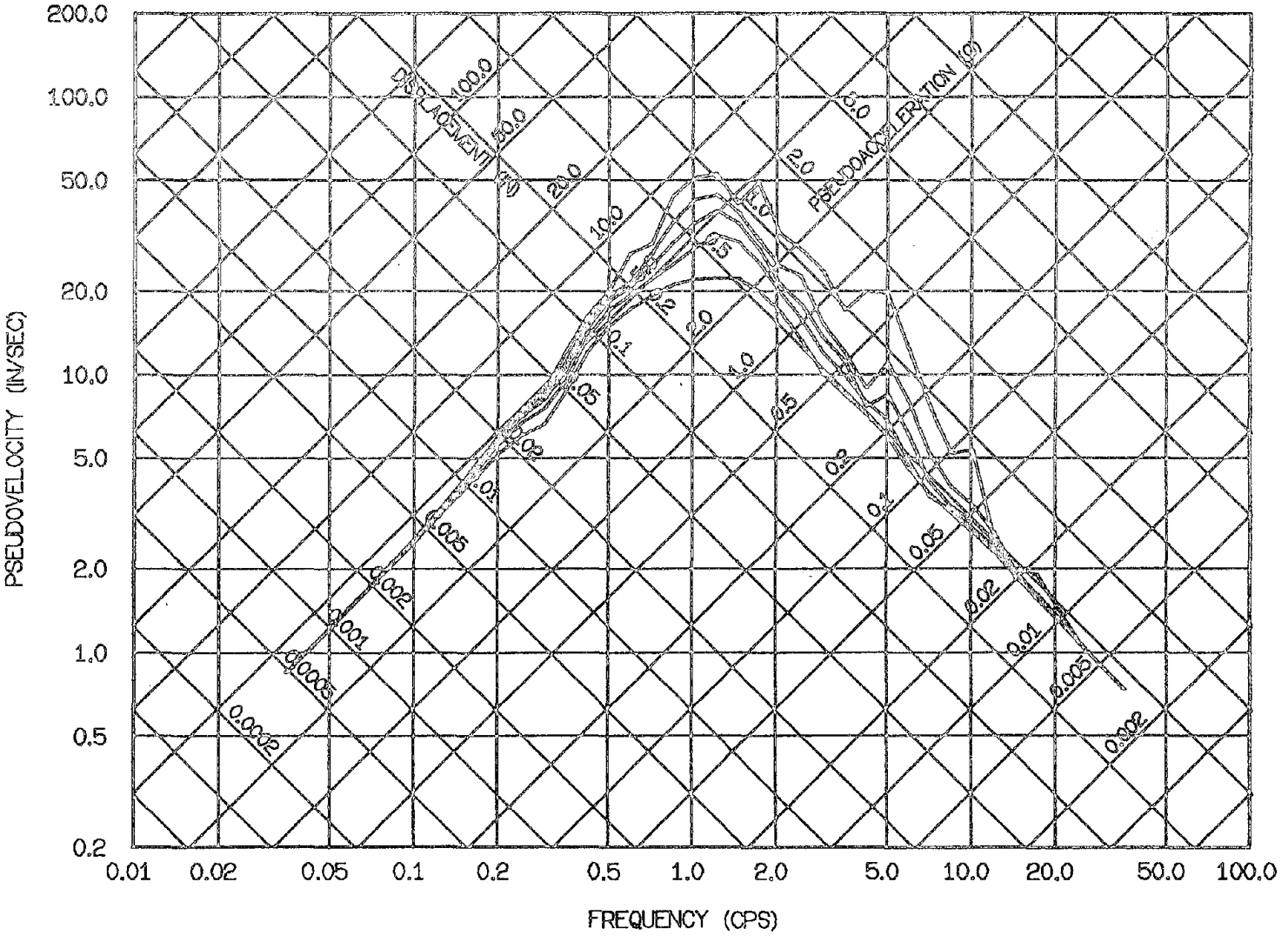

Fig. 3.33 Elastic Spectra for the Gilroy Array No. 6 Record of Aug. 6, 1979, Component 230 Deg: 0, 2, 5, 10, and 20% Damping

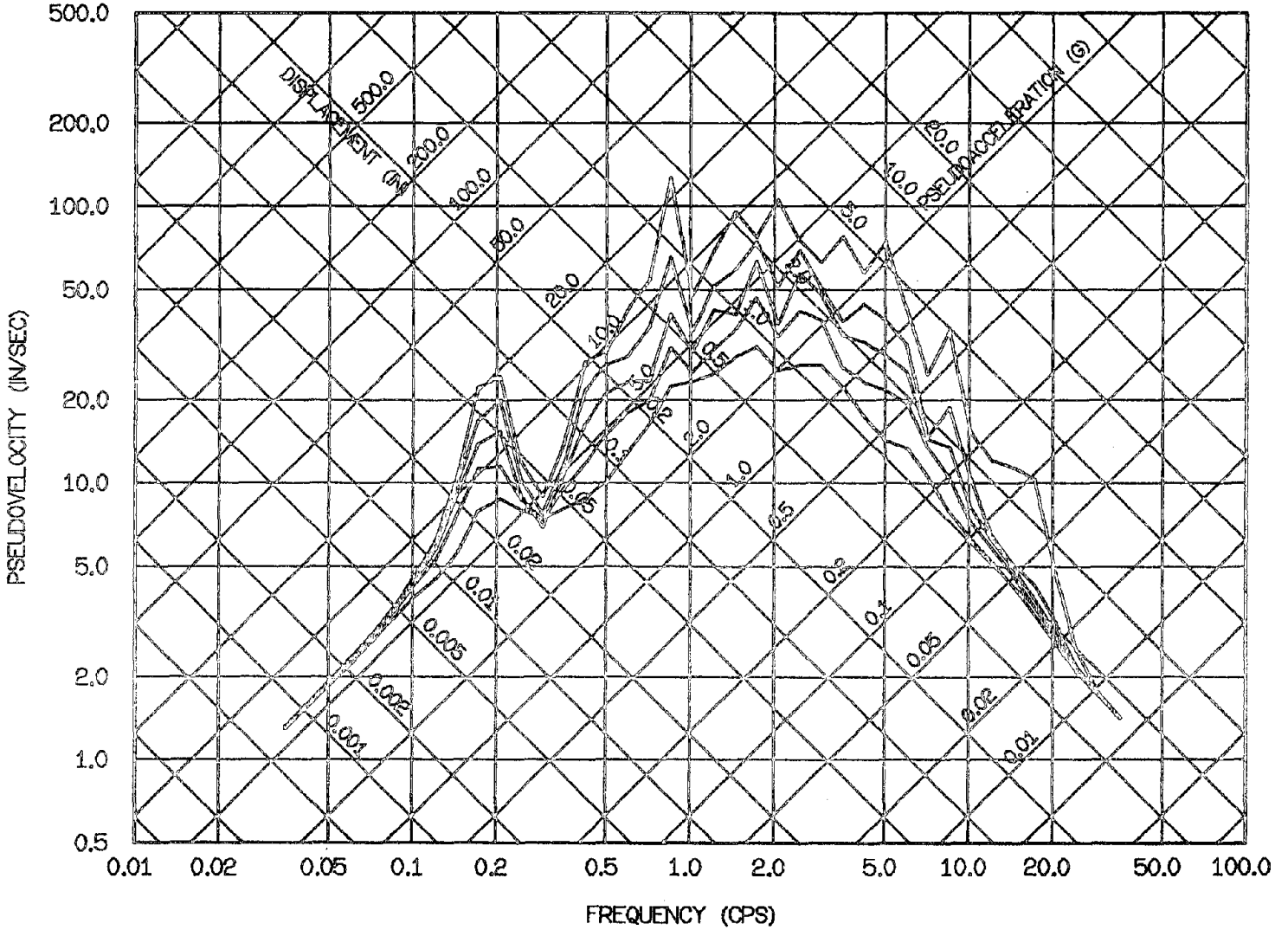

Fig. 3.34 Elastic Spectra for the Bonds Corner Record of Oct. 15, 1979, Component 230 Deg: 0, 2, 5, 10, and 20% Damping

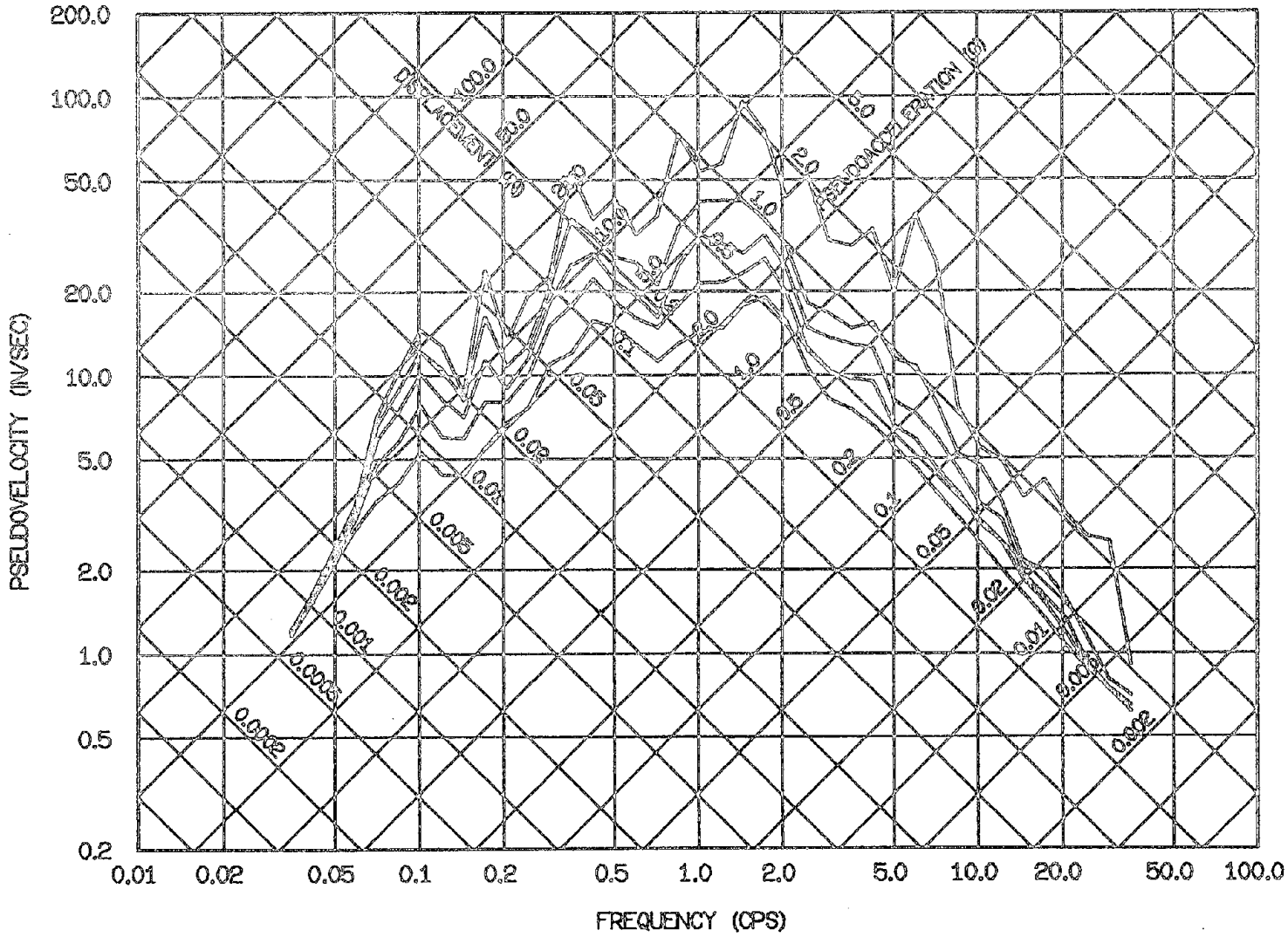

Fig. 3.35 Elastic Spectra for the El Centro Record of May 18, 1940, Component S00E: 0, 2, 5, 10, and 20% Damping

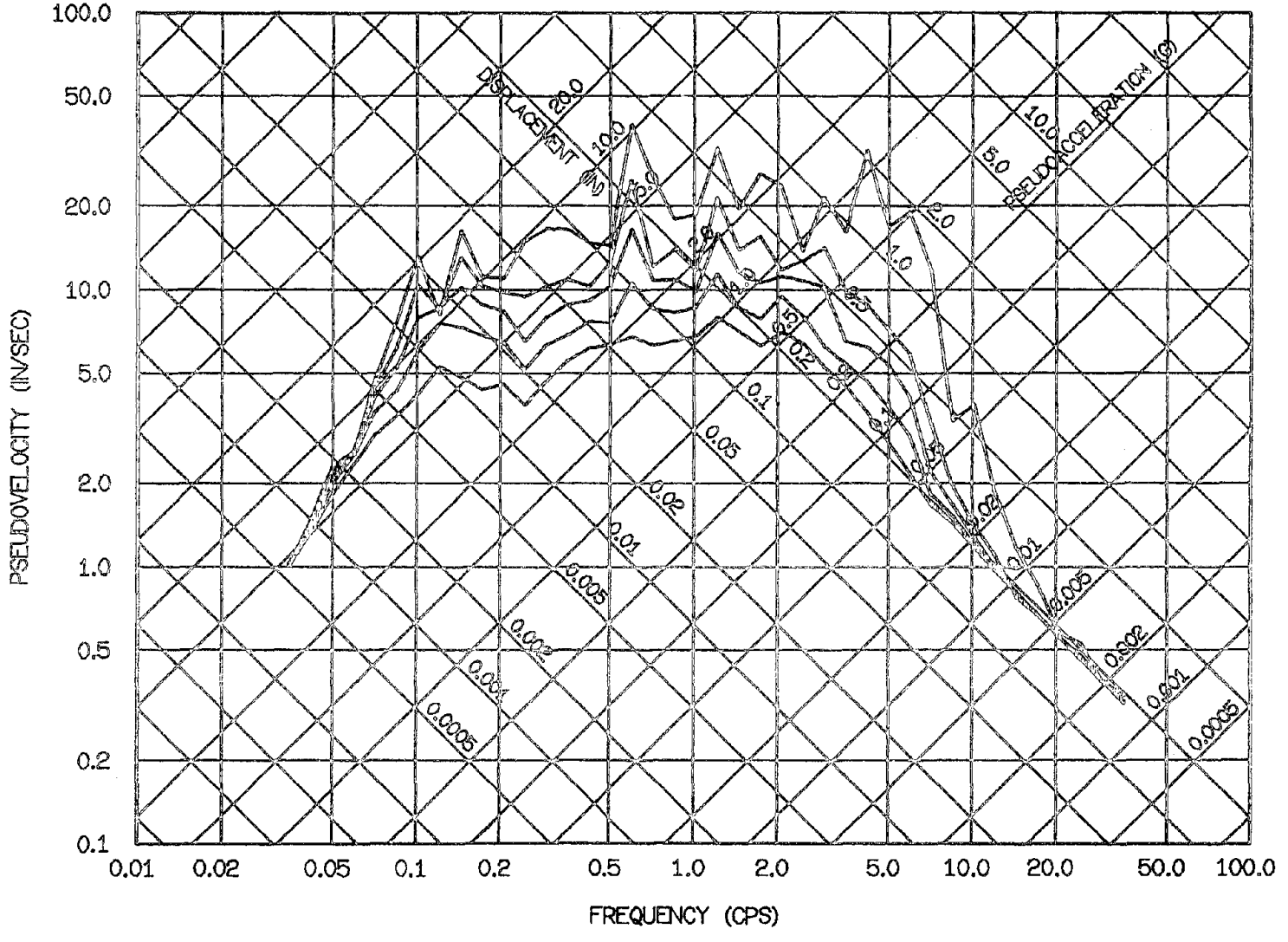

Fig. 3.36 Elastic Spectra for the Taft Record of July 21, 1952, Component S69E: 0, 2, 5, 10, and 20% Damping

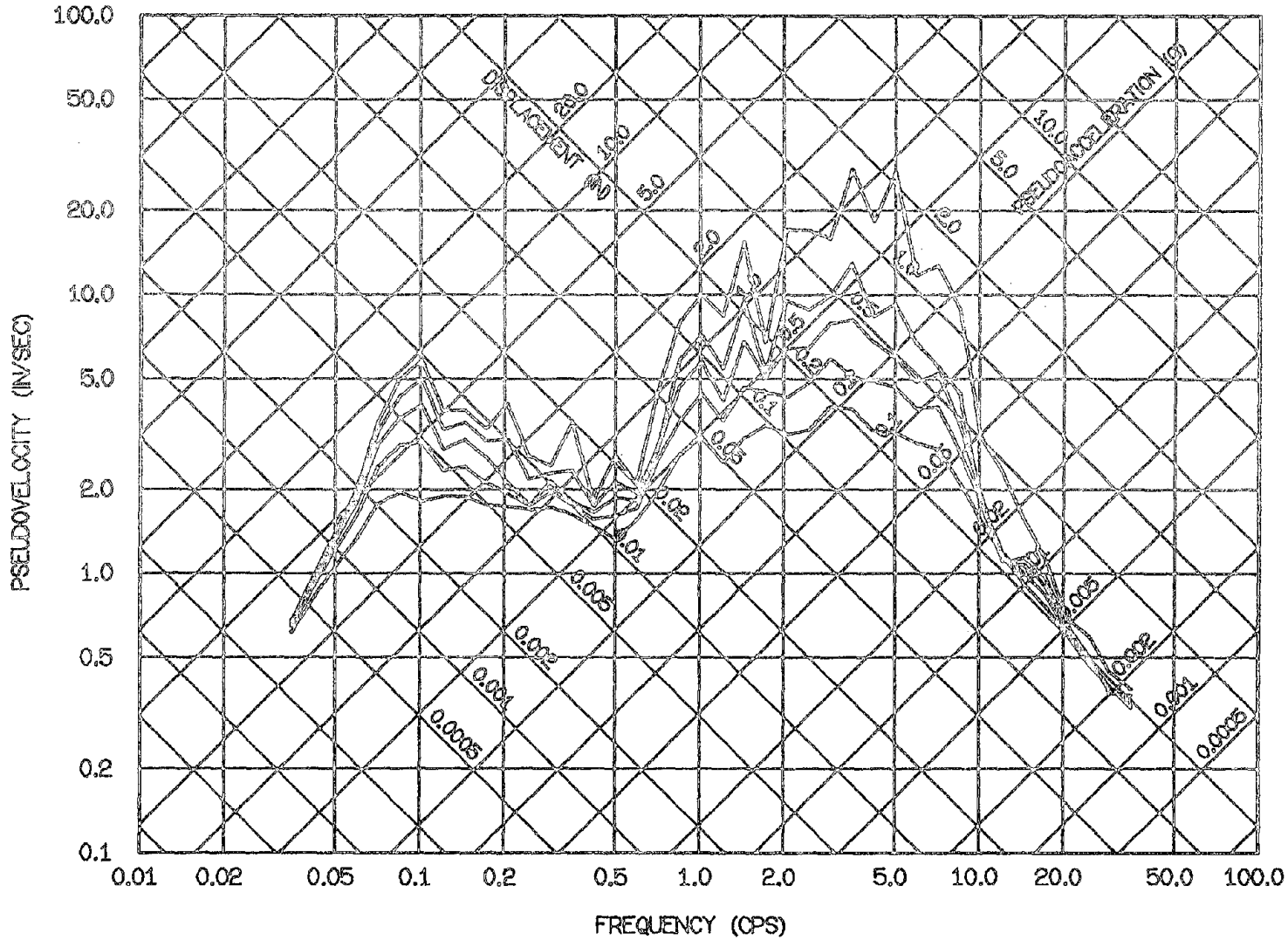

Fig. 3.37 Elastic Spectra for the Adak, Alaska Record of May 1, 1971, Component West: 0, 2, 5, 10, and 20% Damping

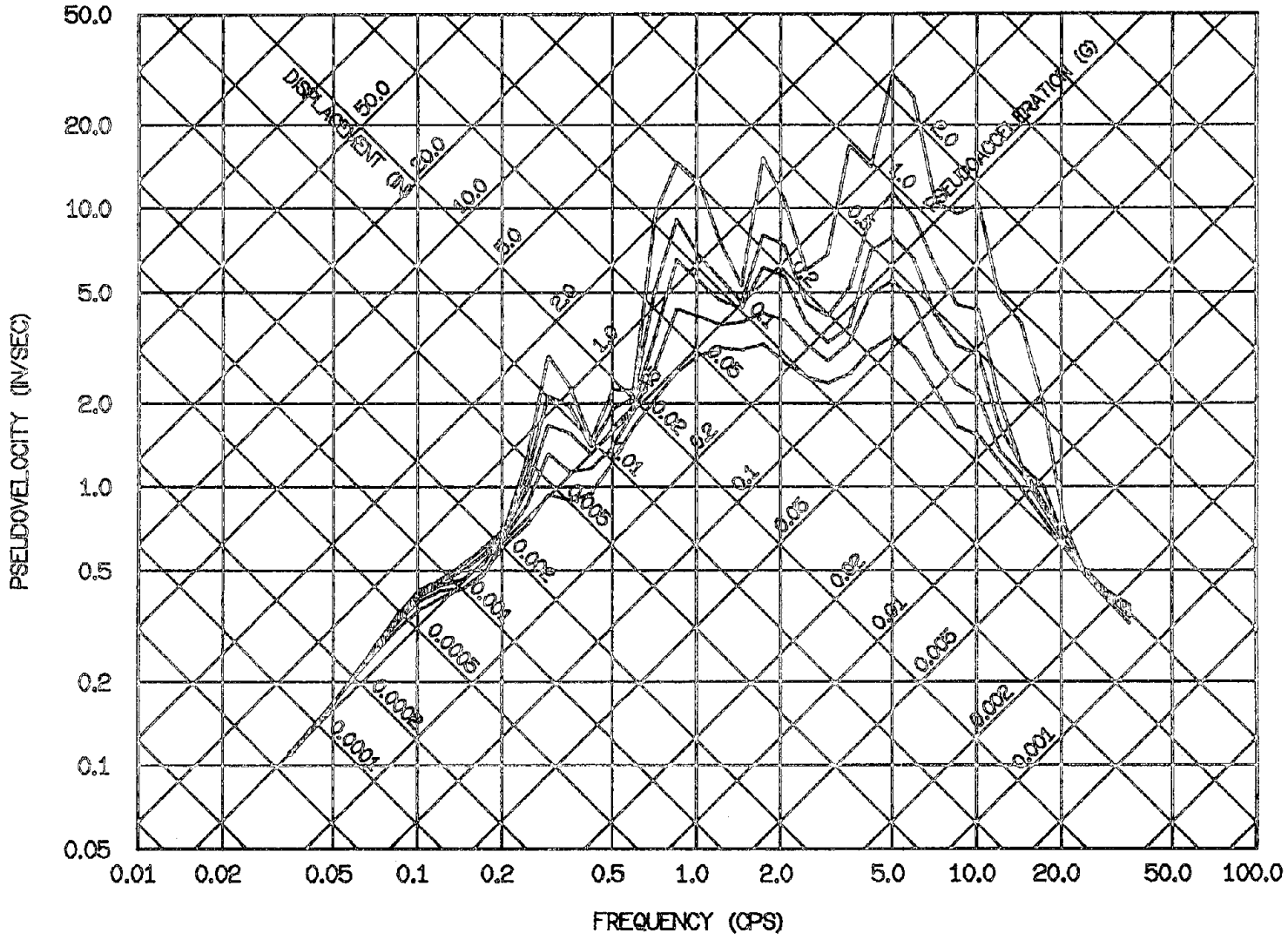

Fig. 3.38 Elastic Spectra for the Kilauea, Hawaii Record of April 26, 1973, Component S30W: 0, 2, 5, 10, and 20% Damping

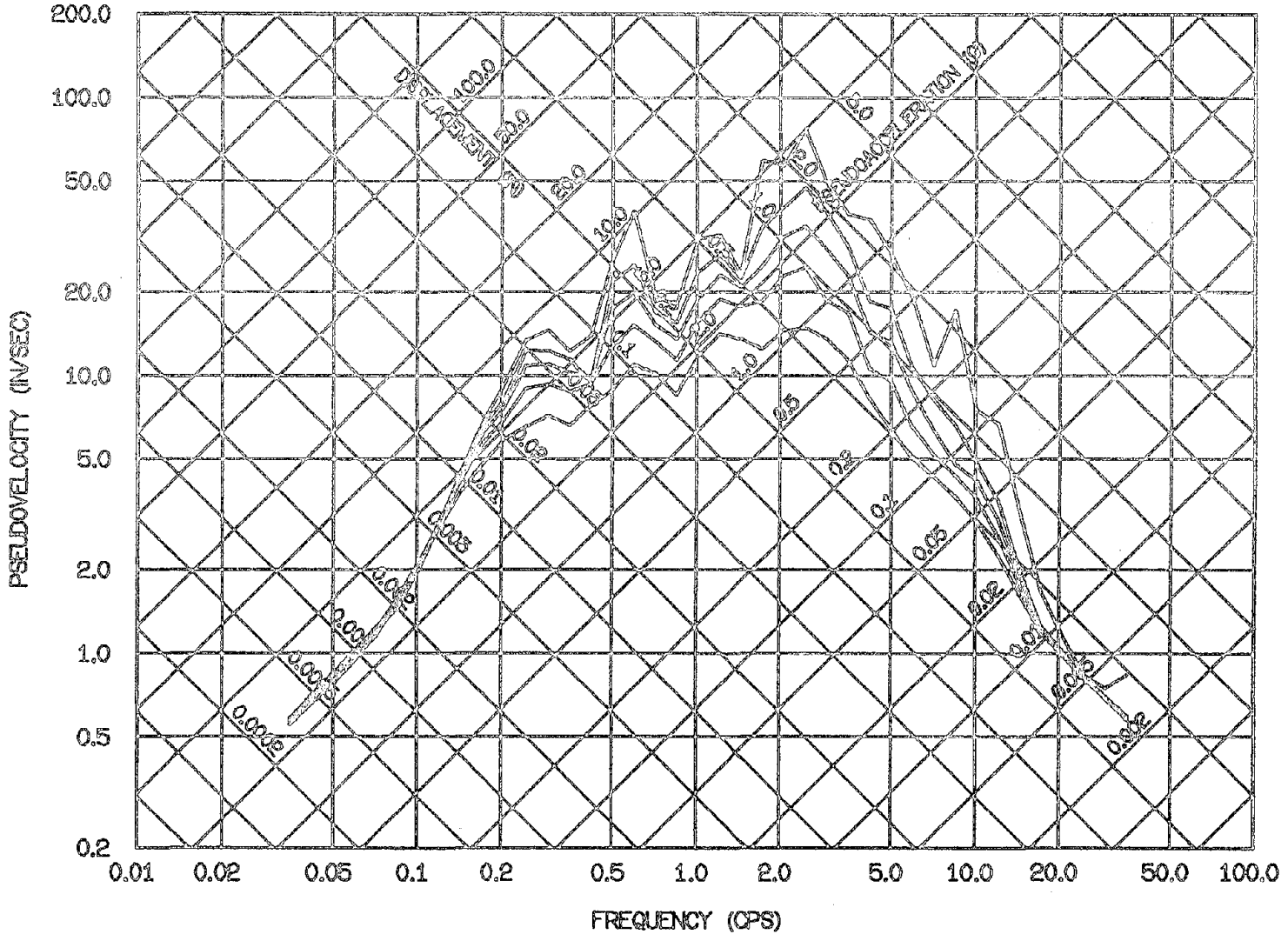

Fig. 3.39 Elastic Spectra for the Managua Record of Dec. 23, 1972, Component South: 0, 2, 5, 10, and 20% Damping

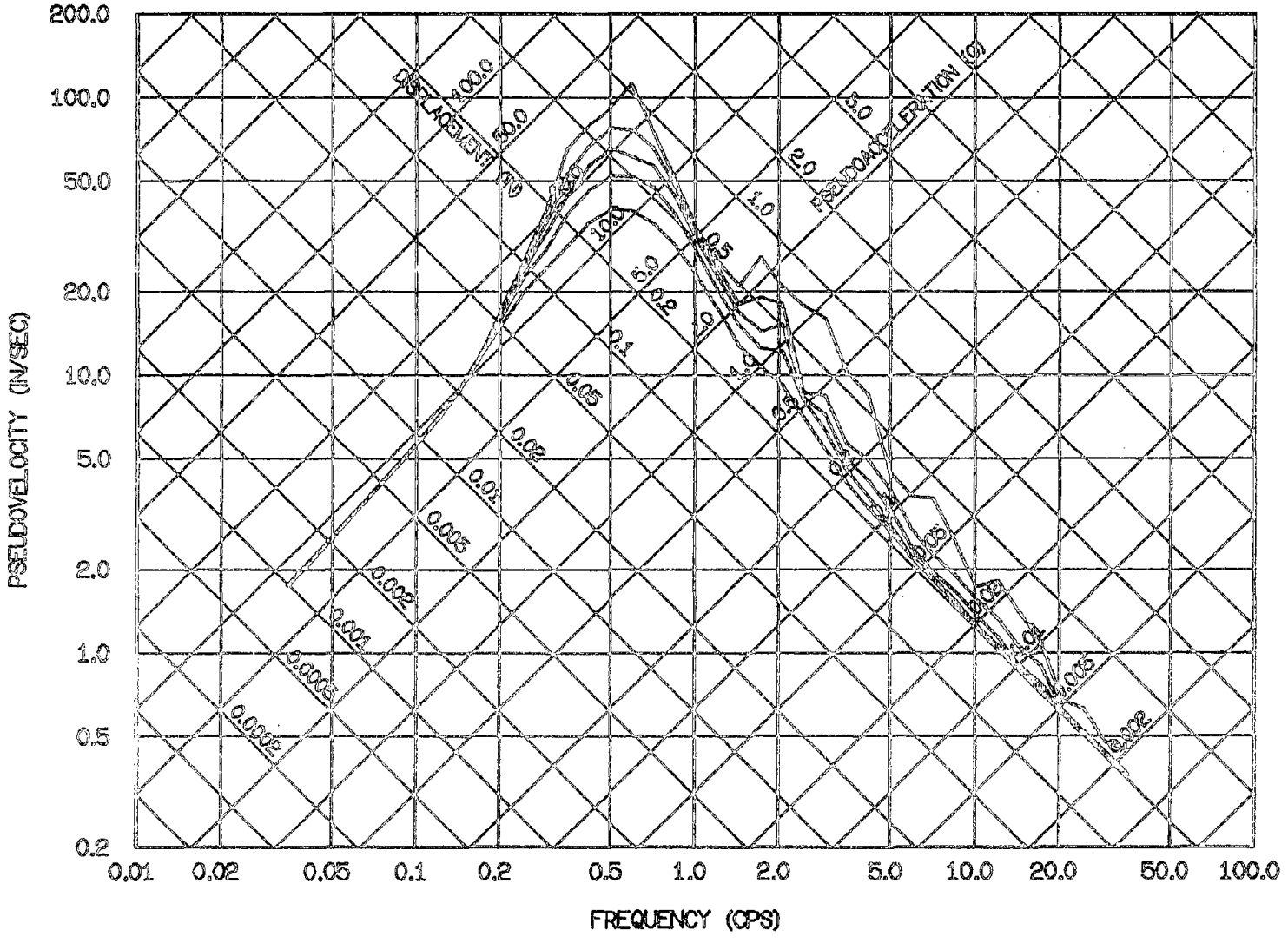

Fig. 3.40 Elastic Spectra for the Bucarest Record of Mar. 4, 1977, Component S-N: 0, 2, 5, 10, and 20% Damping

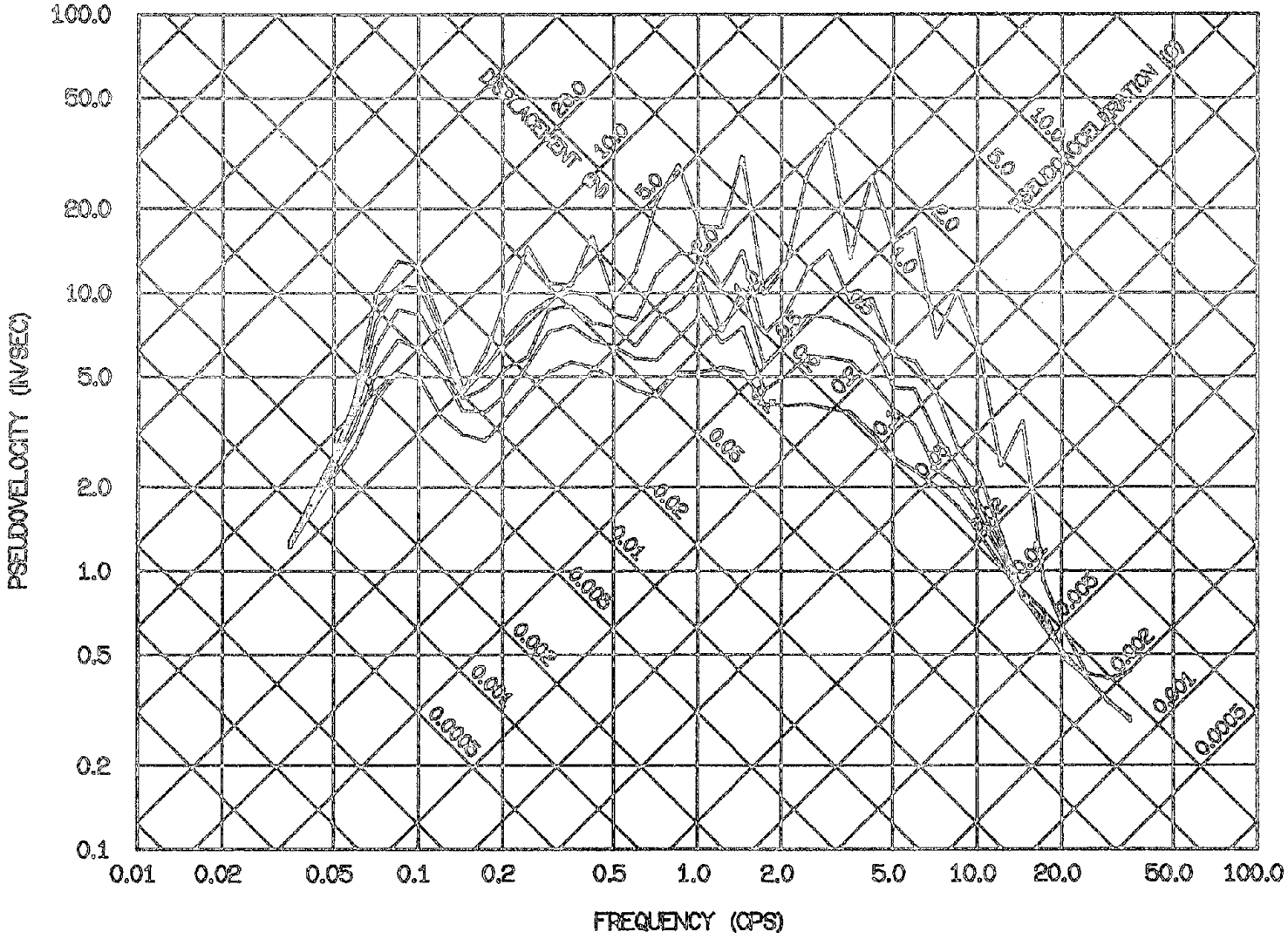

Fig. 3.41 Elastic Spectra for the Santiago Record of July 8, 1971, Component N10W: 0, 2, 5, 10, and 20% Damping

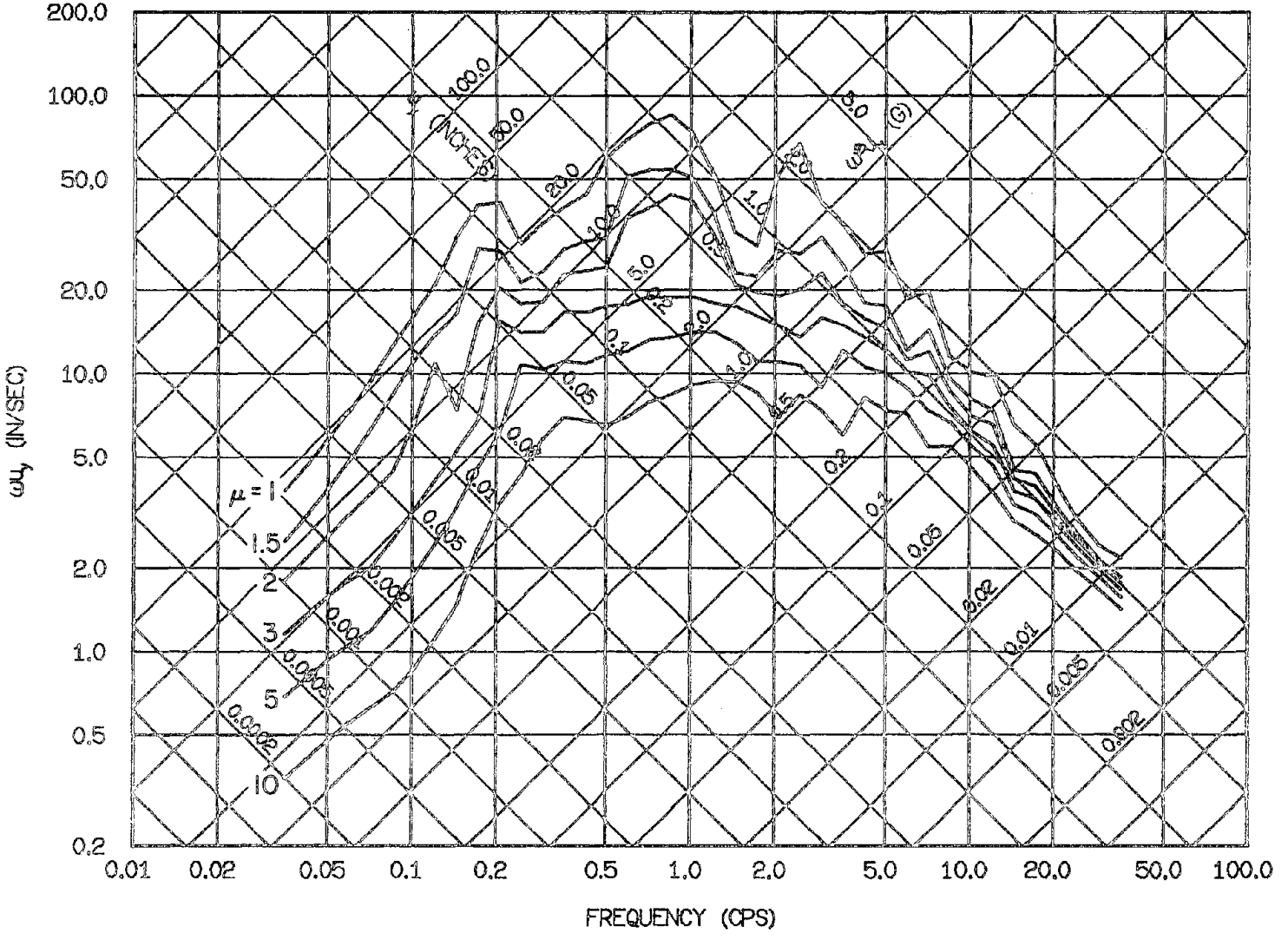

Fig. 3.42 Elastoplastic Yield Spectra for the Pacoima Dam Record of Feb. 9, 1971, Component S16E: 5% Damping

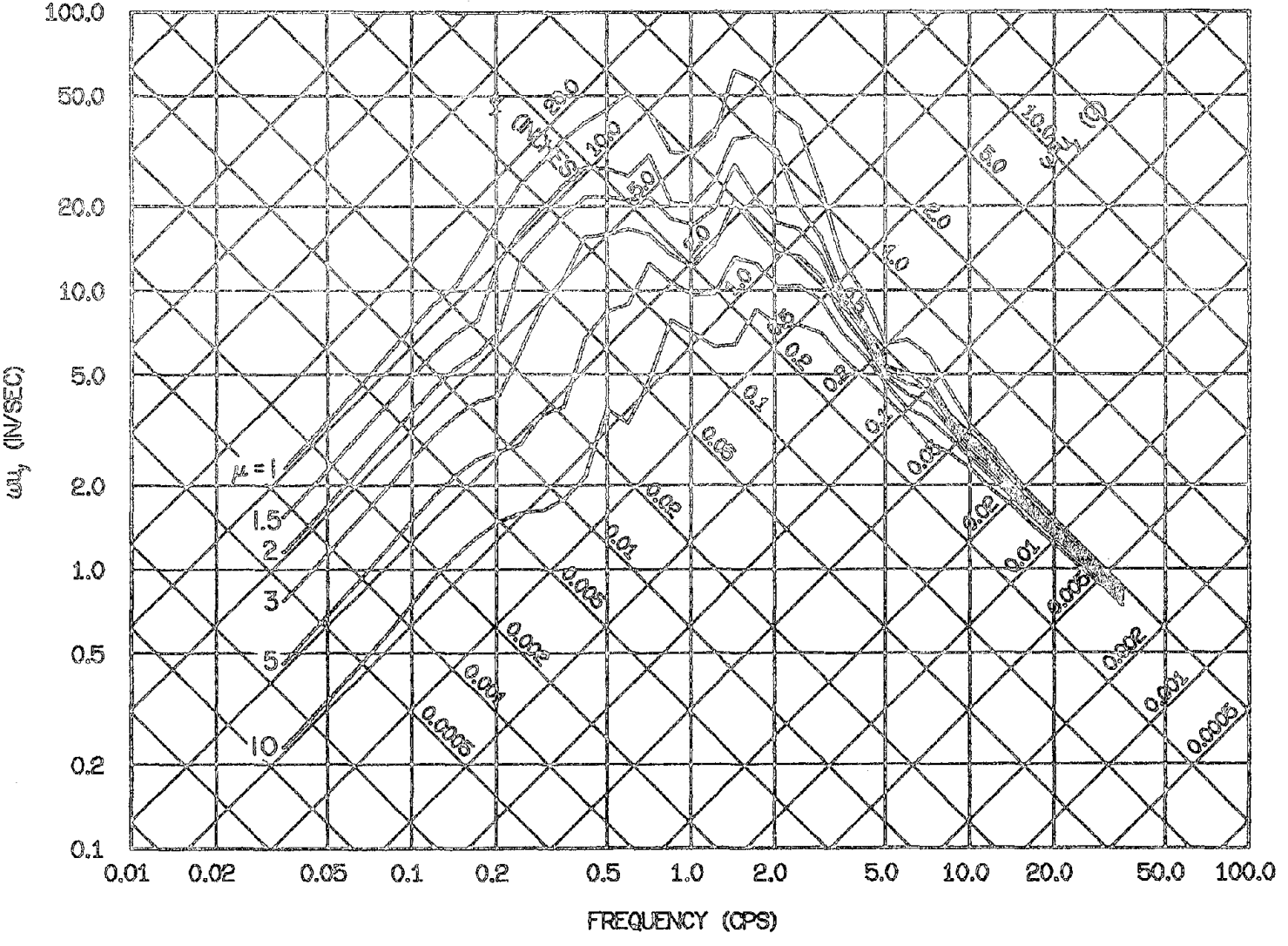

Fig. 3.43 Elastoplastic Yield Spectra for the Cholame-Shandon No. 2 Record of June 27, 1966, Component N65E: 5% Damping

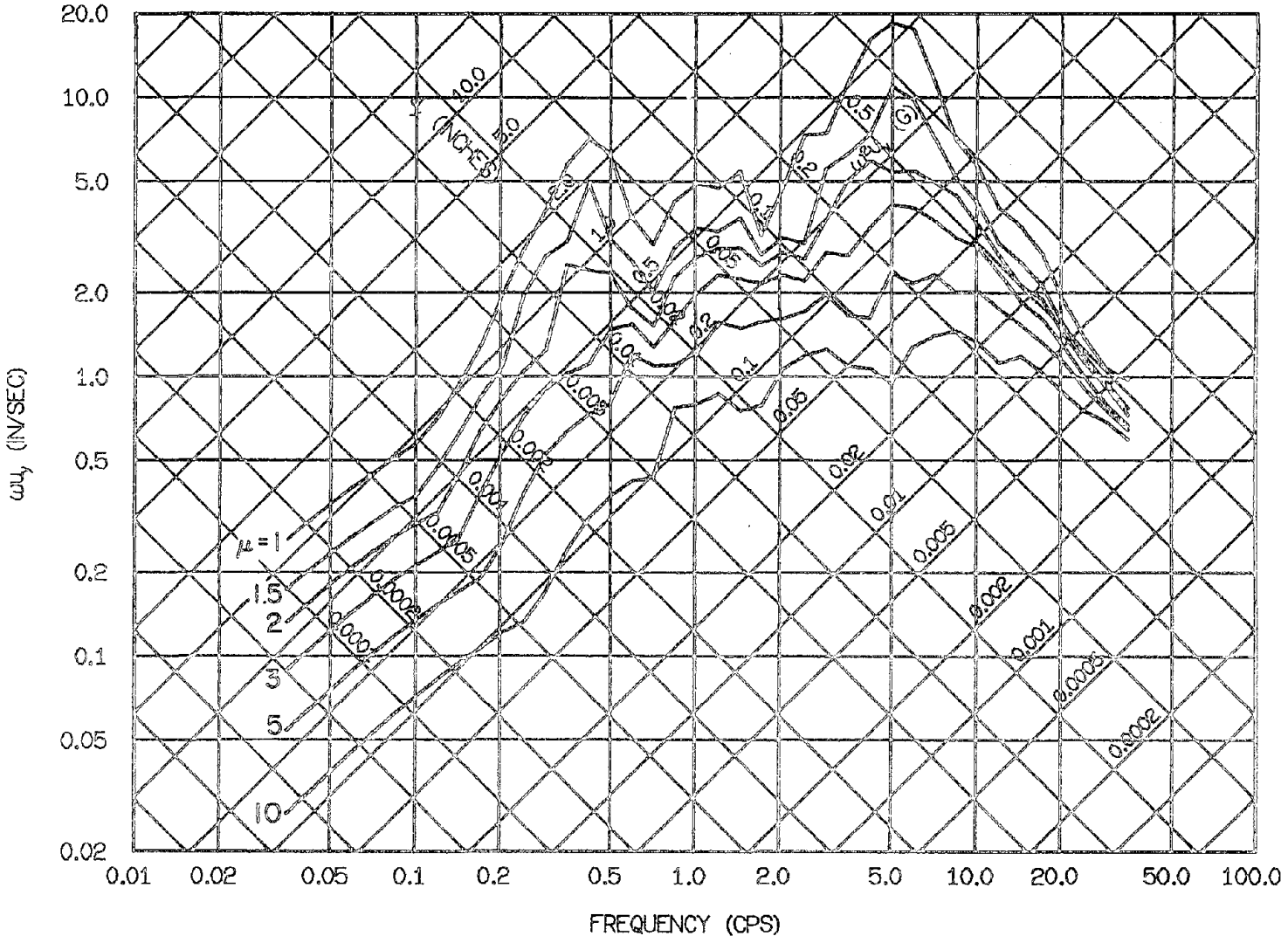

Fig. 3.44 Elastoplastic Yield Spectra for the Melendy Ranch Record of Sept. 4, 1972, Component N29W: 5% Damping

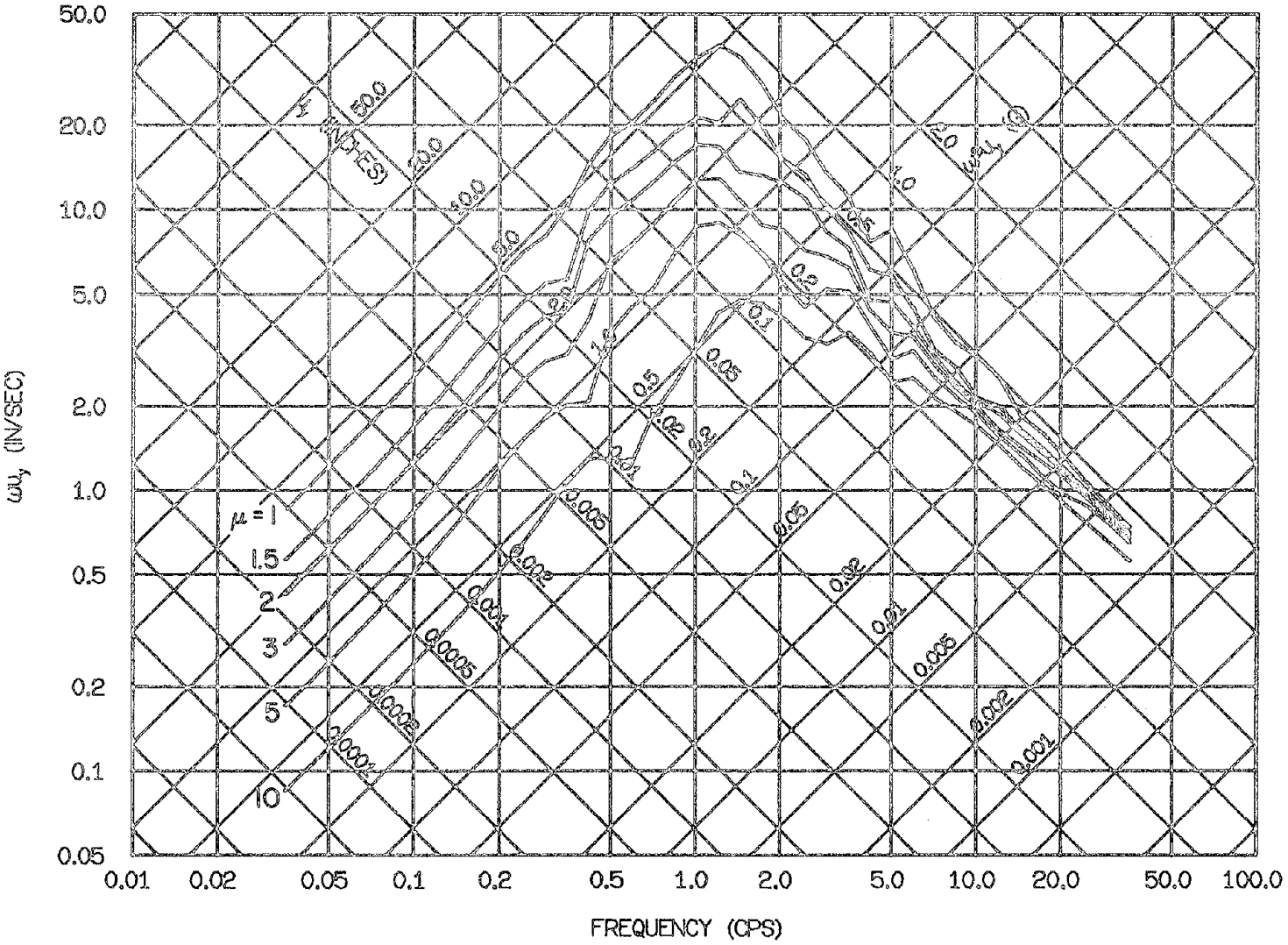

Fig. 3.45 Elastoplastic Yield Spectra for the Gilroy Array No. 6 Record of Aug. 6, 1979, Component 230 Deg: 5% Damping

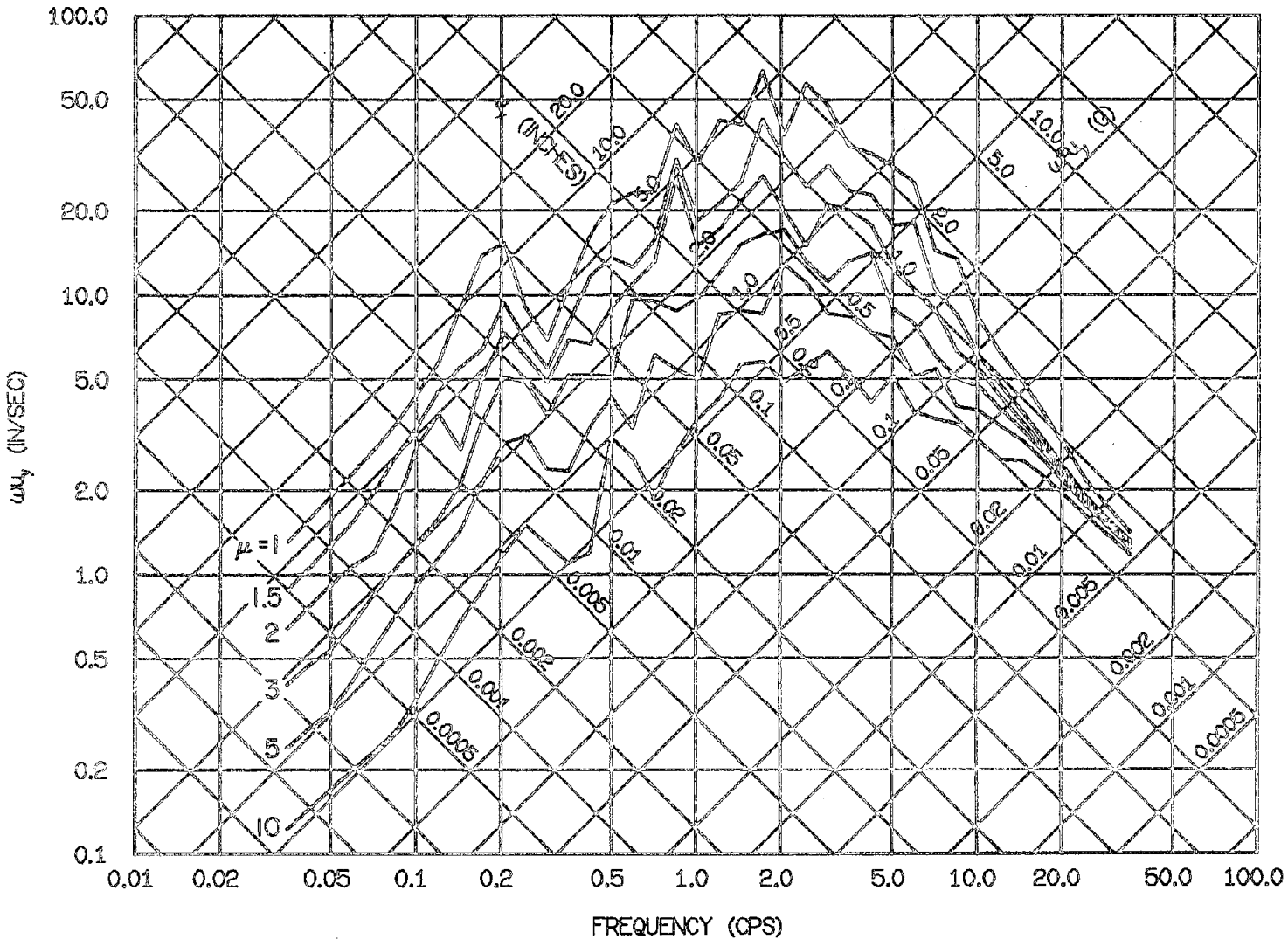

Fig. 3.46 Elastoplastic Yield Spectra for the Bonds Corner Record of Oct. 15, 1979, Component 230 Deg: 5% Damping

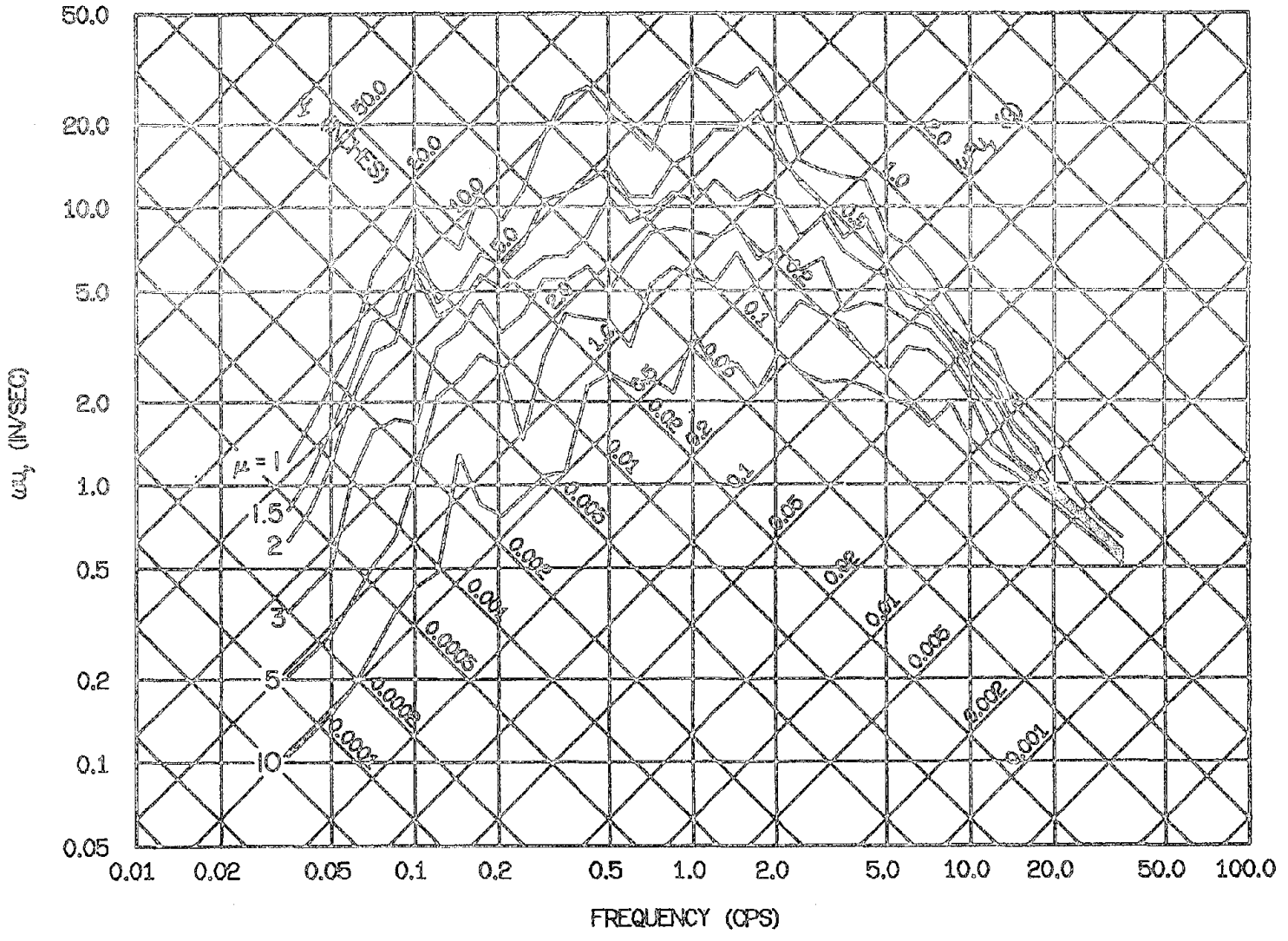

Fig. 3.47 Elastoplastic Yield Spectra for the El Centro Record of May 18, 1940, Component S00E: 5% Damping

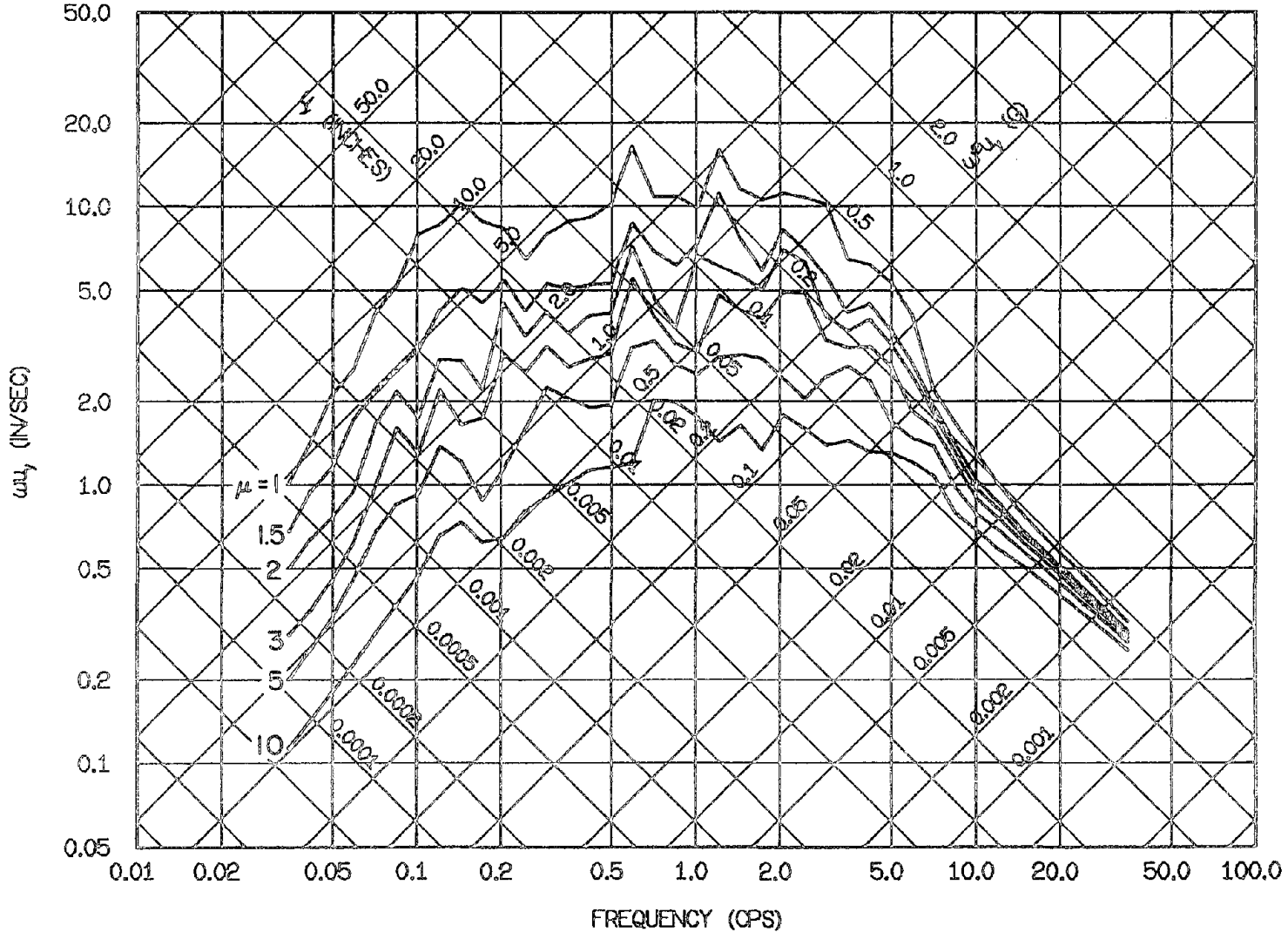

Fig. 3.48 Elastoplastic Yield Spectra for the Taft Record of July 21, 1952, Component S69E: 5% Damping

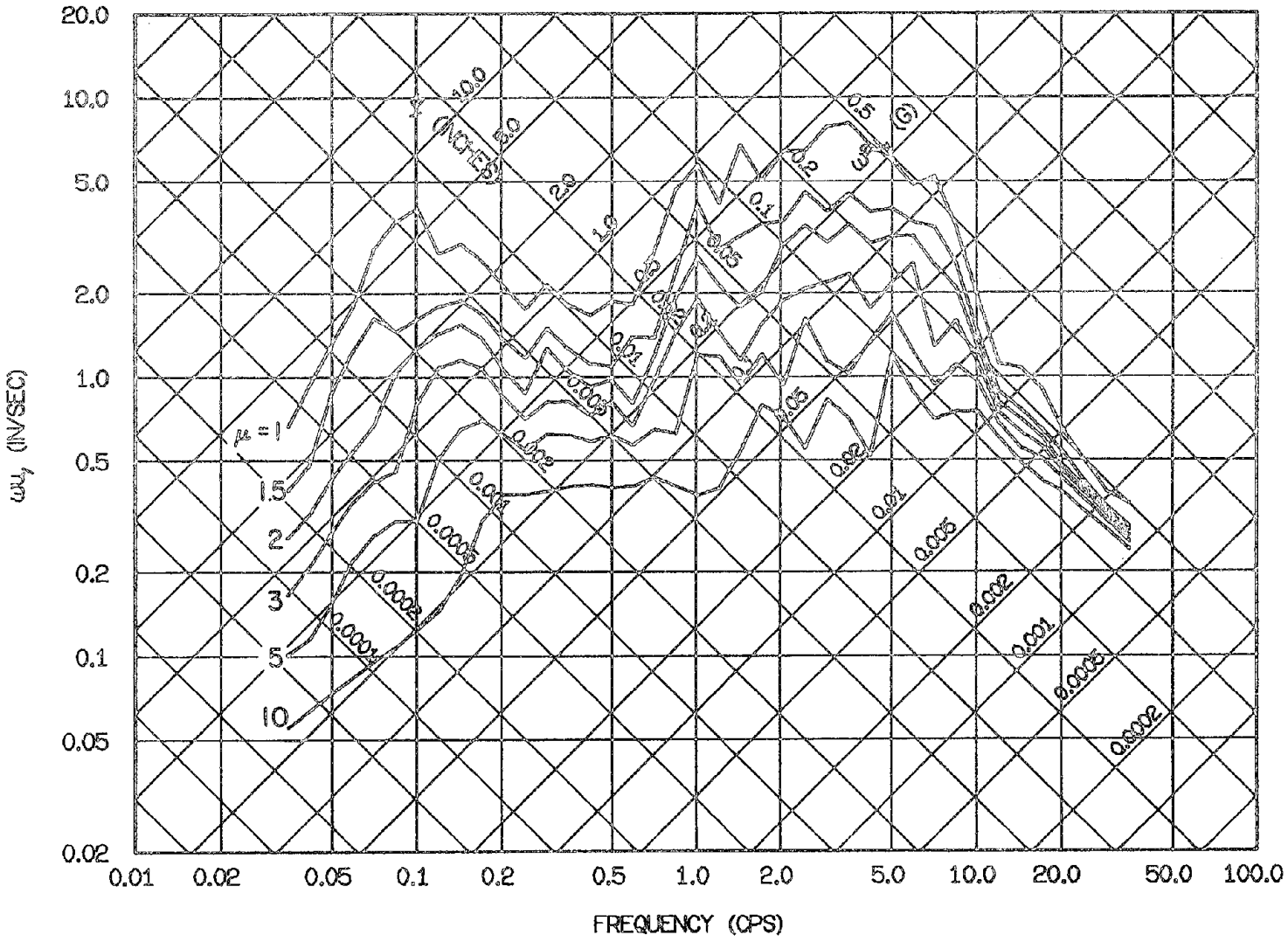

Fig. 3.49 Elastoplastic Yield Spectra for the Adak, Alaska Record of May 1, 1971, Component West: 5% Damping

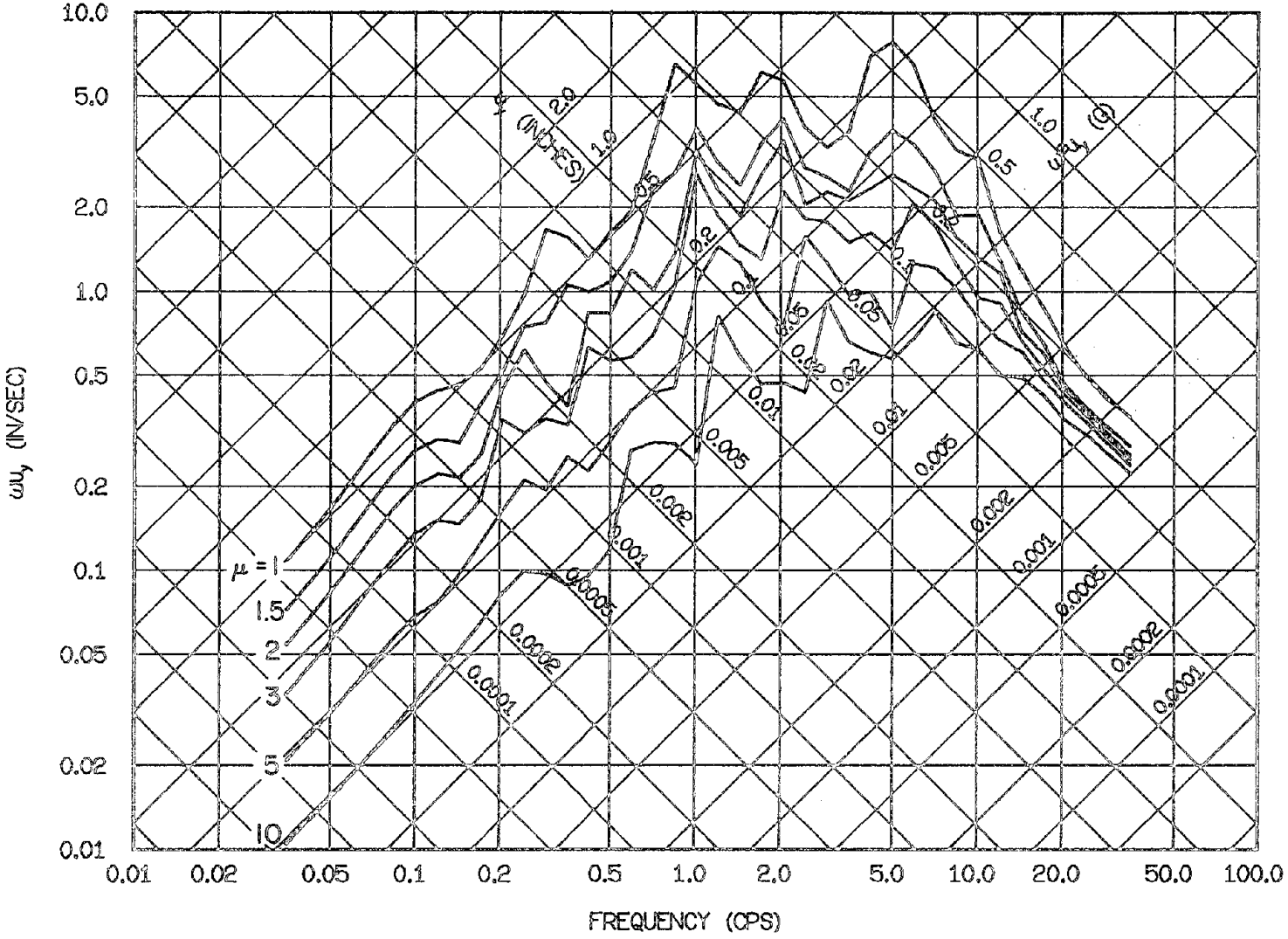

Fig. 3.50 Elastoplastic Yield Spectra for the Kilauea, Hawaii Record of April 26, 1973, Component S30W: 5% Damping

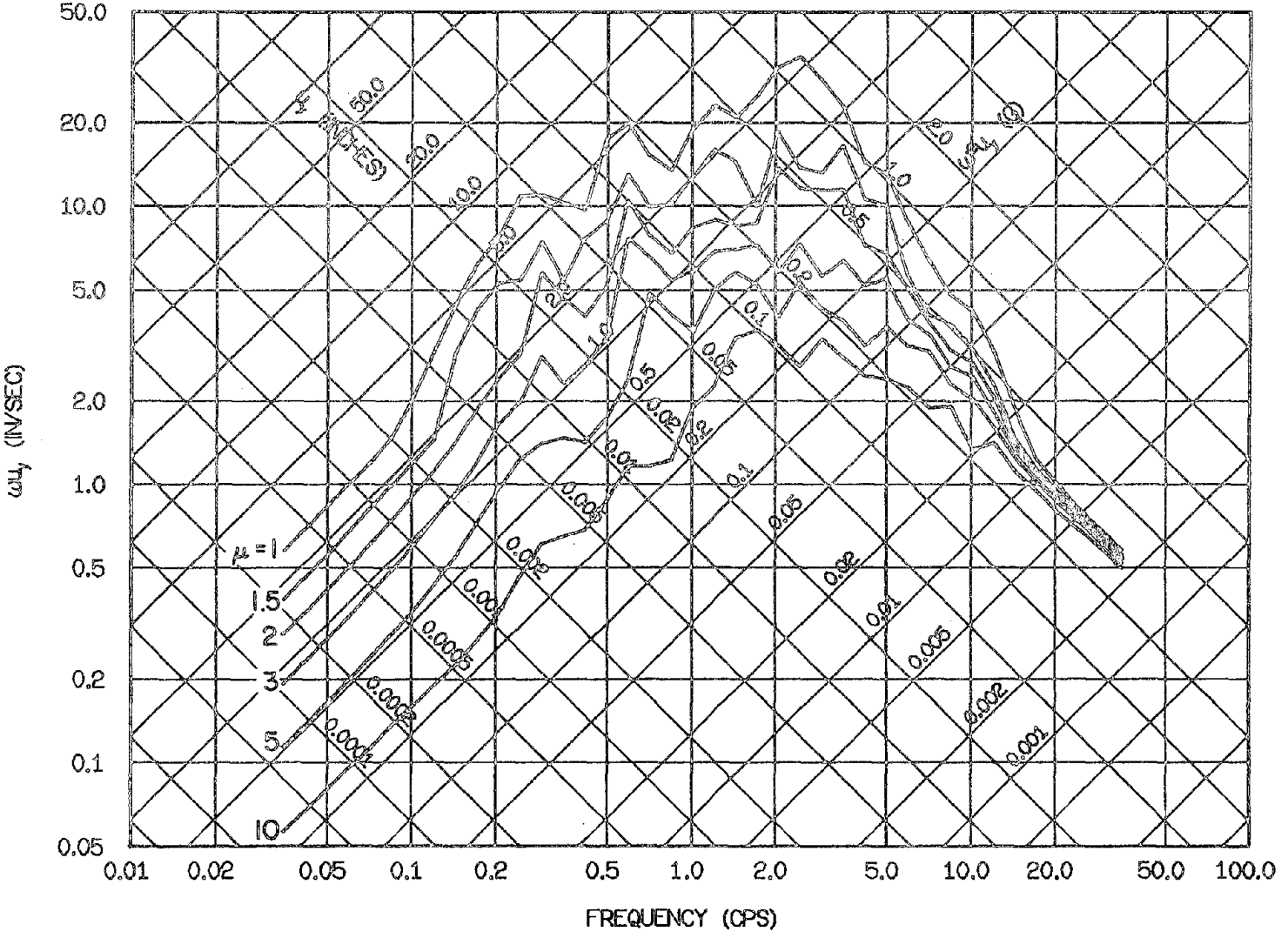

Fig. 3.51 Elastoplastic Yield Spectra for the Managua Record of Dec. 23, 1972, Component South: 5% Damping

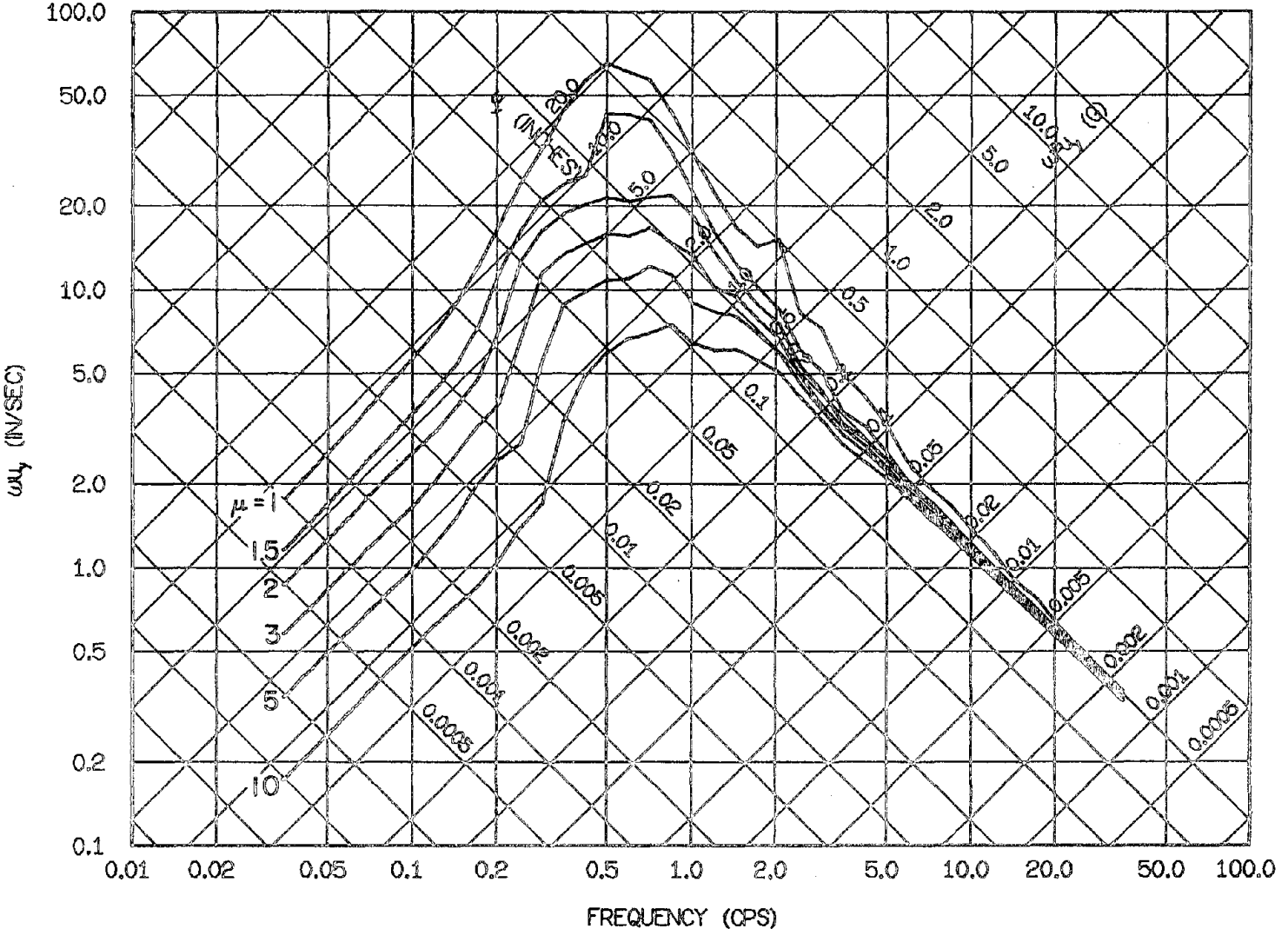

Fig. 3.52 Elastoplastic Yield Spectra for the Bucarest Record of Mar. 4, 1977, Component S-N: 5% Damping

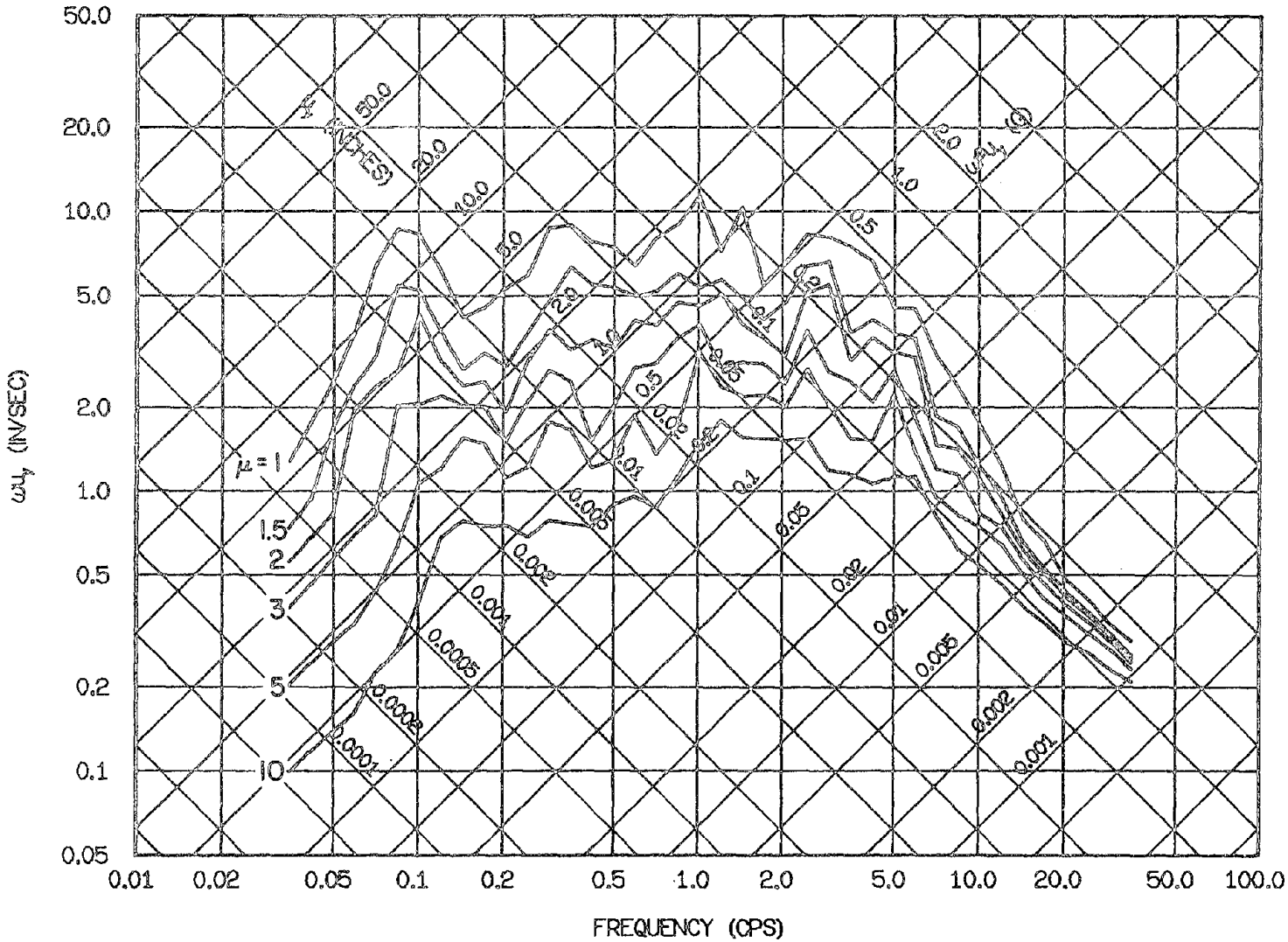

Fig. 3.53 Elastoplastic Yield Spectra for the Santiago Record of July 8, 1971, Component N10W: 5% Damping

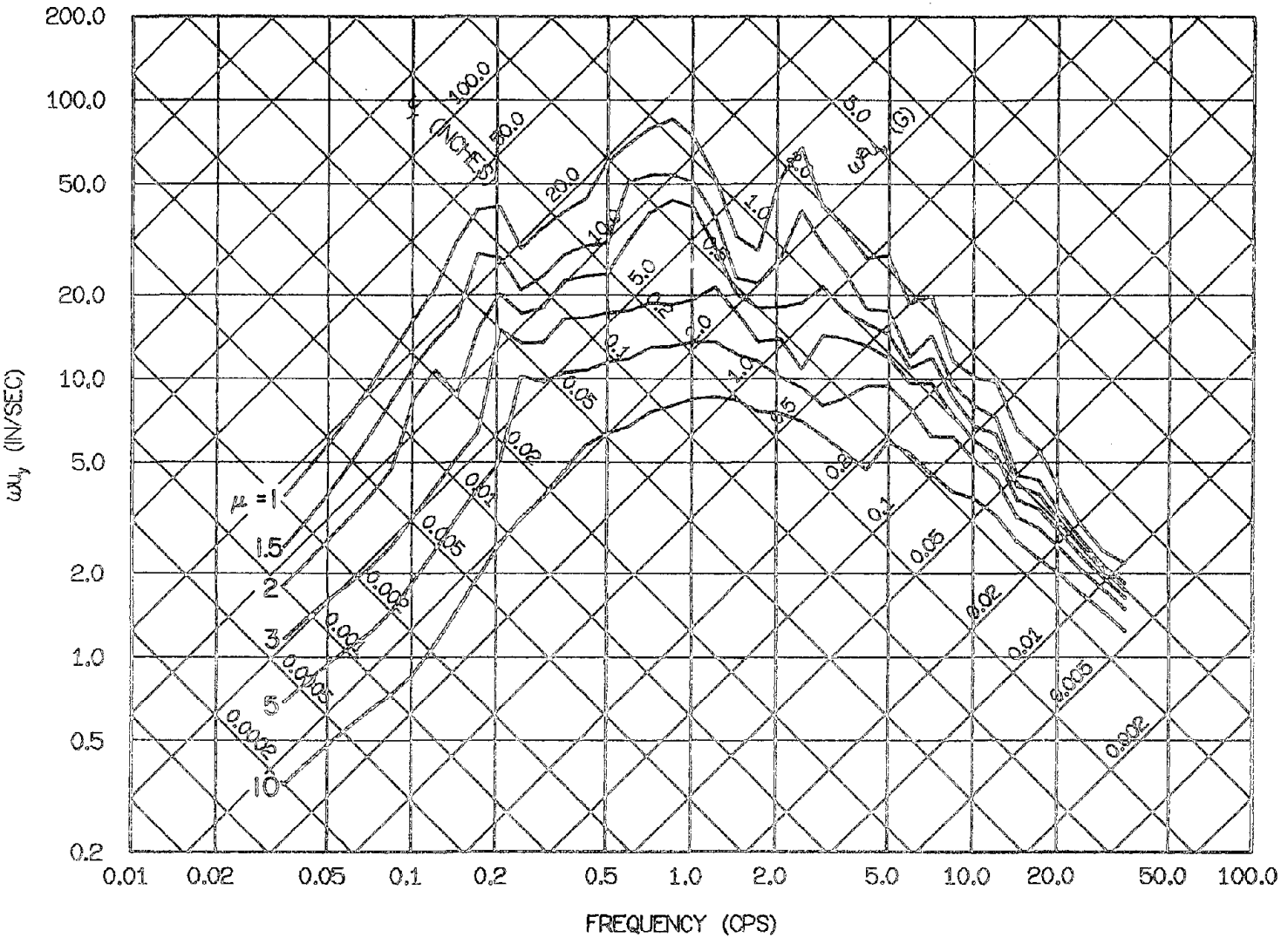

Fig. 3.54 Bilinear Yield Spectra for the Pacoima Dam Record of Feb. 9, 1971, Component S16E: 5% Strain-Hardening and 5% Damping

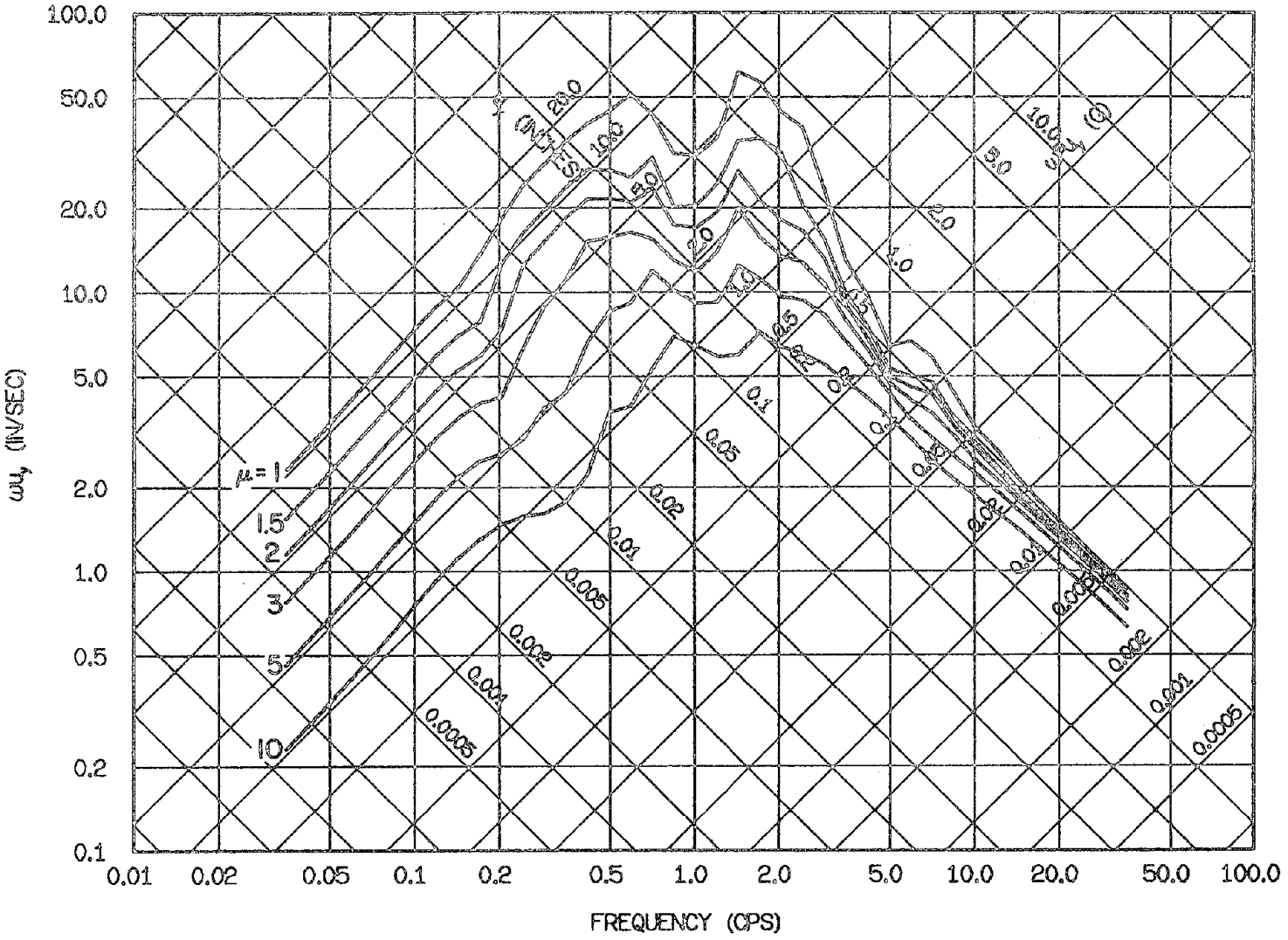

Fig. 3.55 Bilinear Yield Spectra for the Cholame-Shandon No. 2 Record of June 27, 1966, Component N65E: 5% Strain-Hardening and 5% Damping

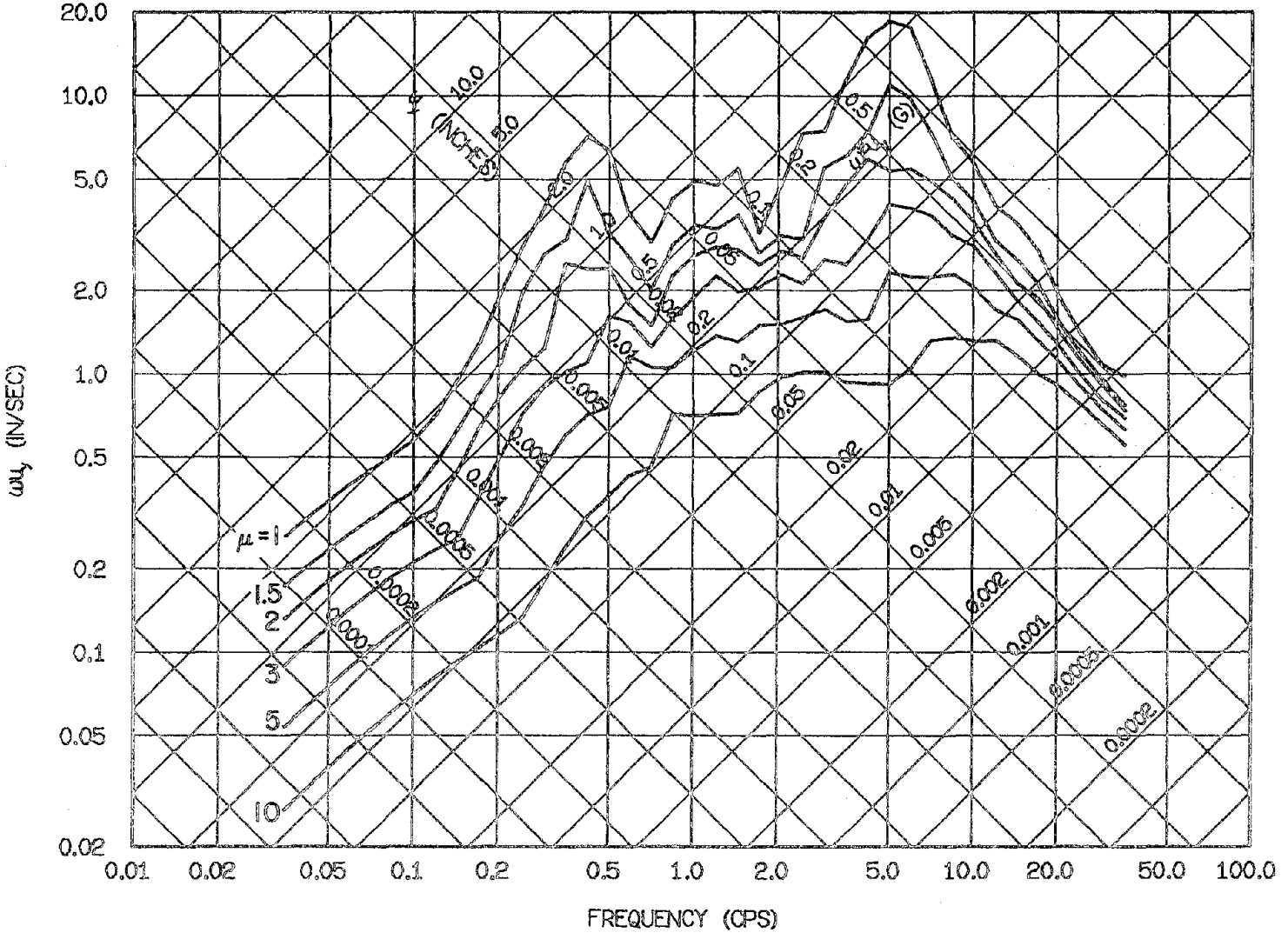

Fig. 3.56 Bilinear Yield Spectra for the Melendy Ranch Record of Sept. 4, 1972, Component N29W: 5% Strain-Hardening and 5% Damping

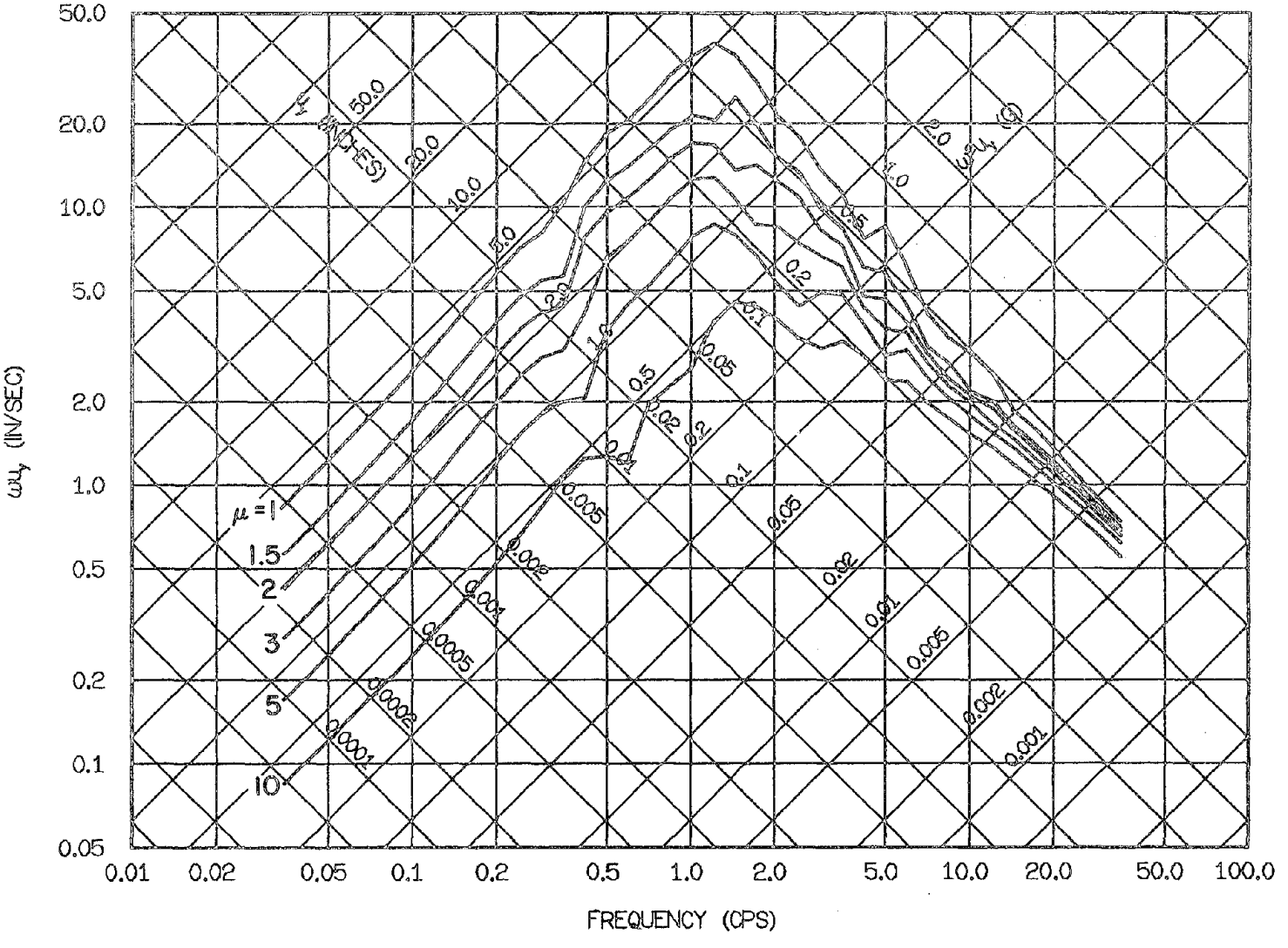

Fig. 3.57 Bilinear Yield Spectra for the Gilroy Array No. 6 Record of Aug. 6, 1979, Component 230 Deg: 5% Strain-Hardening and 5% Damping

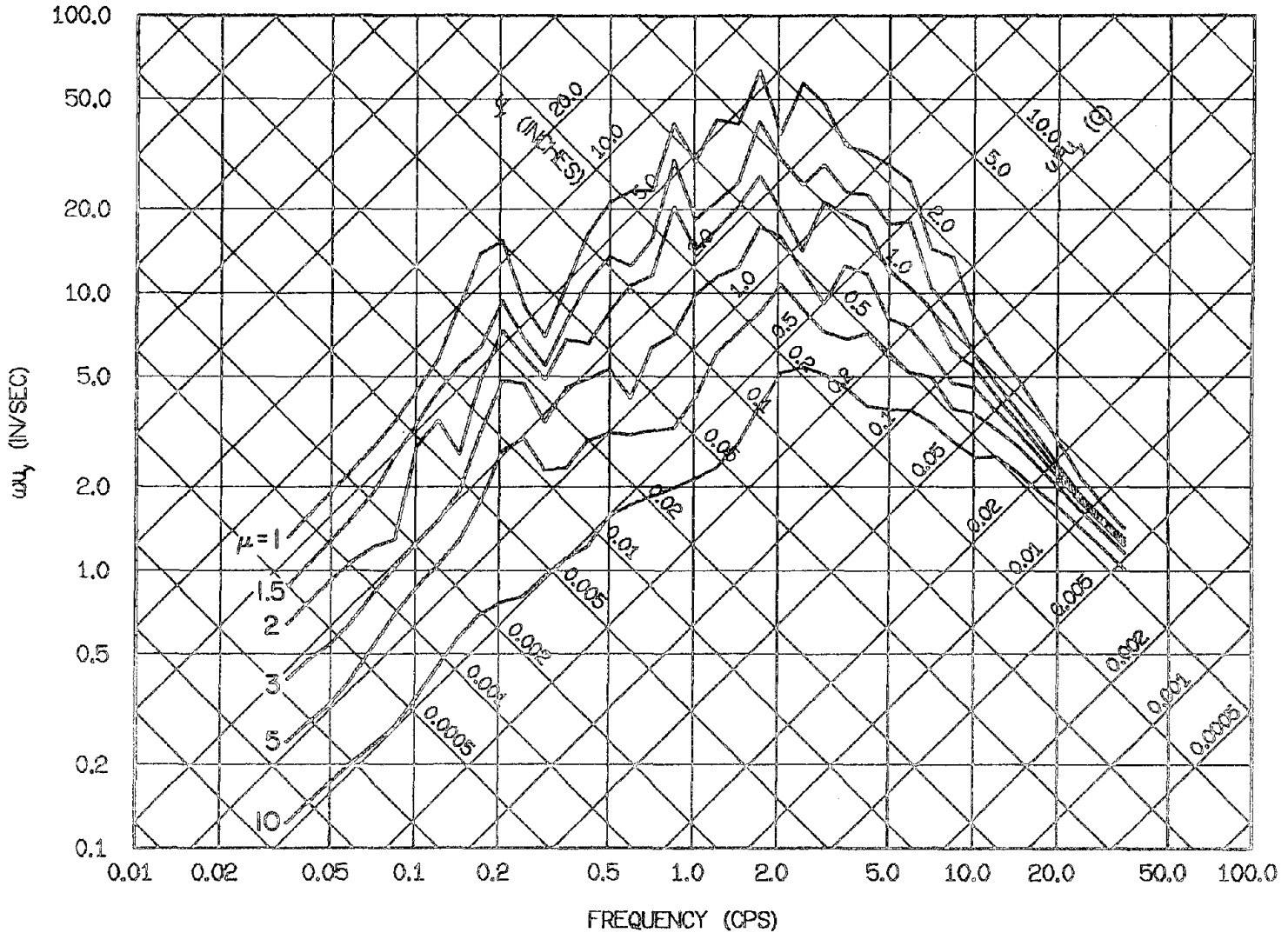

Fig. 3.58 Bilinear Yield Spectra for the Bonds Corner Record of Oct. 15, 1979, Component 230 Deg: 5% Strain-Hardening and 5% Damping

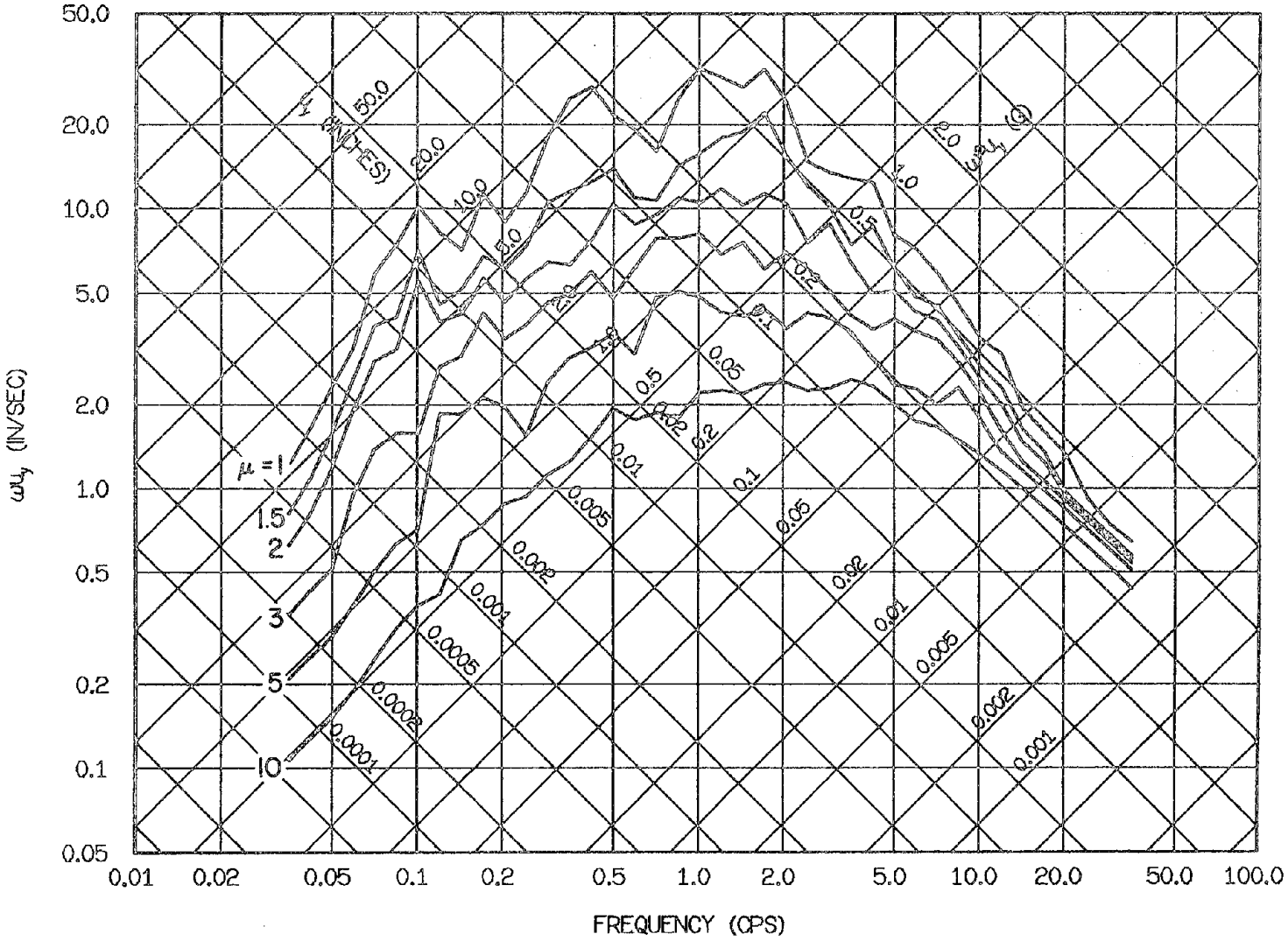

Fig. 3.59 Bilinear Yield Spectra for the El Centro Record of May 18, 1940, Component S00E: 5% Strain-Hardening and 5% Damping

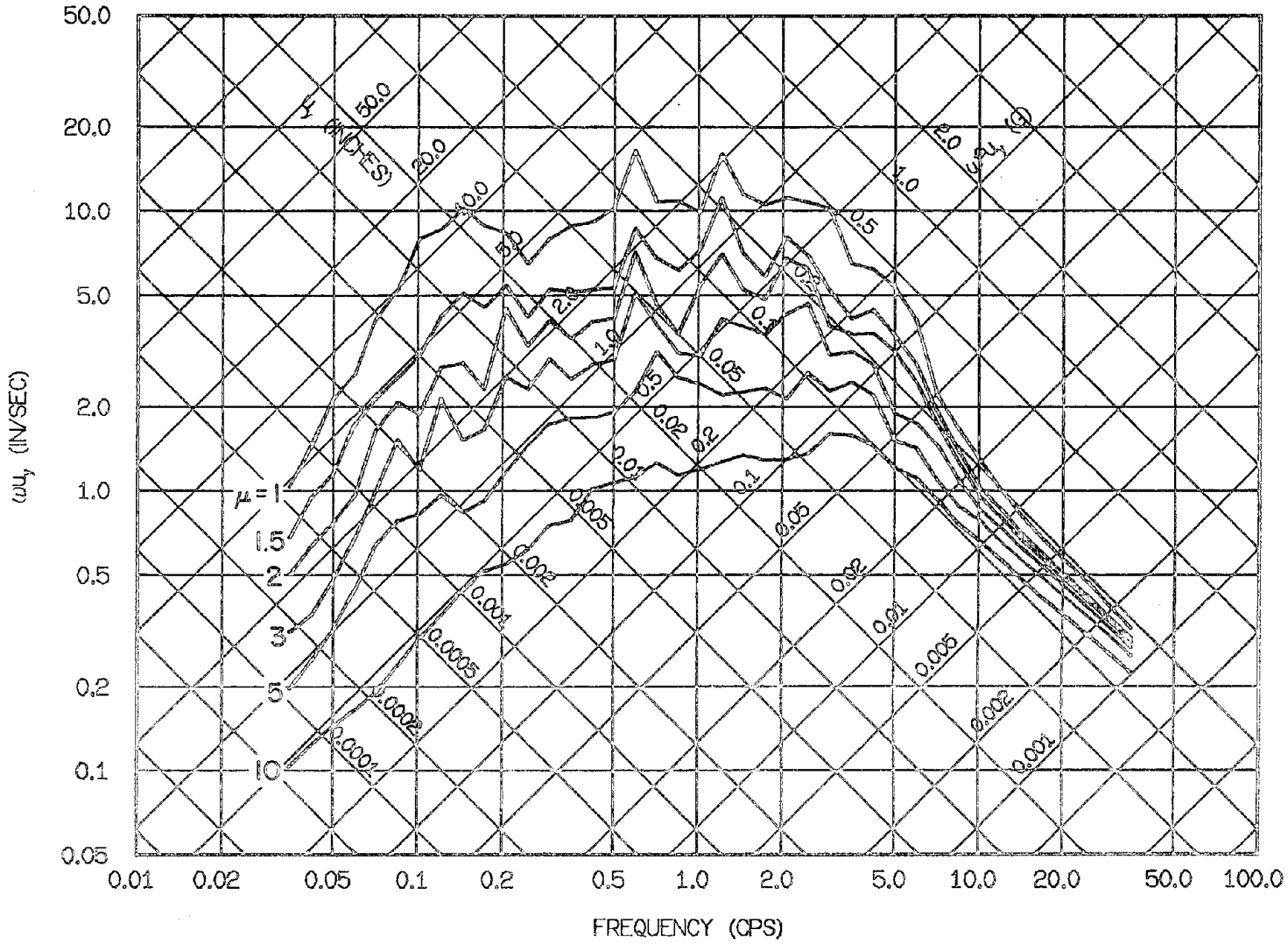

Fig. 3.60 Bilinear Yield Spectra for the Taft Record of July 21, 1952, Component S69E: 5% Strain-Hardening and 5% Damping

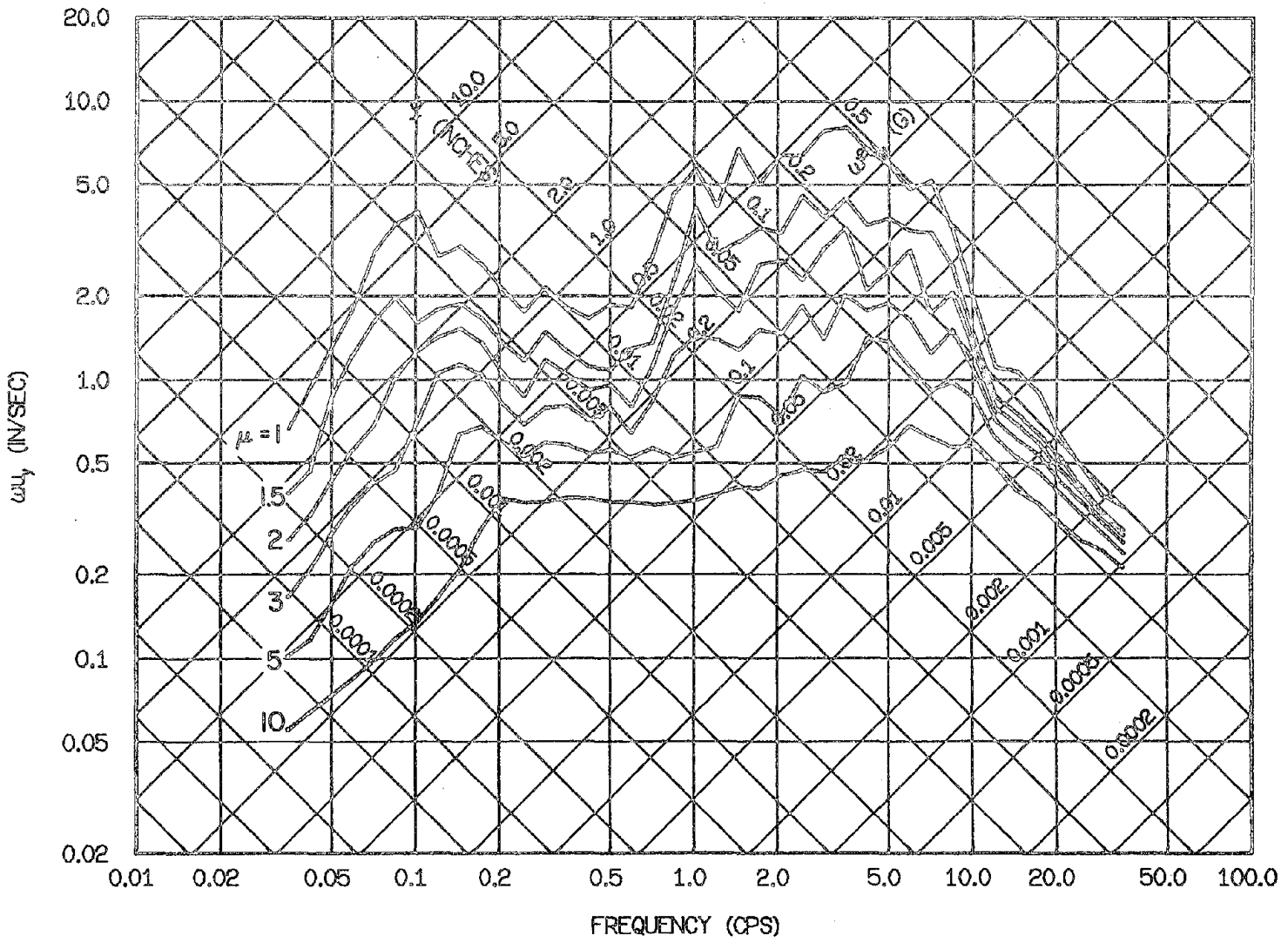

Fig. 3.61 Bilinear Yield Spectra for the Adak, Alaska Record of May 1, 1971, Component West: 5% Strain-Hardening and 5% Damping

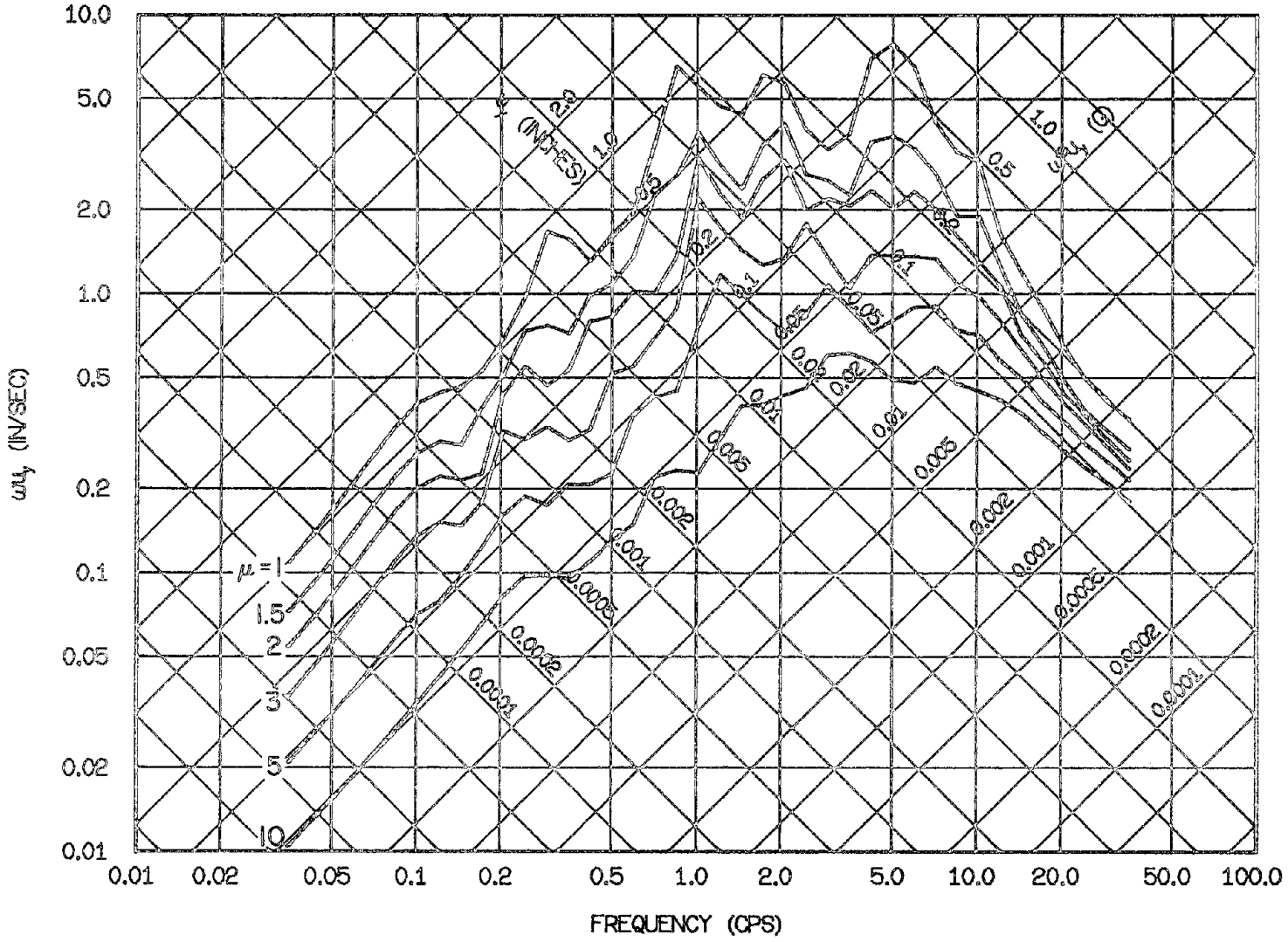

Fig. 3.62 Bilinear Yield Spectra for the Kilauea, Hawaii Record of April 26, 1973, Component S30W: 5% Strain-Hardening and 5% Damping

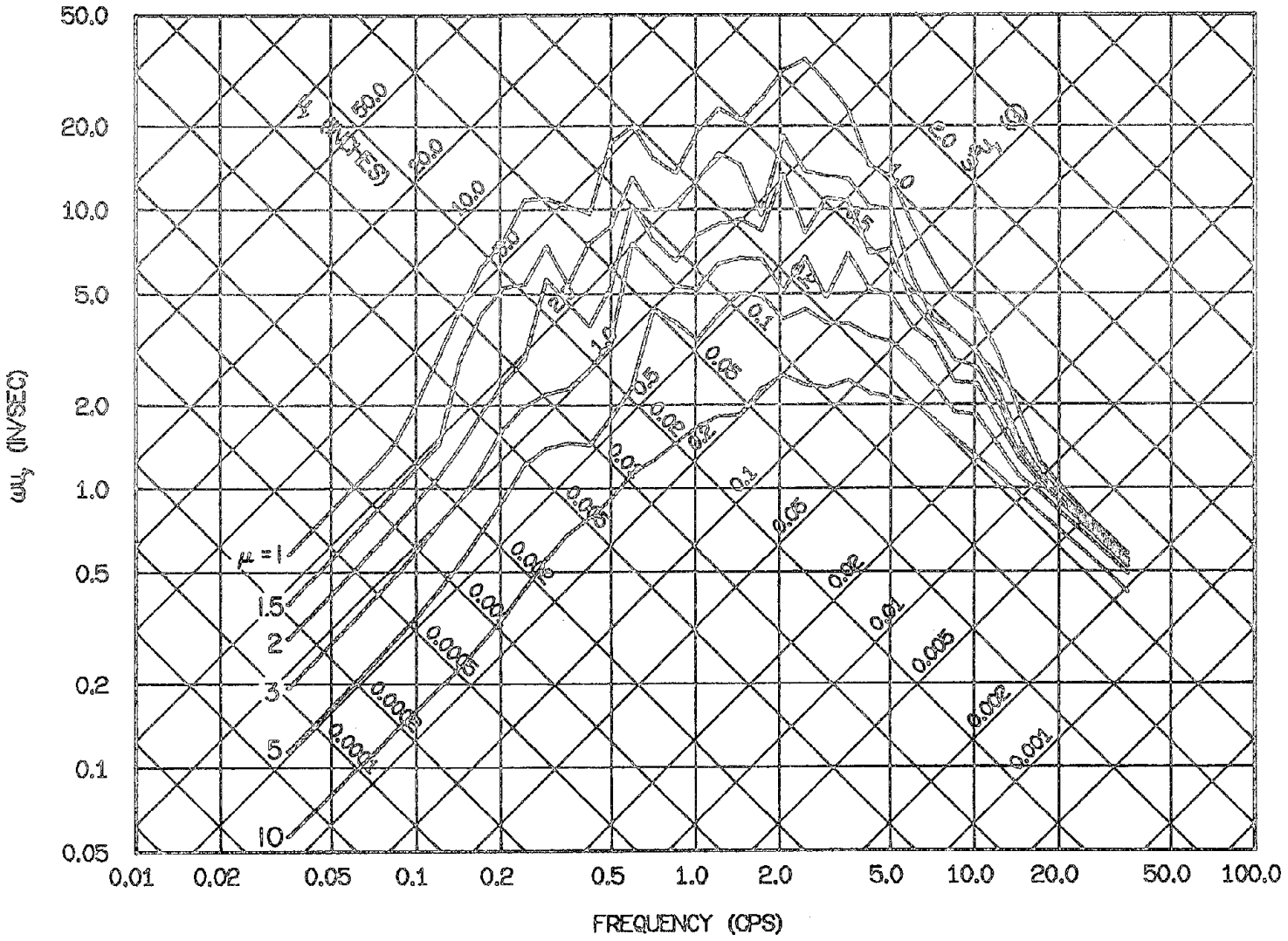

Fig. 3.63 Bilinear Yield Spectra for the Managua Record of Dec. 23, 1972, Component South: 5% Strain-Hardening and 5% Damping

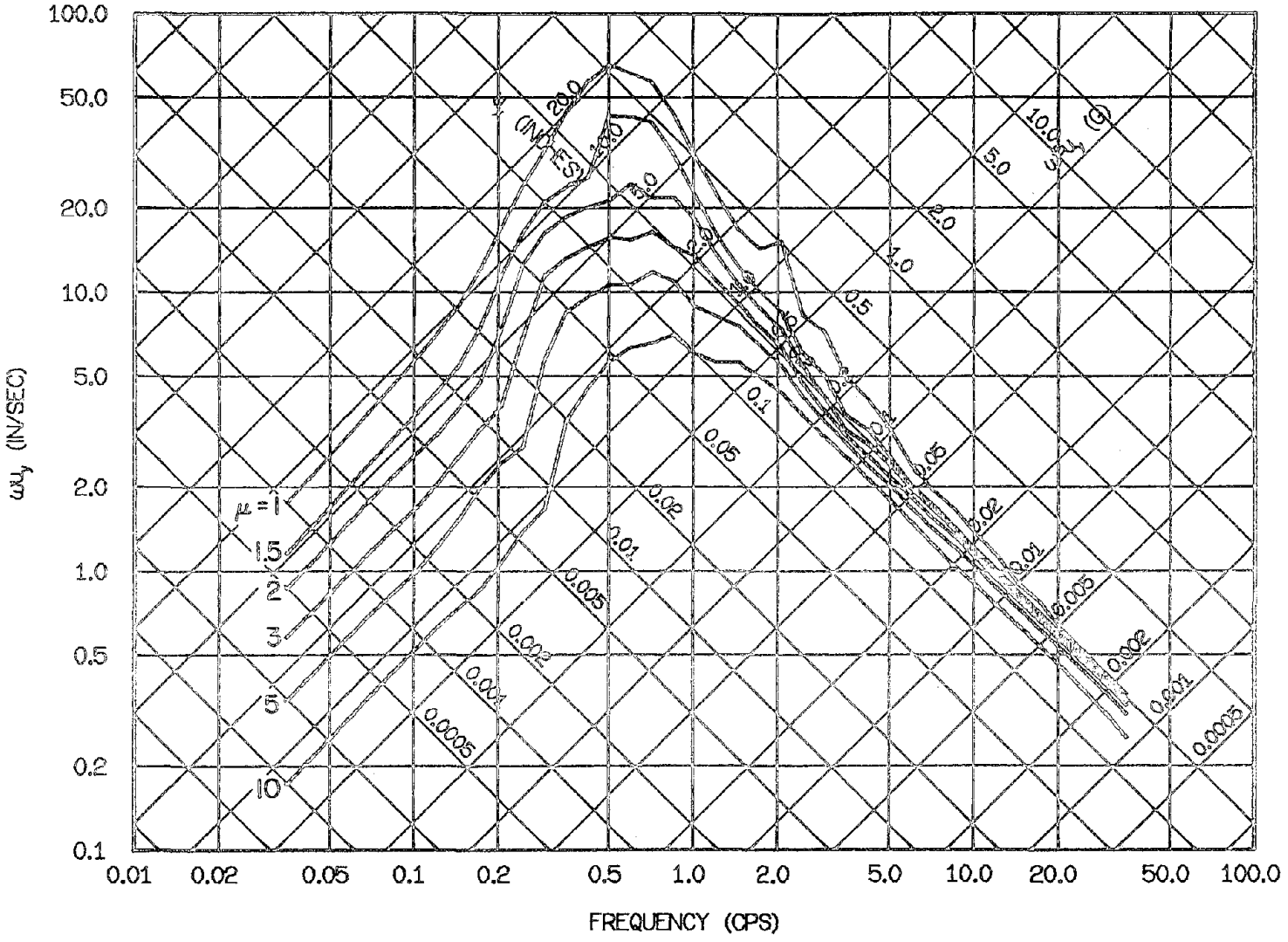

Fig. 3.64 Bilinear Yield Spectra for the Bucarest Record of Mar. 4, 1977, Component S-N: 5% Strain-Hardening and 5% Damping

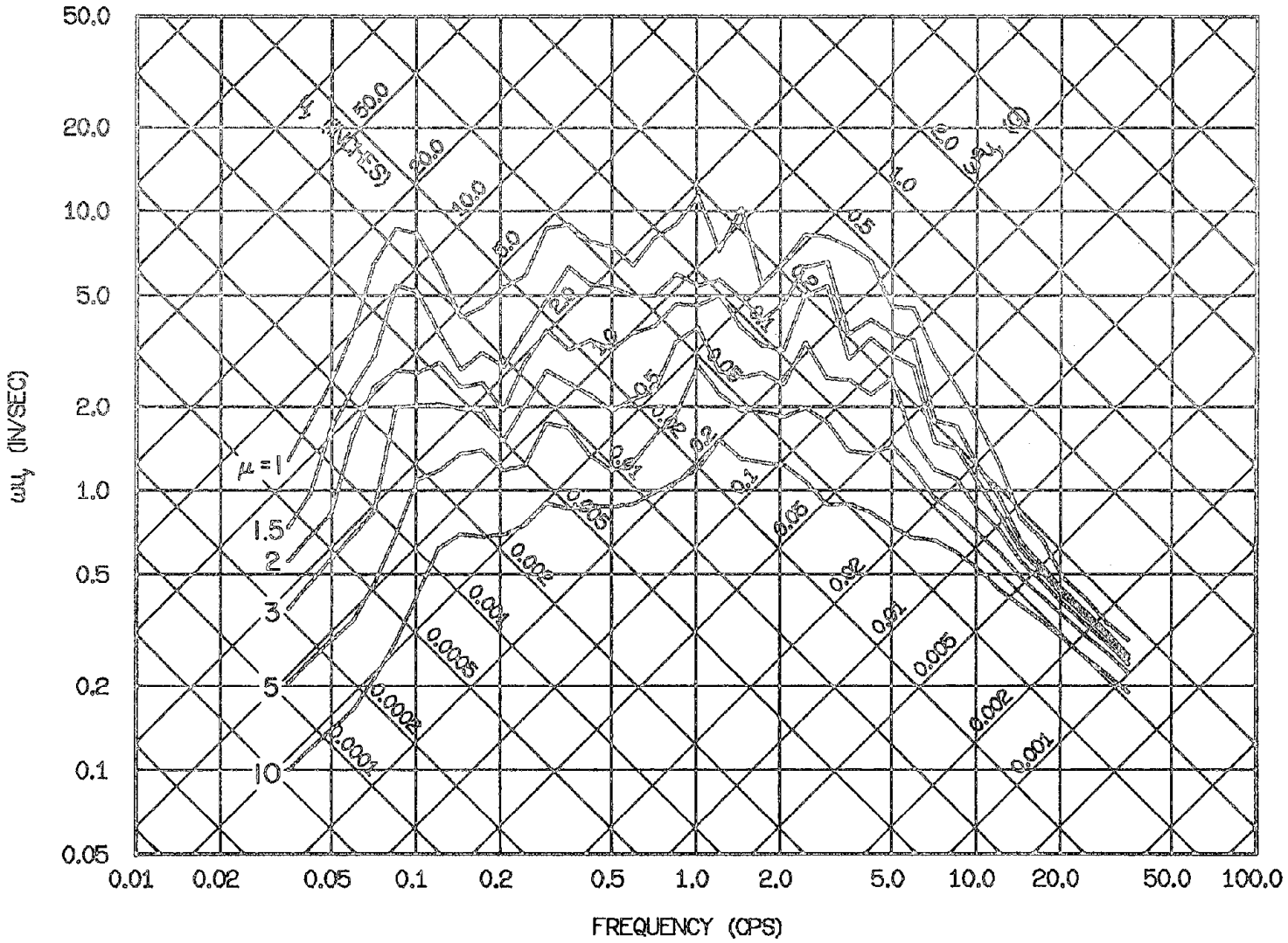

Fig. 3.65 Bilinear Yield Spectra for the Santiago Record of July 8, 1971, Component N10W: 5% Strain-Hardening and 5% Damping

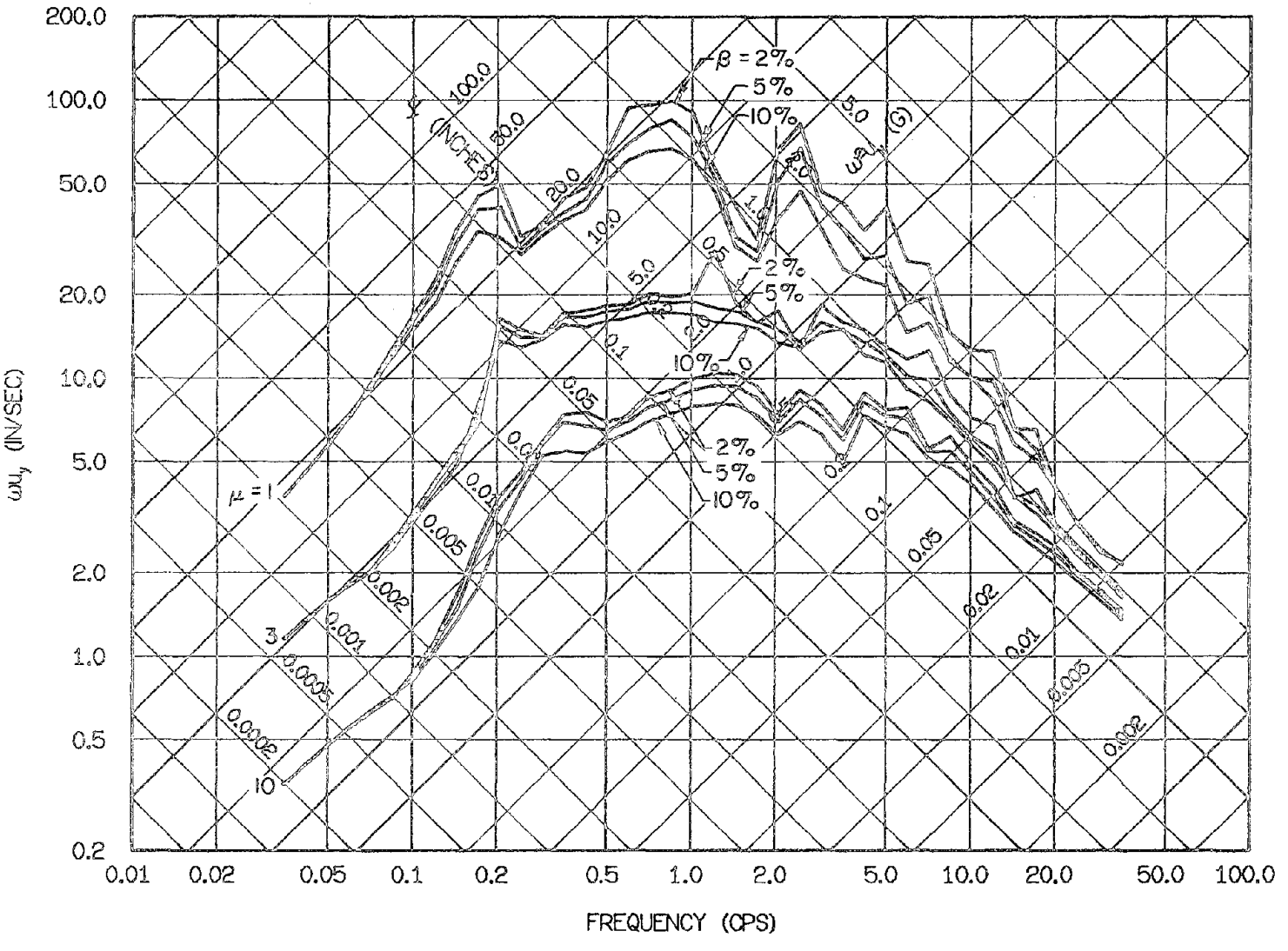

Fig. 3.66 Comparison of Elastoplastic Yield Spectra for the Pacoima Dam Record of Feb. 9, 1971, Component S16E

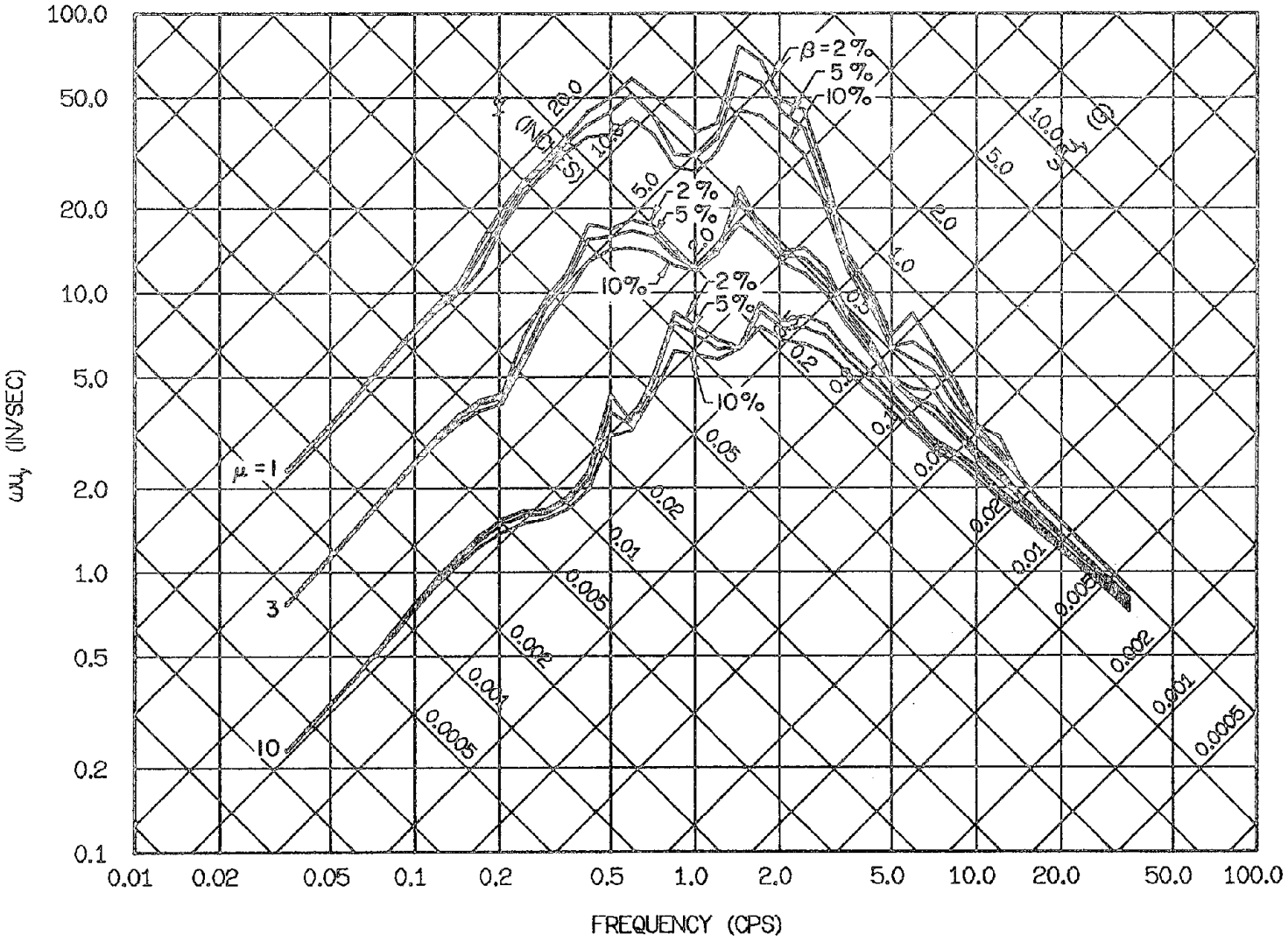

Fig. 3.67 Comparison of Elastoplastic Yield Spectra for the Cholame-Shandon No. 2 Record of June 27, 1966, Component N65E

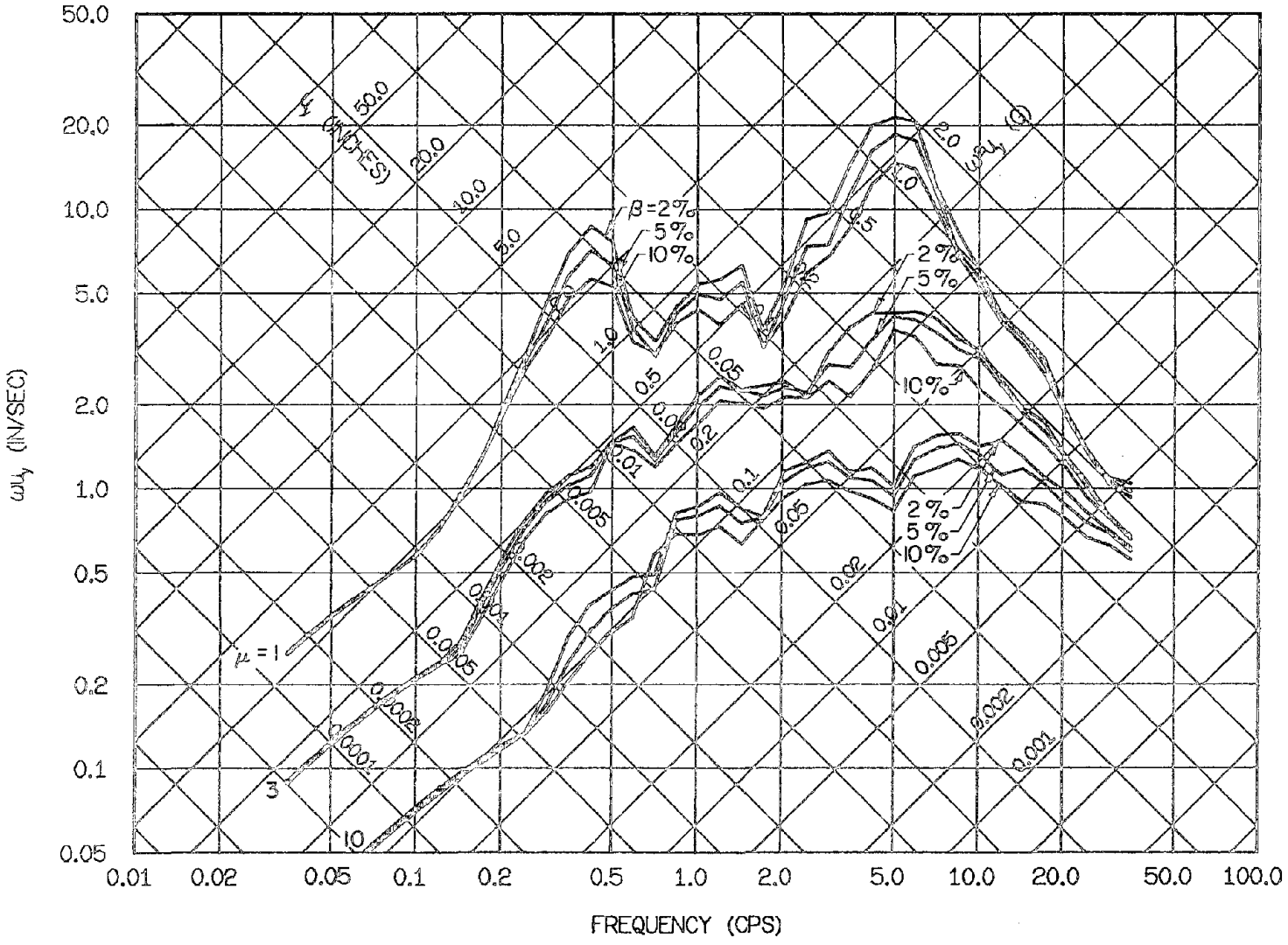

Fig. 3.68 Comparison of Elastoplastic Yield Spectra for the Melendy Ranch Record of Sept. 4, 1972, Component N29W

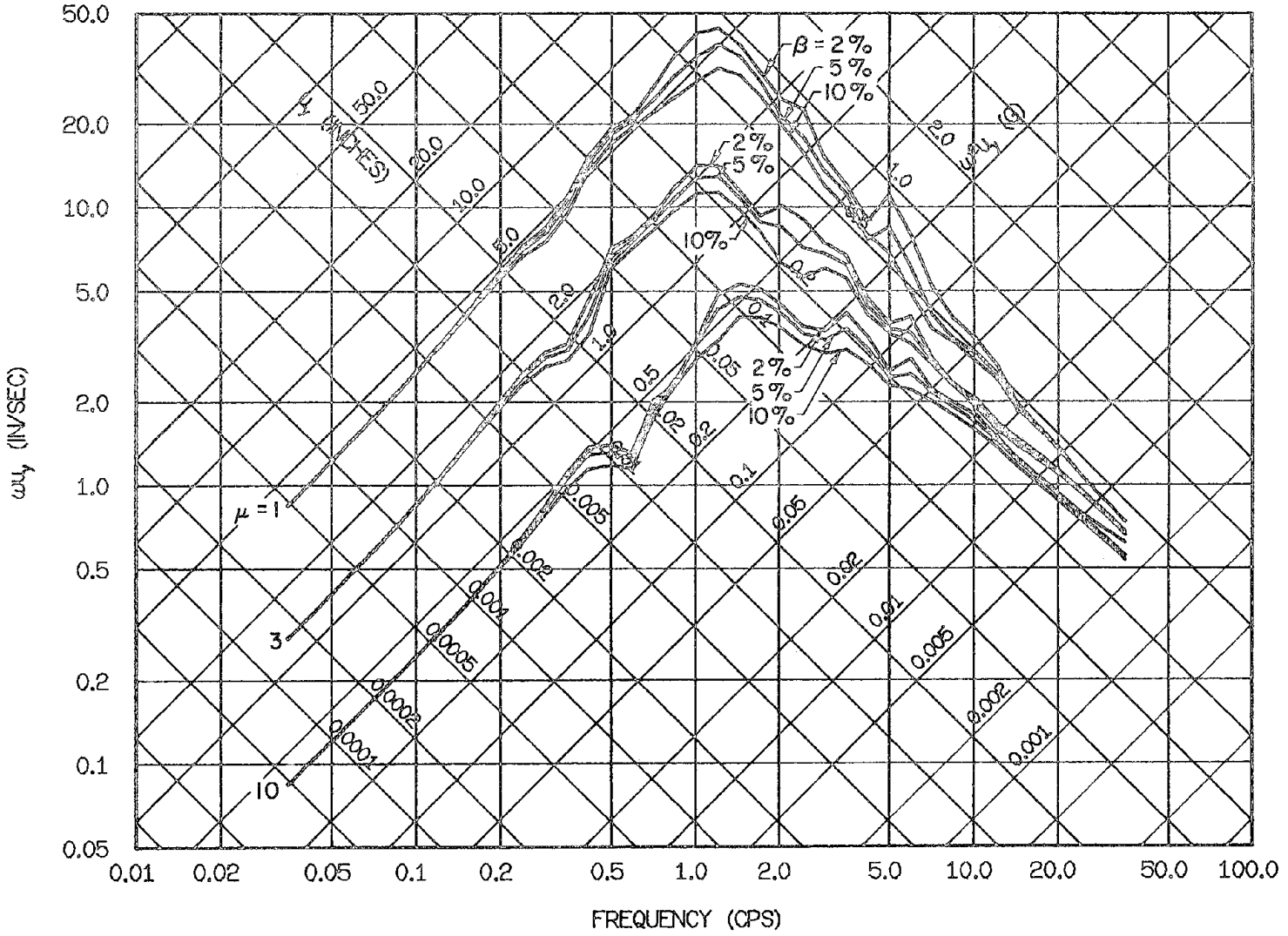

Fig. 3.69 Comparison of Elastoplastic Yield Spectra for the Gilroy Array No. 6 Record of Aug. 6, 1979, Component 230 Deg

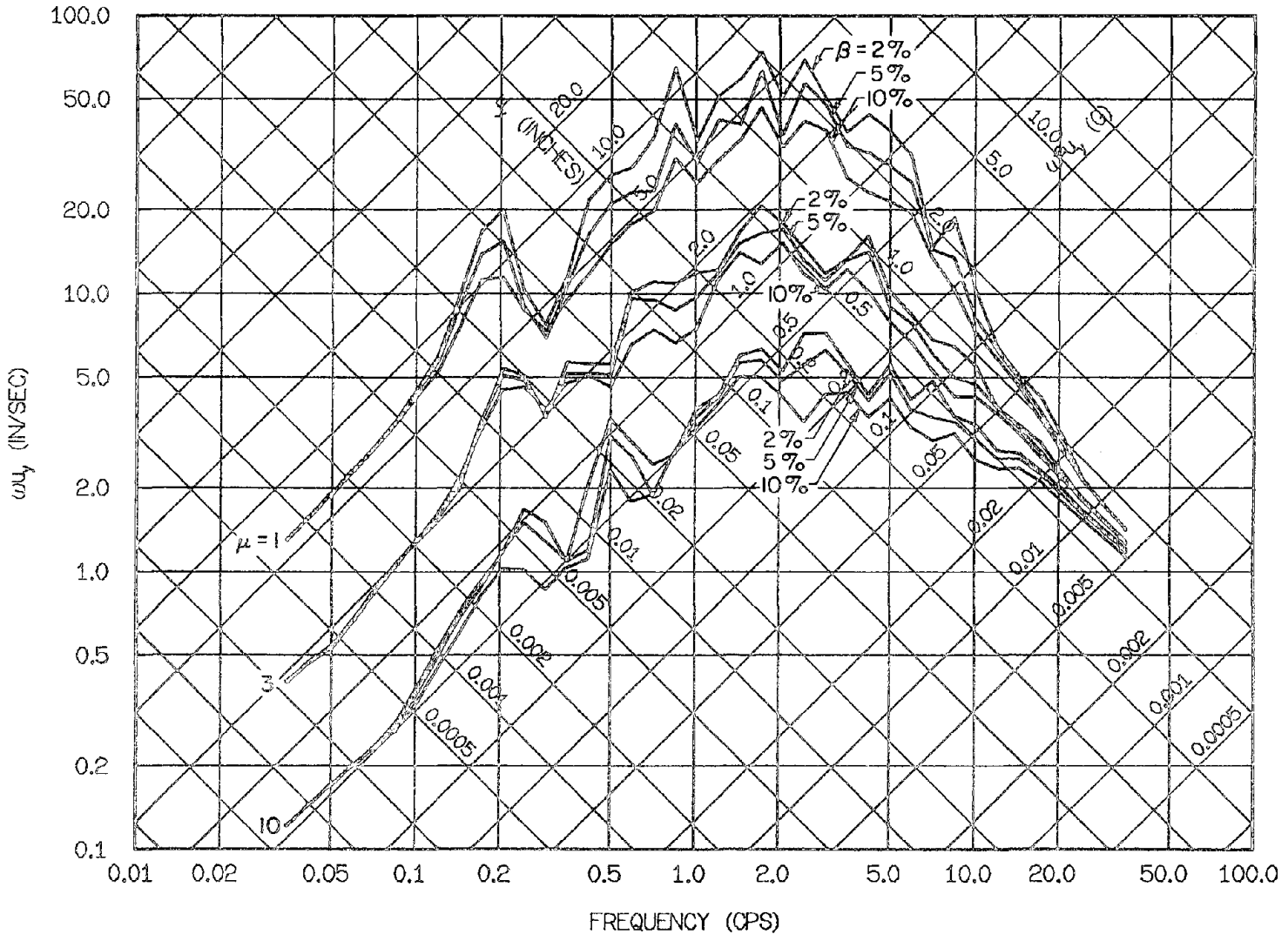

Fig. 3.70 Comparison of Elastoplastic Yield Spectra for the Bonds Corner Record of Oct. 15, 1979, Component 230 Deg

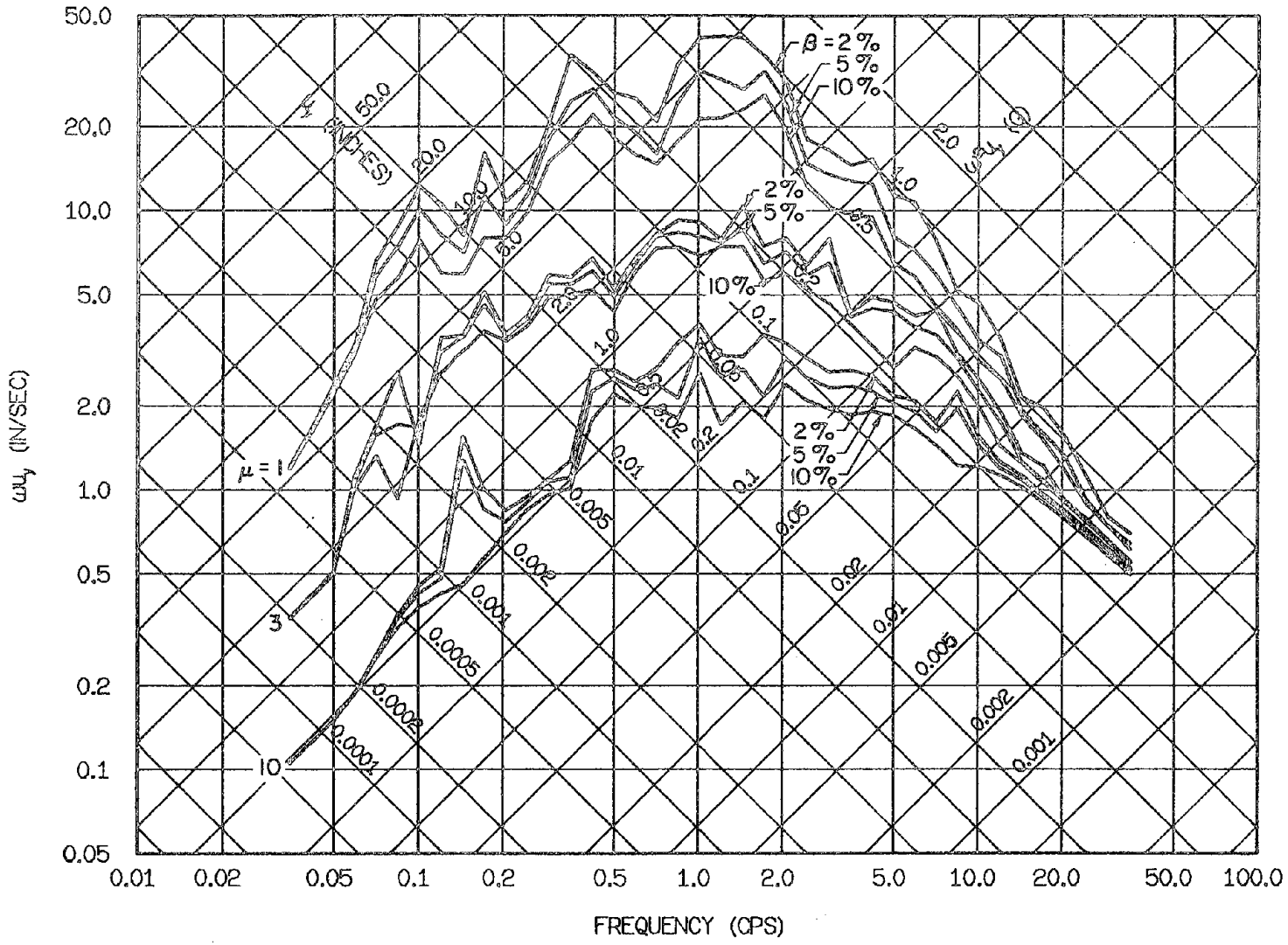

Fig. 3.71 Comparison of Elastoplastic Yield Spectra for the El Centro Record of May 18, 1940, Component S00E

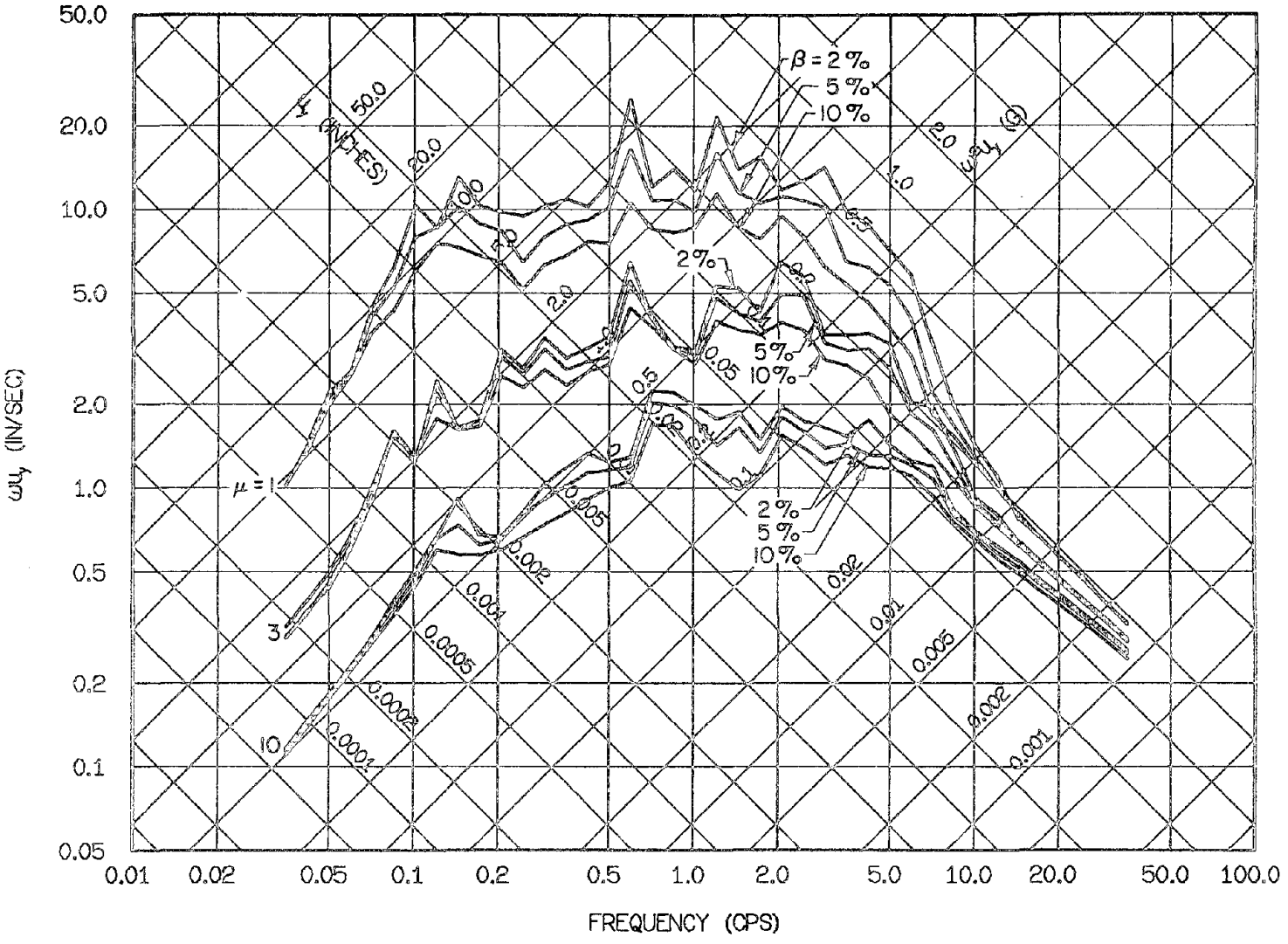

Fig. 3.72 Comparison of Elastoplastic Yield Spectra for the Taft Record of July 21, 1952, Component S69E

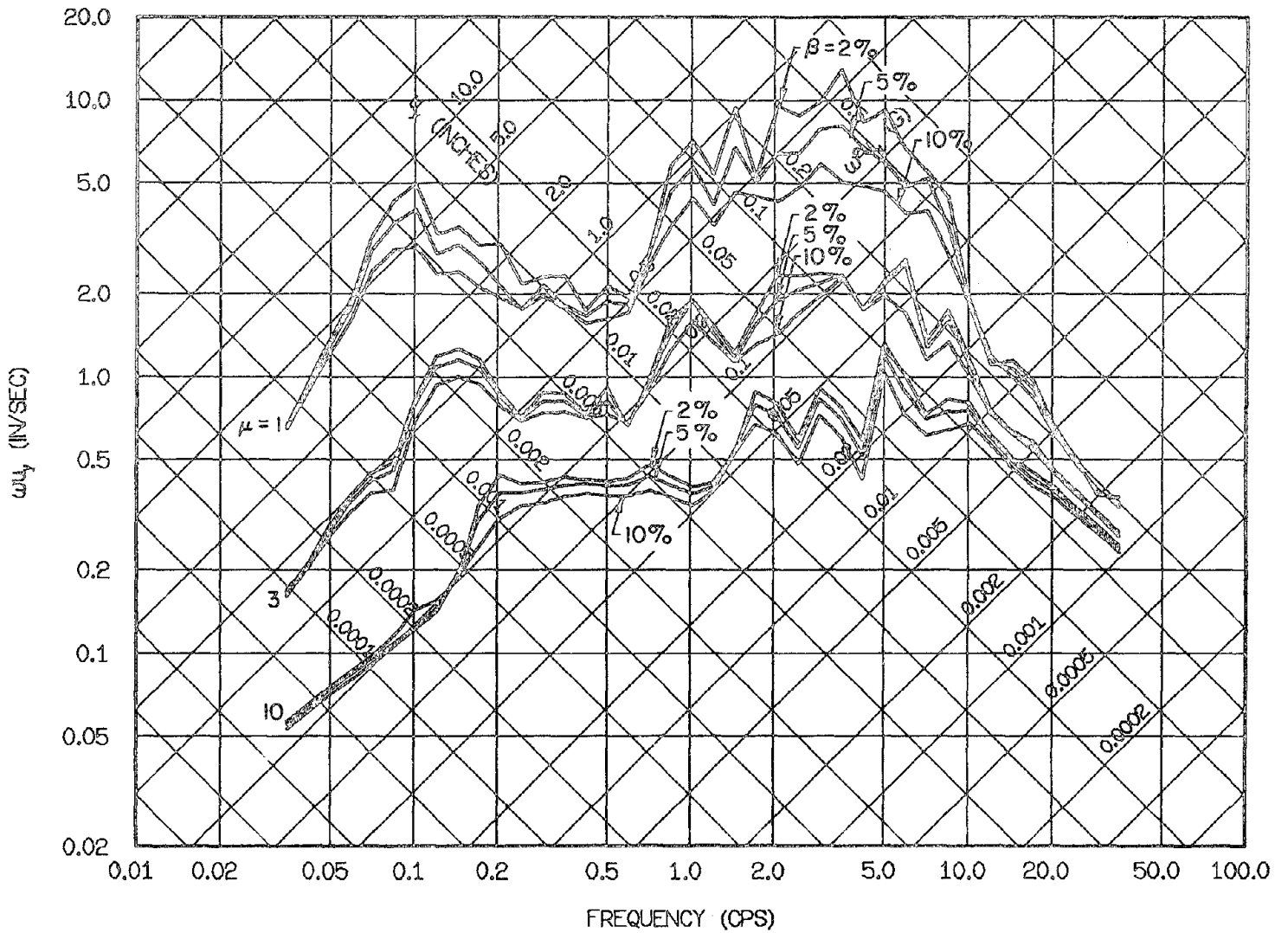

Fig. 3.73 Comparison of Elastoplastic Yield Spectra for the Adak, Alaska Record of May 1, 1971, Component West

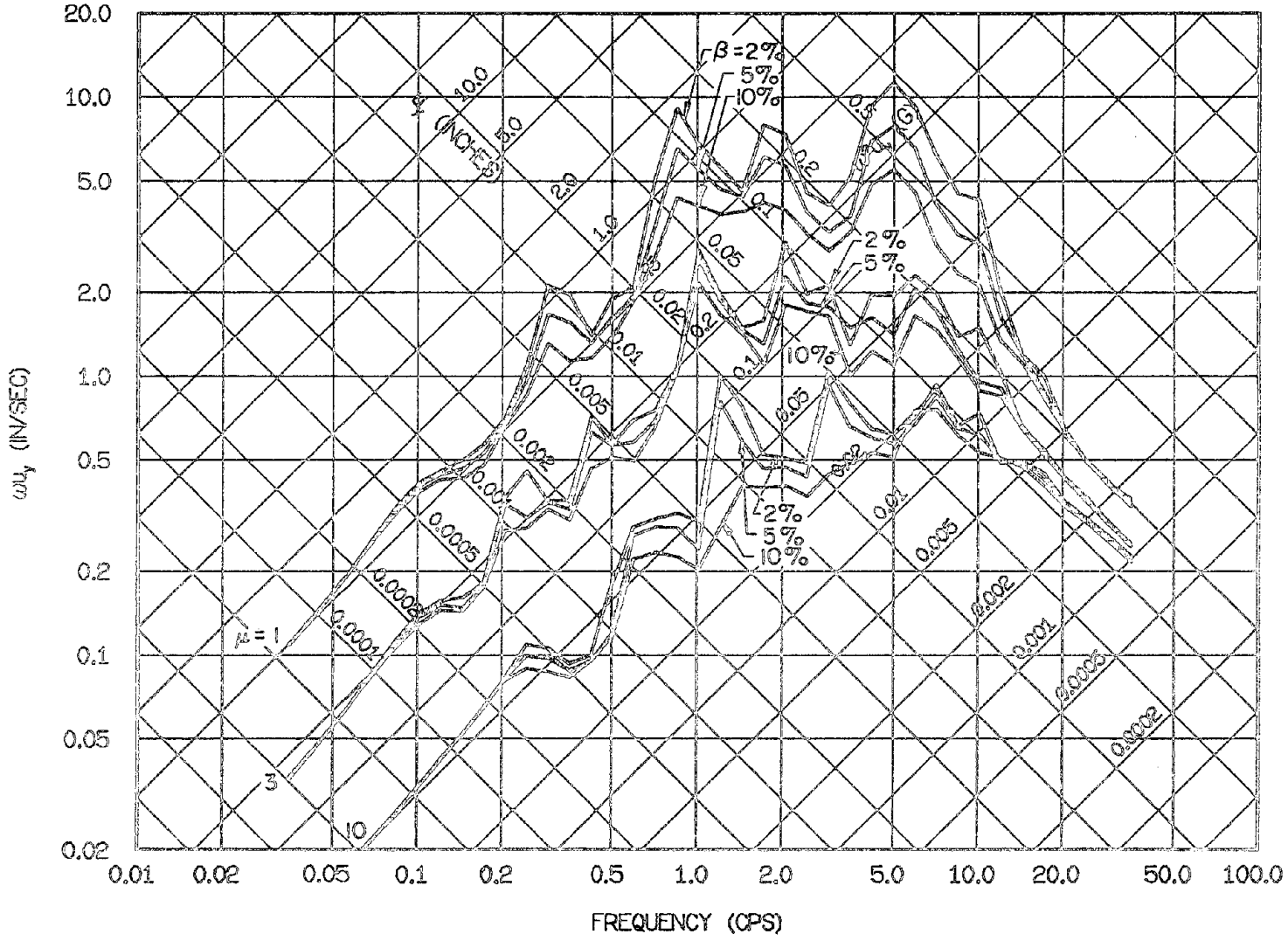

Fig. 3.74 Comparison of Elastoplastic Yield Spectra for the Kilauea, Hawaii Record of April 26, 1973, Component S30W

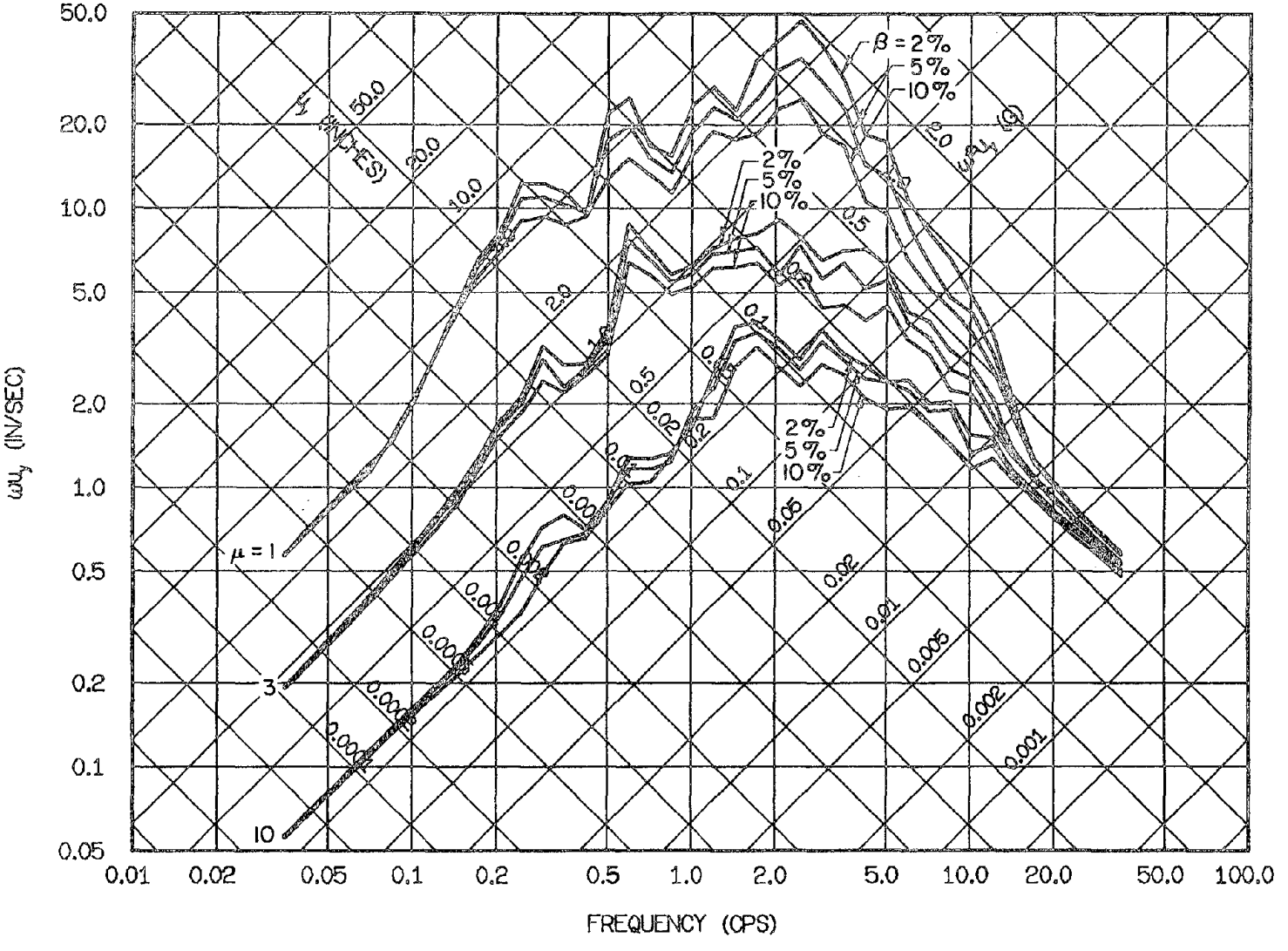

Fig. 3.75 Comparison of Elastoplastic Yield Spectra for the Managua Record of Dec. 23, 1972, Component South

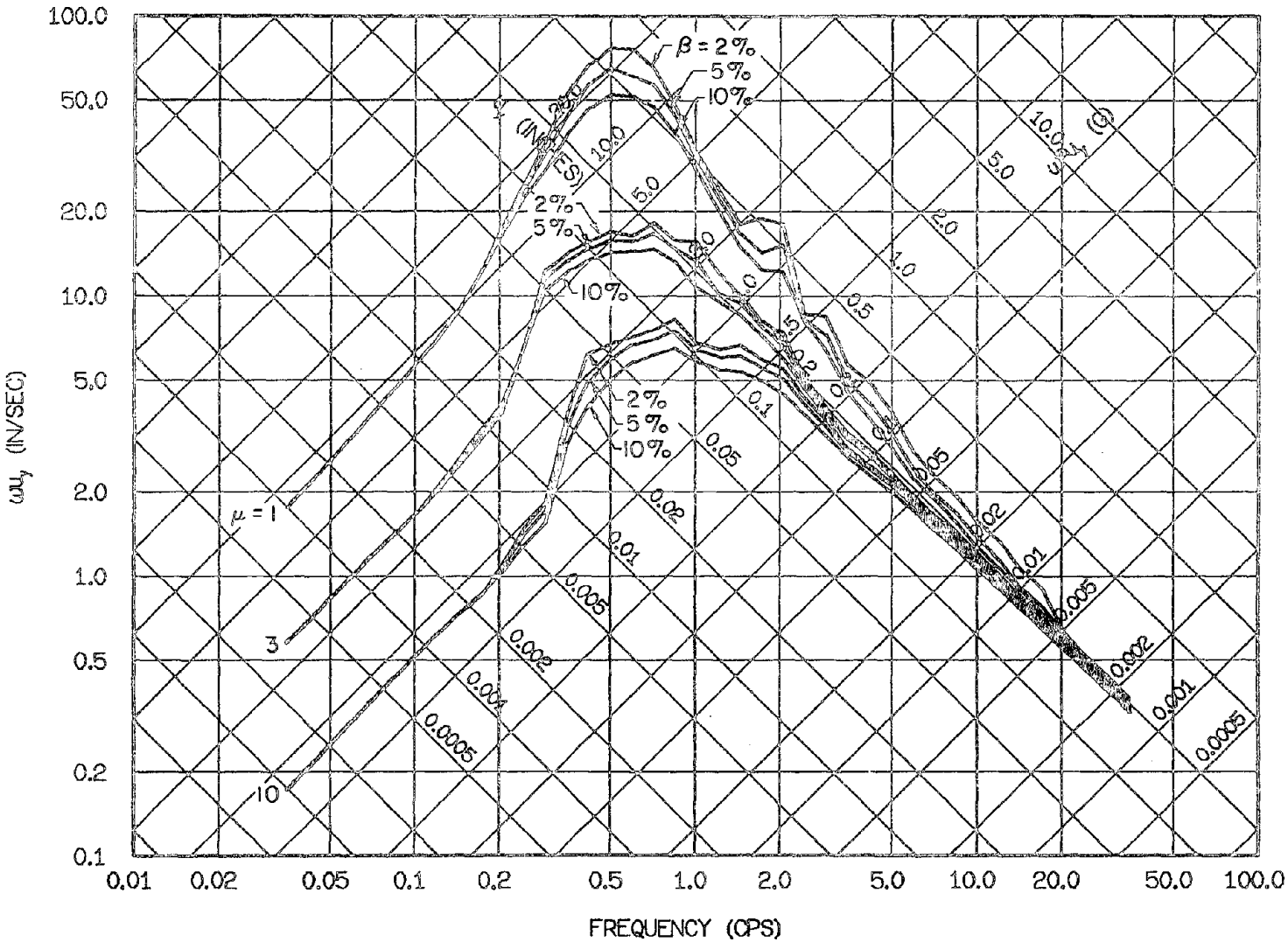

Fig. 3.76 Comparison of Elastoplastic Yield Spectra for the Bucarest Record of Mar. 4, 1977, Component S-N

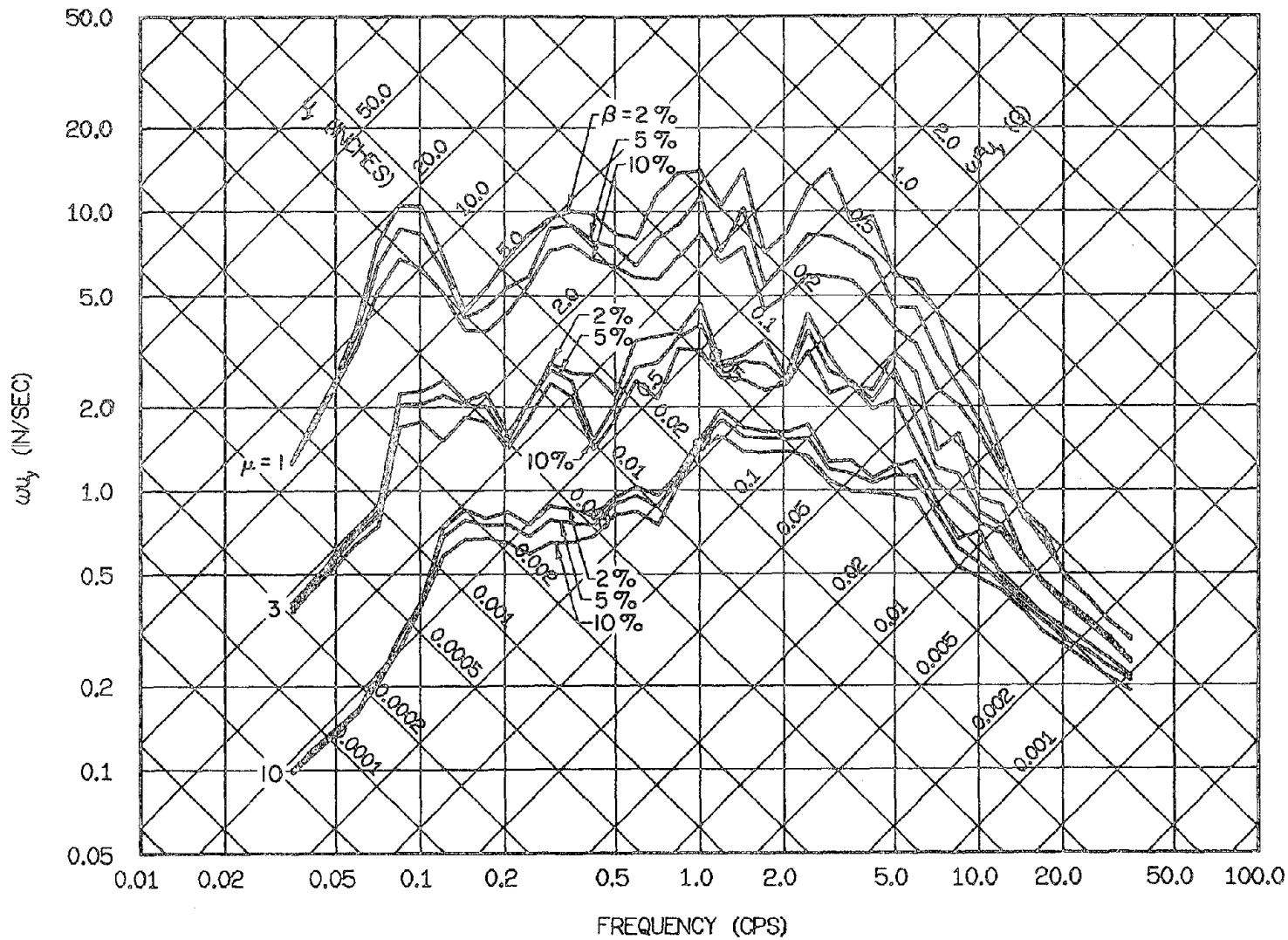

Fig. 3.77 Comparison of Elastoplastic Yield Spectra for the Santiago Record of July 8, 1971, Component N10W

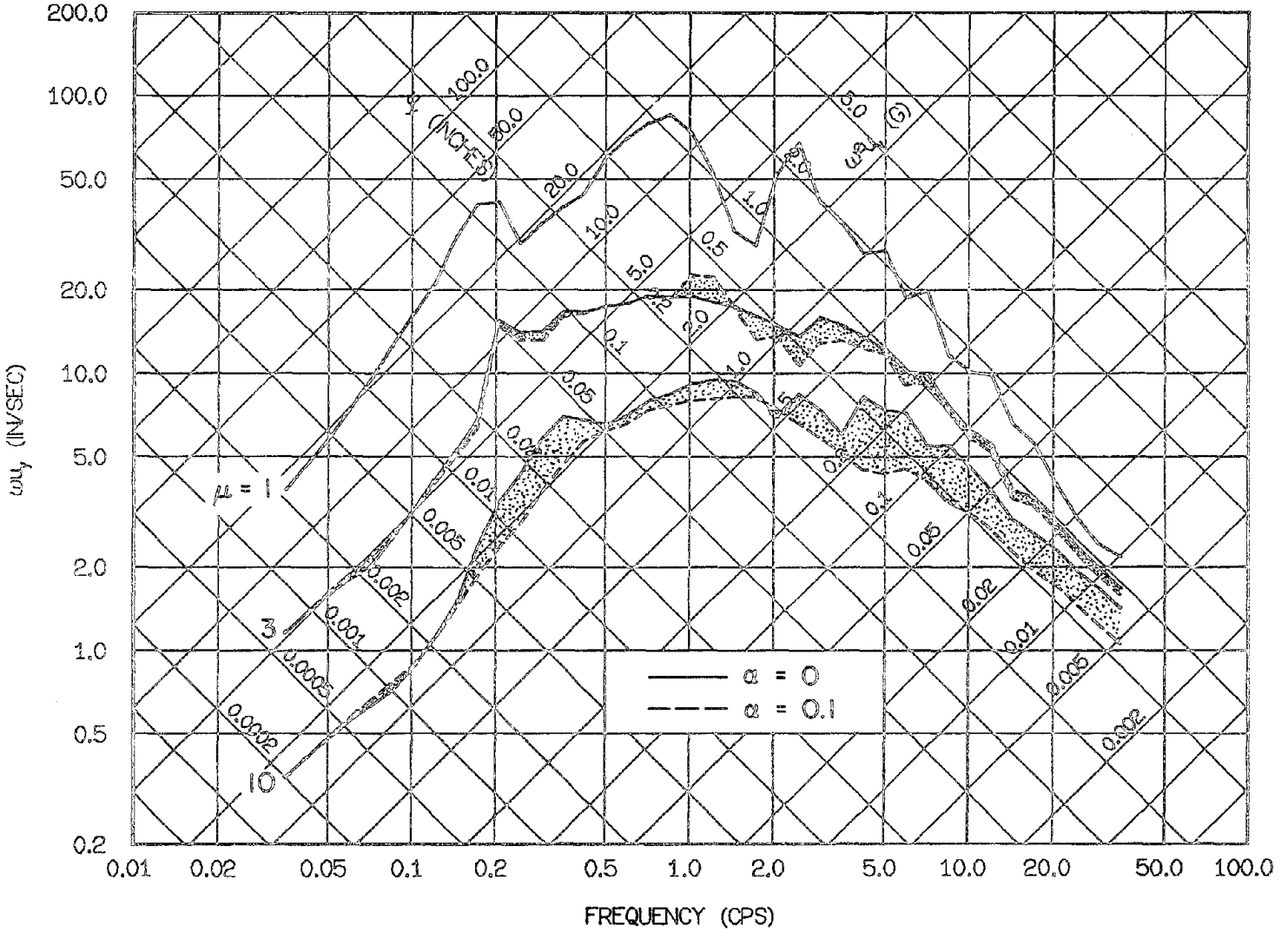

Fig. 3.78 Comparison of Elastoplastic and Bilinear Yield Spectra for the Pacoima Dam Record of Feb. 9, 1971, Component S16E: 5% Damping

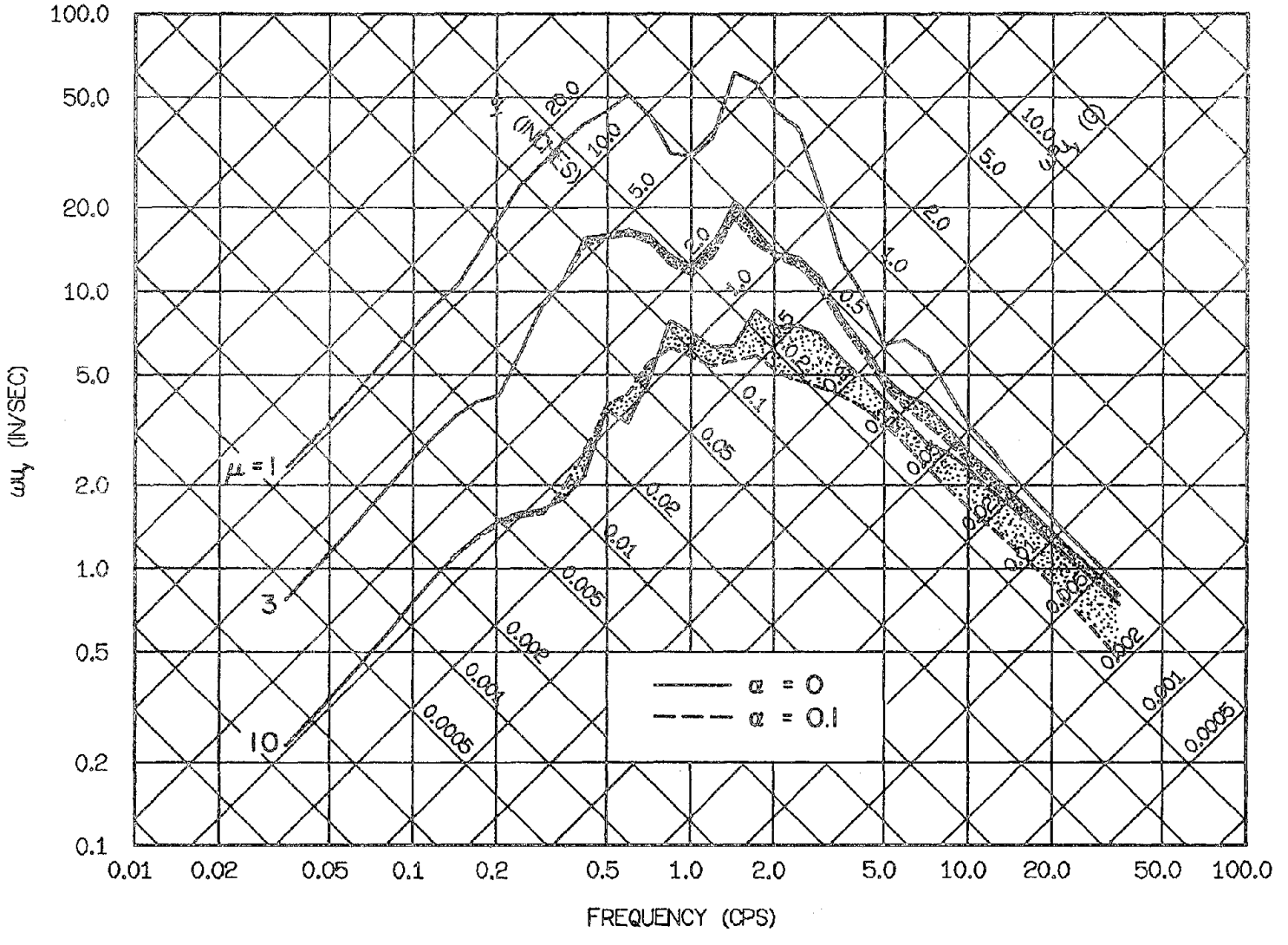

Fig. 3.79 Comparison of Elastoplastic and Bilinear Yield Spectra for the Cholame-Shandon No. 2 Record of June 27, 1966, Component N65E: 5% Damping

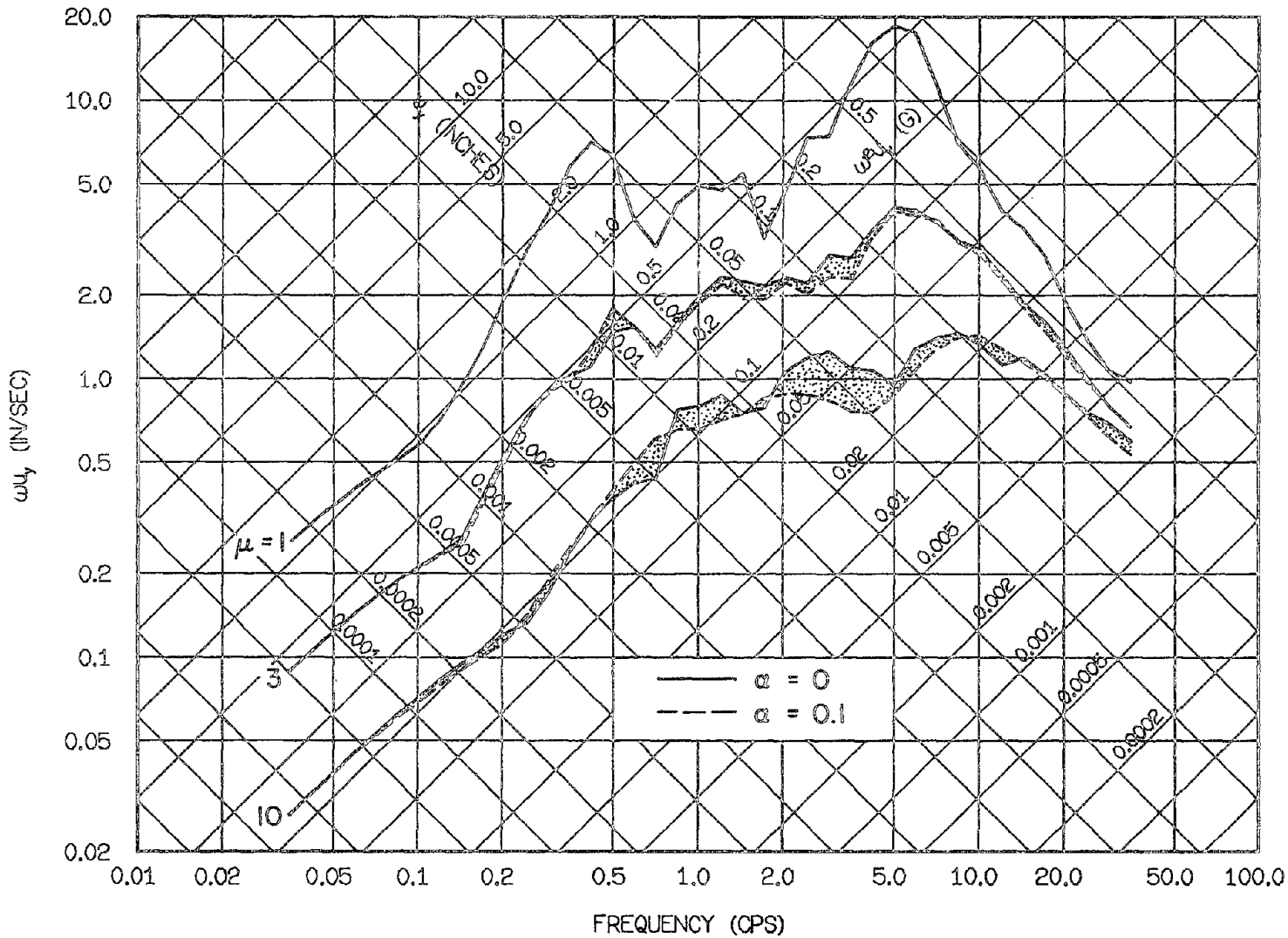

Fig. 3.80 Comparison of Elastoplastic and Bilinear Yield Spectra for the Melendy Ranch Record of Sept. 4, 1972, Component N29W: 5% Damping

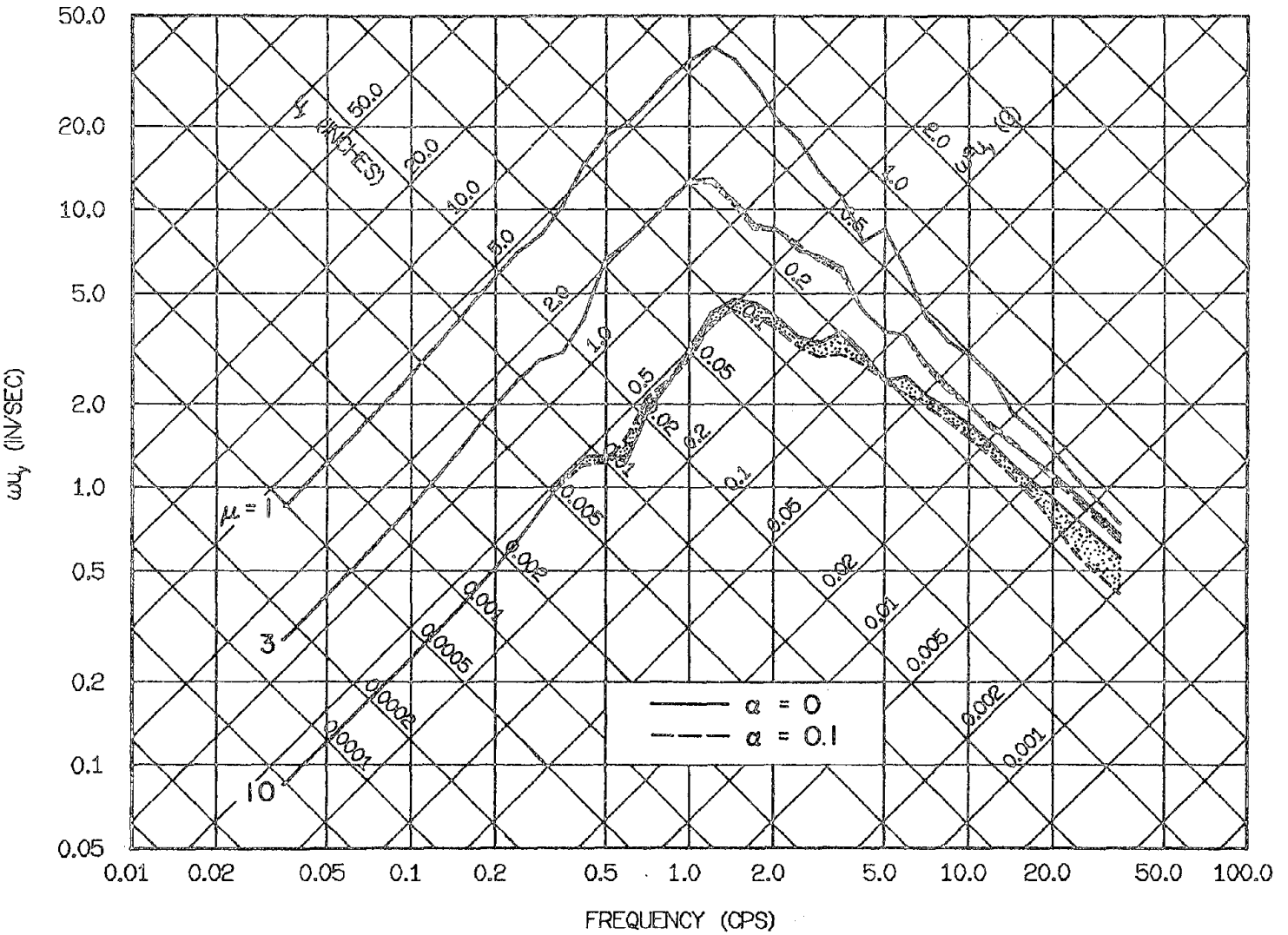

Fig. 3.81 Comparison of Elastoplastic and Bilinear Yield Spectra for the Gilroy Array No. 6 Record of Aug. 6, 1979, Component 230 Deg: 5% Damping

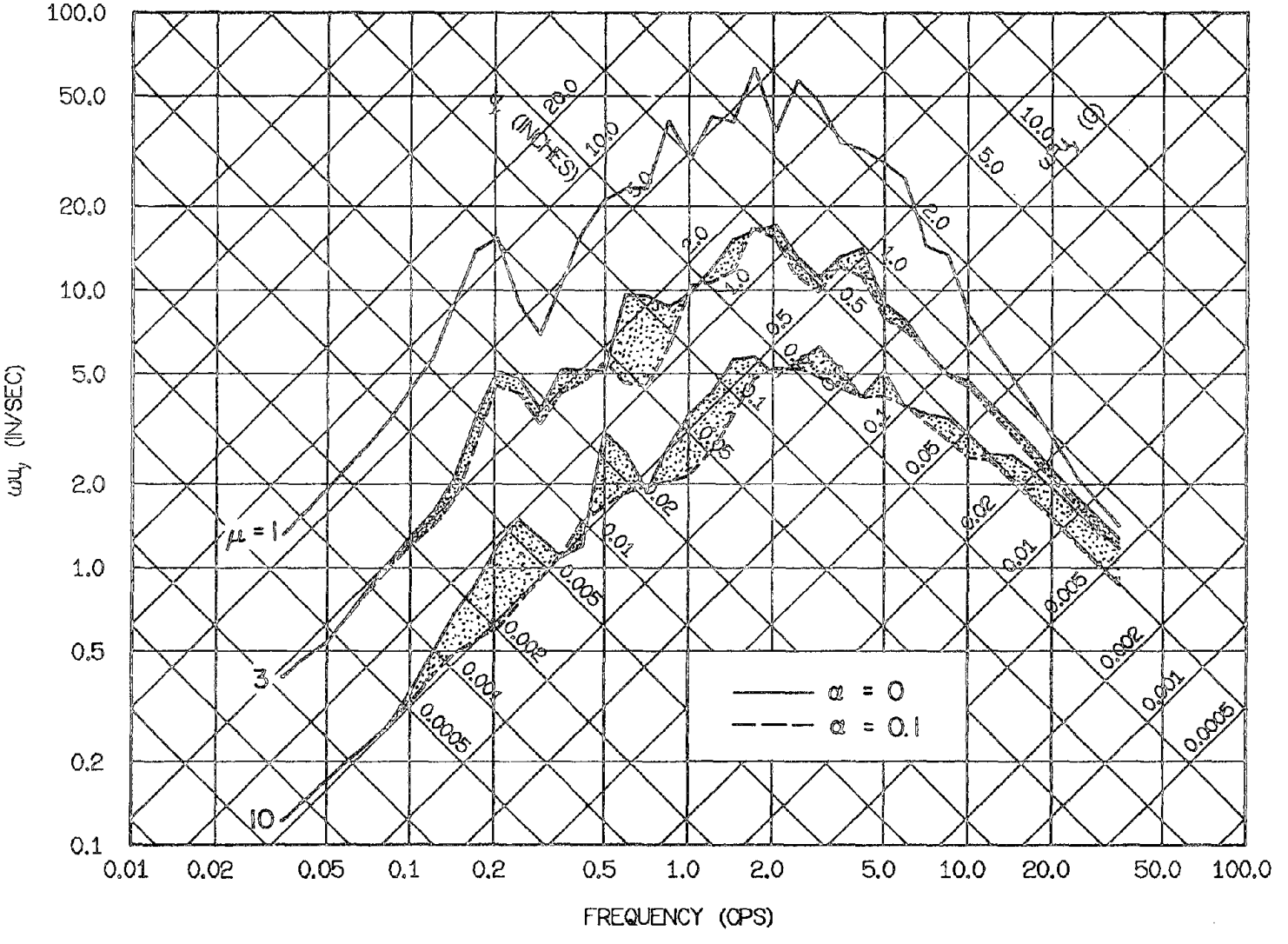

Fig. 3.82 Comparison of Elastoplastic and Bilinear Yield Spectra for the Bonds Corner Record of Oct. 15, 1979, Component 230 Deg: 5% Damping

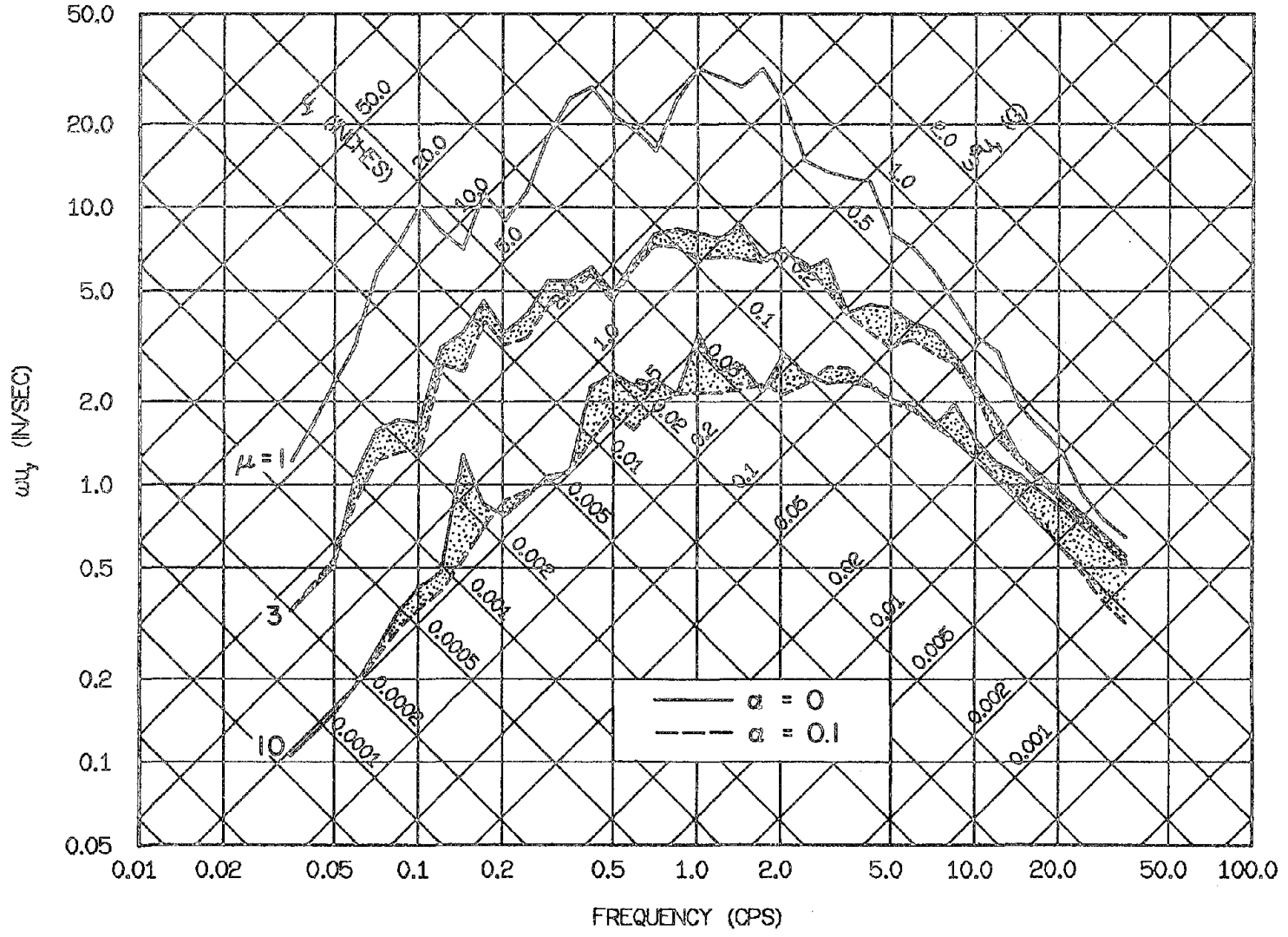

Fig. 3.83 Comparison of Elastoplastic and Bilinear Yield Spectra for the El Centro Record of May 18, 1940, Component S00E: 5% Damping

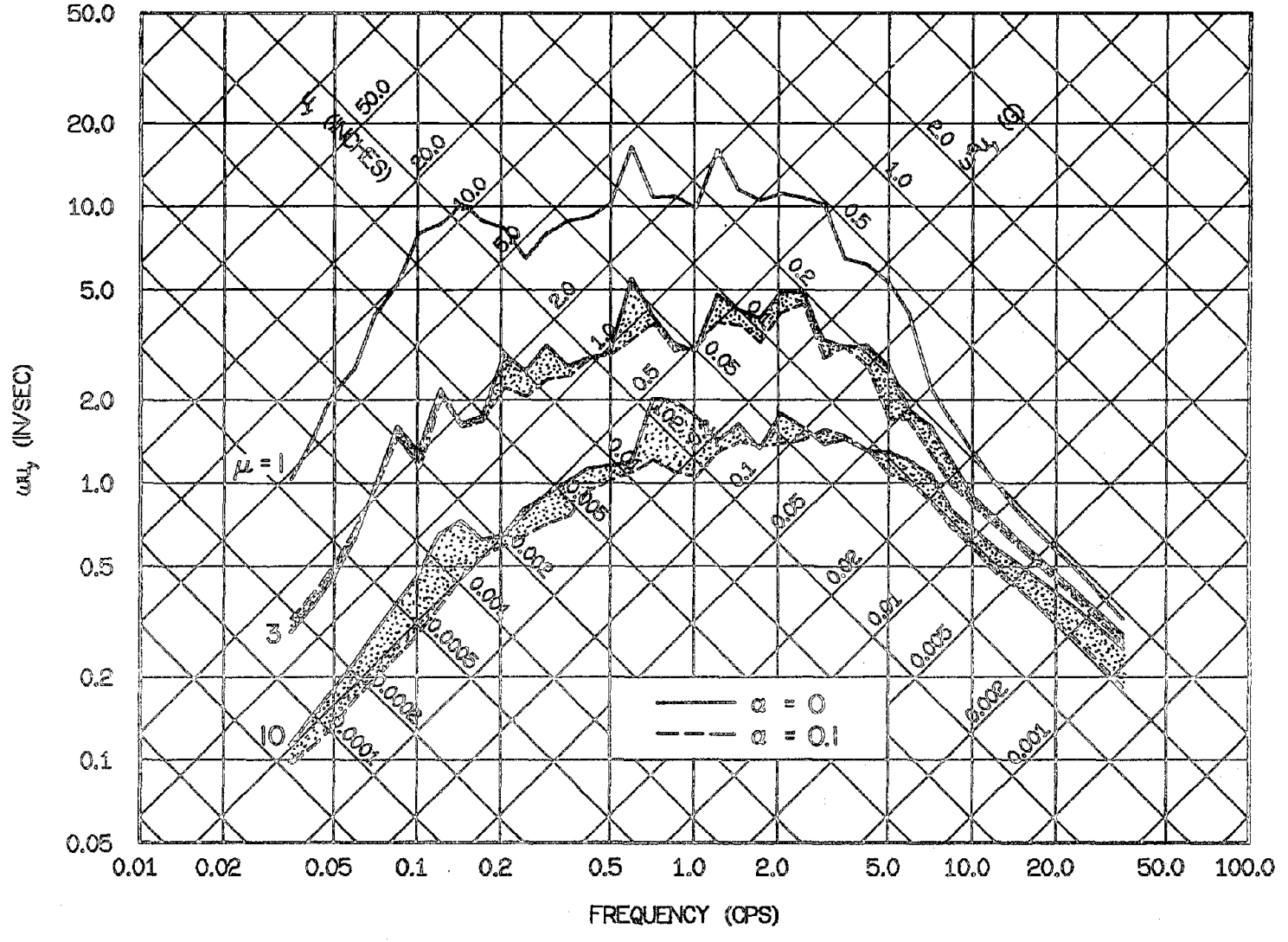

Fig. 3.84 Comparison of Elastoplastic and Bilinear Yield Spectra for the Taft Record of July 21, 1952, Component S69E: 5% Damping

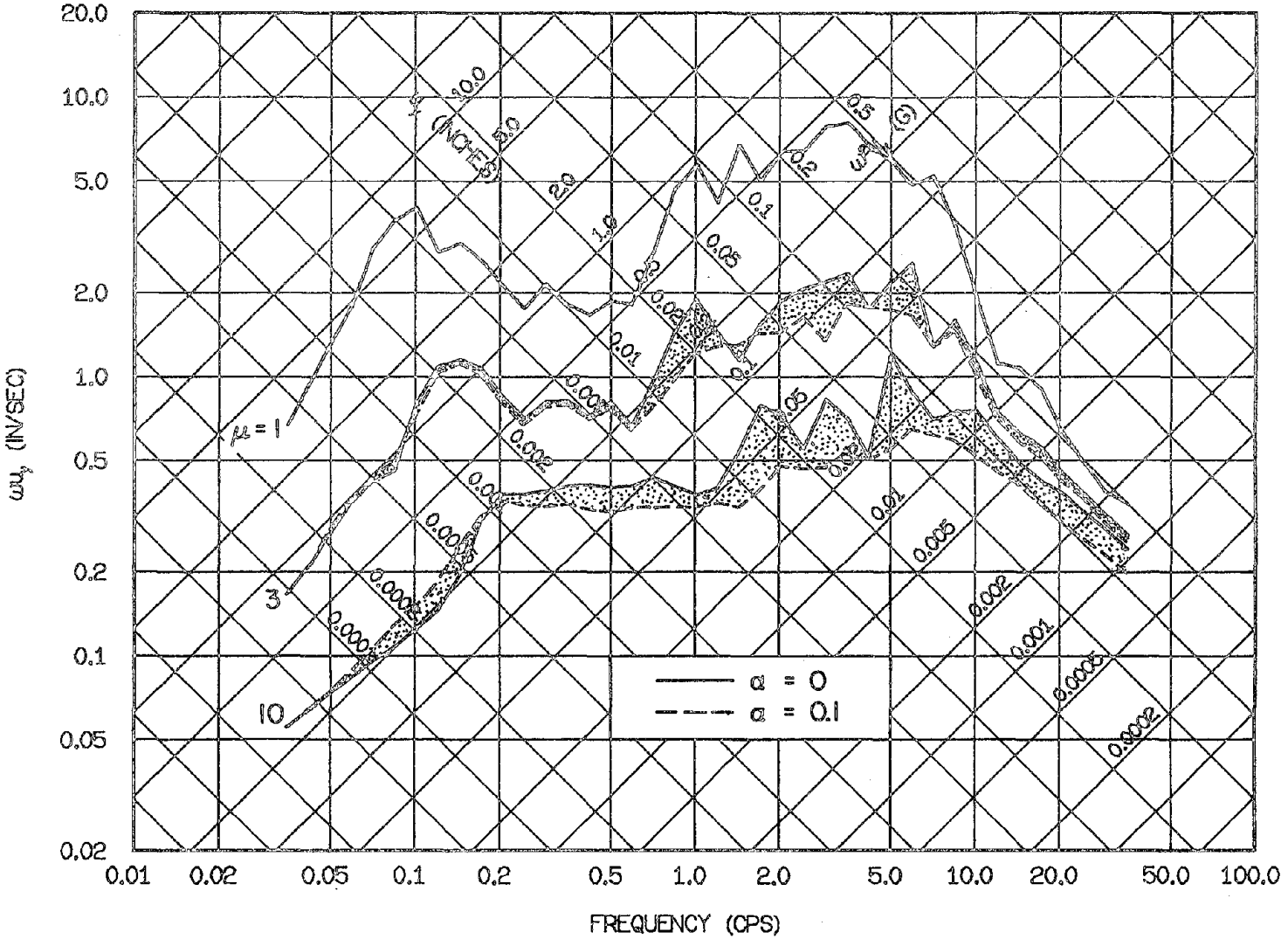

Fig. 3.85 Comparison of Elastoplastic and Bilinear Yield Spectra for the Adak, Alaska Record of May 1, 1971, Component West: 5% Damping

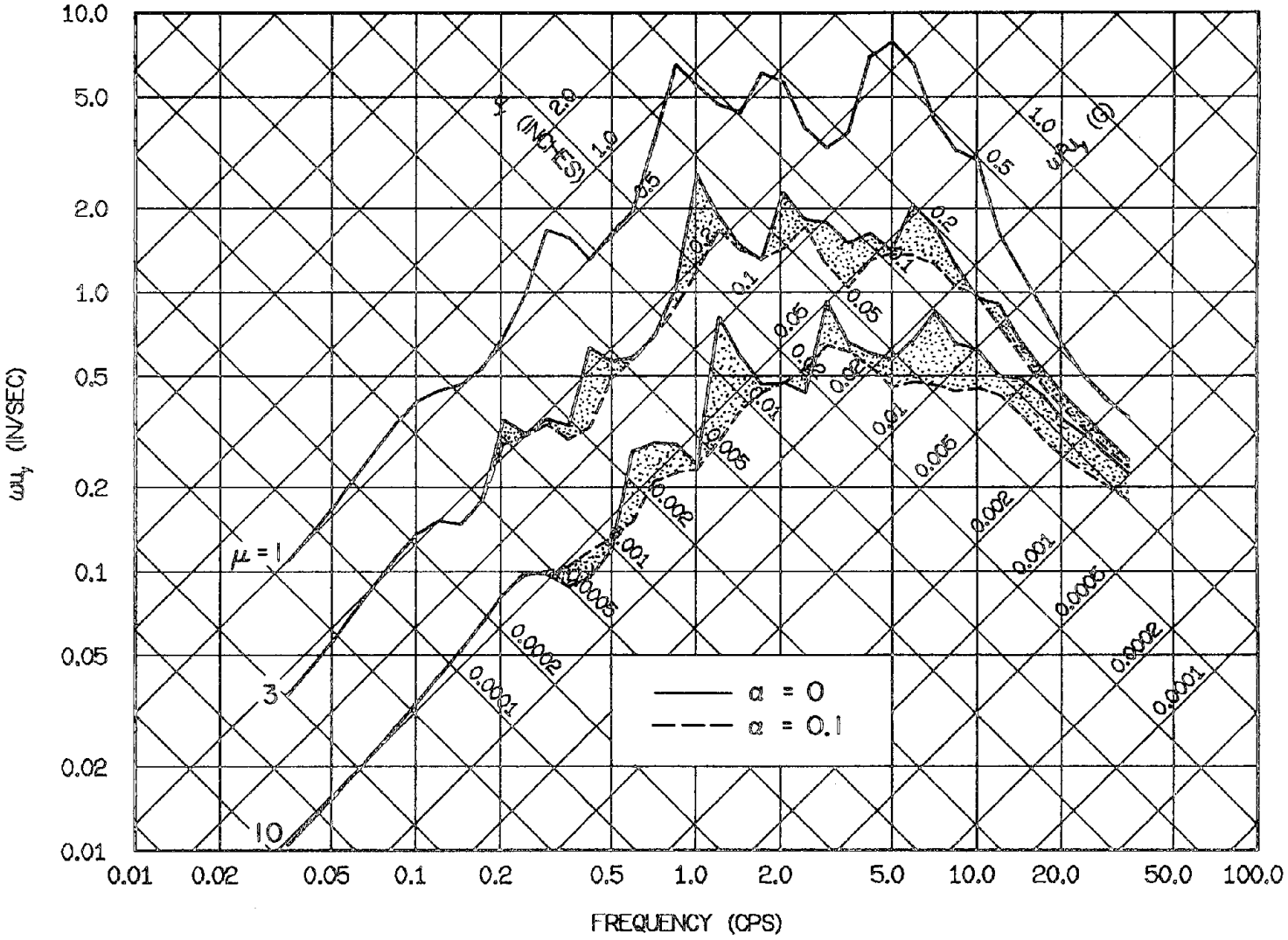

Fig. 3.86 Comparison of Elastoplastic and Bilinear Yield Spectra for the Kilauea, Hawaii Record of April 26, 1973, Component S30W: 5% Damping

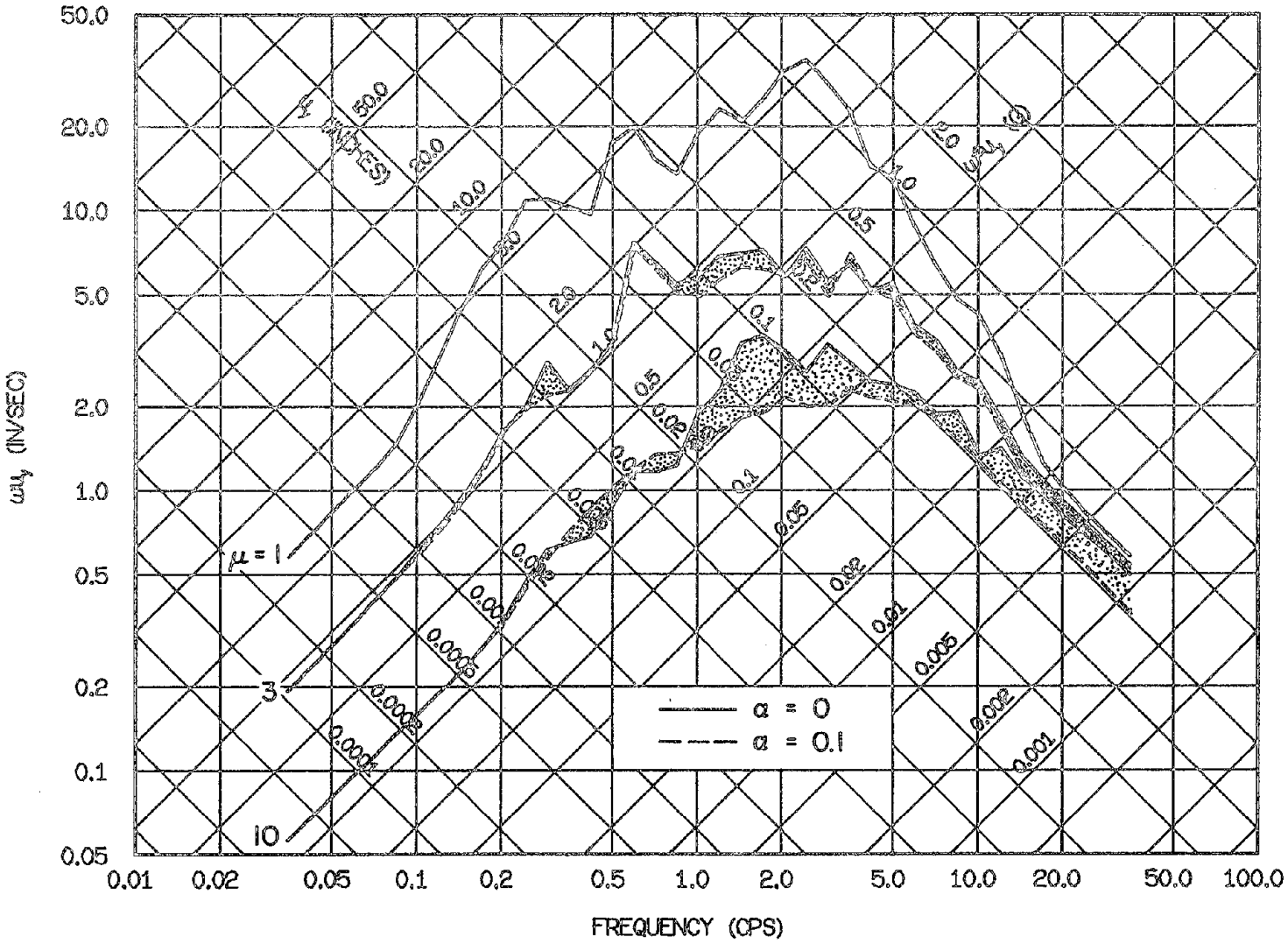

Fig. 3.87 Comparison of Elastoplastic and Bilinear Yield Spectra for the Managua Record of Dec. 23, 1972, Component South: 5% Damping

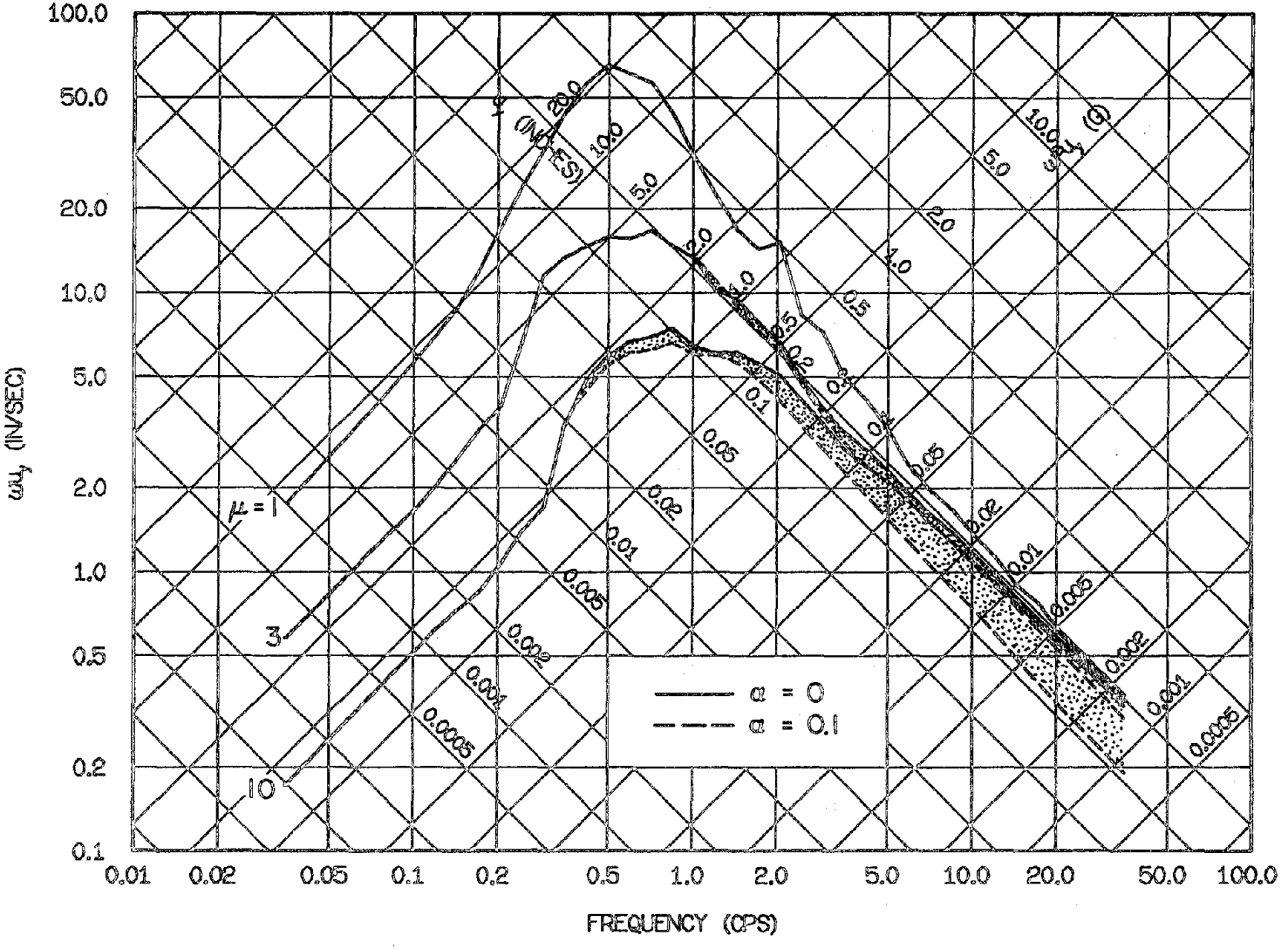

Fig. 3.88 Comparison of Elastoplastic and Bilinear Yield Spectra for the Bucarest Record of Mar. 4, 1977, Component S-N: 5% Damping

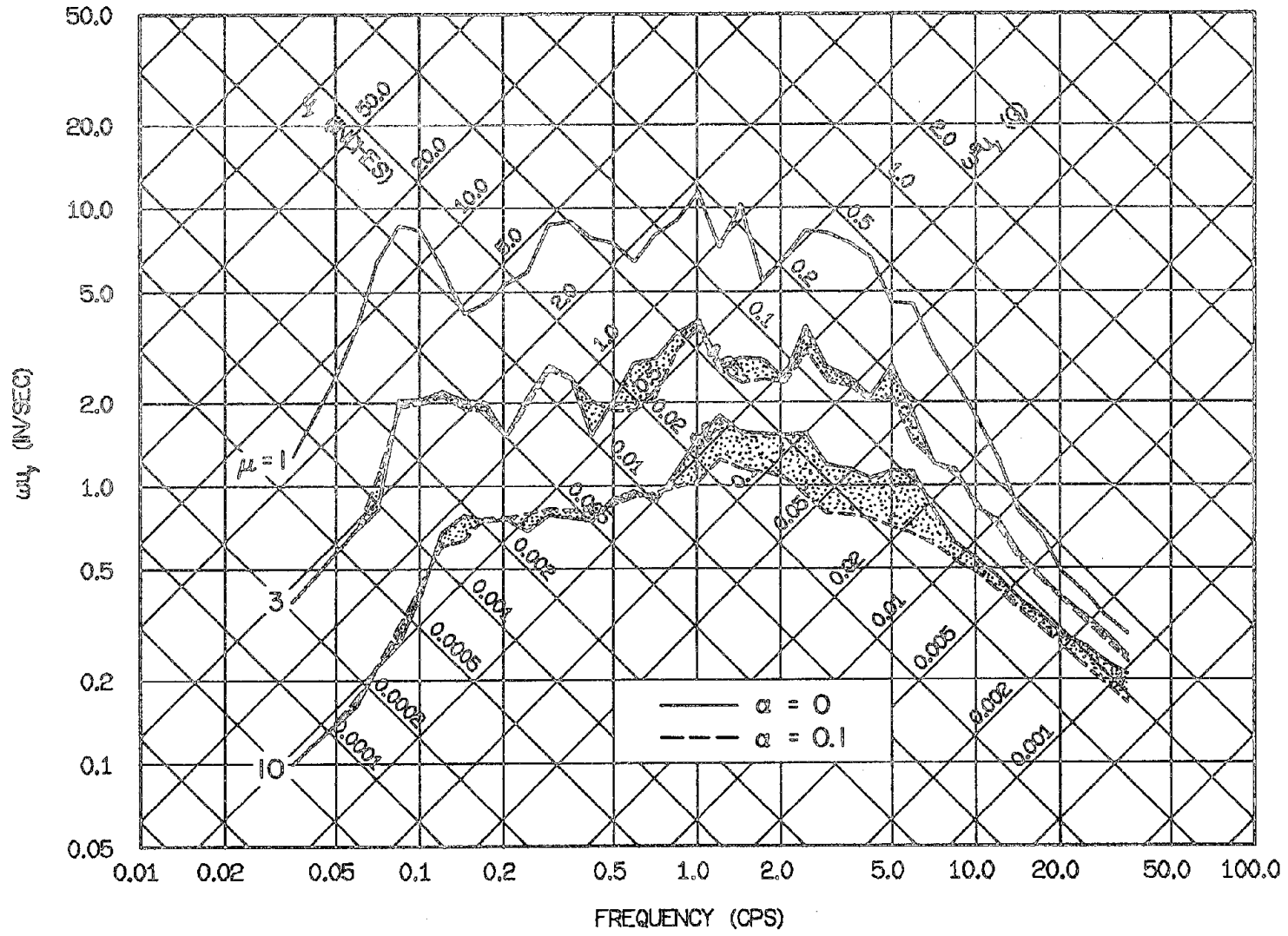

Fig. 3.89 Comparison of Elastoplastic and Bilinear Yield Spectra for the Santiago Record of July 8, 1971, Component N10W: 5% Damping

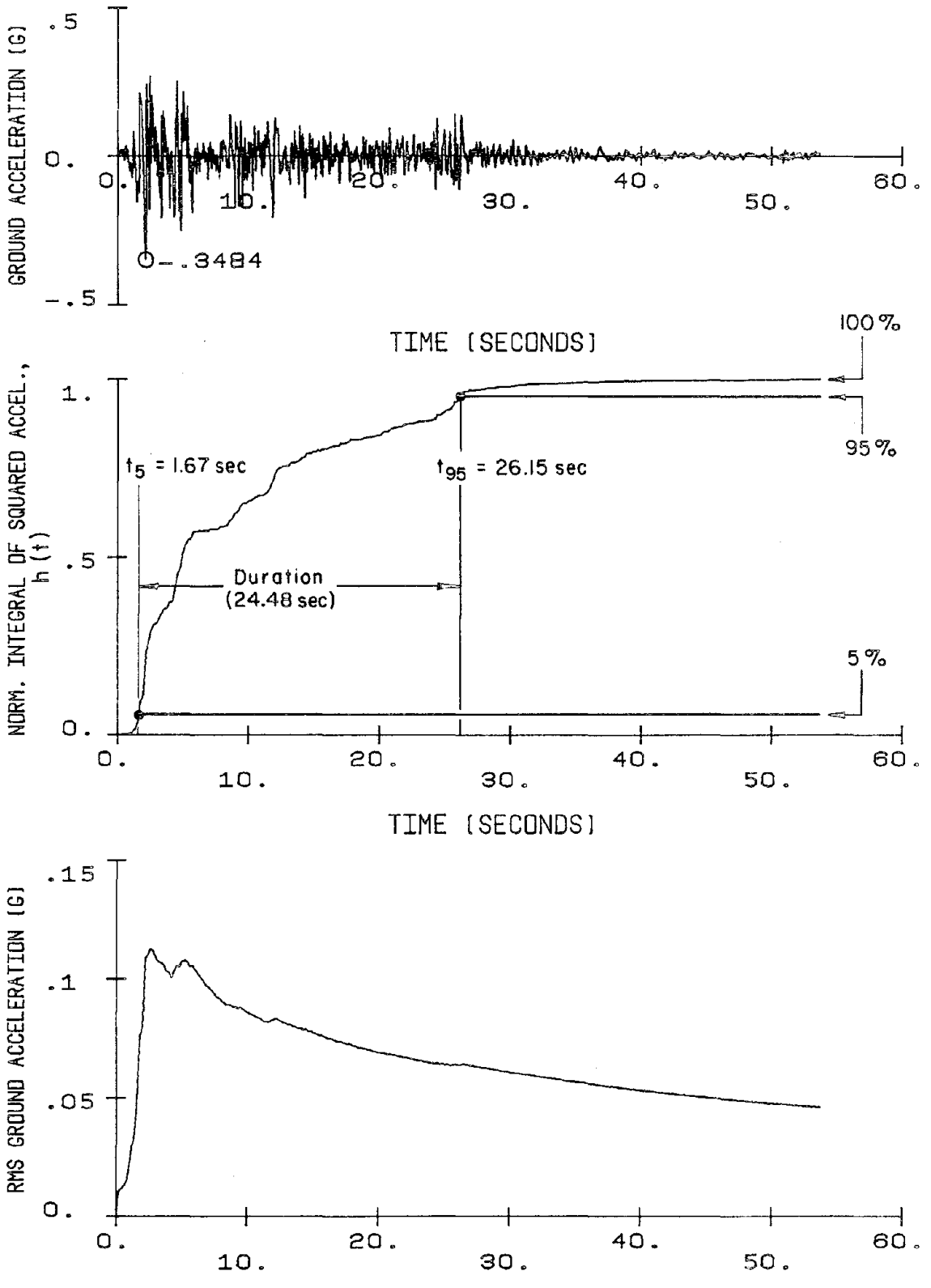

Fig. 4.1 Ground Acceleration, Husid Plot, and RMS Acceleration for the El Centro Record without a Prefixed Pulse

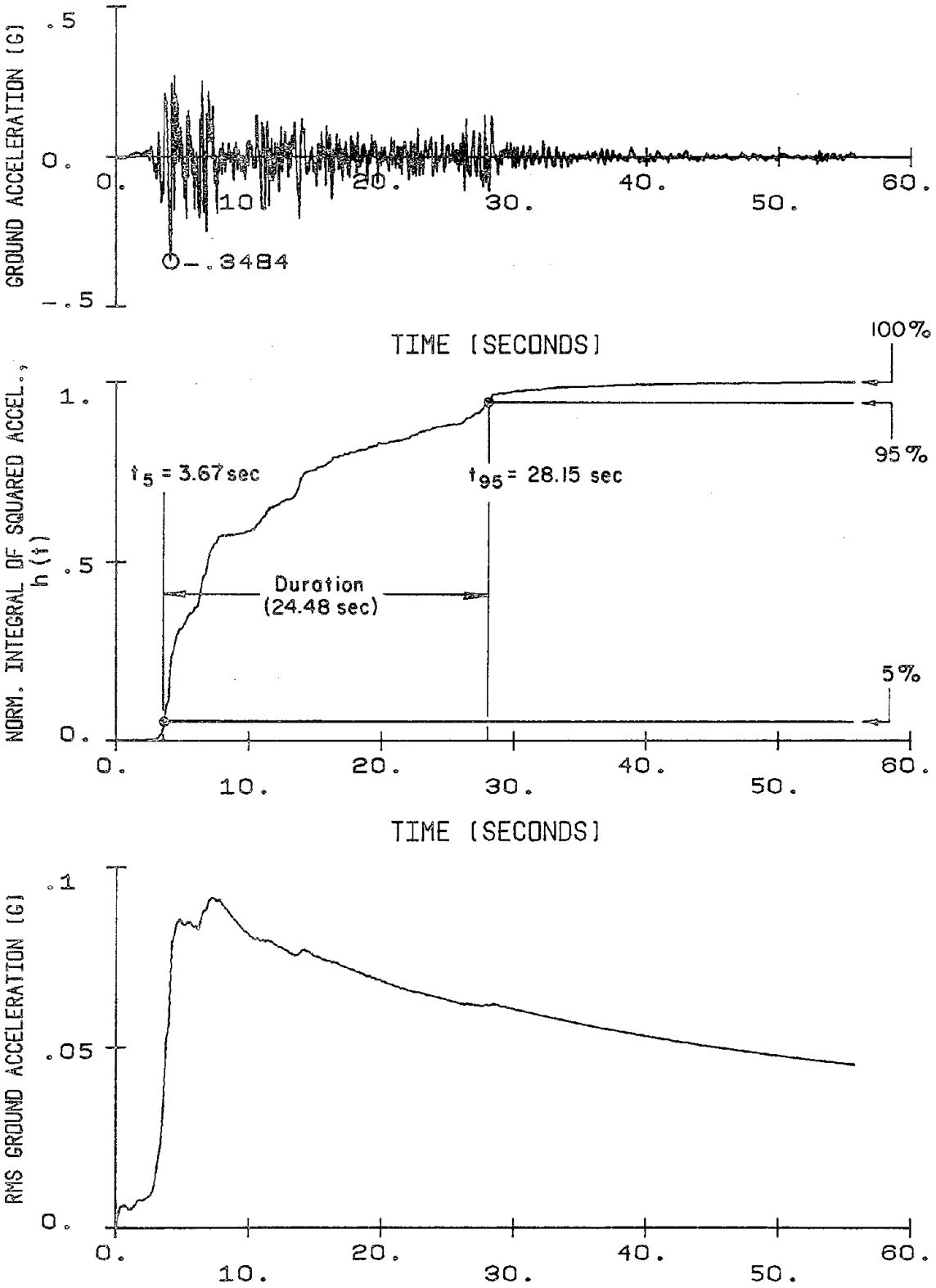

Fig. 4.2 Ground Acceleration, Husid Plot, and RMS Acceleration for the El Centro Record with a Prefixed Pulse

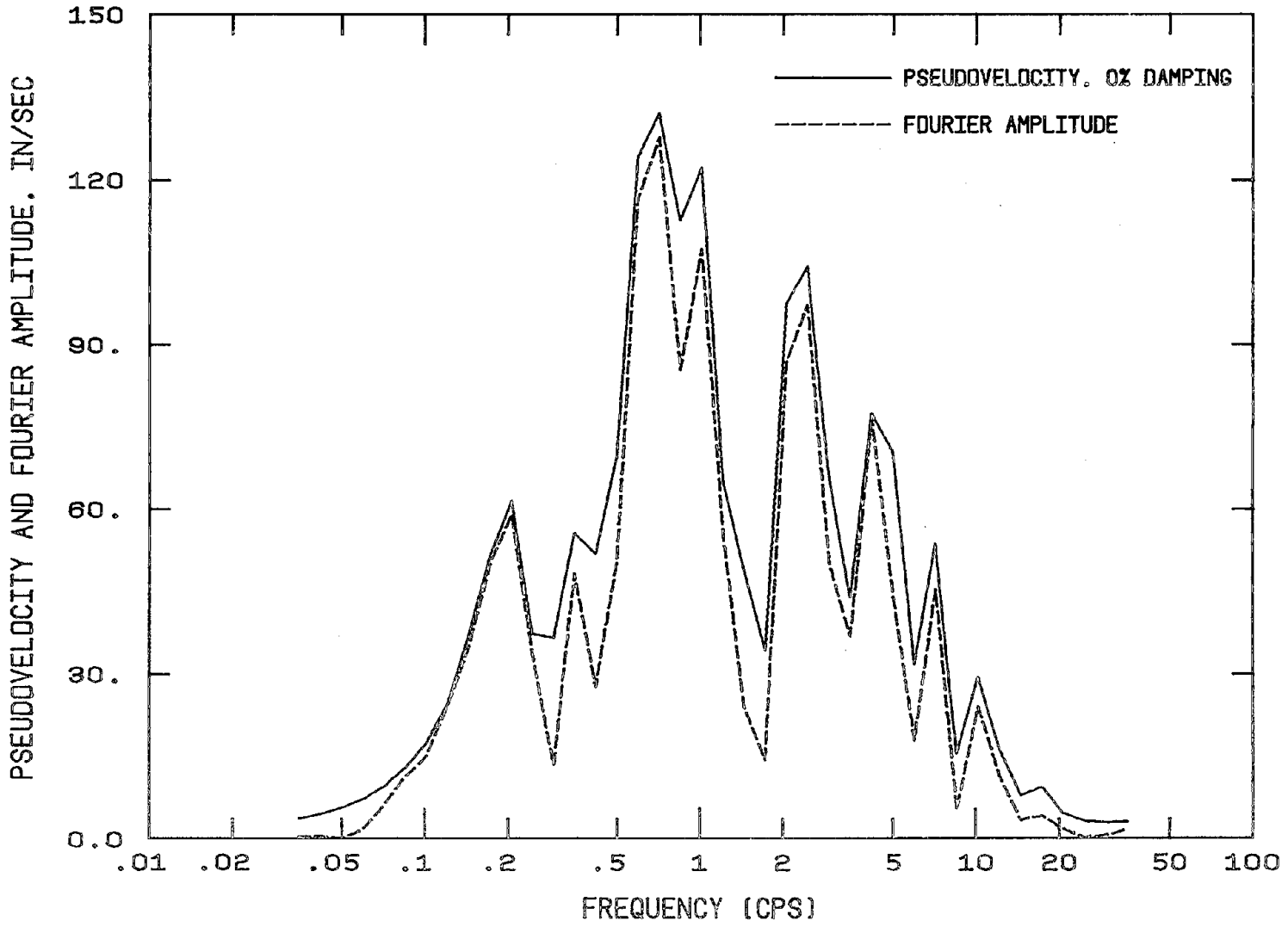

Fig. 4.3 Undamped Pseudovelocity and Fourier Amplitude Spectra for the Pacoima Dam Record of Feb. 9, 1971, Component S16E

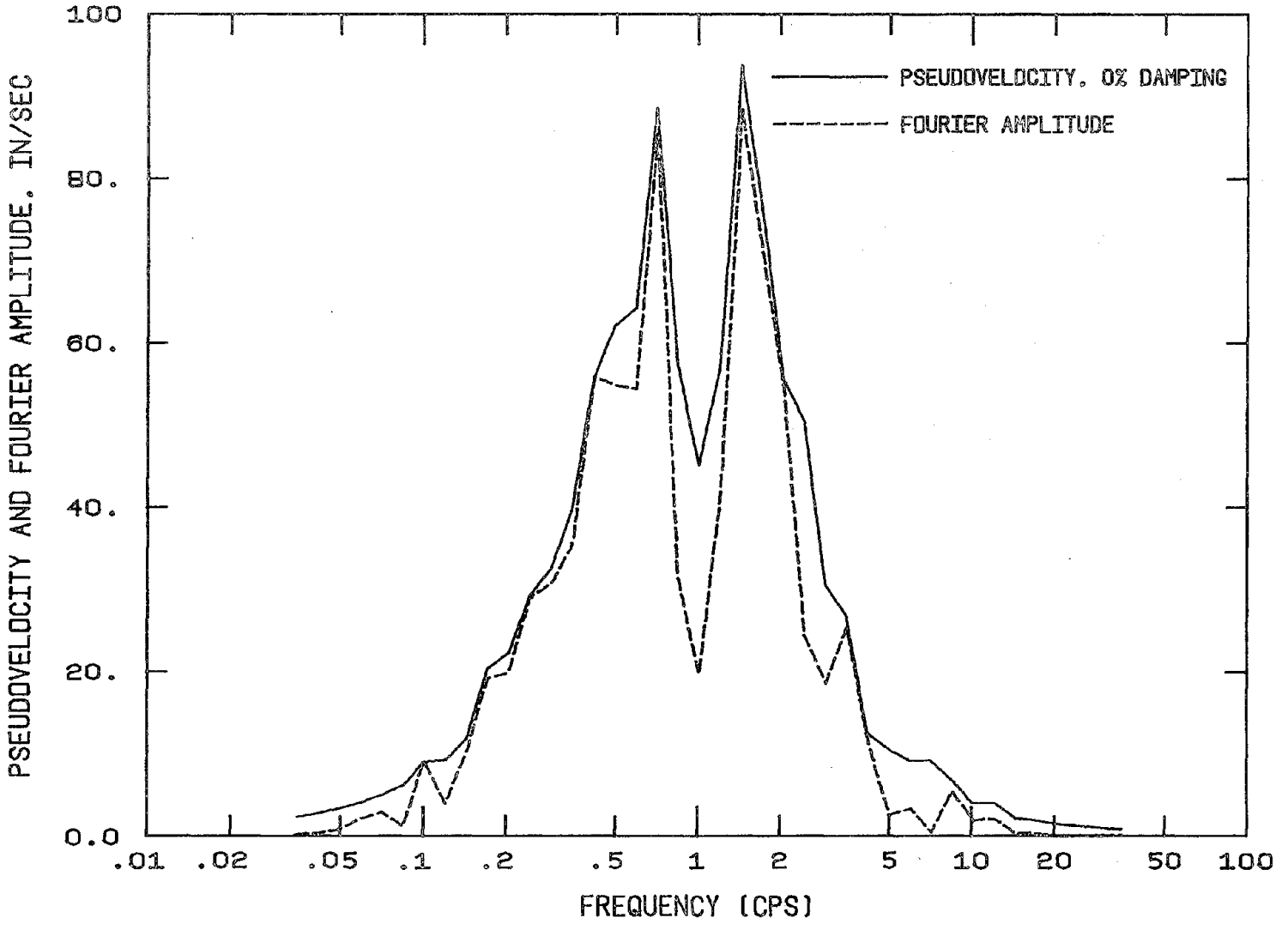

Fig. 4.4 Undamped Pseudovelocity and Fourier Amplitude Spectra for the Cholame-Shandon No. 2 Record of June 27, 1966, Component N65E

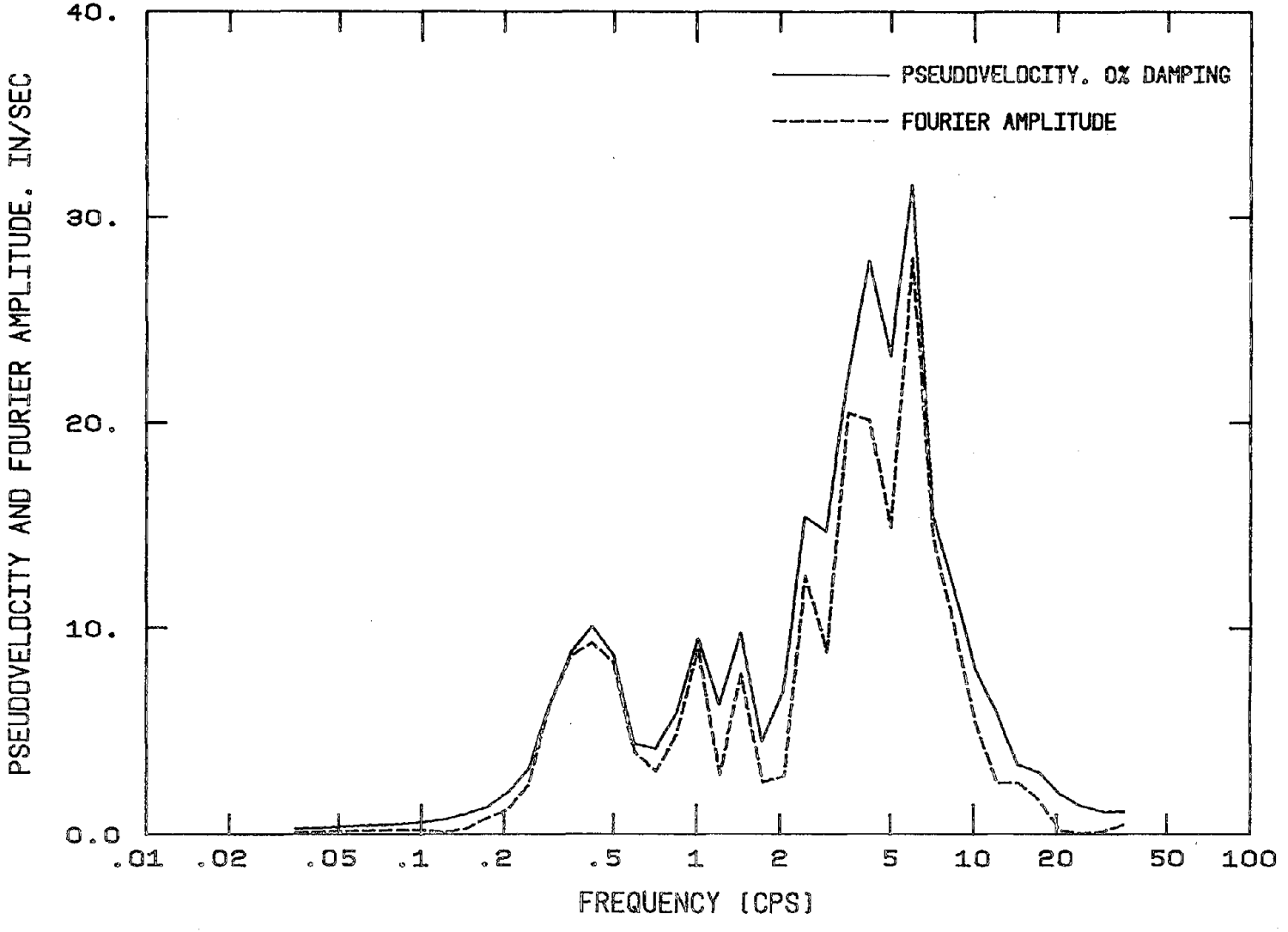

Fig. 4.5 Undamped Pseudovelocity and Fourier Amplitude Spectra for the Melendy Ranch Record of Sept. 4, 1972, Component N29W

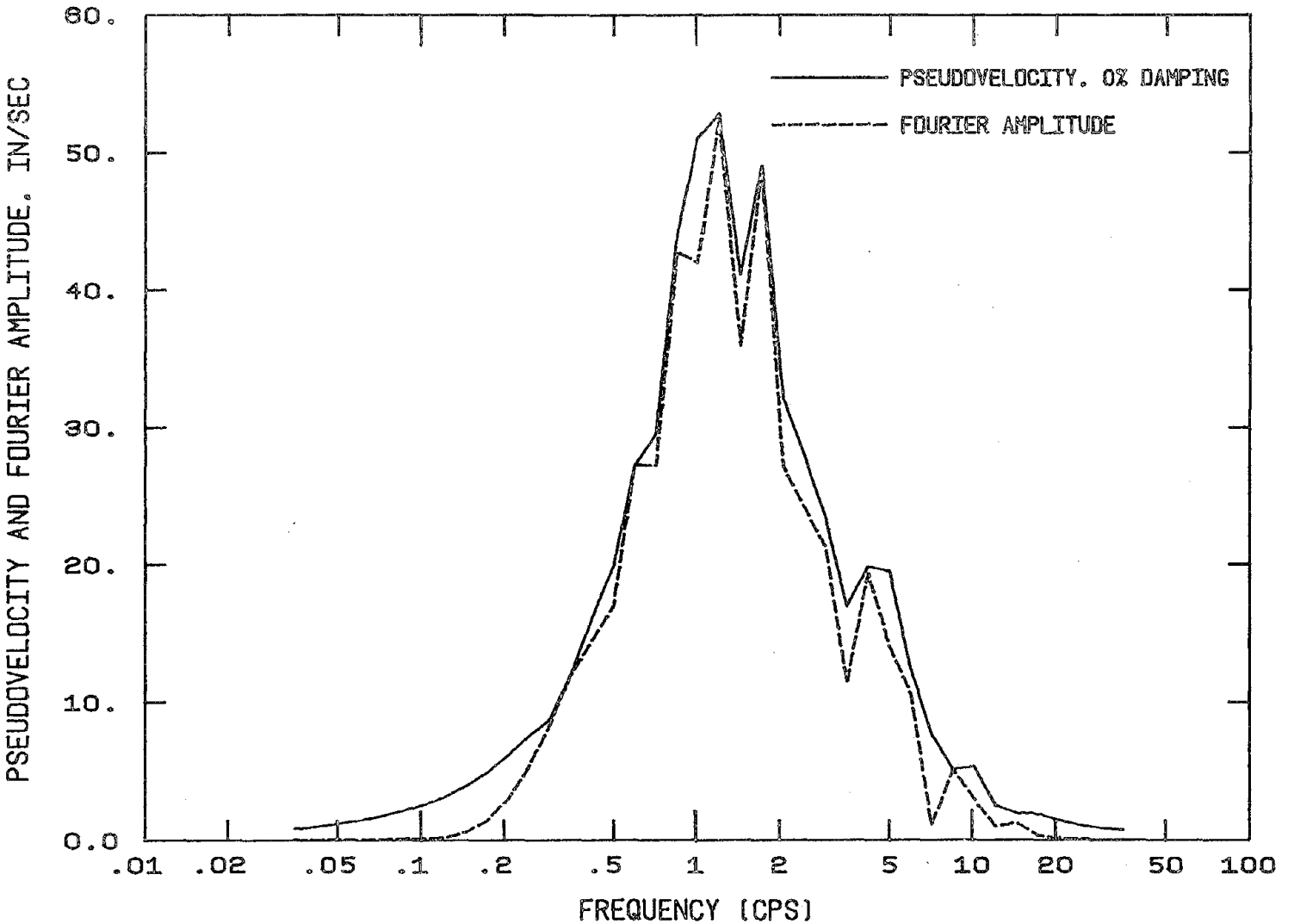

Fig. 4.6 Undamped Pseudovelocity and Fourier Amplitude Spectra for the Gilroy Array No. 6 Record of Aug. 6, 1979, Component 230 Deg

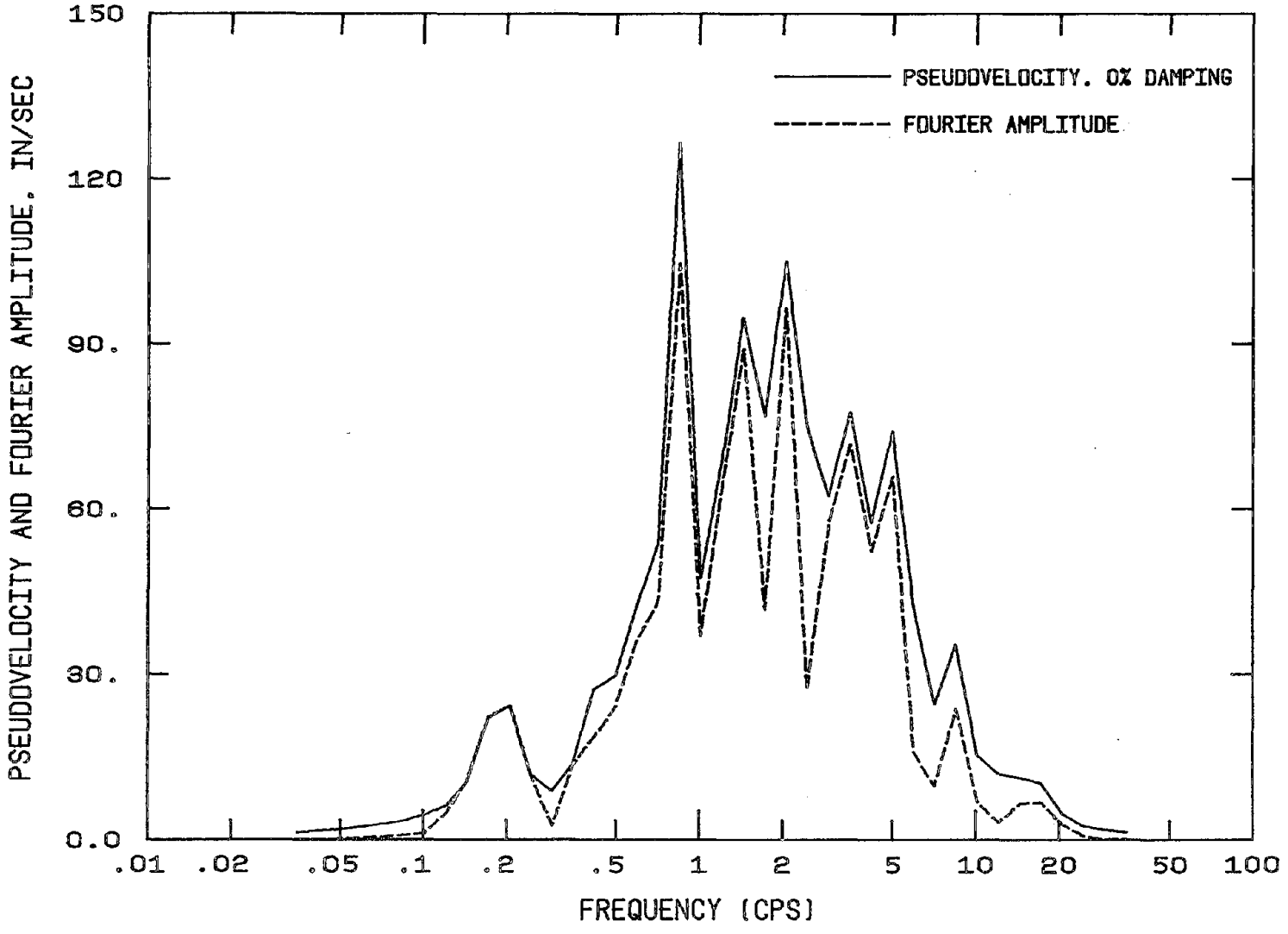

Fig. 4.7 Undamped Pseudovelocity and Fourier Amplitude Spectra for the Bonds Corner Record of Oct. 15, 1979, Component 230 Deg

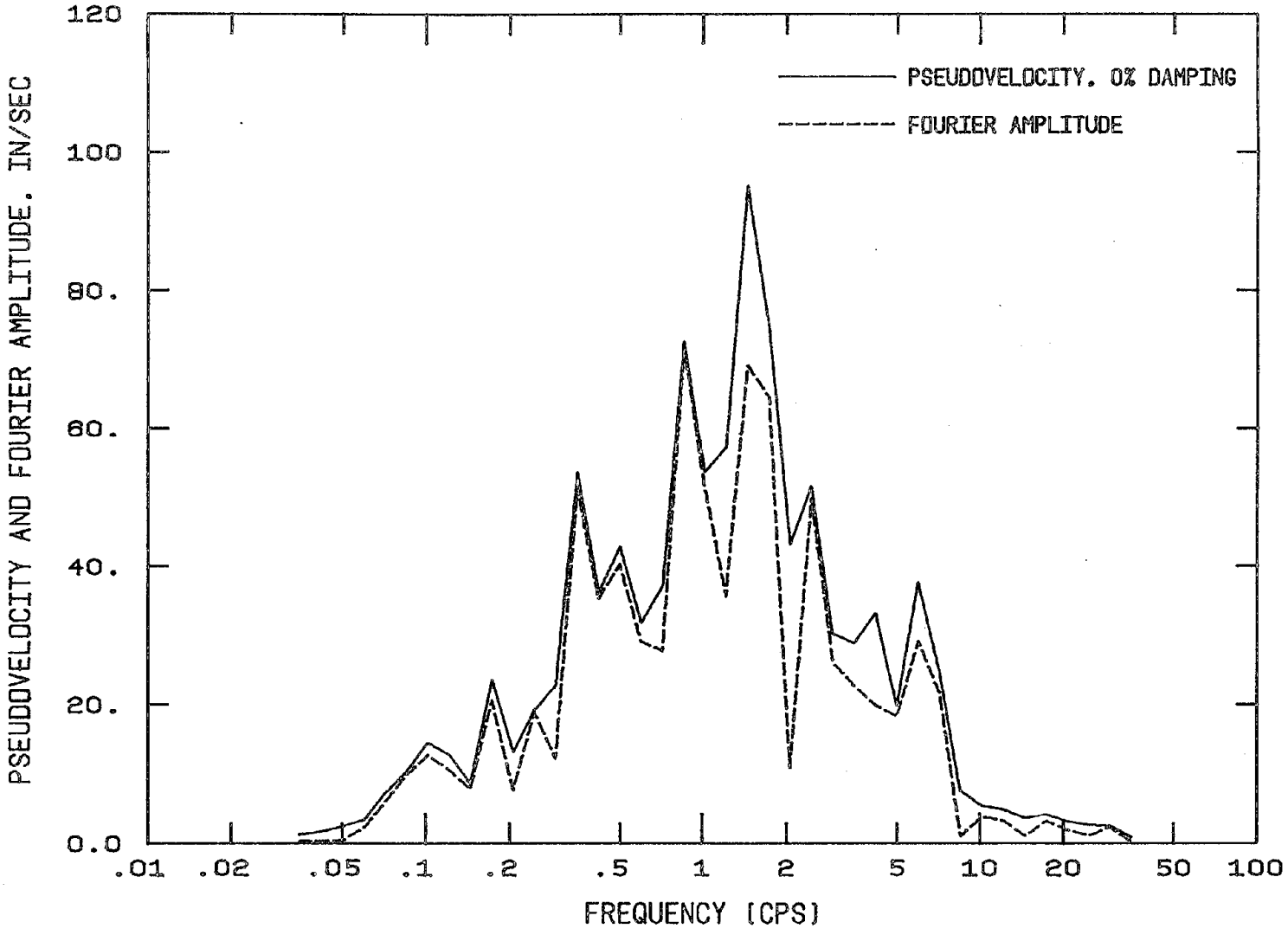

Fig. 4.8 Undamped Pseudovelocity and Fourier Amplitude Spectra for the El Centro Record of May 18, 1940, Component S00E

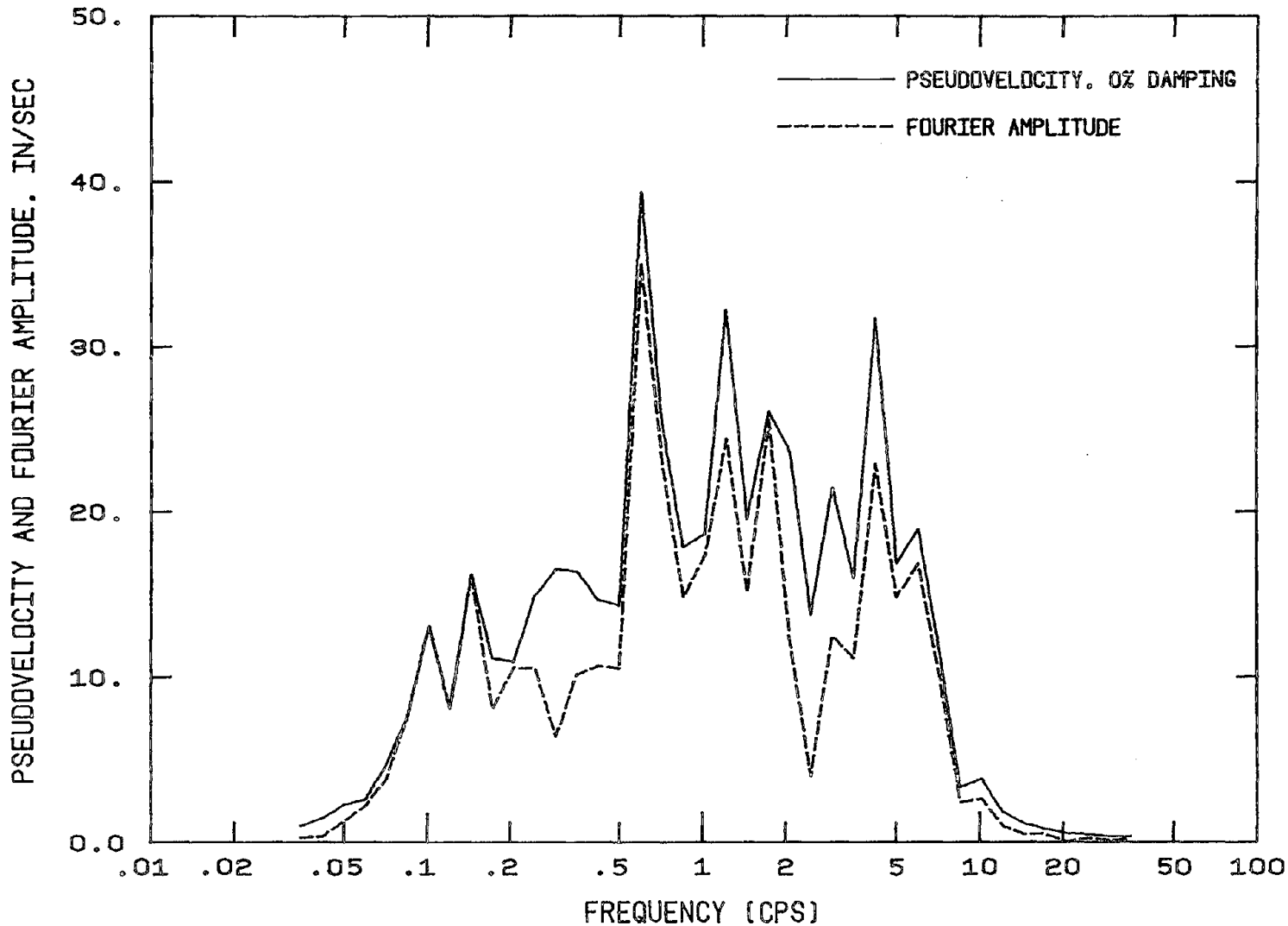

Fig. 4.9 Undamped Pseudovelocity and Fourier Amplitude Spectra for the Taft Record of July 21, 1952, Component S69E

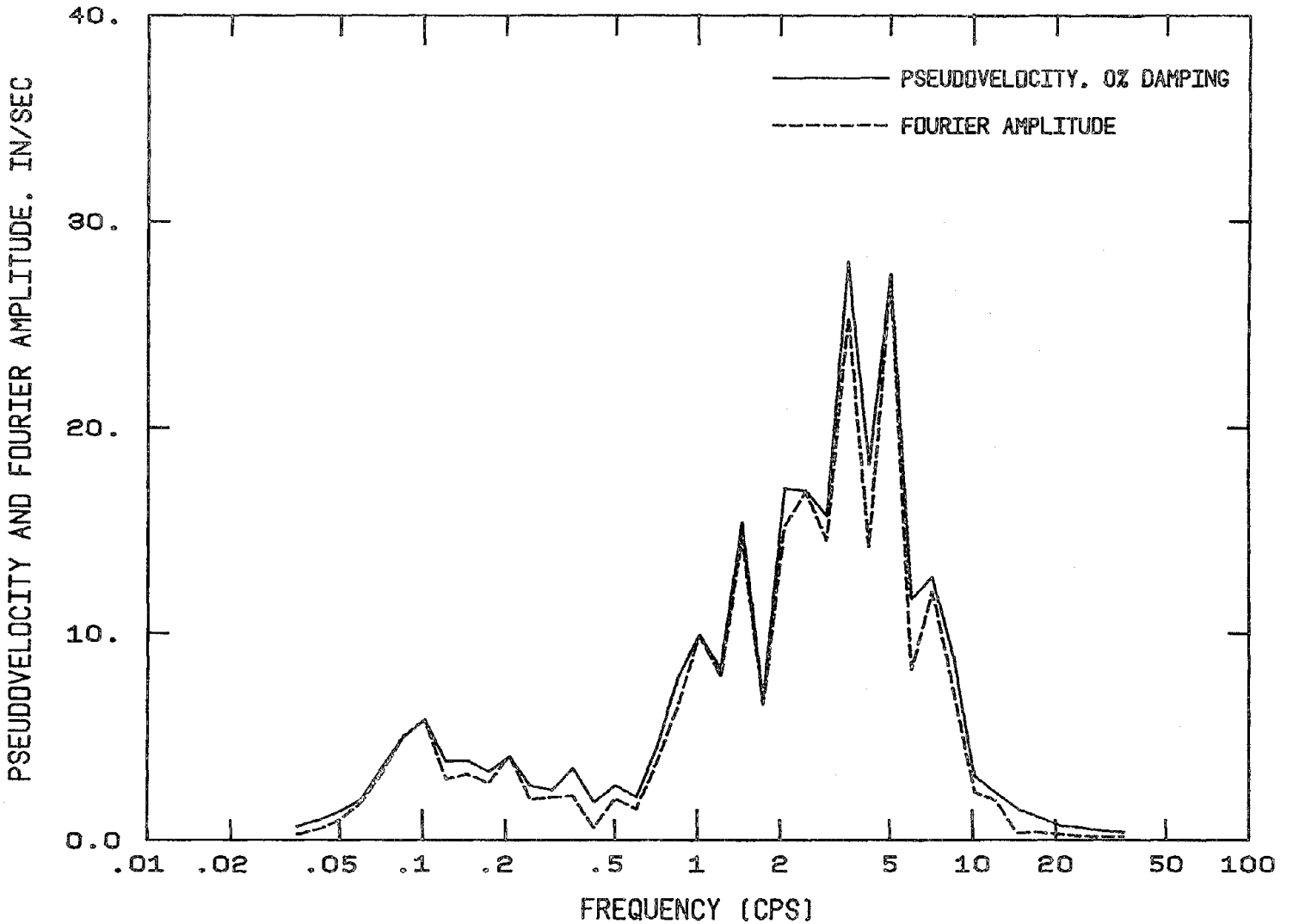

Fig. 4.10 Undamped Pseudovelocity and Fourier Amplitude Spectra for the Adak, Alaska Record of May 1, 1971, Component West

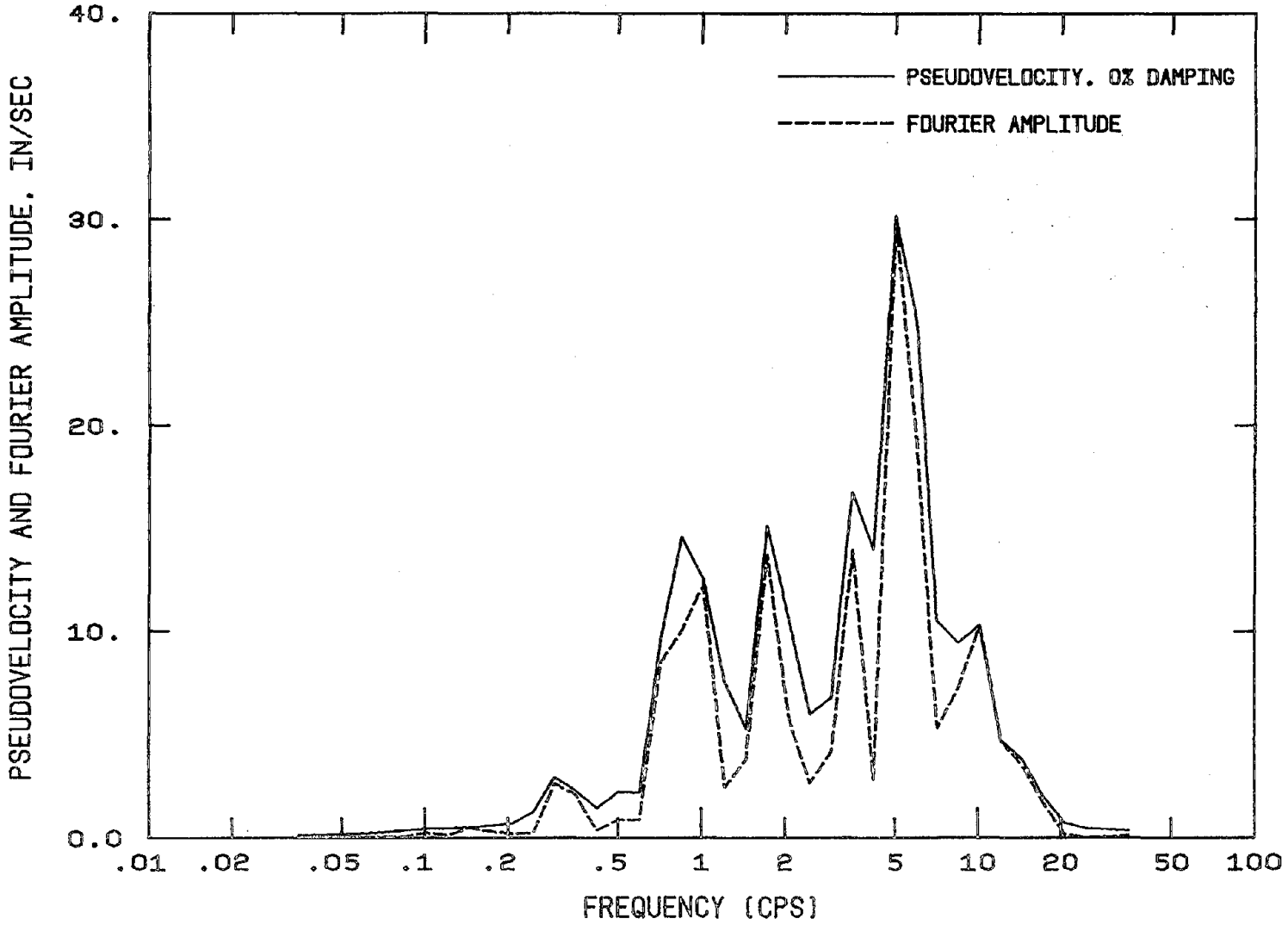

Fig. 4.11 Undamped Pseudovelocity and Fourier Amplitude Spectra for the Kilauea, Hawaii Record of April 26, 1973, Component S30W

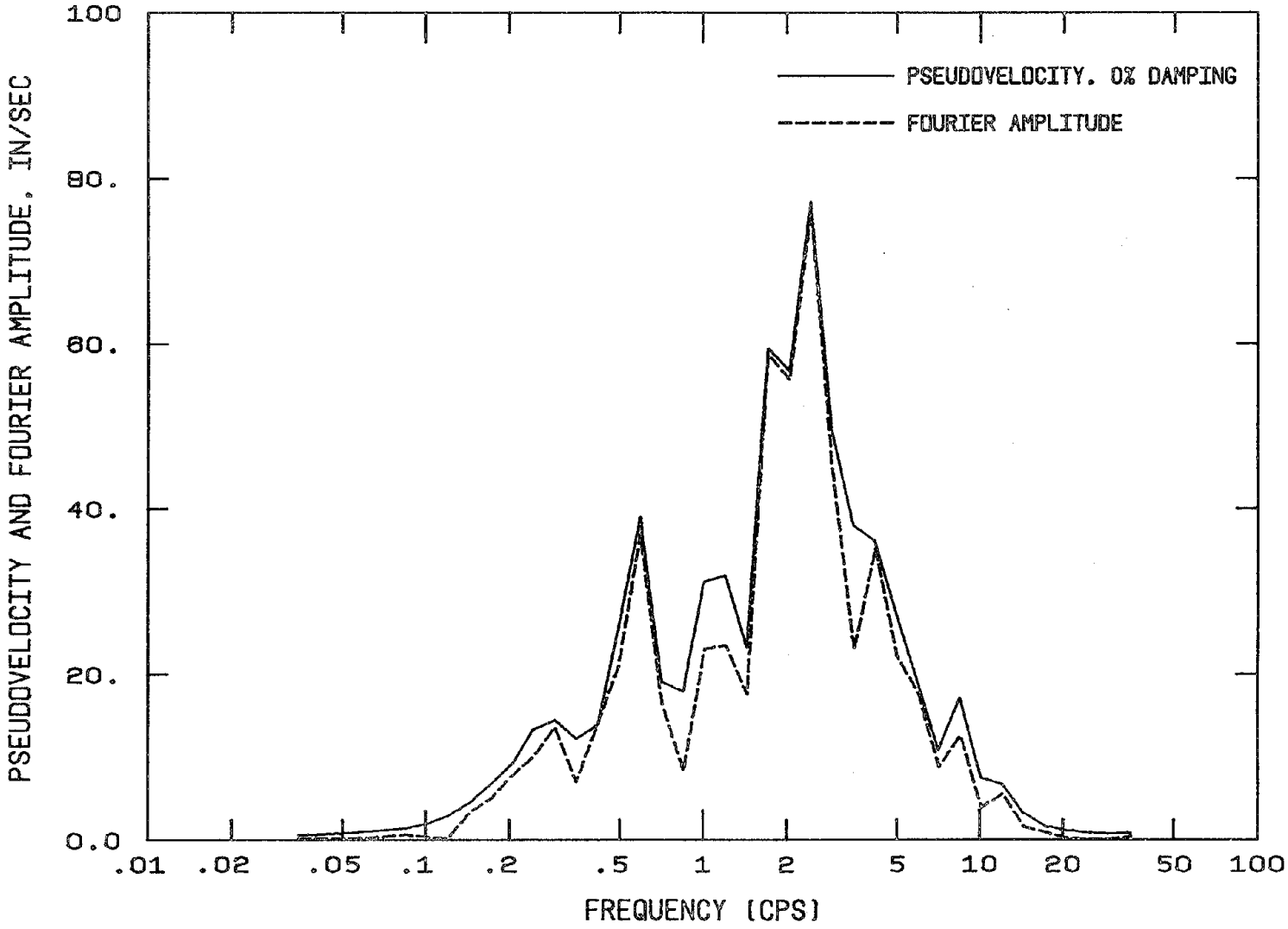

Fig. 4.12 Undamped Pseudovelocity and Fourier Amplitude Spectra for the Managua Record of Dec. 23, 1972, Component South

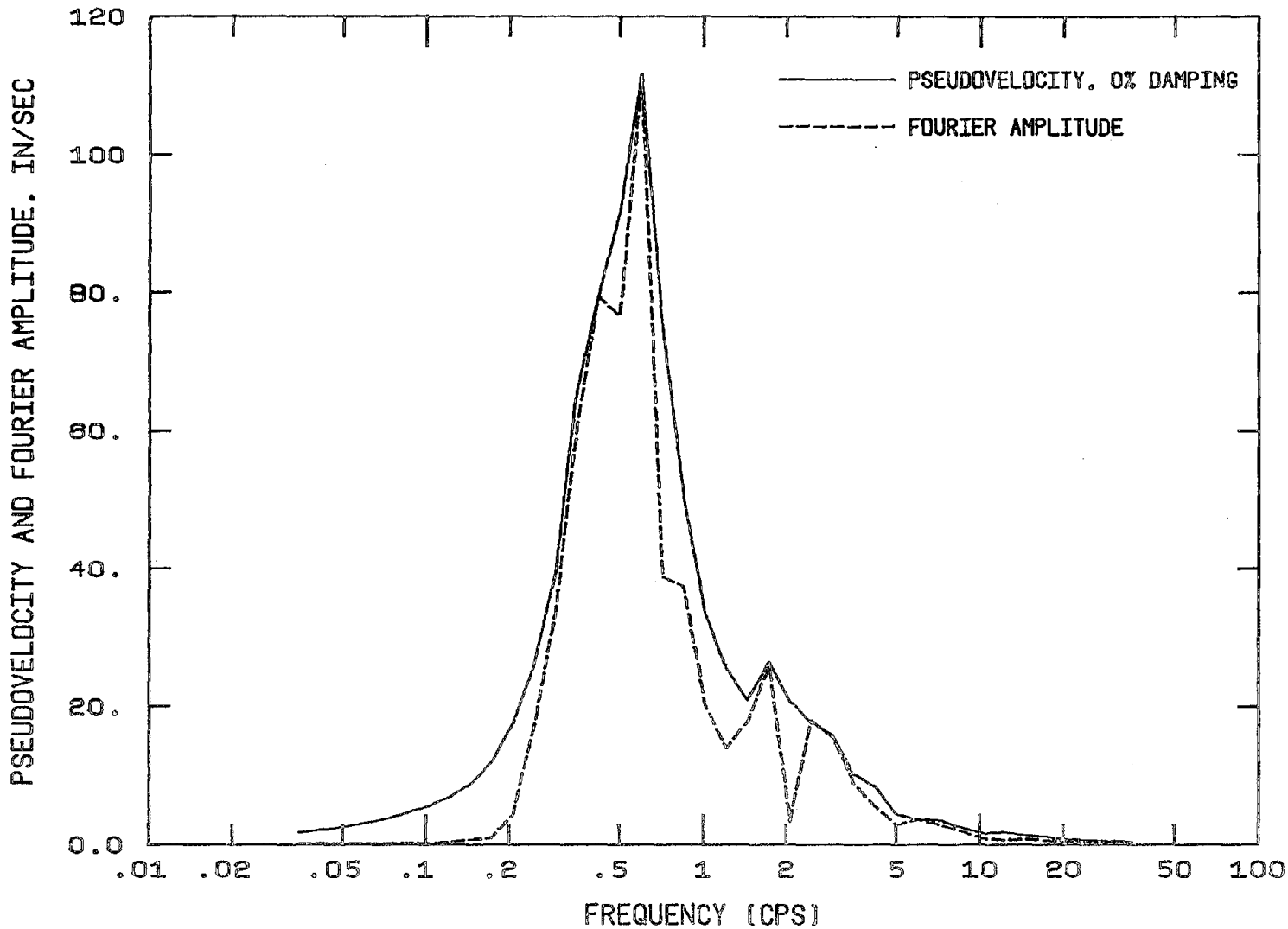

Fig. 4.13 Undamped Pseudovelocity and Fourier Amplitude Spectra for the Bucarest Record of Mar. 4, 1977, Component S-N

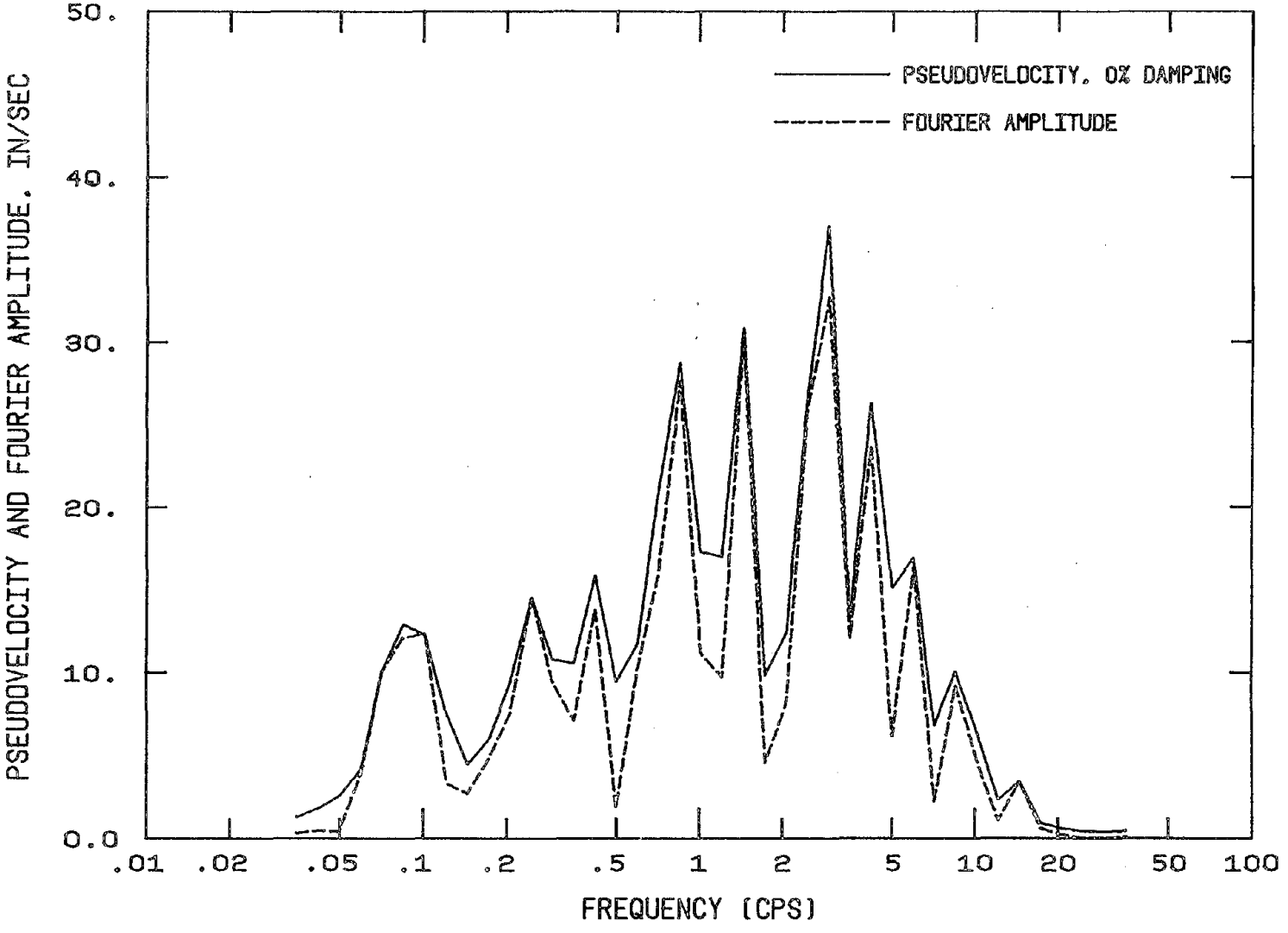

Fig. 4.14 Undamped Pseudovelocity and Fourier Amplitude Spectra for the Santiago Record of July 8, 1971, Component N10W

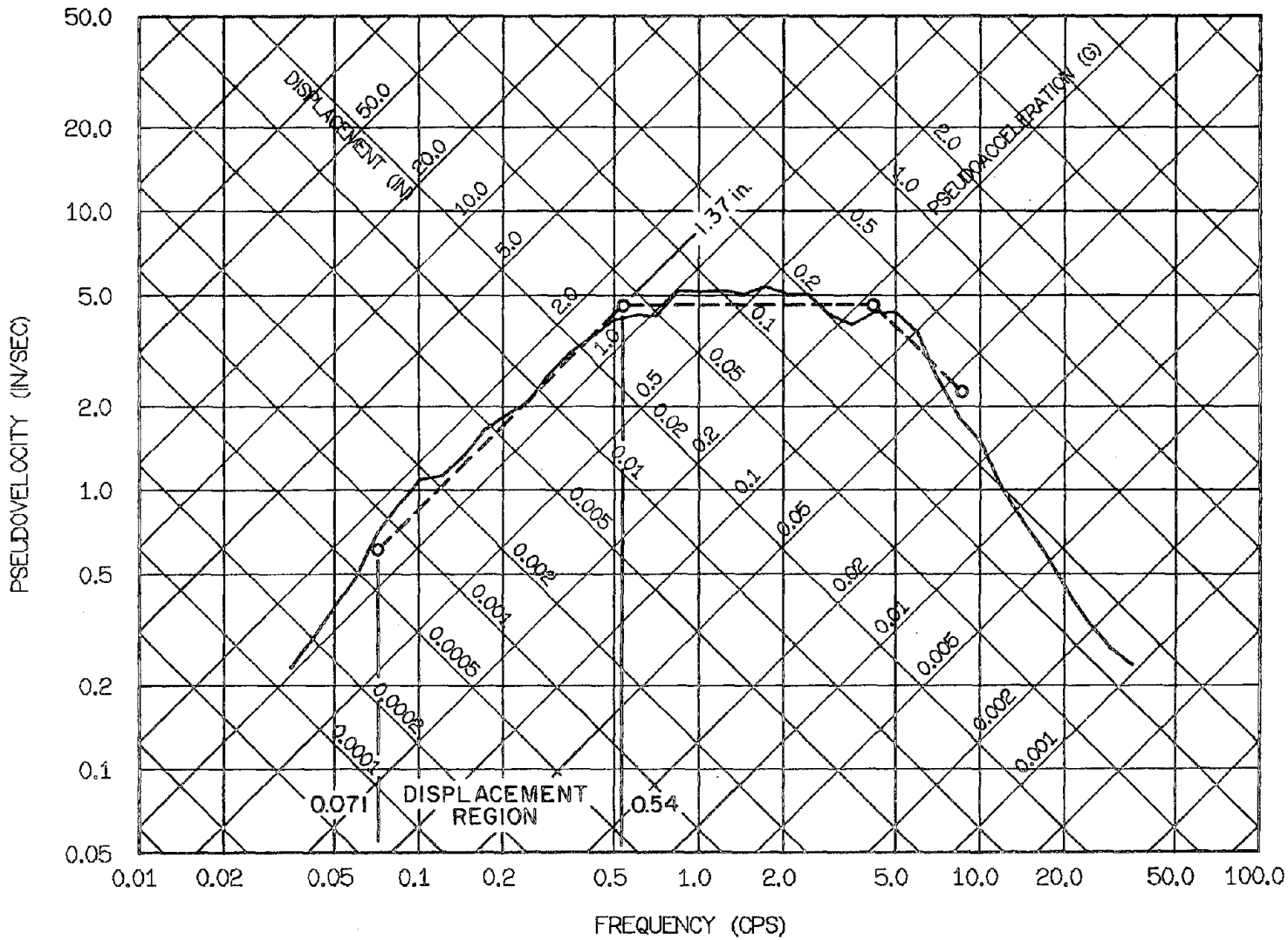

Fig. 5.1 Mean of Elastic Spectra Normalized by Peak Ground Displacement: 5% Damping

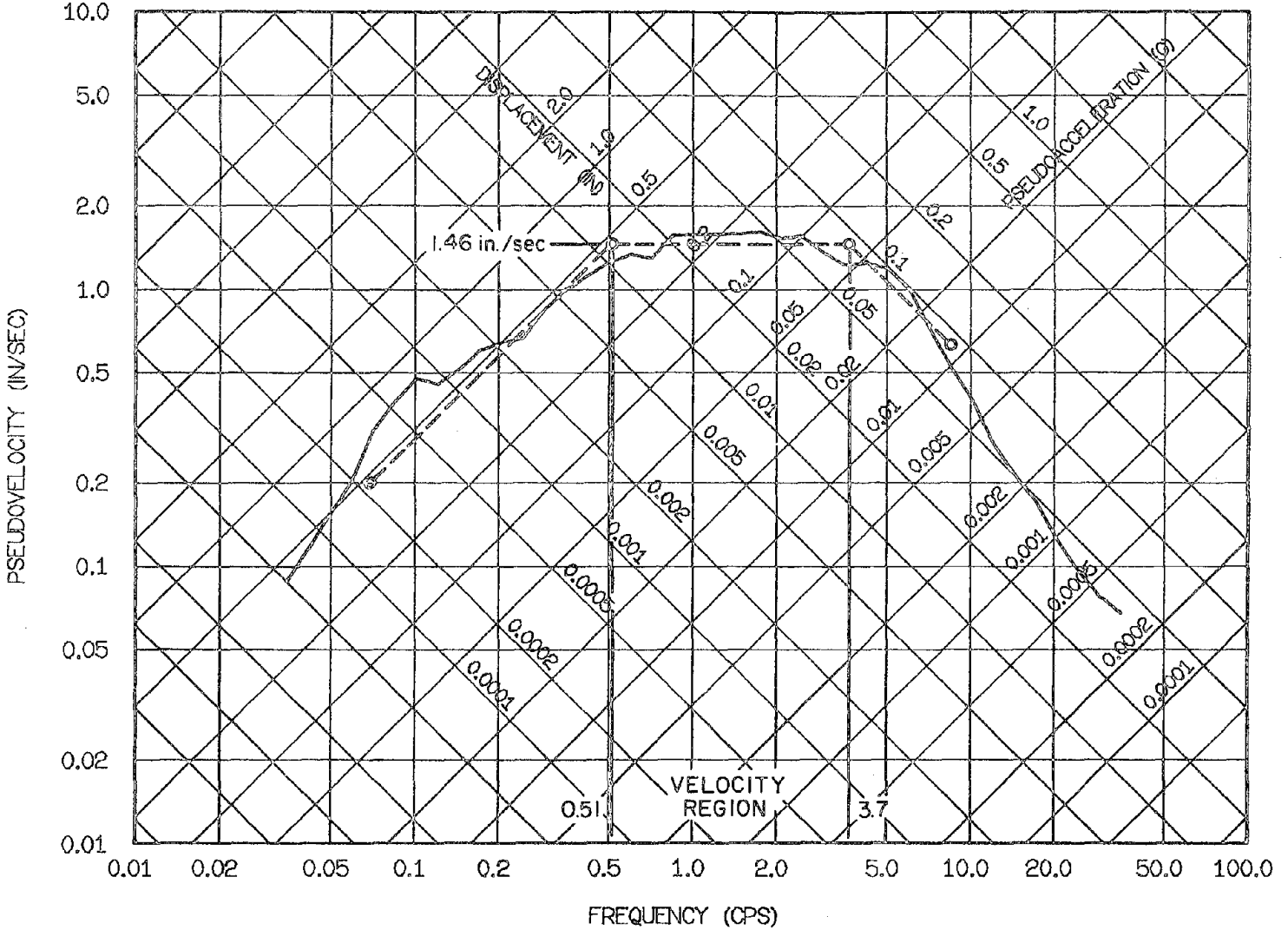

Fig. 5.2 Mean of Elastic Spectra Normalized by Peak Ground Velocity: 5% Damping

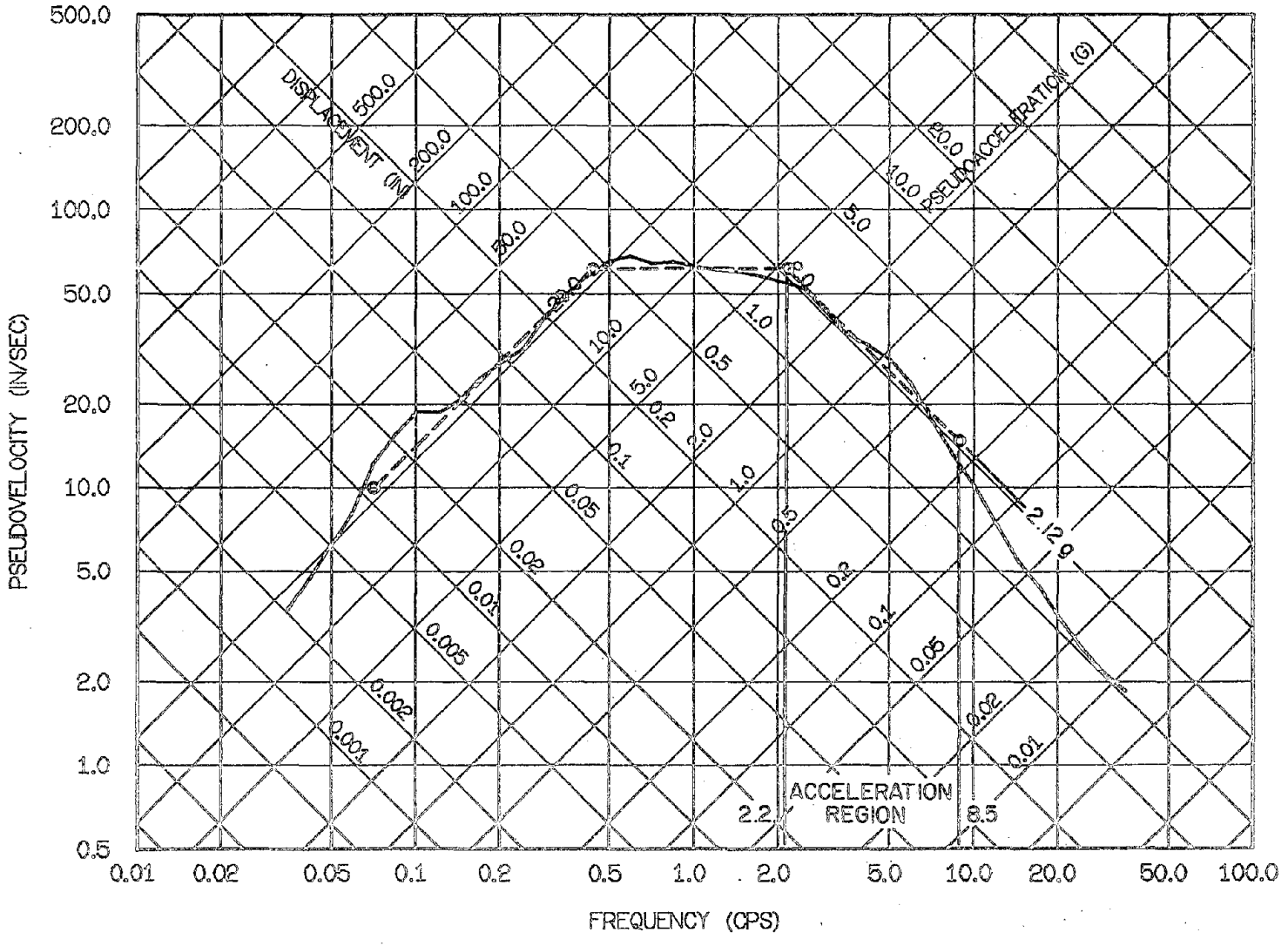

Fig. 5.3 Mean of Elastic Spectra Normalized by Peak Ground Acceleration: 5% Damping

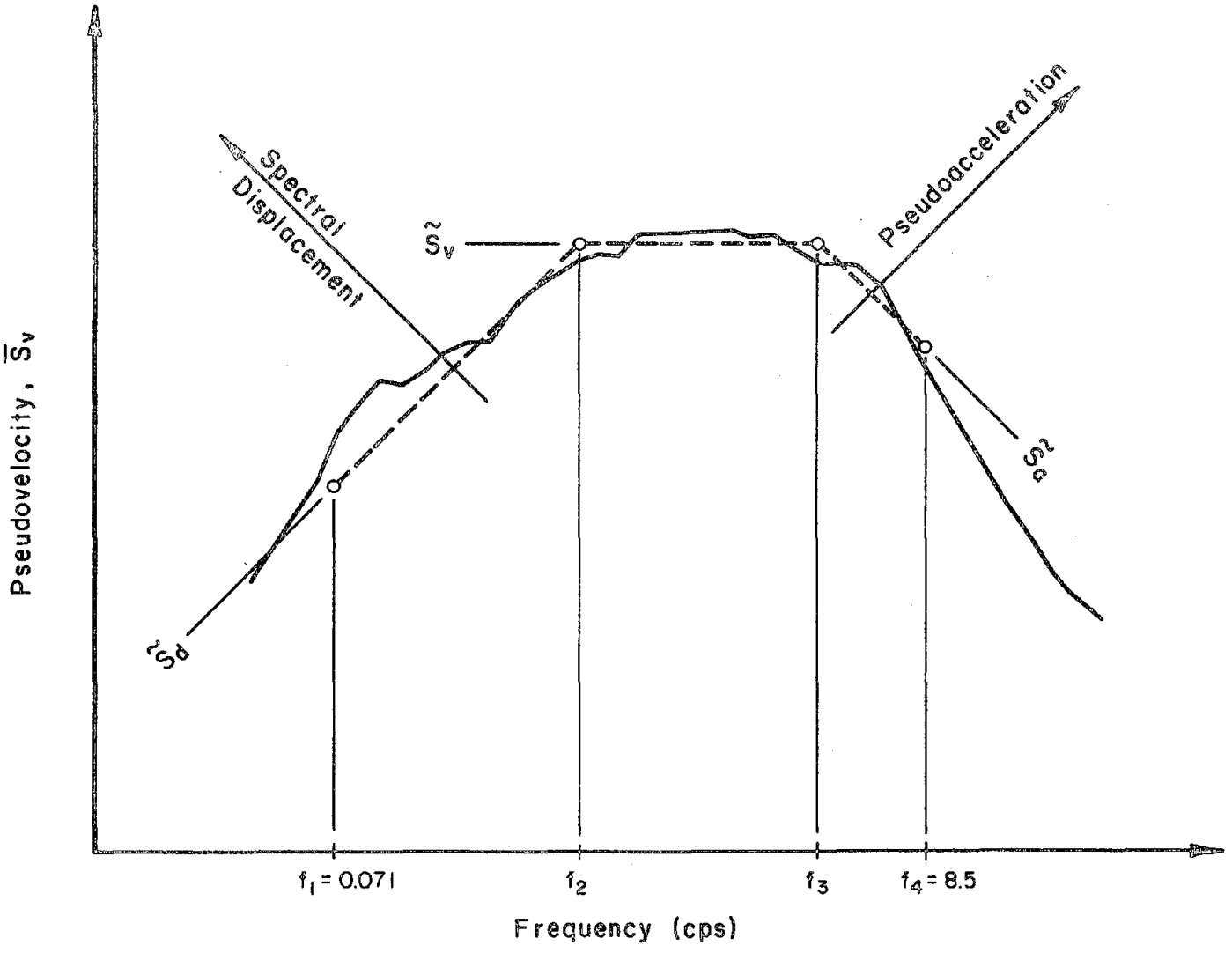

Fig. 5.4 Lines of Best Fit for Mean Normalized Spectra

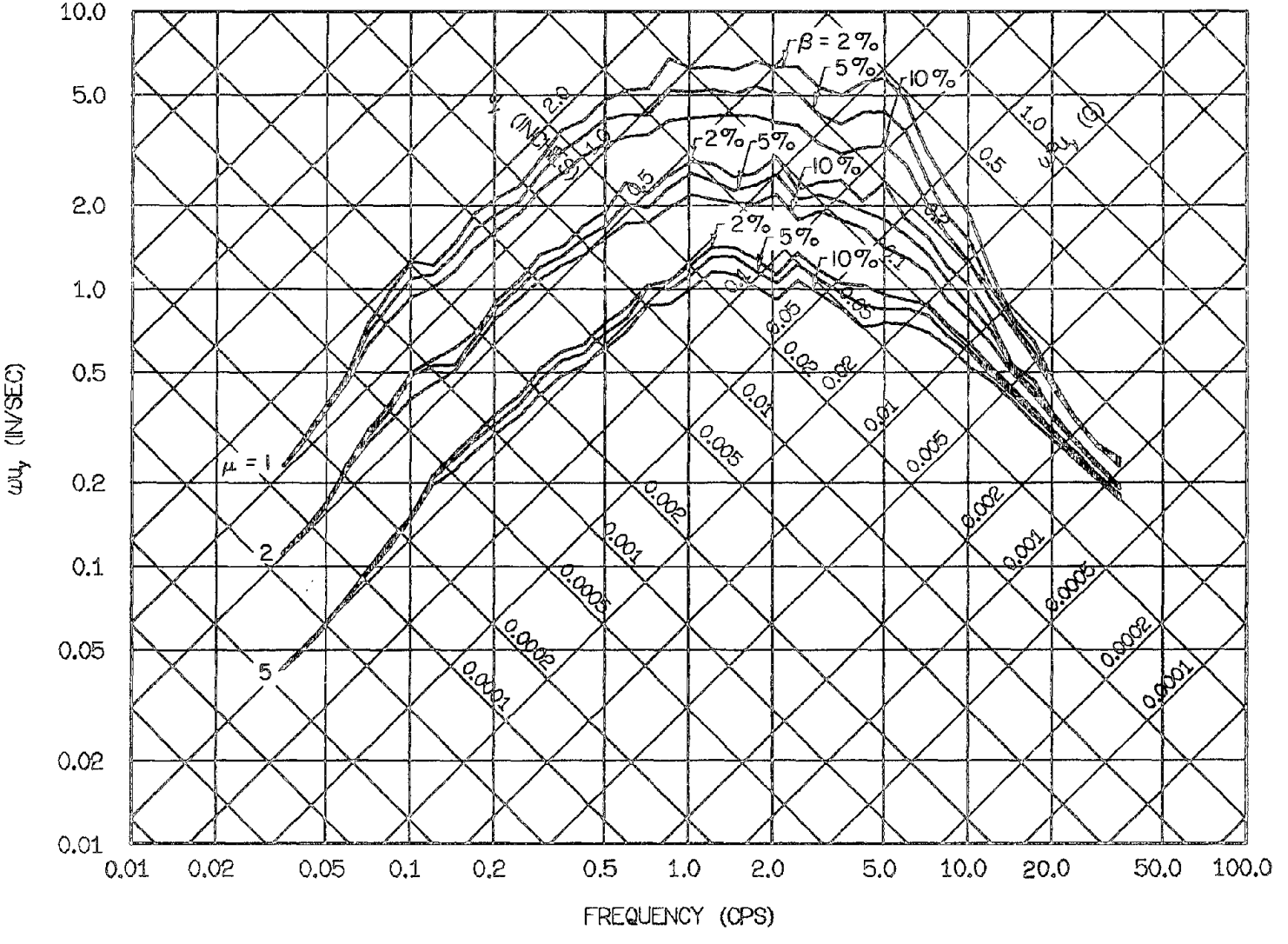

Fig. 5.5 Mean of Elastoplastic Yield Spectra Normalized by Peak Ground Displacement: Ductilities = 1, 2, and 5

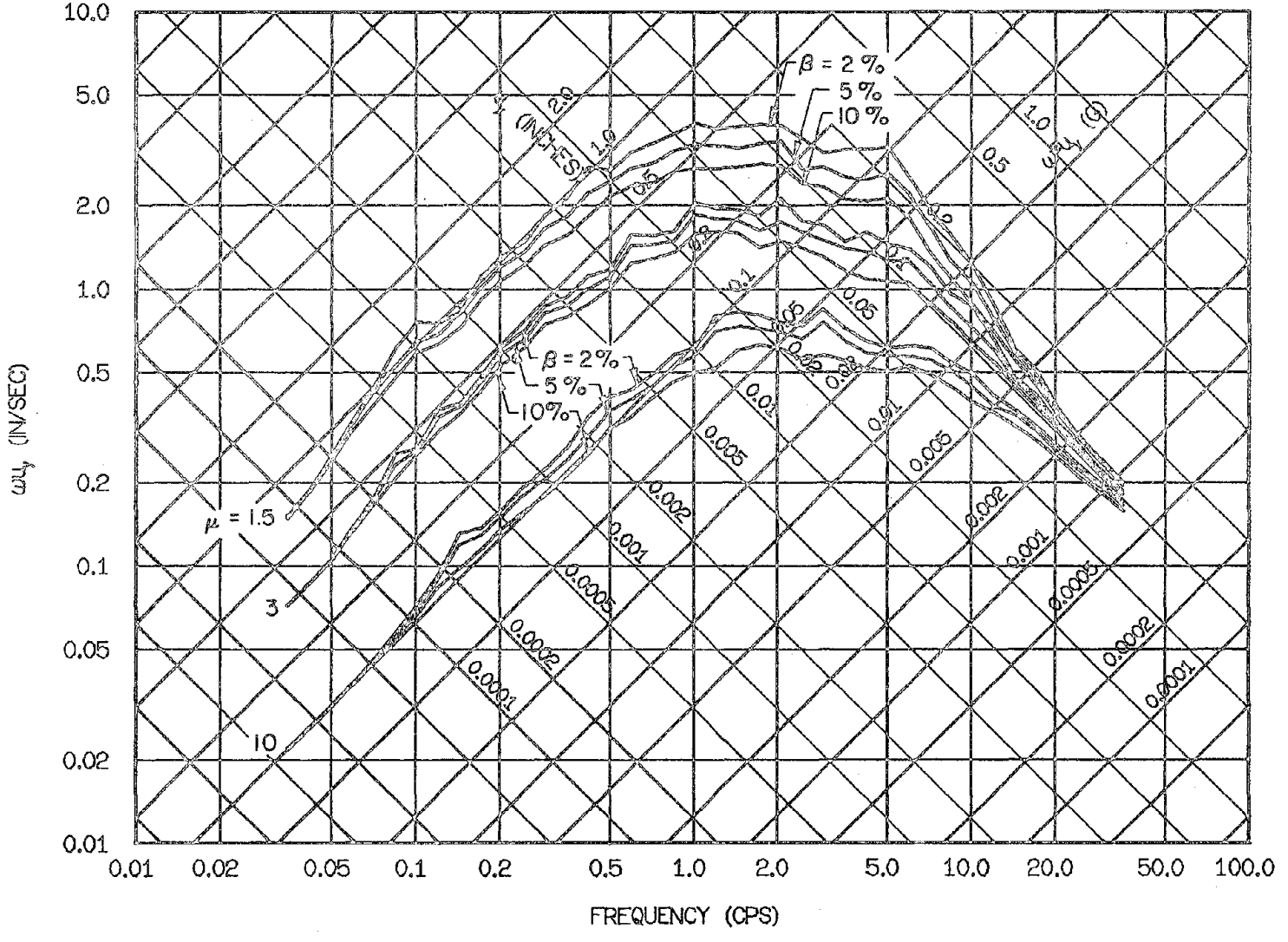

Fig. 5.6 Mean of Elastoplastic Yield Spectra Normalized by Peak Ground Displacement: Ductilities = 1.5, 3, and 10

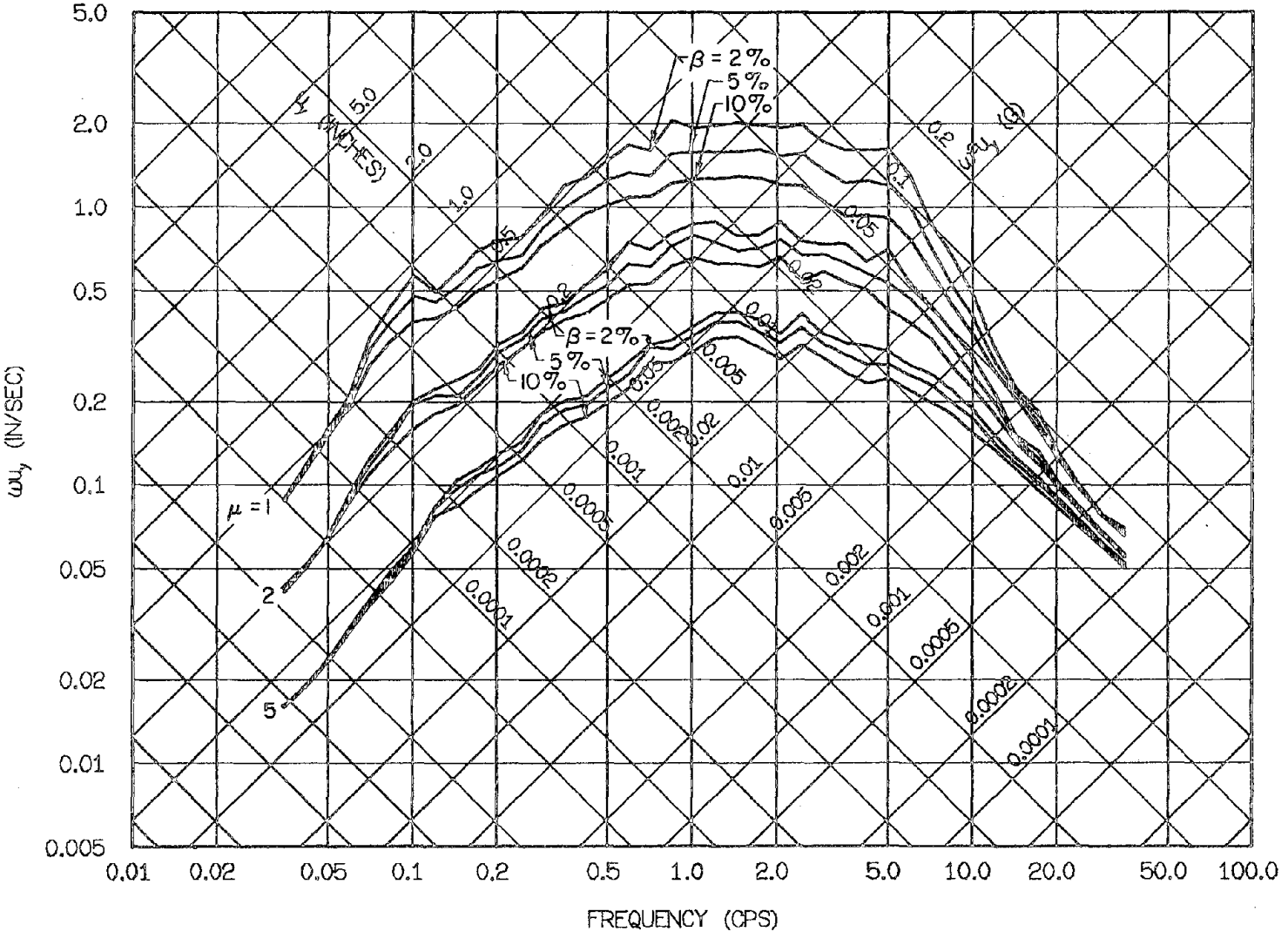

Fig. 5.7 Mean of Elastoplastic Yield Spectra Normalized by Peak Ground Velocity: Ductilities = 1, 2, and 5

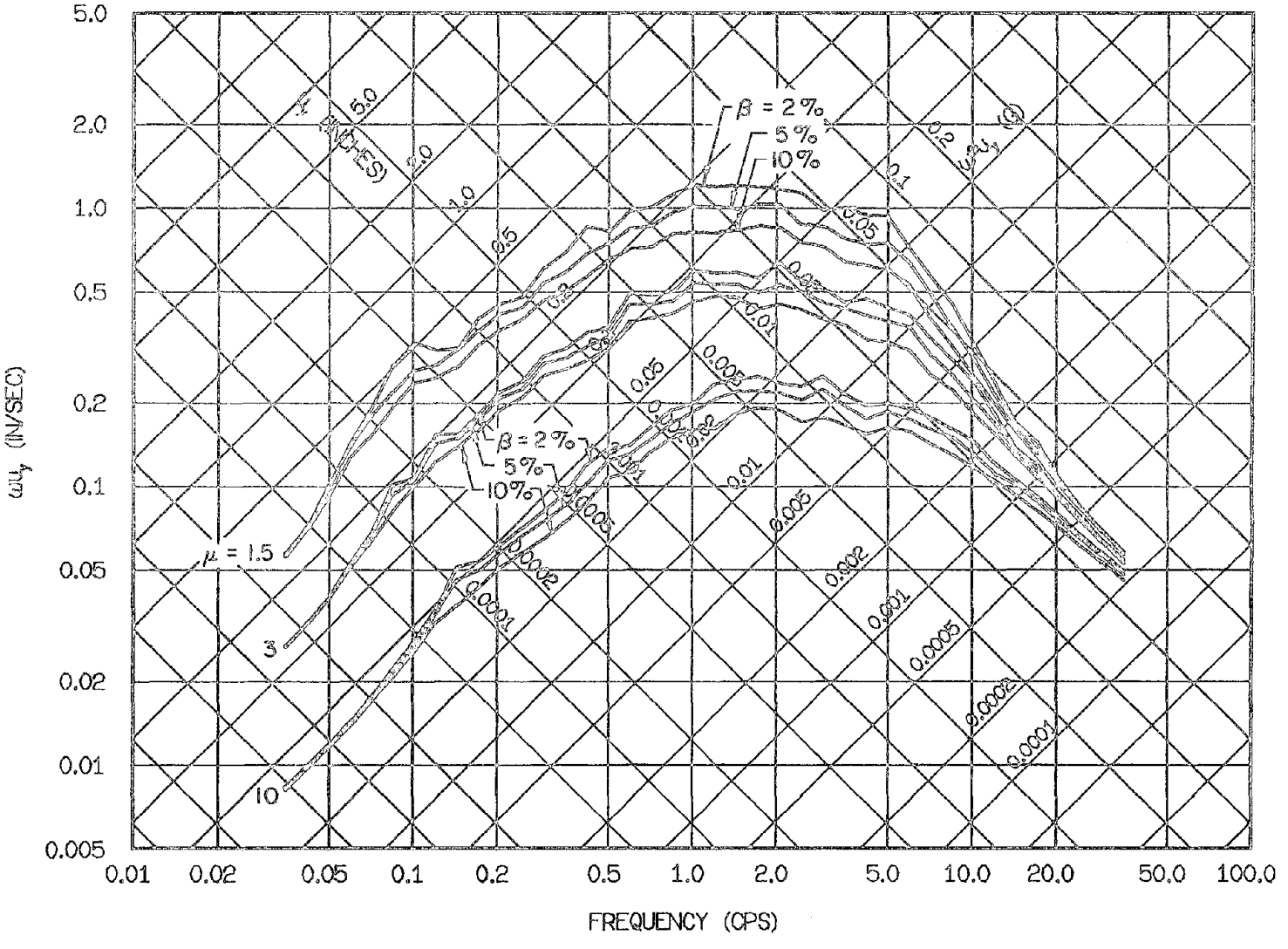

Fig. 5.8 Mean of Elastoplastic Yield Spectra Normalized by Peak Ground Velocity: Ductilities = 1.5, 3, and 10

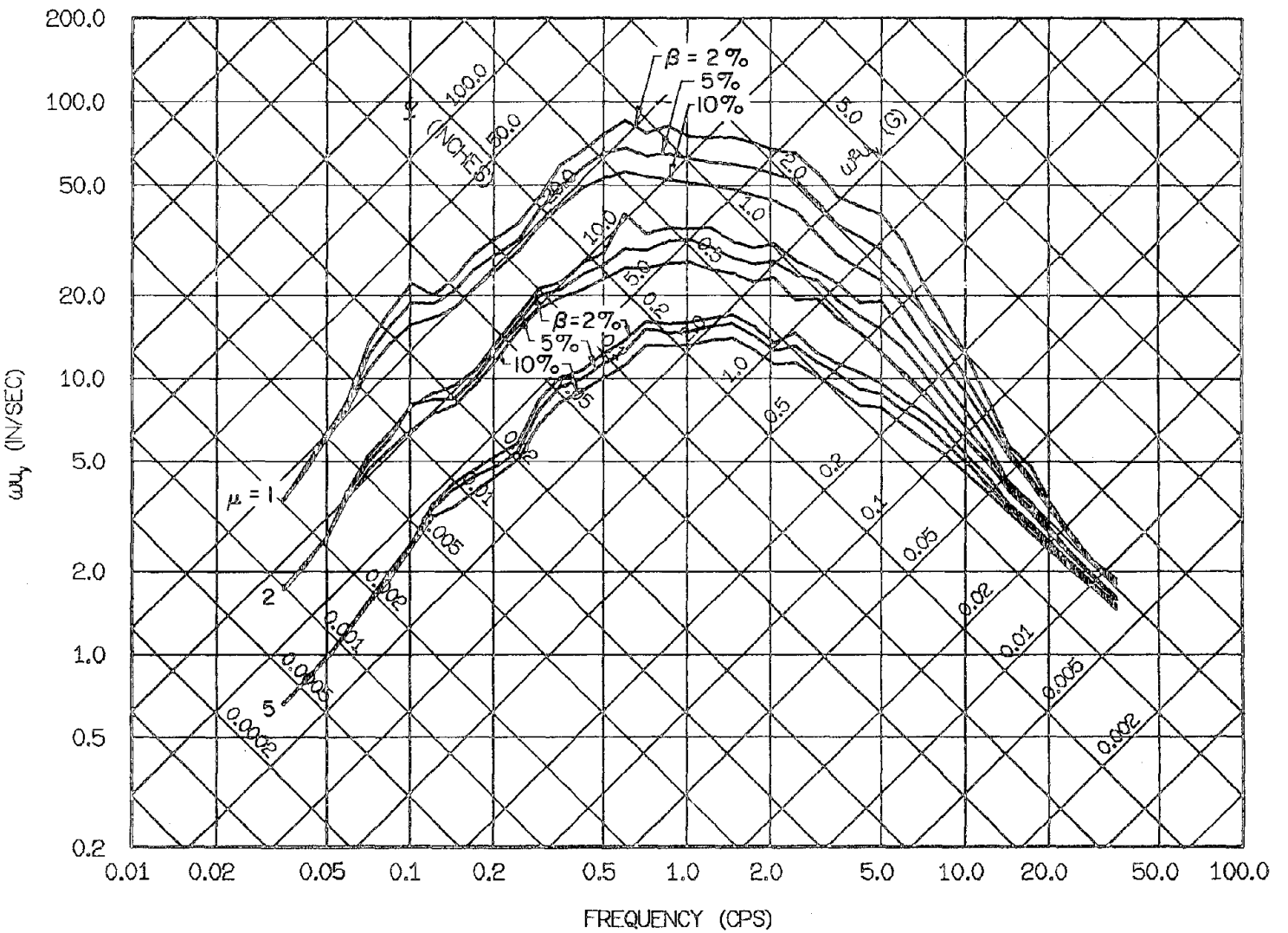

Fig. 5.9 Mean of Elastoplastic Yield Spectra Normalized by Peak Ground Acceleration: Ductilities = 1, 2, and 5

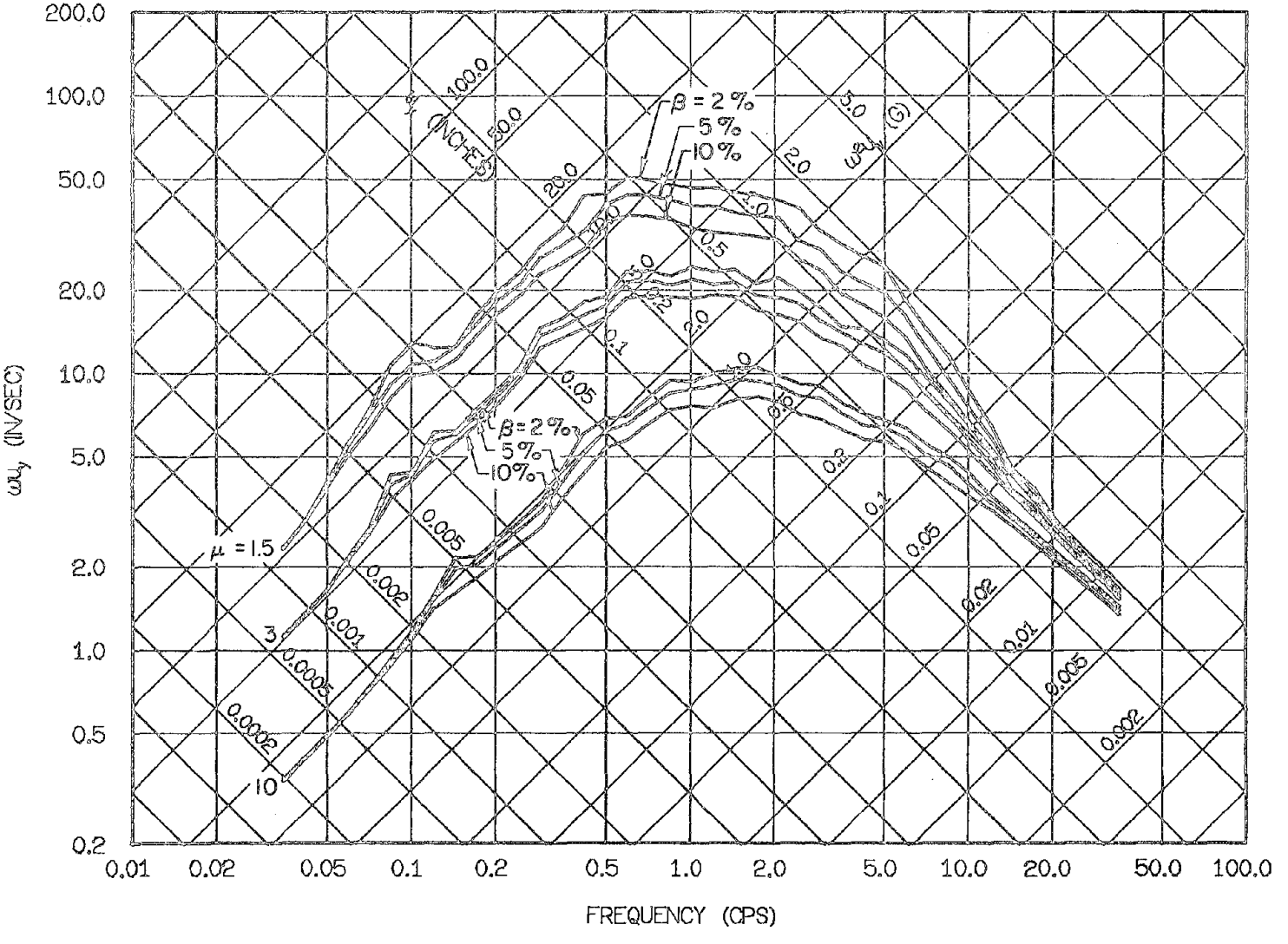

Fig. 5.10 Mean of Elastoplastic Yield Spectra Normalized by Peak Ground Acceleration: Ductilities = 1.5, 3, and 10

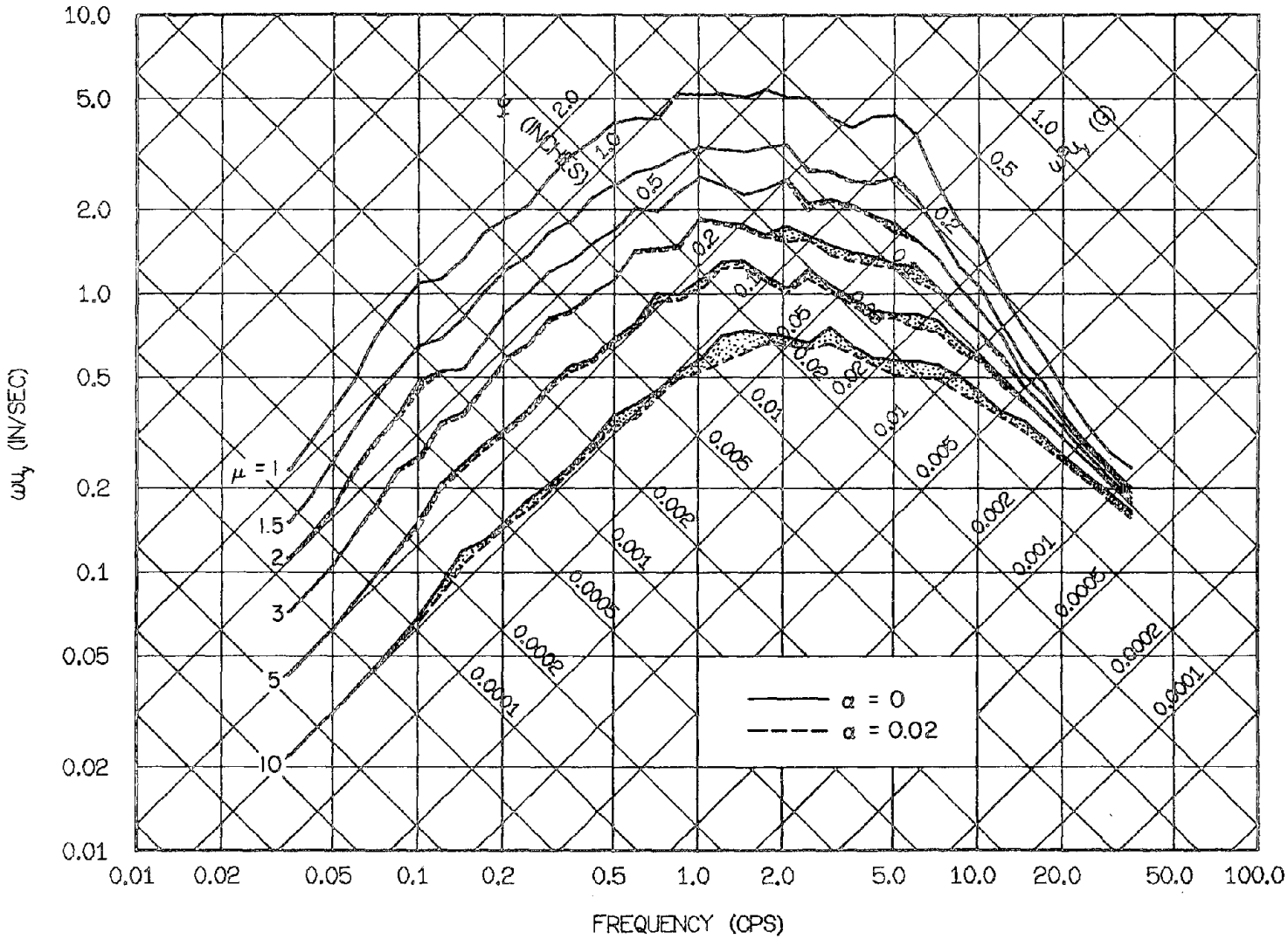

Fig. 5.11 Comparison of Mean Elastoplastic and Bilinear Yield Spectra with 2% Strain-Hardening, Normalized by Peak Ground Displacement

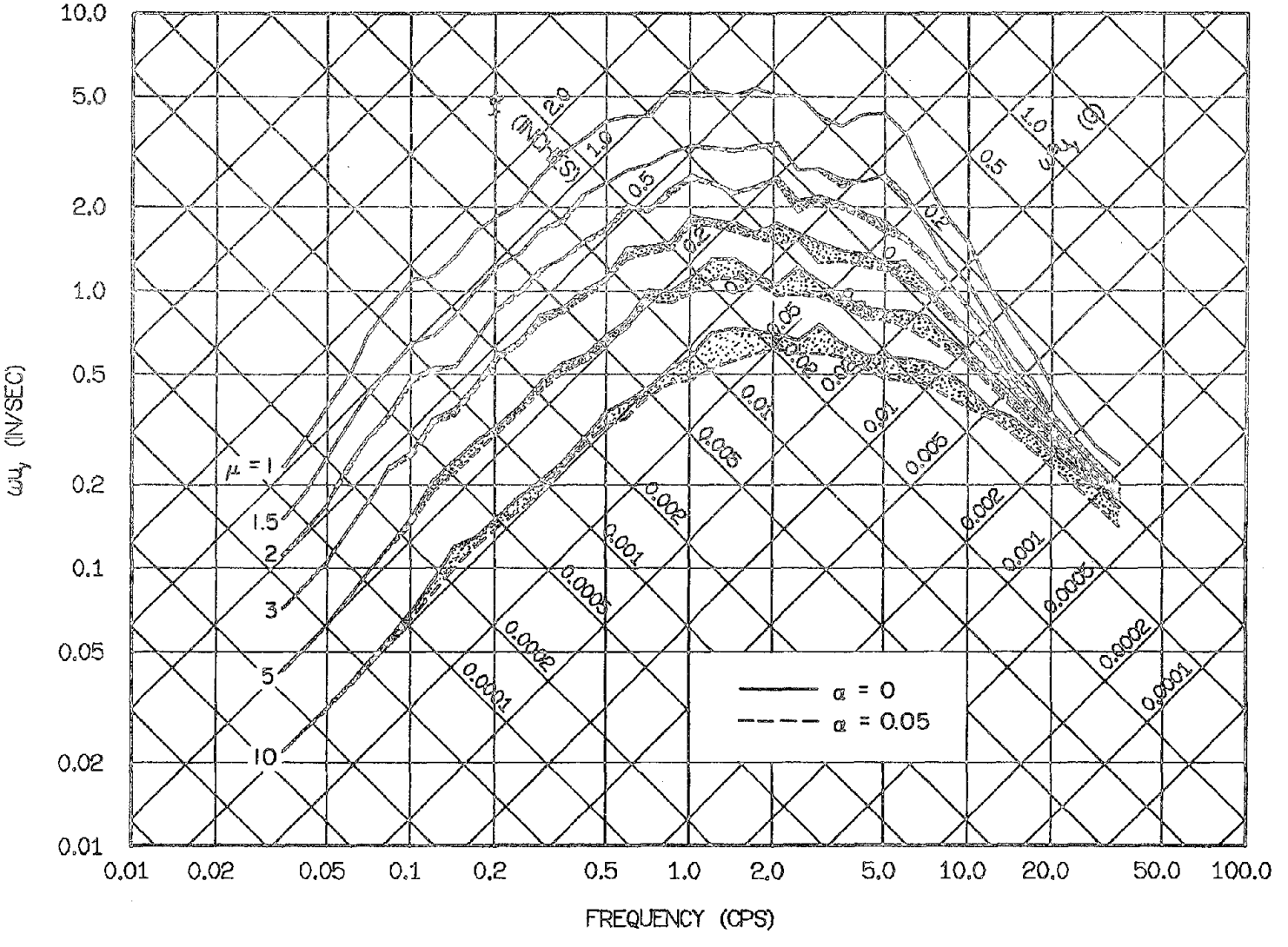

Fig. 5.12 Comparison of Mean Elastoplastic and Bilinear Yield Spectra with 5% Strain-Hardening, Normalized by Peak Ground Displacement

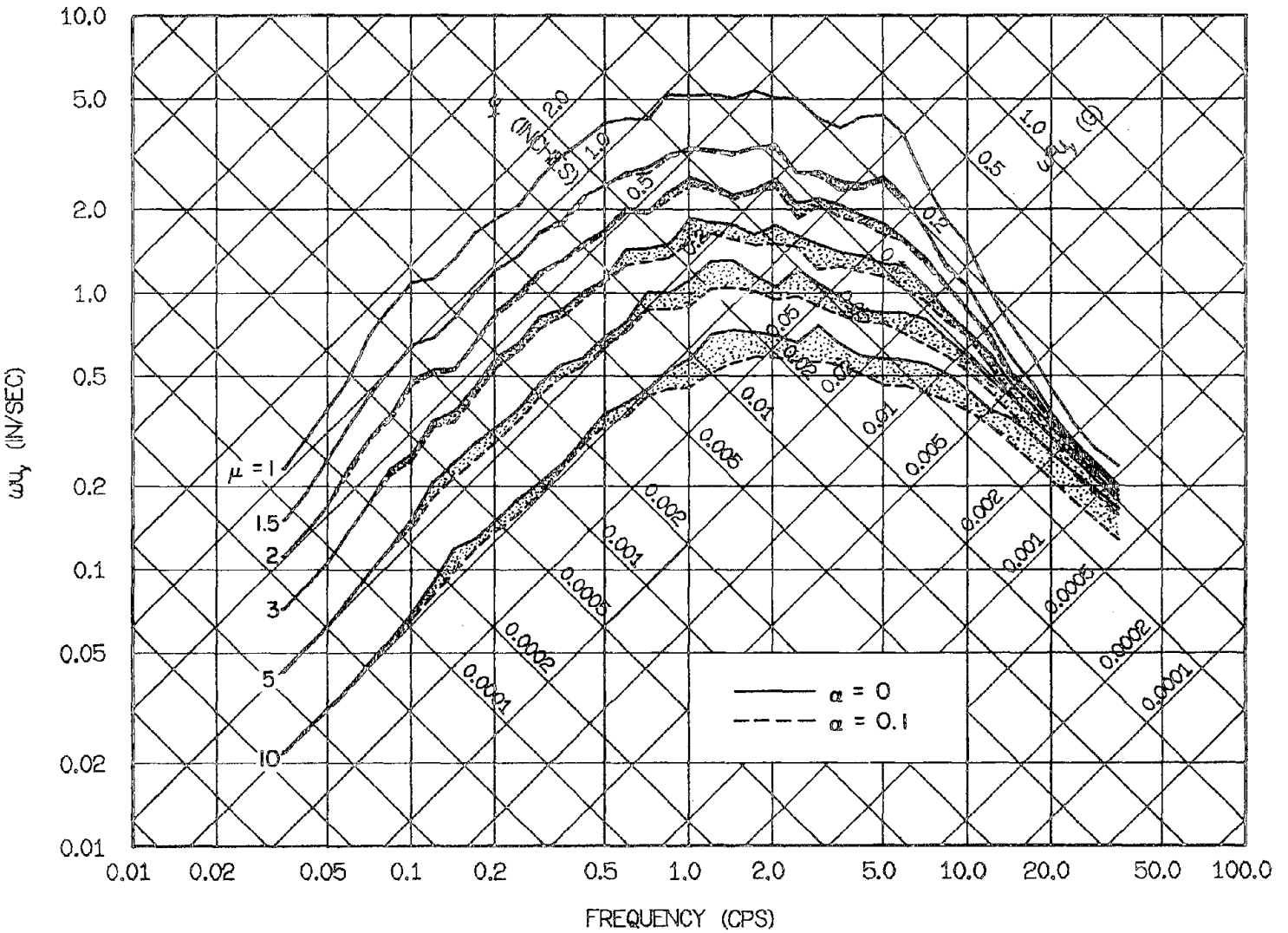

Fig. 5.13 Comparison of Mean Elastoplastic and Bilinear Yield Spectra with 10% Strain-Hardening, Normalized by Peak Ground Displacement

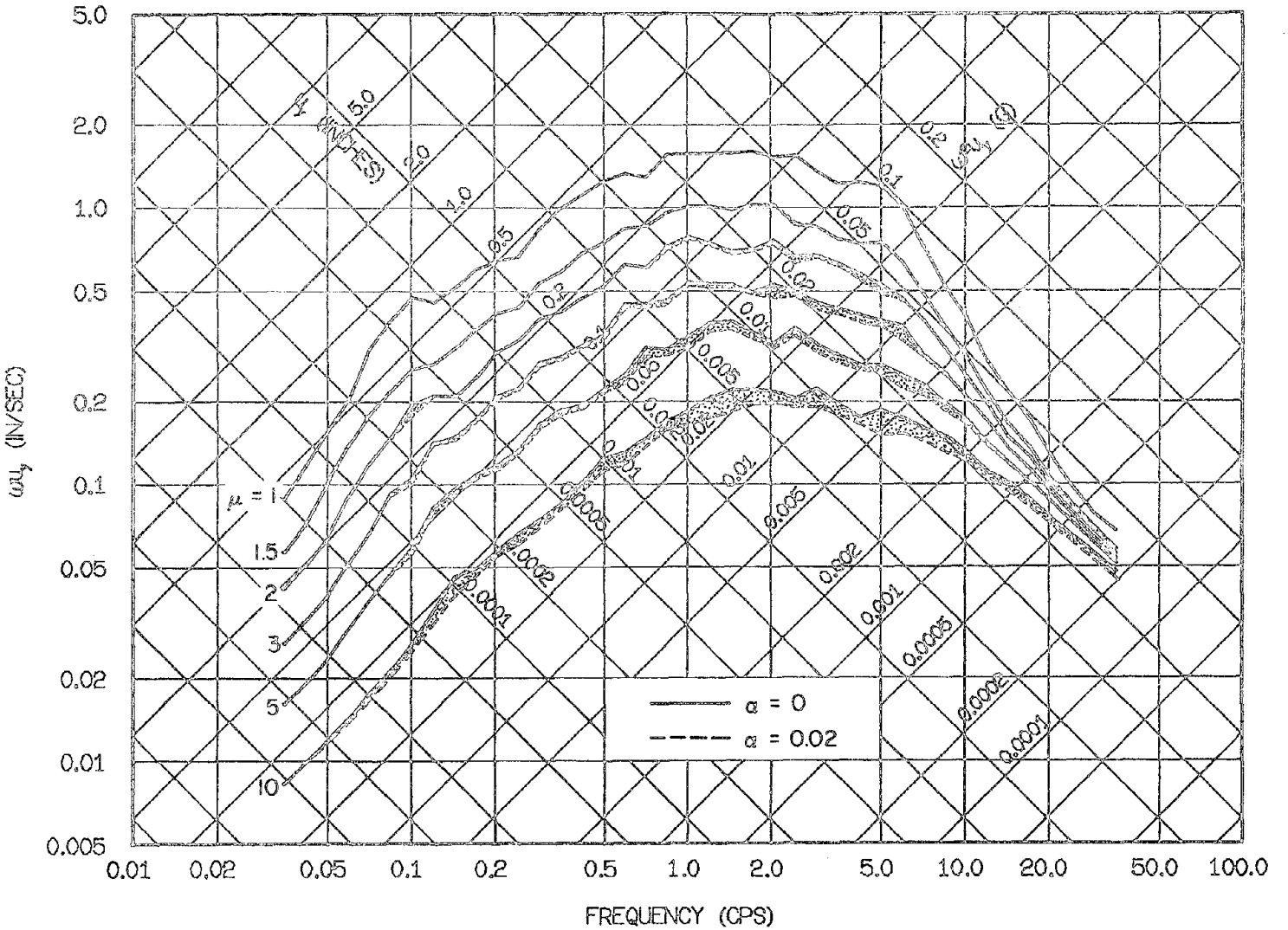

Fig. 5.14 Comparison of Mean Elastoplastic and Bilinear Yield Spectra with 2% Strain-Hardening, Normalized by Peak Ground Velocity

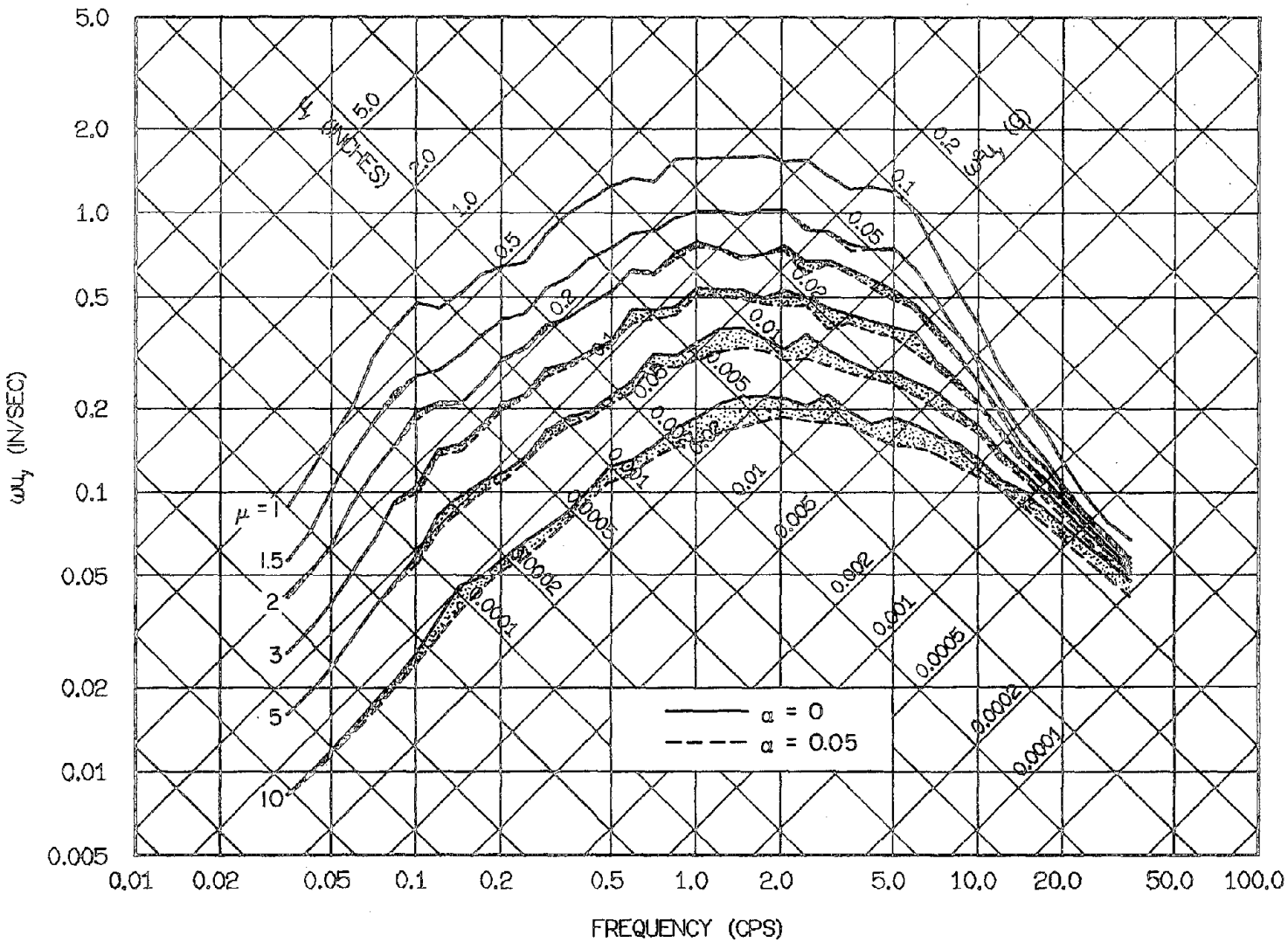

Fig. 5.15 Comparison of Mean Elastoplastic and Bilinear Yield Spectra with 5% Strain-Hardening, Normalized by Peak Ground Velocity

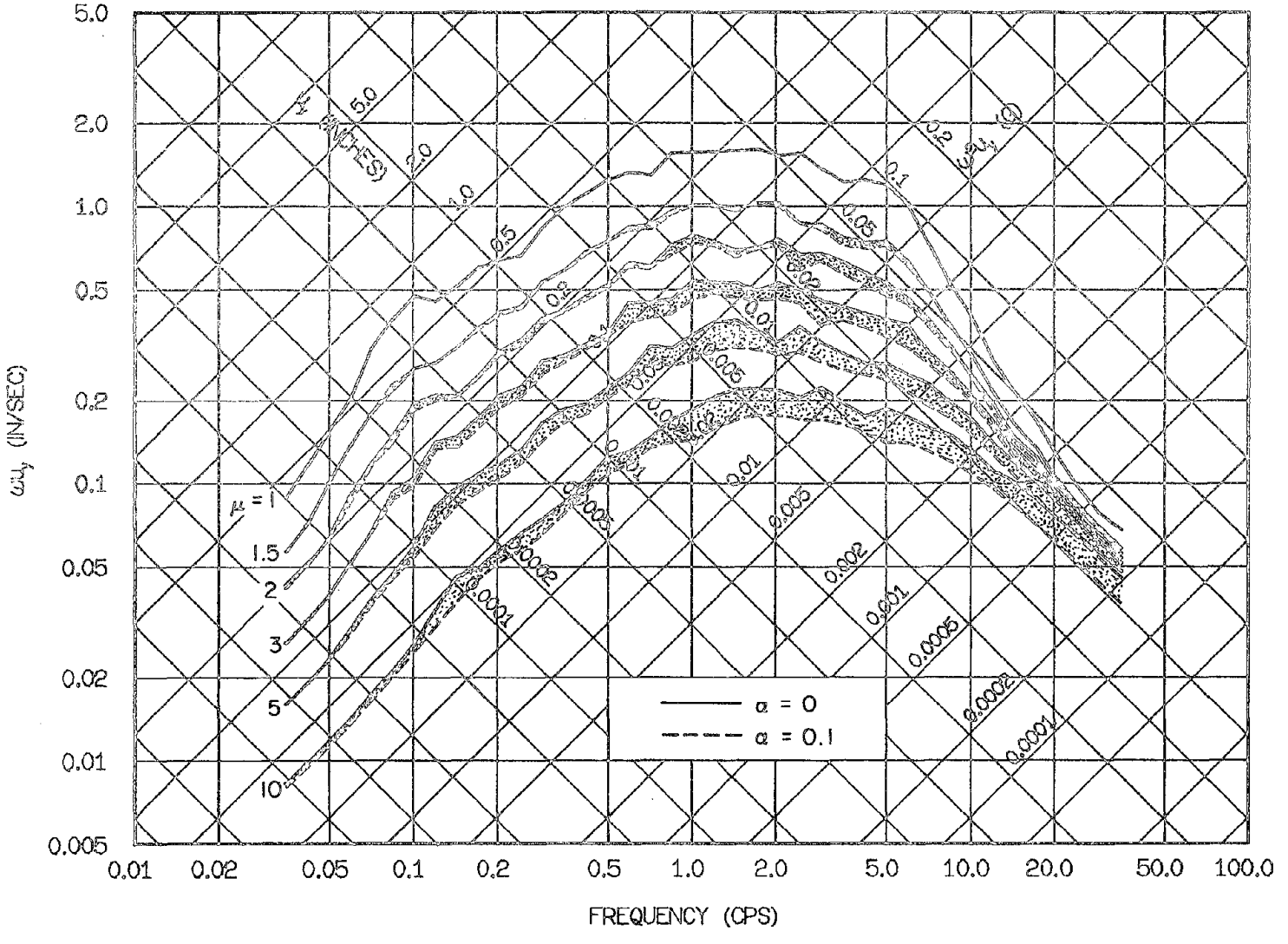

Fig. 5.16 Comparison of Mean Elastoplastic and Bilinear Yield Spectra with 10% Strain-Hardening, Normalized by Peak Ground Velocity

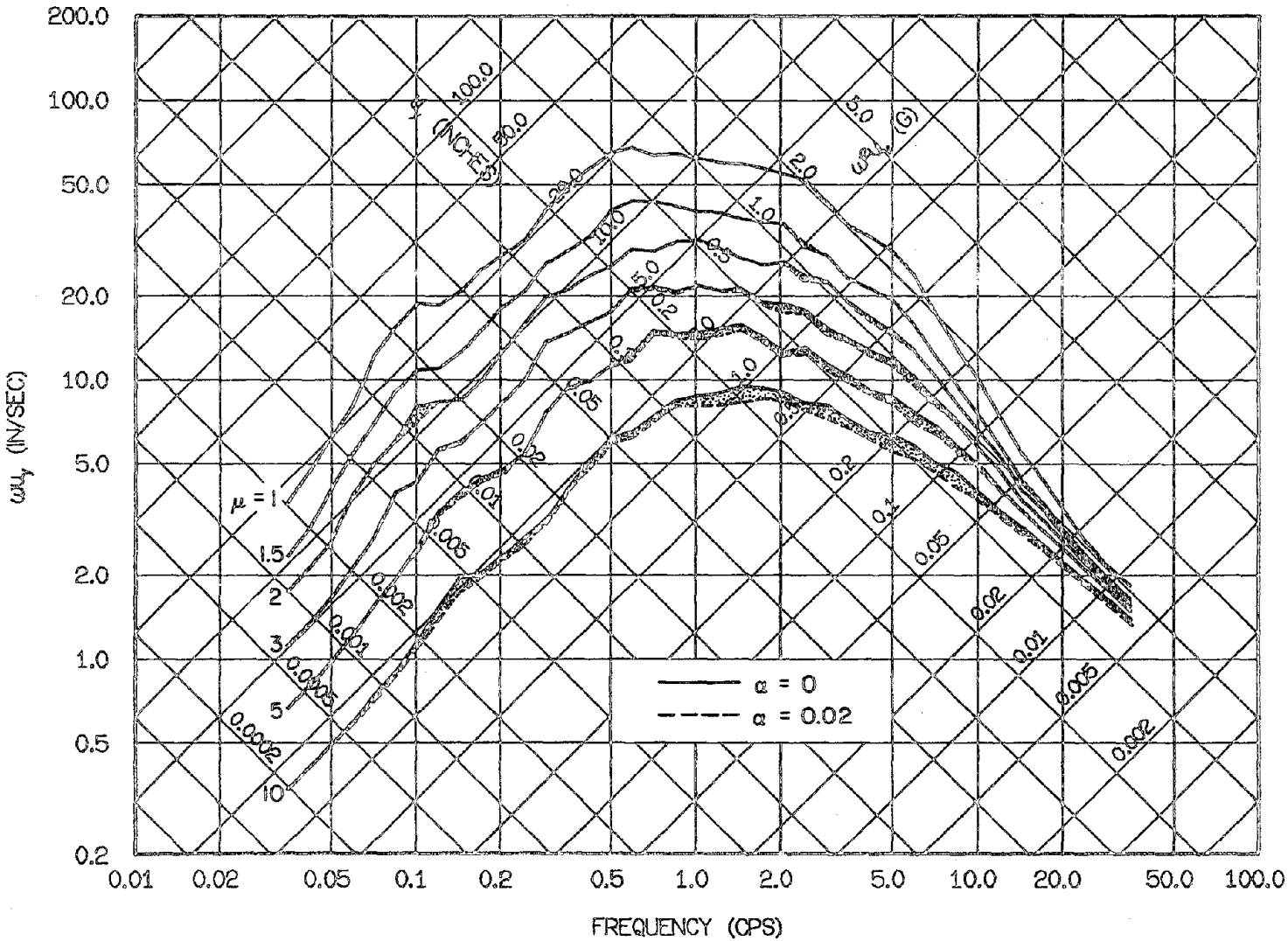

Fig. 5.17 Comparison of Mean Elastoplastic and Bilinear Yield Spectra with 2% Strain-Hardening, Normalized by Peak Ground Acceleration

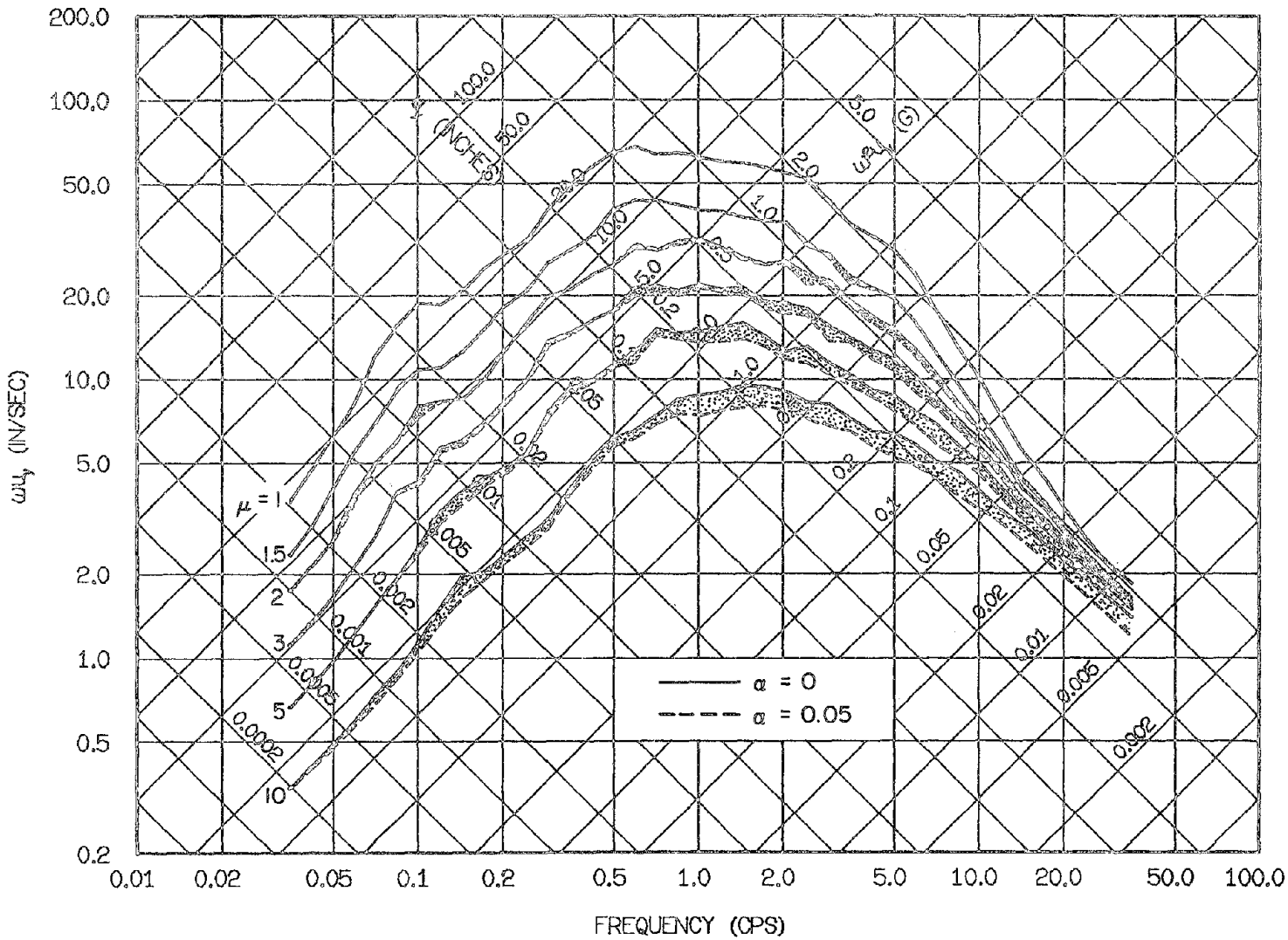

Fig. 5.18 Comparison of Mean Elastoplastic and Bilinear Yield Spectra with 5% Strain-Hardening, Normalized by Peak Ground Acceleration

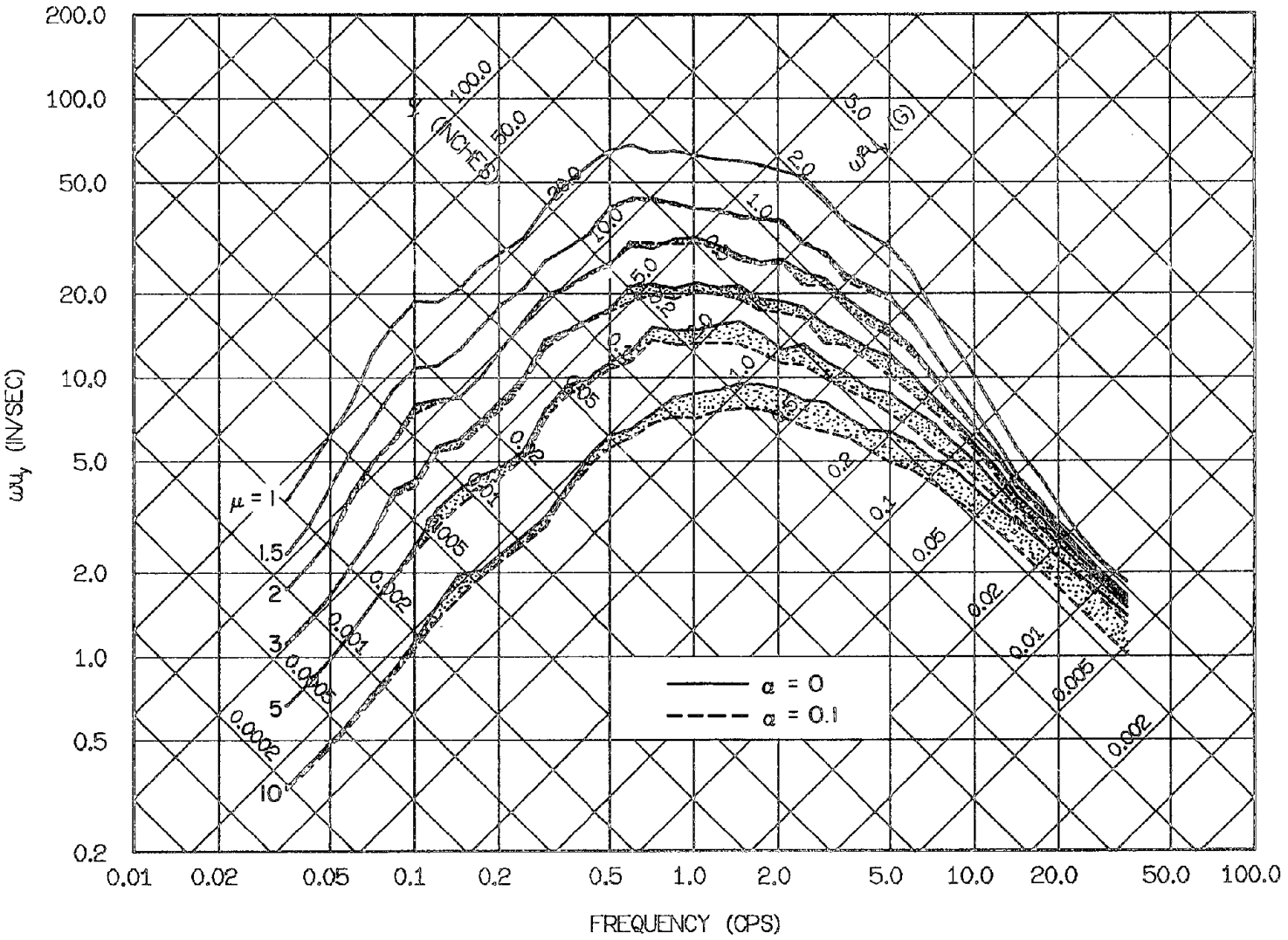

Fig. 5.19 Comparison of Mean Elastoplastic and Bilinear Yield Spectra with 10% Strain-Hardening, Normalized by Peak Ground Acceleration

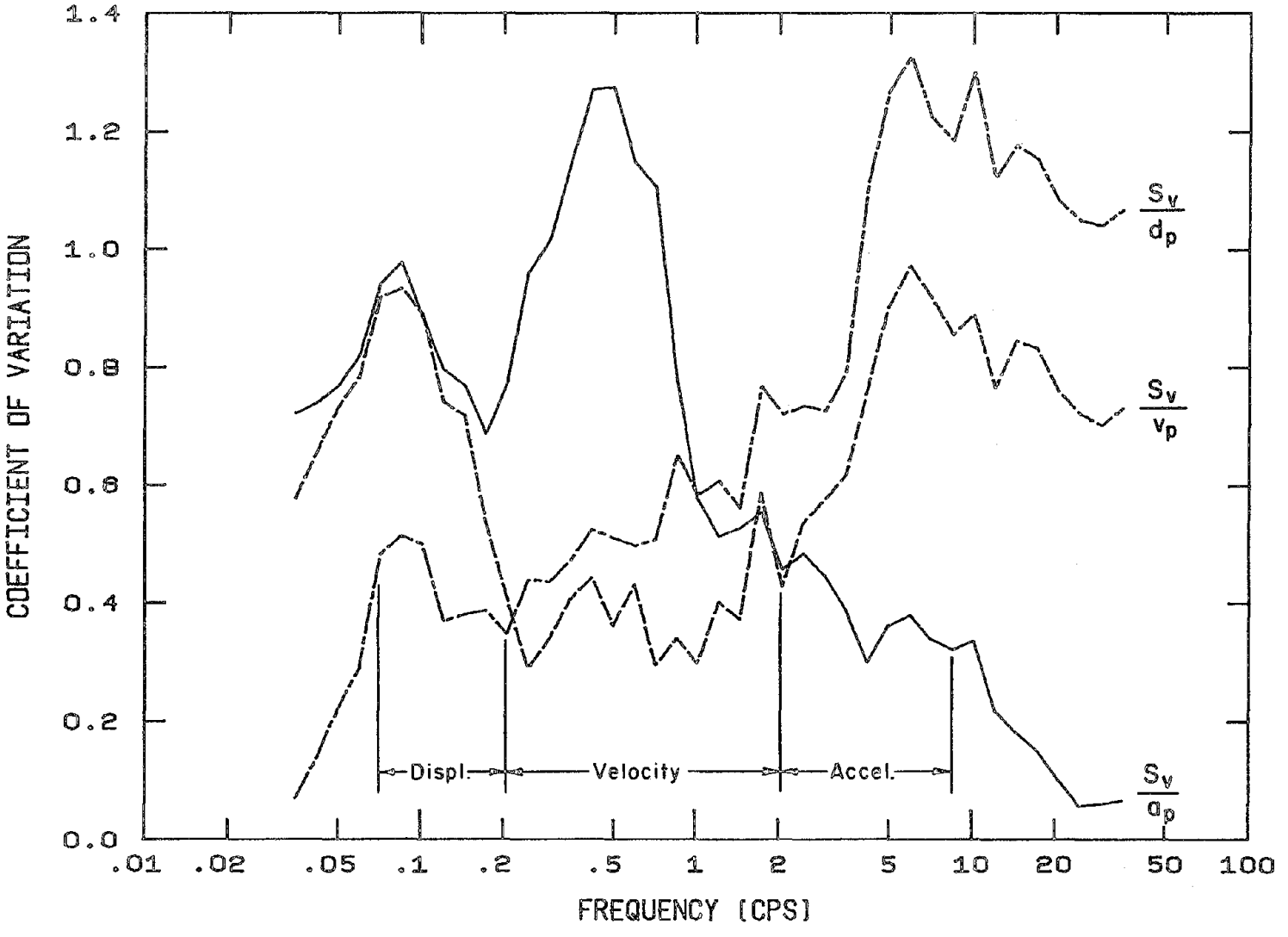

Fig. 5.20 Coefficients of Variation for Elastoplastic Yield Spectra with 5% Damping Normalized by Peak Ground Motions: Ductility = 1 (Elastic)

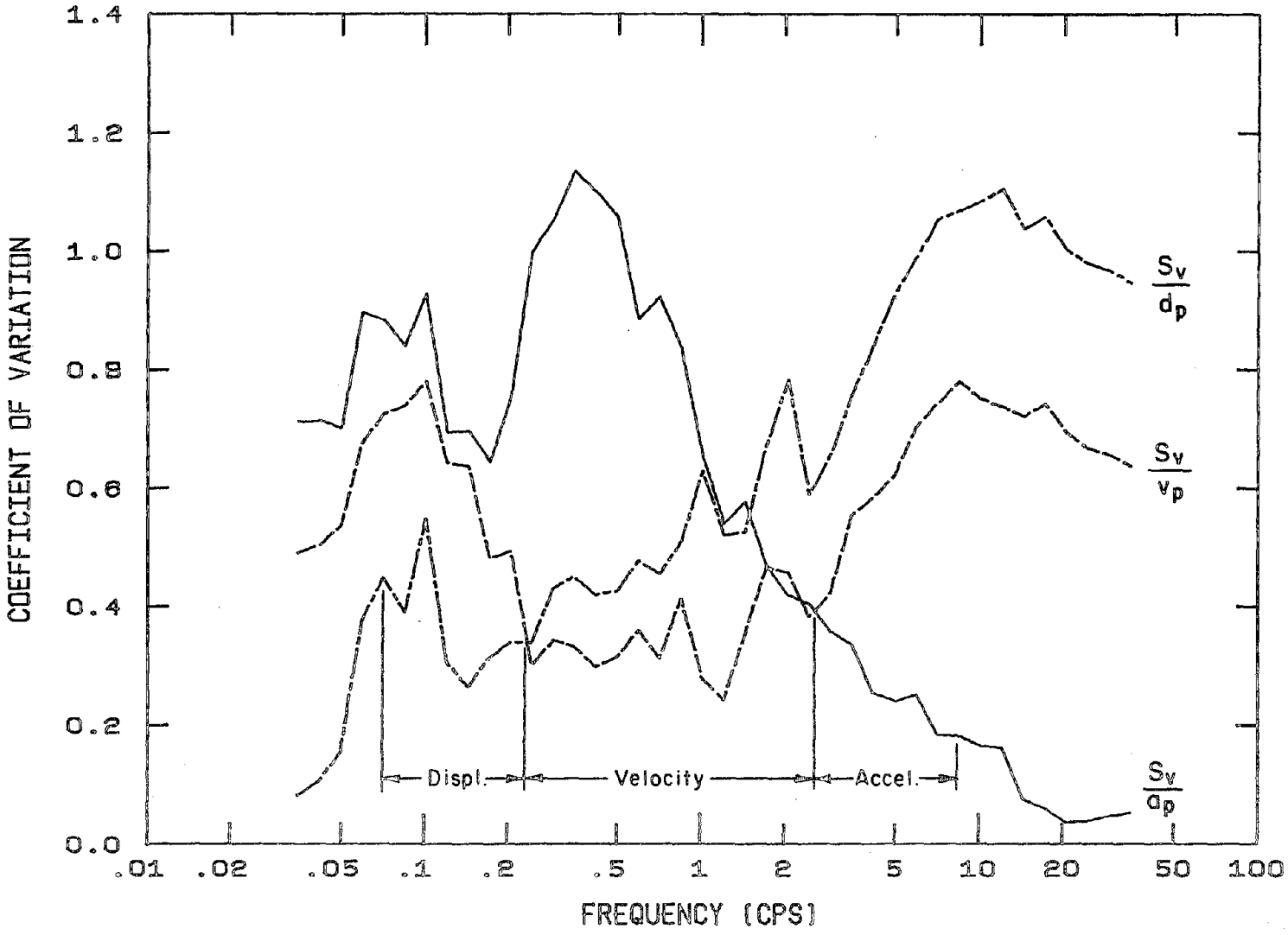

Fig. 5.21 Coefficients of Variation for Elastoplastic Yield Spectra with 5% Damping Normalized by Peak Ground Motions: Ductility = 2

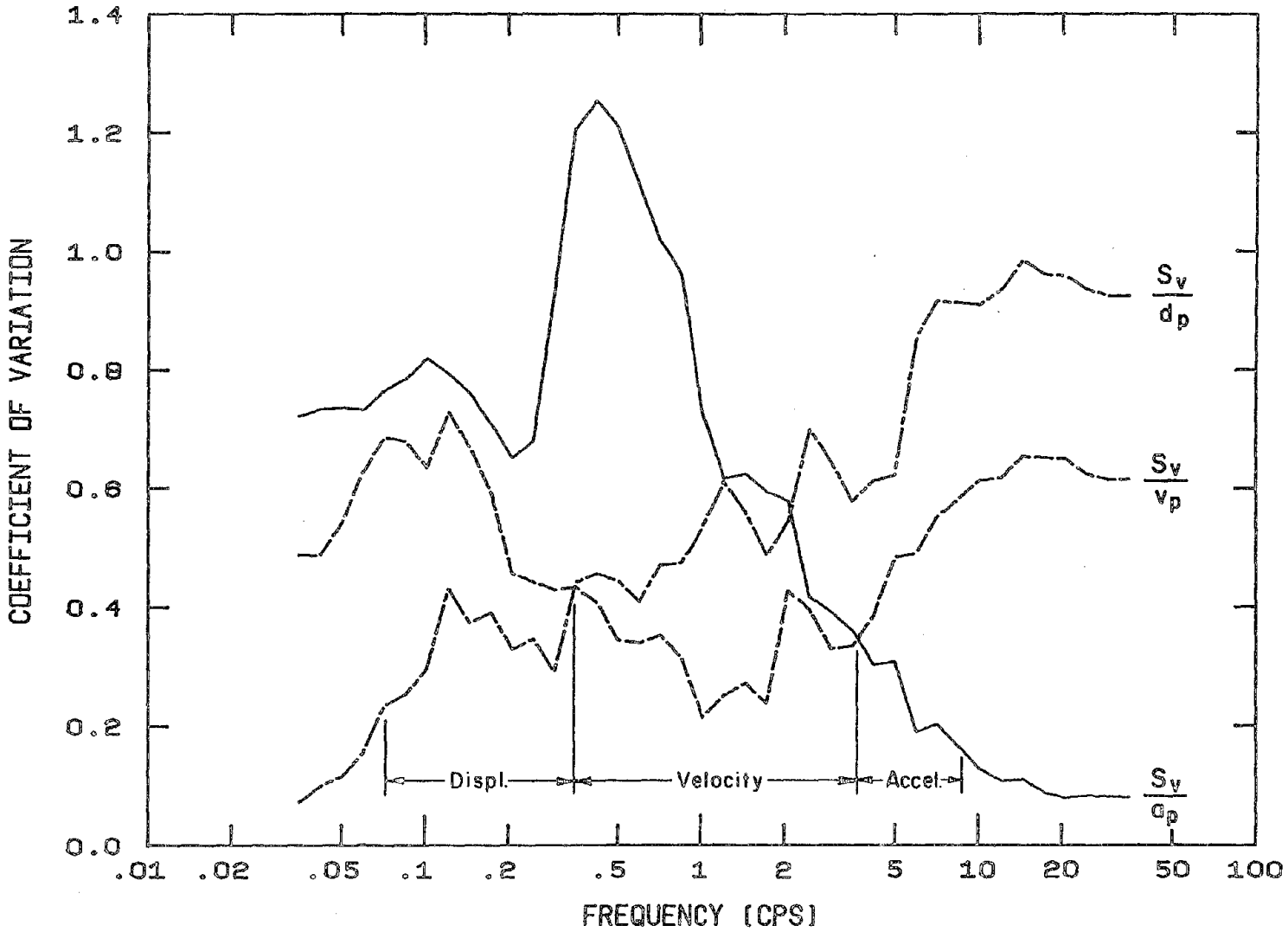

Fig. 5.22 Coefficients of Variation for Elastoplastic Yield Spectra with 5% Damping Normalized by Peak Ground Motions: Ductility = 5

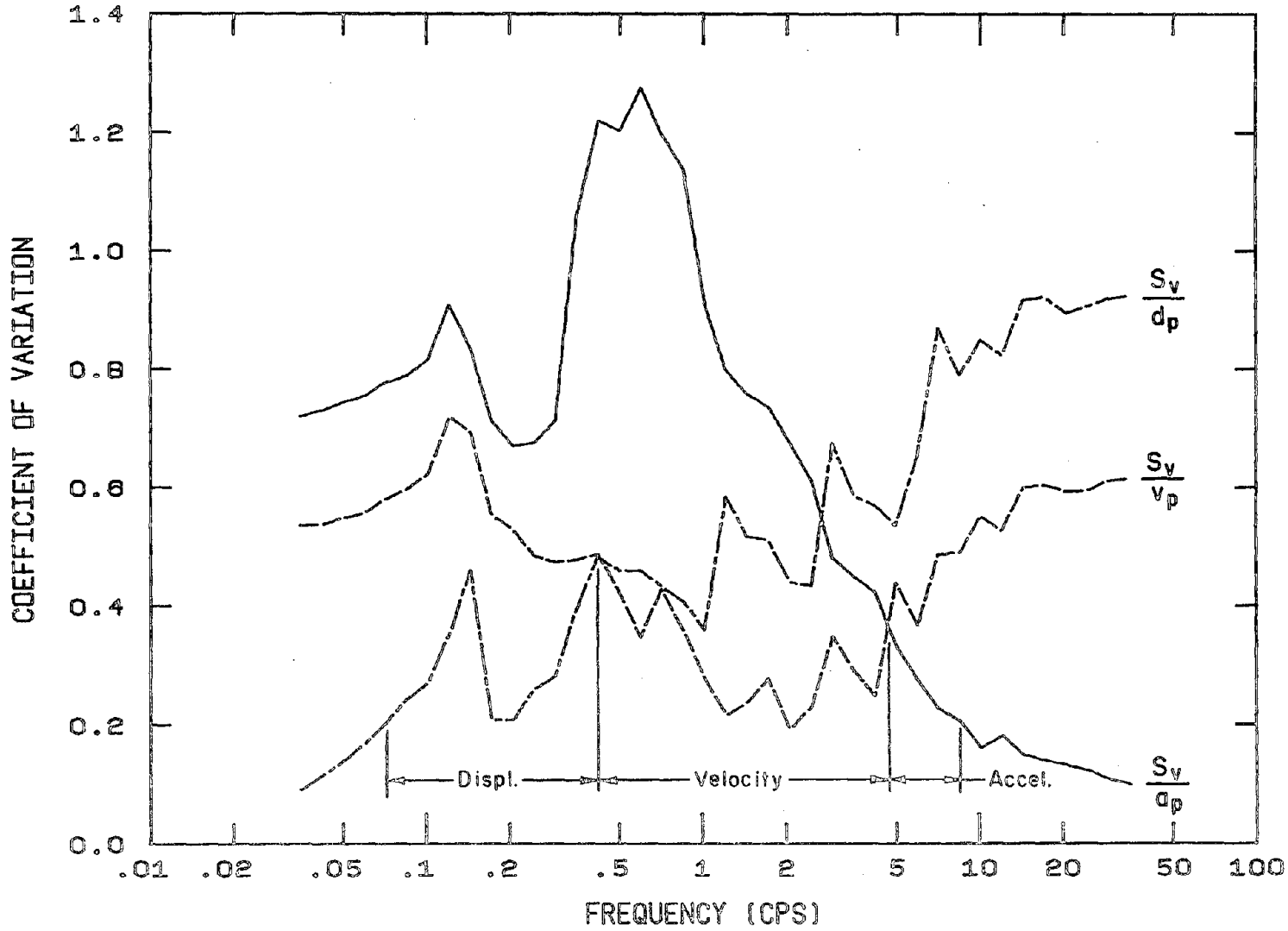

Fig. 5.23 Coefficients of Variation for Elastoplastic Yield Spectra with 5% Damping Normalized by Peak Ground Motions: Ductility = 10

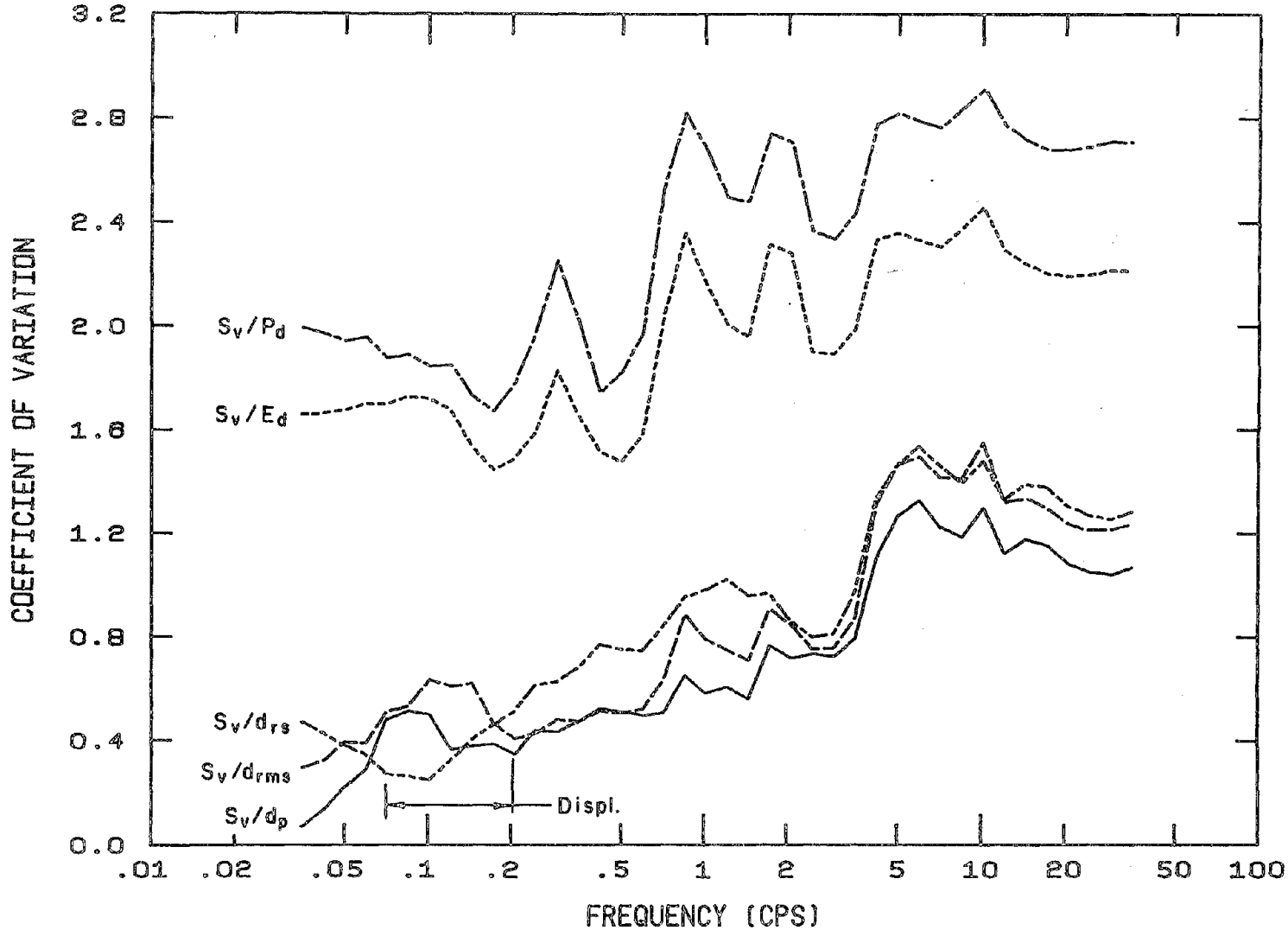

Fig. 5.24 Comparison of Displacement-Related Normalizing Factors: Coefficients of Variation for Elastoplastic Yield Spectra with 5% Damping and Ductility = 1 (Elastic)

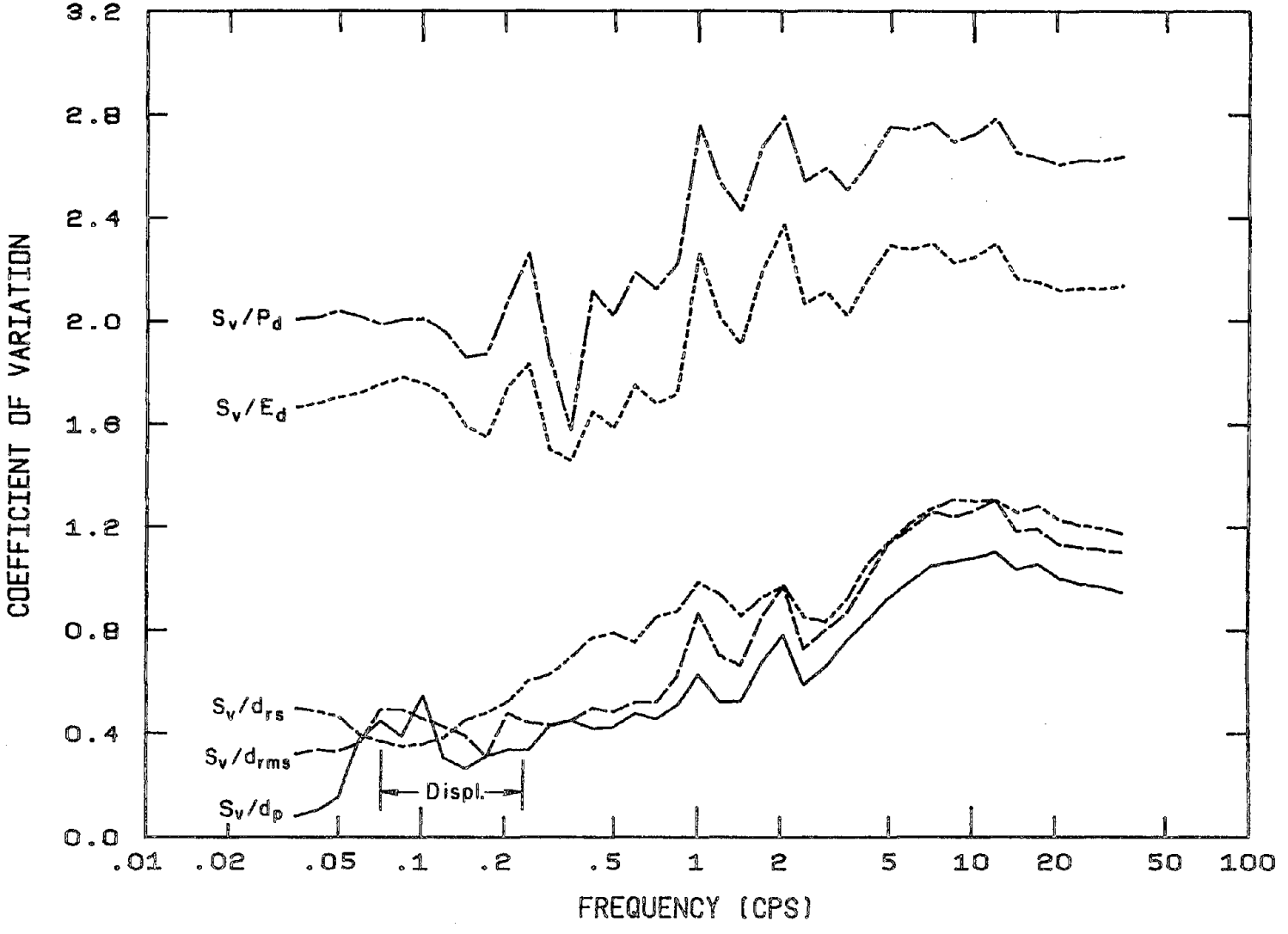

Fig. 5.25 Comparison of Displacement-Related Normalizing Factors: Coefficients of Variation for Elastoplastic Yield Spectra with 5% Damping and Ductility = 2

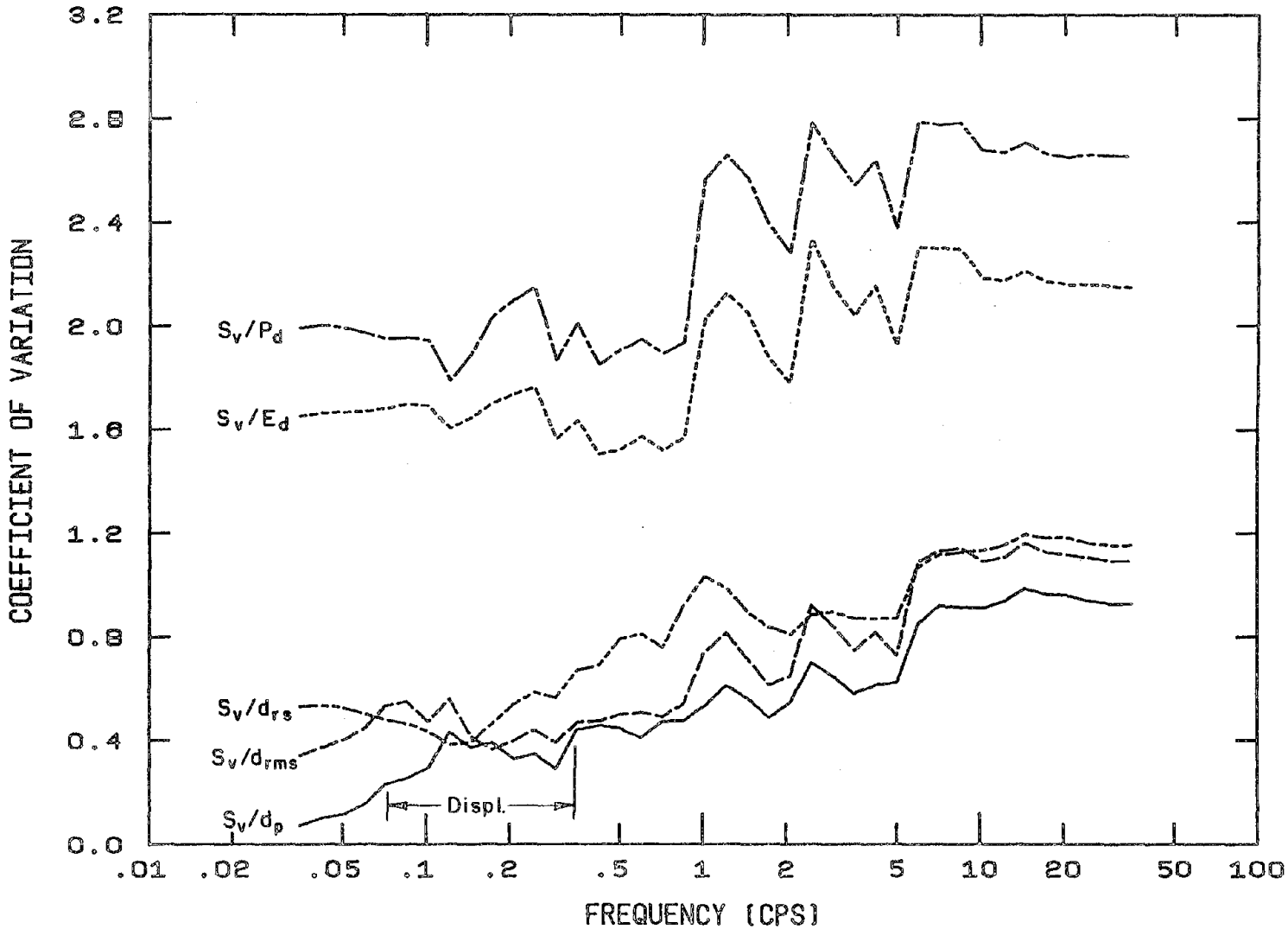

Fig. 5.26 Comparison of Displacement-Related Normalizing Factors: Coefficients of Variation for Elastoplastic Yield Spectra with 5% Damping and Ductility = 5

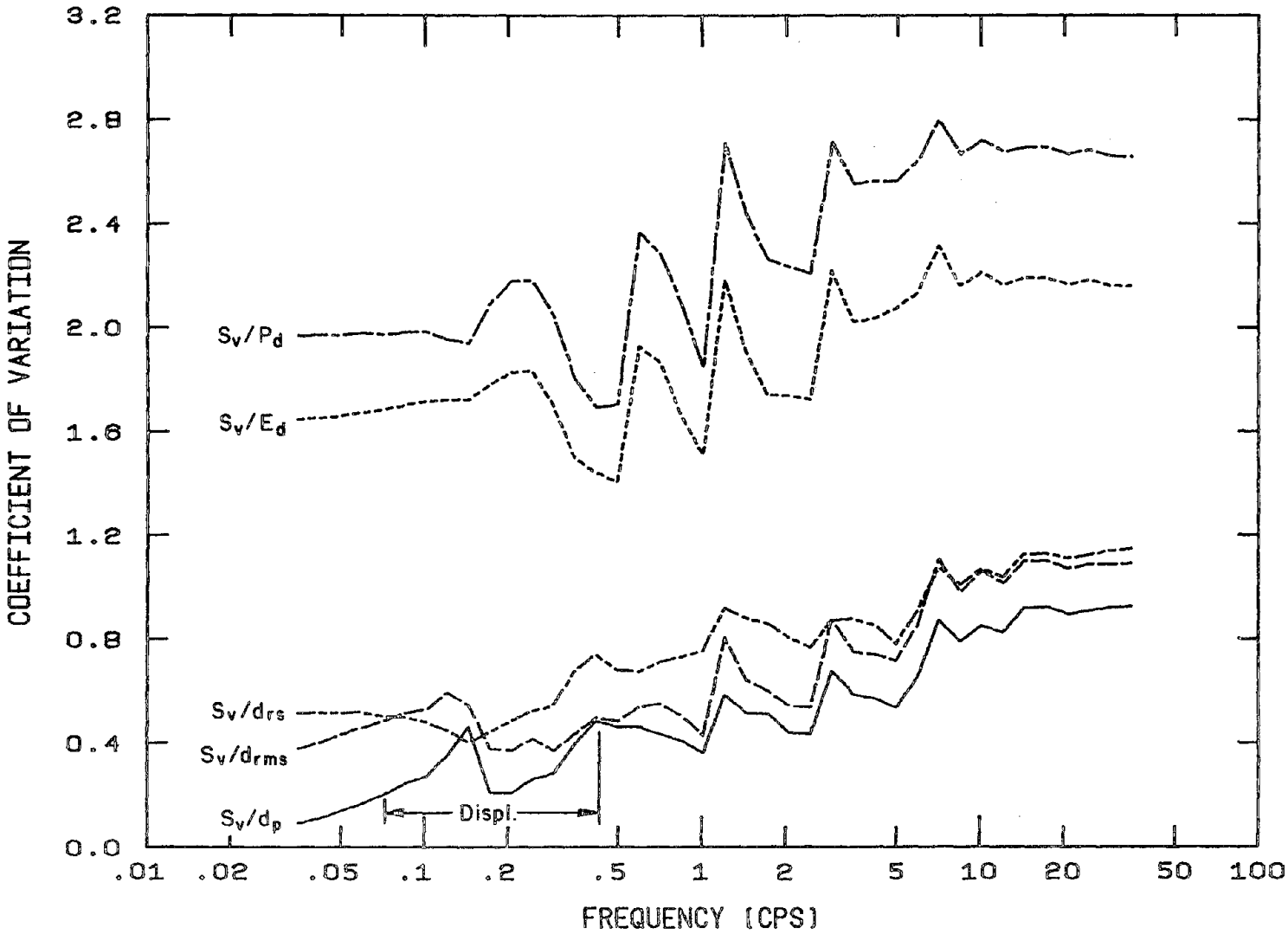

Fig. 5.27 Comparison of Displacement-Related Normalizing Factors: Coefficients of Variation for Elastoplastic Yield Spectra with 5% Damping and Ductility = 10

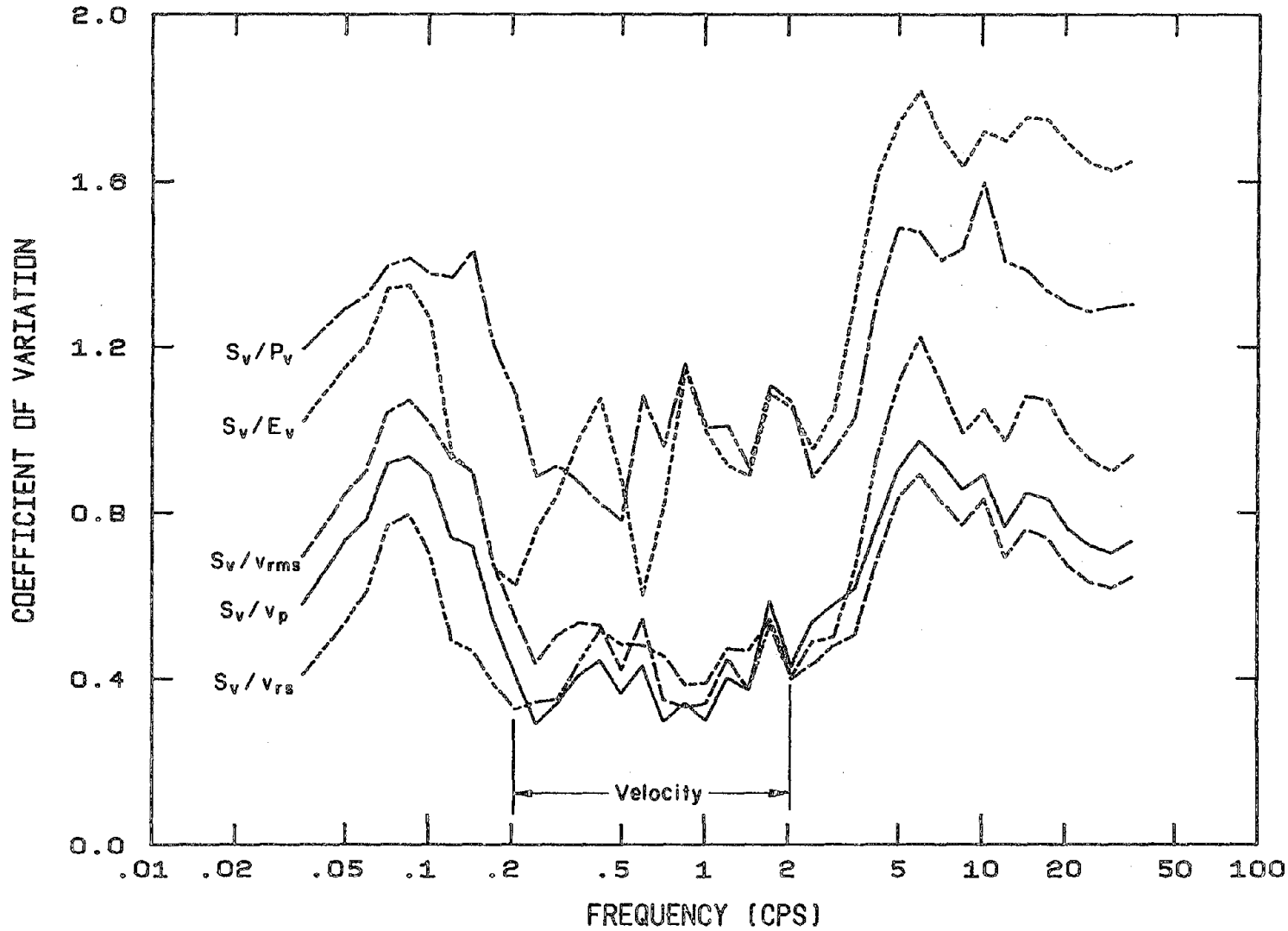

Fig. 5.28 Comparison of Velocity-Related Normalizing Factors: Coefficients of Variation for Elastoplastic Yield Spectra with 5% Damping and Ductility = 1 (Elastic)

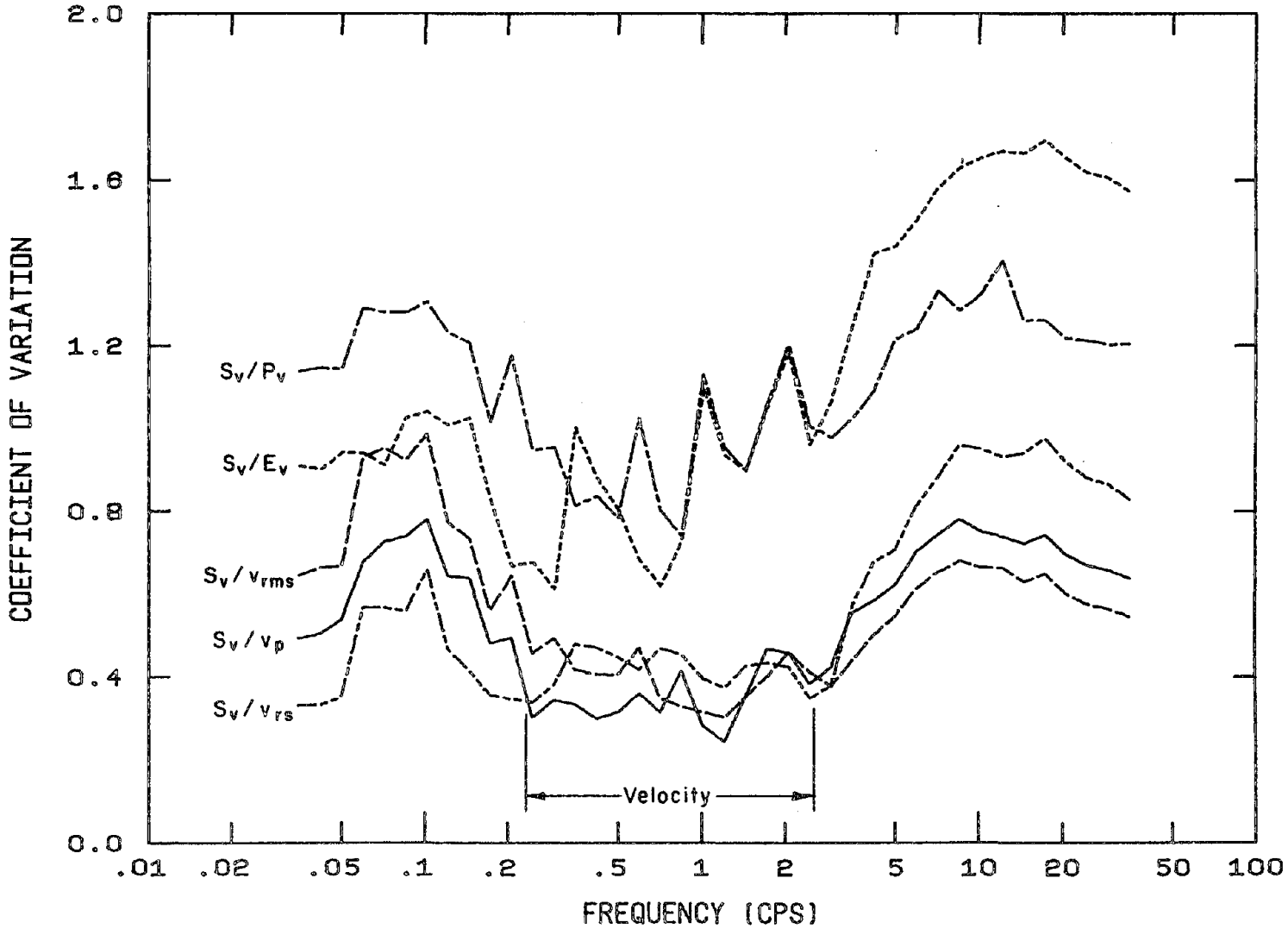

Fig. 5.29 Comparison of Velocity-Related Normalizing Factors: Coefficients of Variation for Elastoplastic Yield Spectra with 5% Damping and Ductility = 2

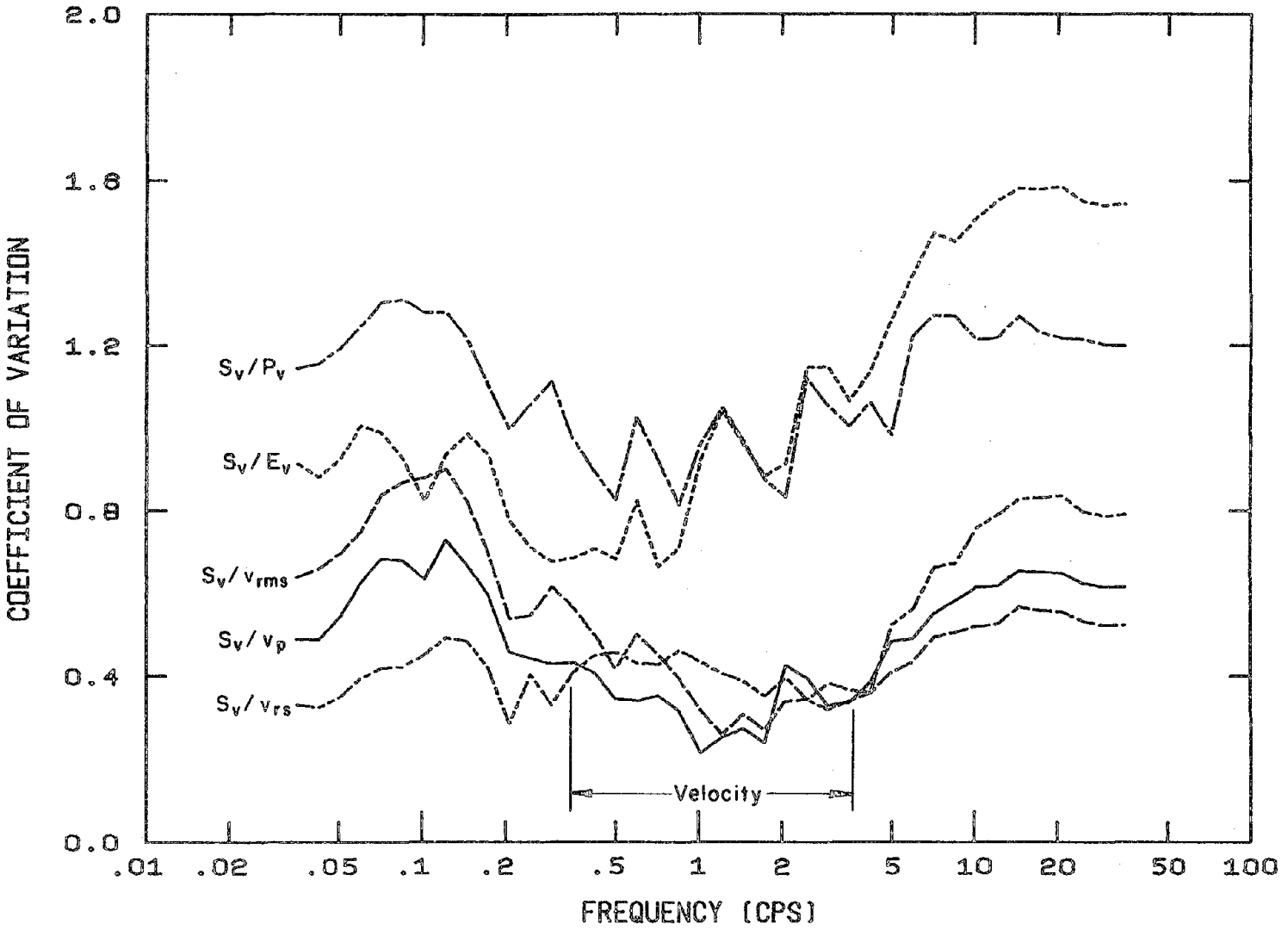

Fig. 5.30 Comparison of Velocity-Related Normalizing Factors: Coefficients of Variation for Elastoplastic Yield Spectra with 5% Damping and Ductility = 5

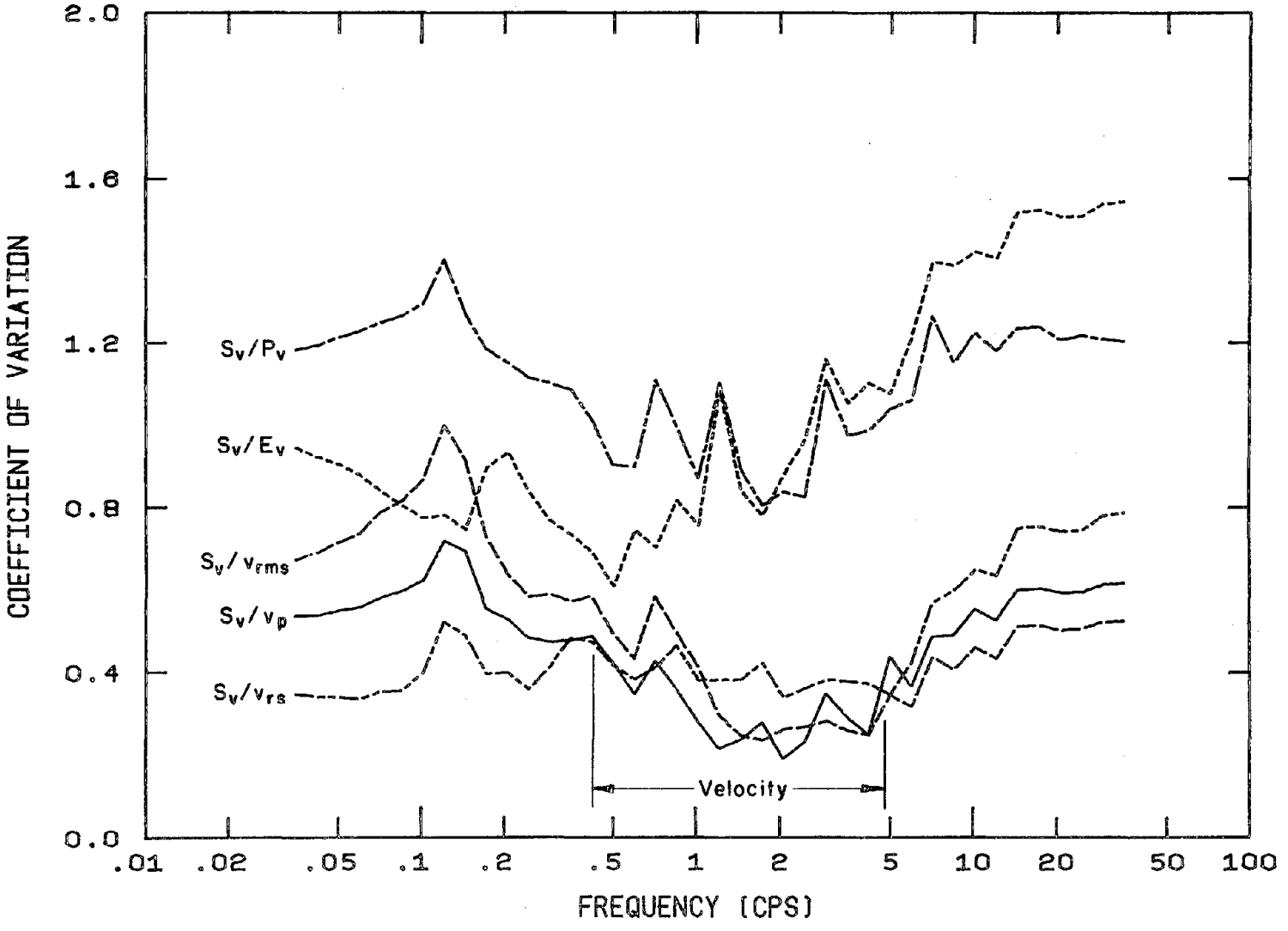

Fig. 5.31 Comparison of Velocity-Related Normalizing Factors: Coefficients of Variation for Elastoplastic Yield Spectra with 5% Damping and Ductility = 10

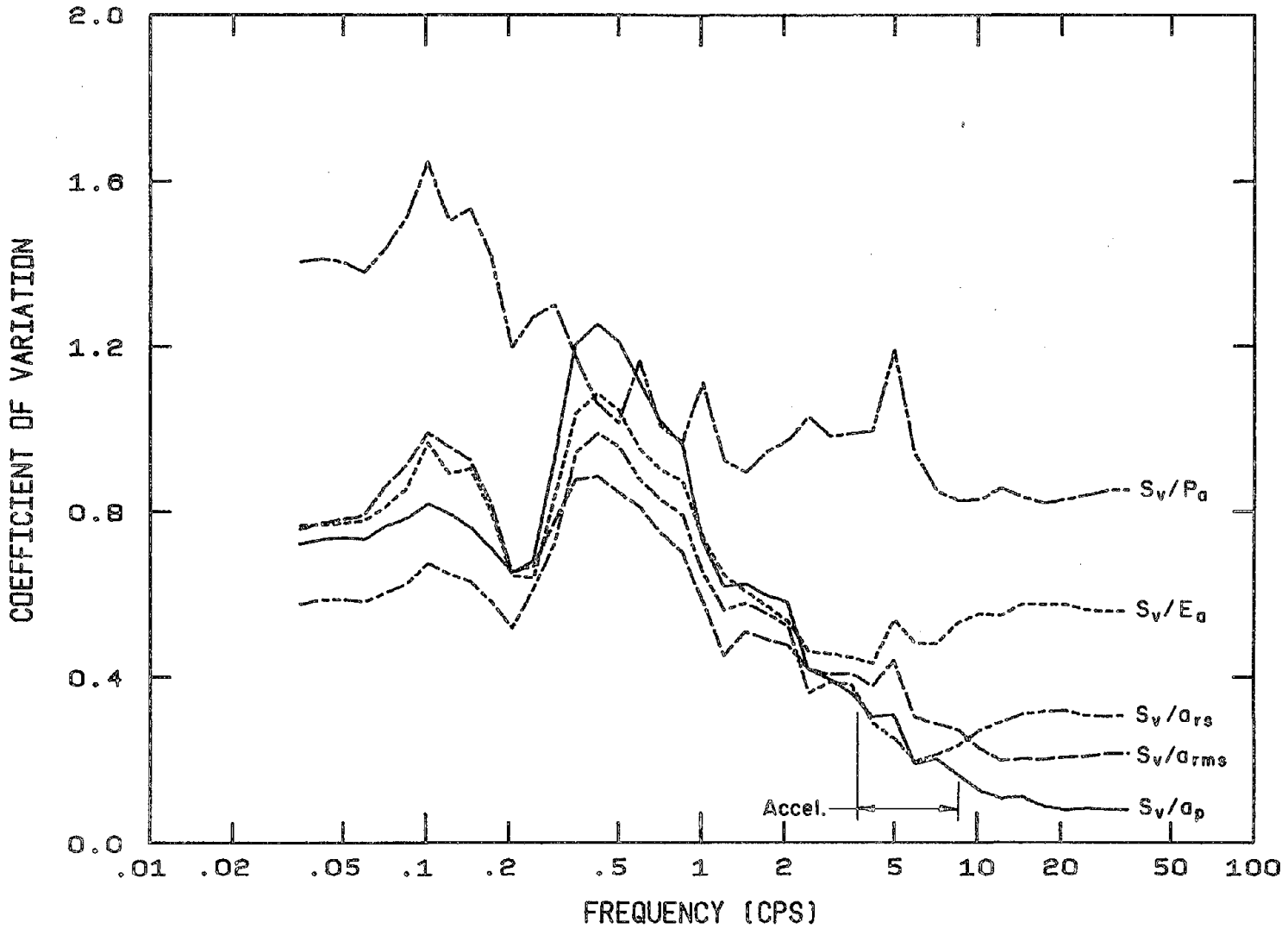

Fig. 5.34 Comparison of Acceleration-Related Normalizing Factors: Coefficients of Variation for Elastoplastic Yield Spectra with 5% Damping and Ductility = 5

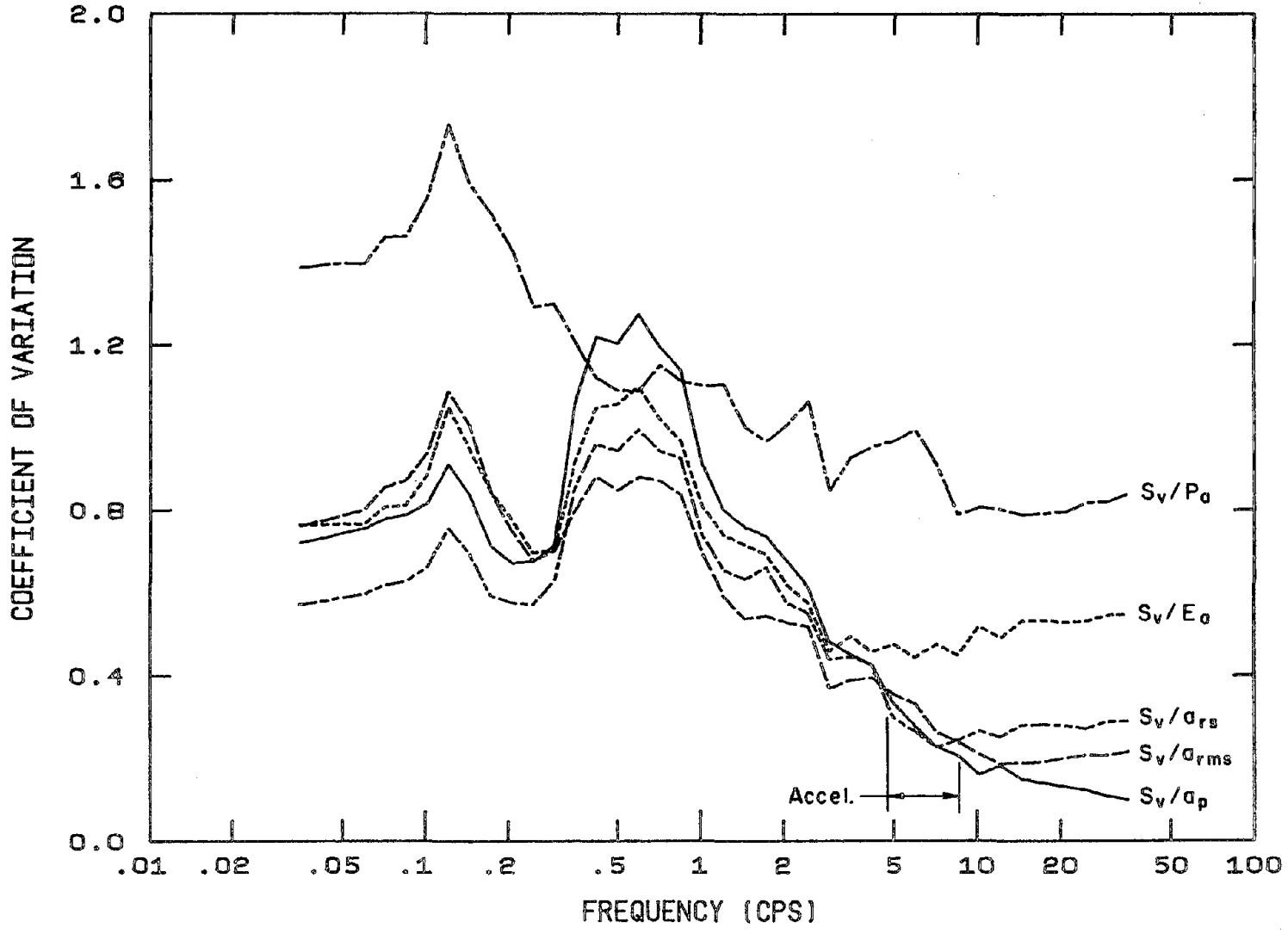

Fig. 5.35 Comparison of Acceleration-Related Normalizing Factors: Coefficients of Variation for Elastoplastic Yield Spectra with 5% Damping and Ductility = 10

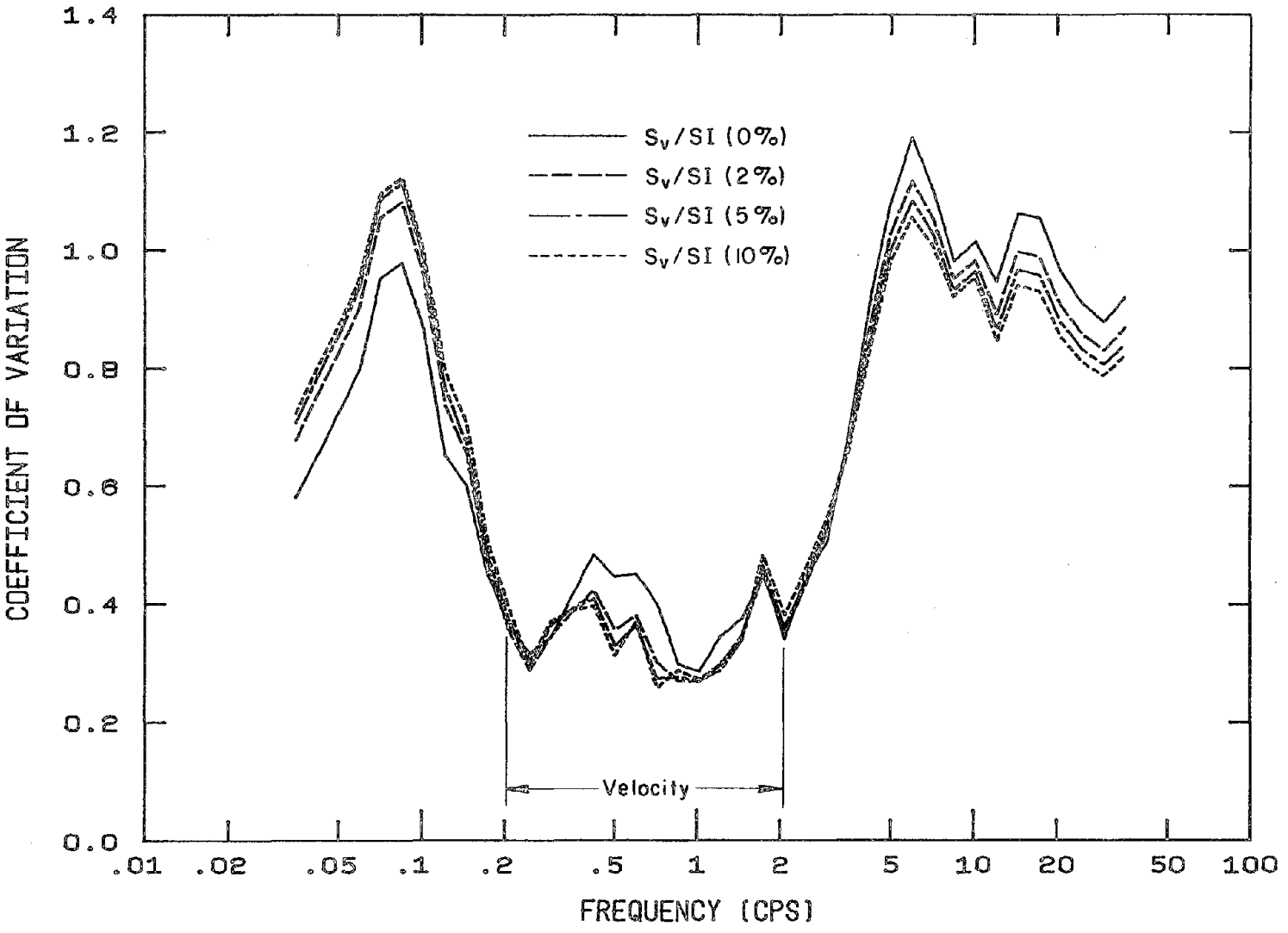

Fig. 5.36 Coefficients of Variation for Elastic Spectra with 5% Damping Normalized by Spectrum Intensities between 0.4 and 10 cps

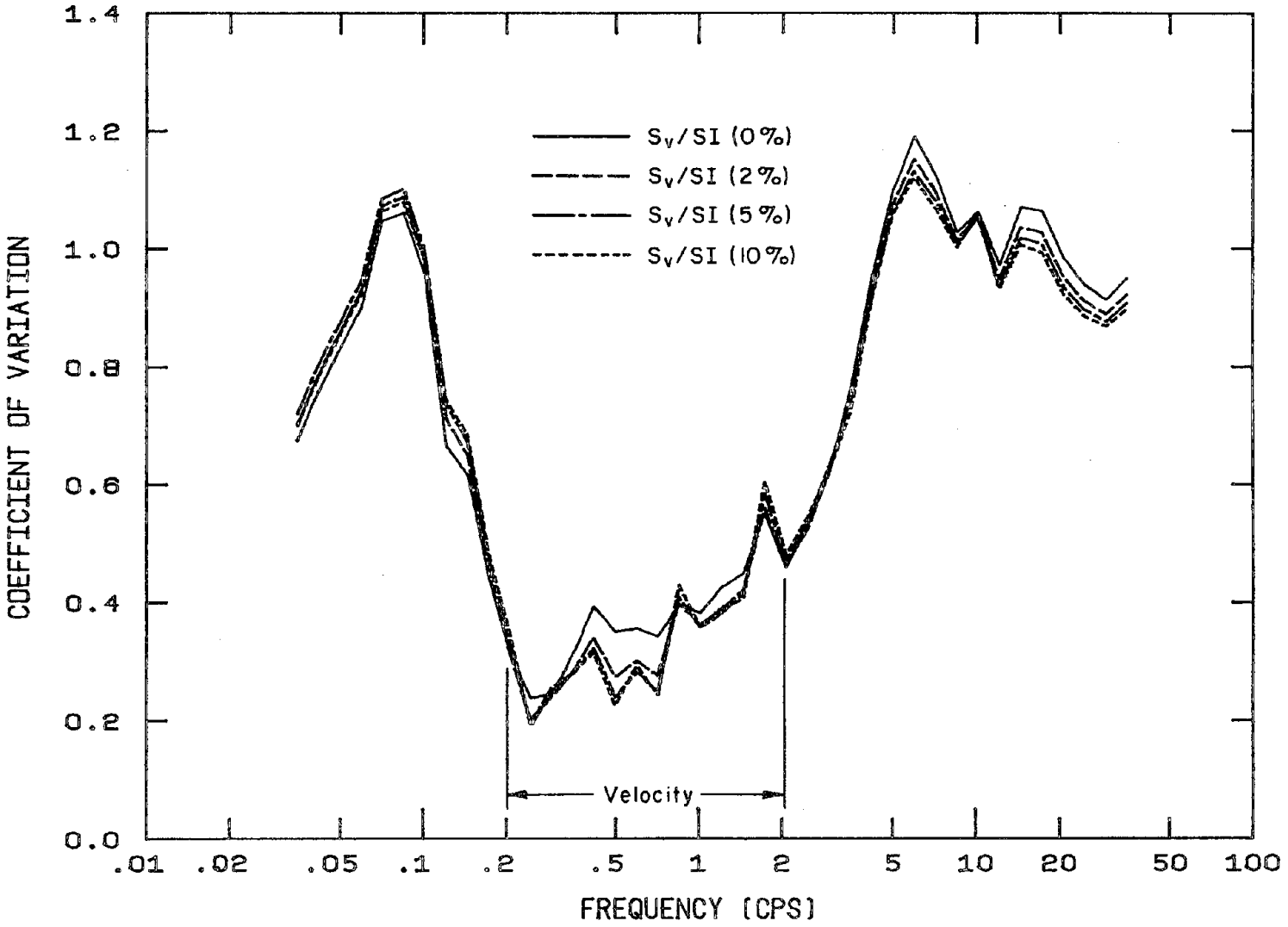

Fig. 5.37 Coefficients of Variation for Elastic Spectra with 5% Damping Normalized by Spectrum Intensities between 0.2 and 2 cps

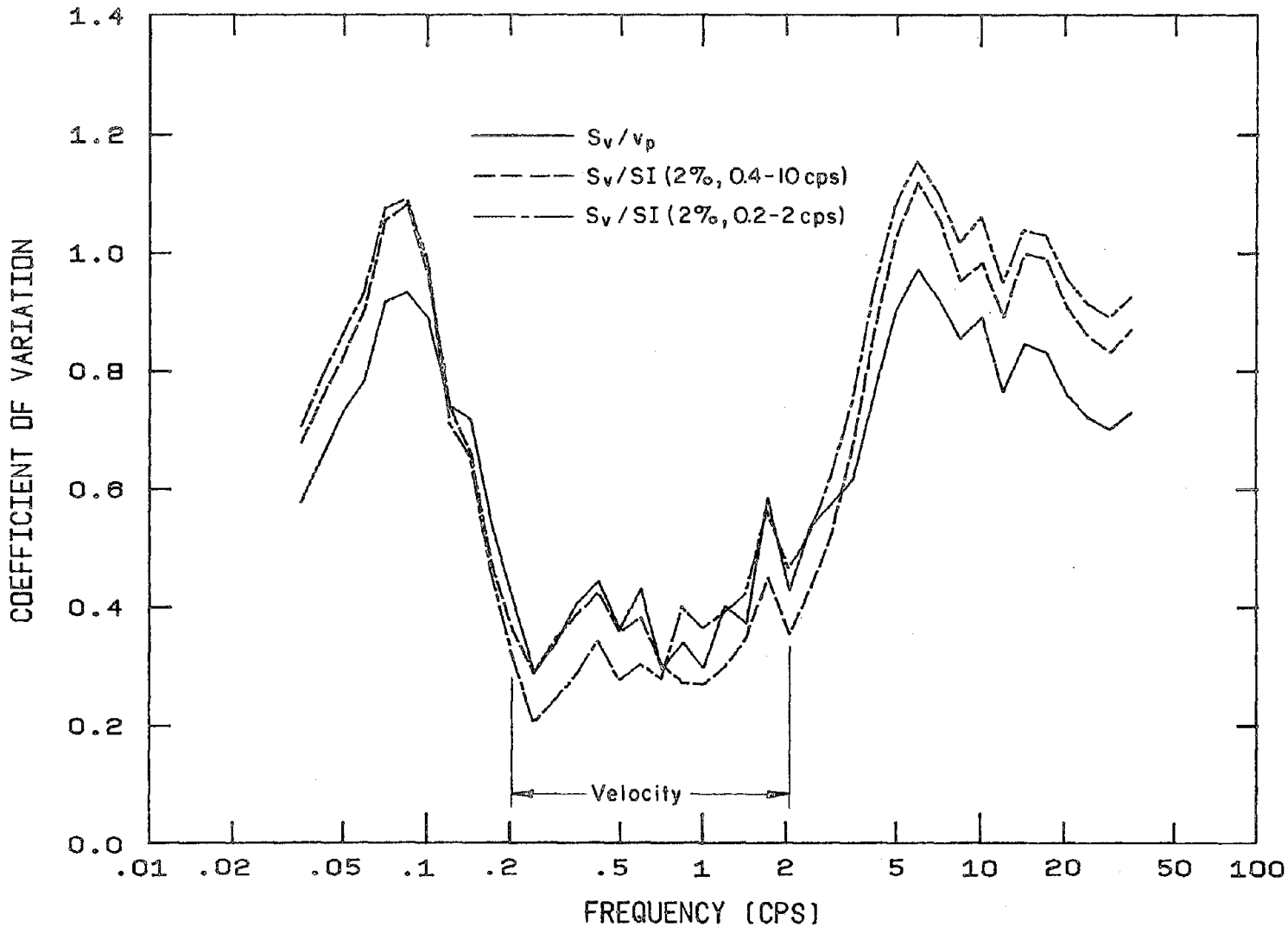

Fig. 5.38 Coefficients of Variation for Elastic Spectra with 5% Damping Normalized by Peak Ground Velocity and 2% Spectrum Intensities

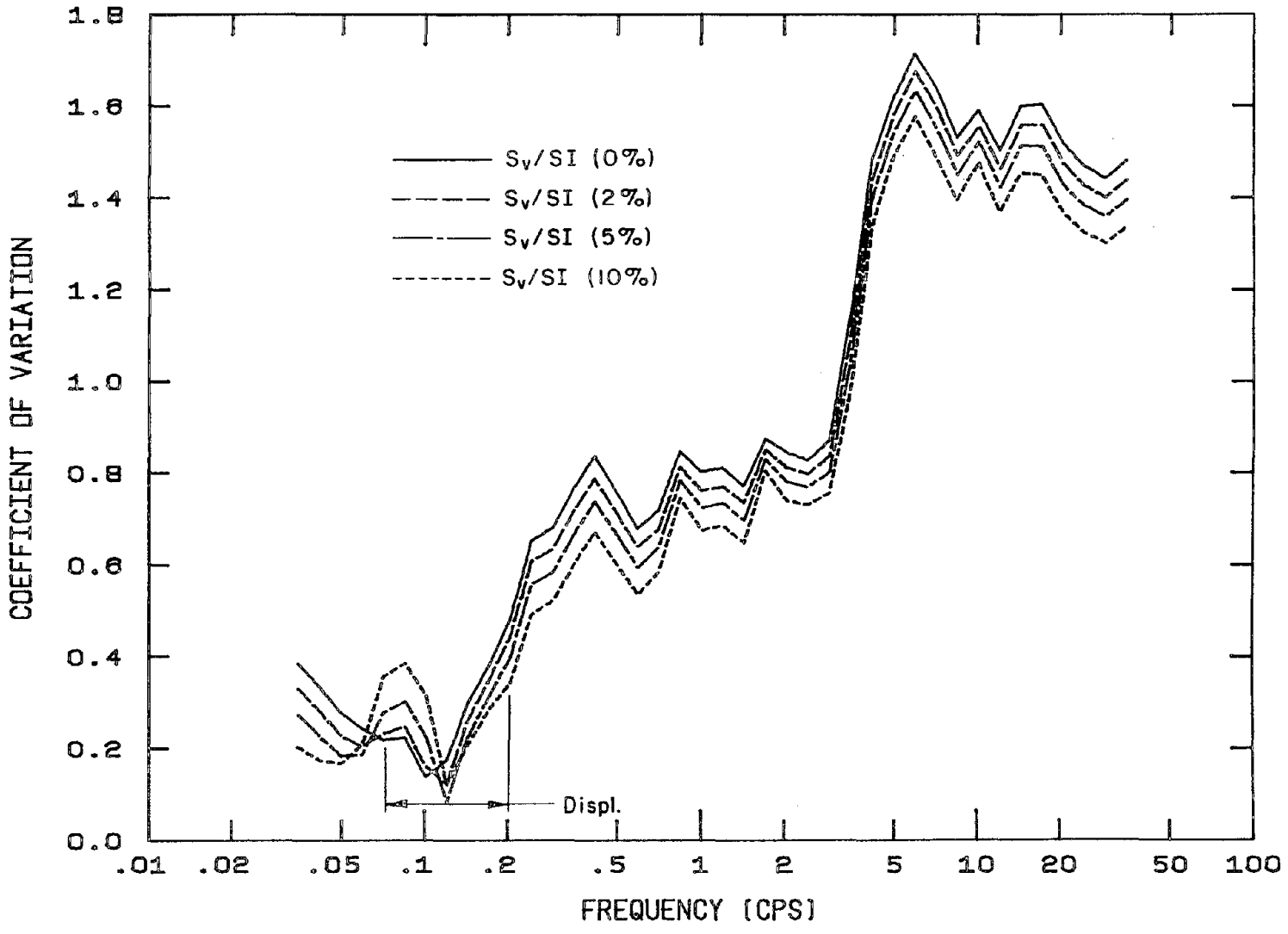

Fig. 5.39 Coefficients of Variation for Elastic Spectra with 5% Damping Normalized by Spectrum Intensities between 0.071 and 0.2 cps

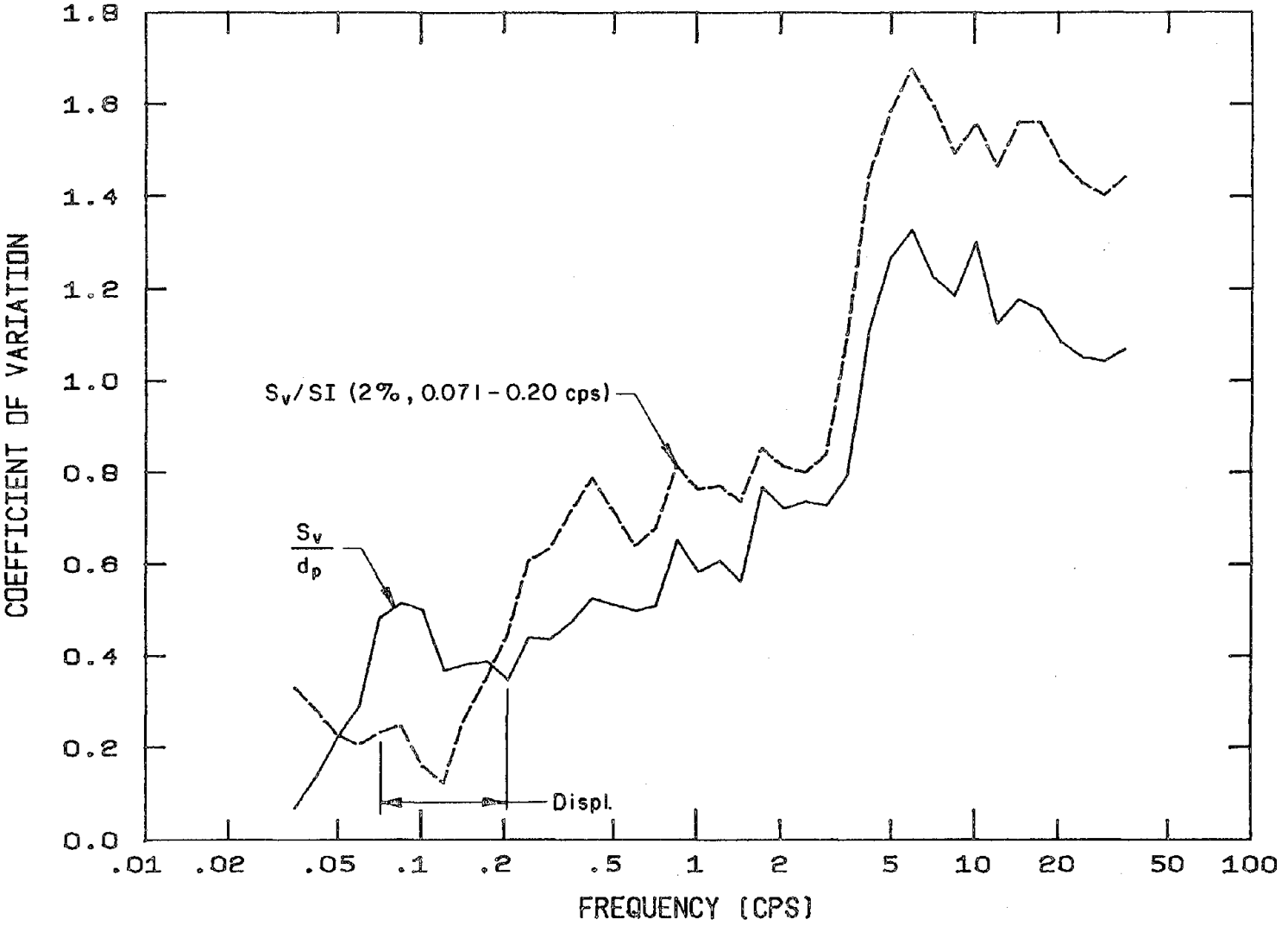

Fig. 5.40 Coefficients of Variation for Elastic Spectra with 5% Damping Normalized by Peak Ground Displacement and 2% Spectrum Intensity

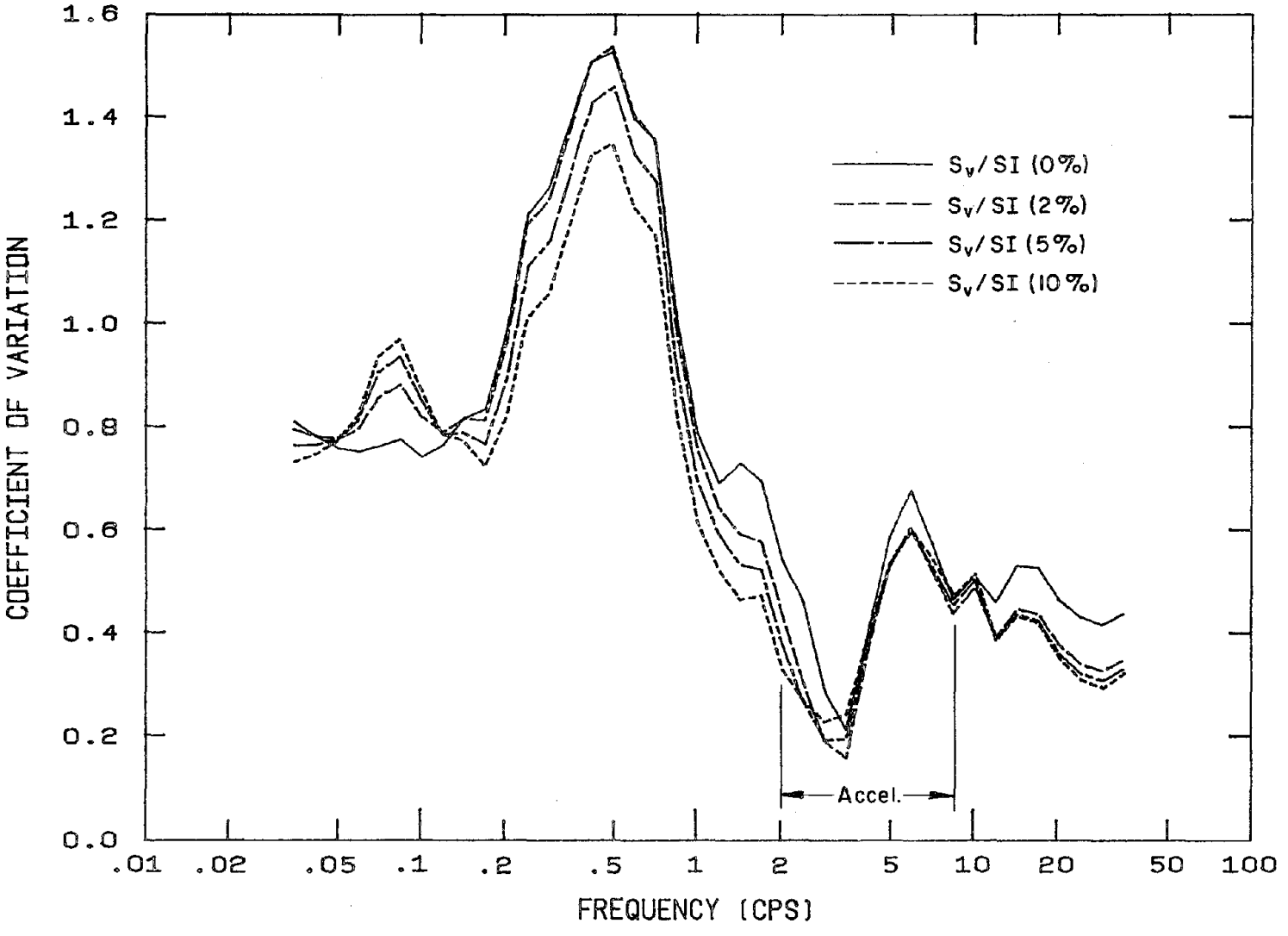

Fig. 5.41 Coefficients of Variation for Elastic Spectra with 5% Damping Normalized by Spectrum Intensities between 2 and 8.5 cps

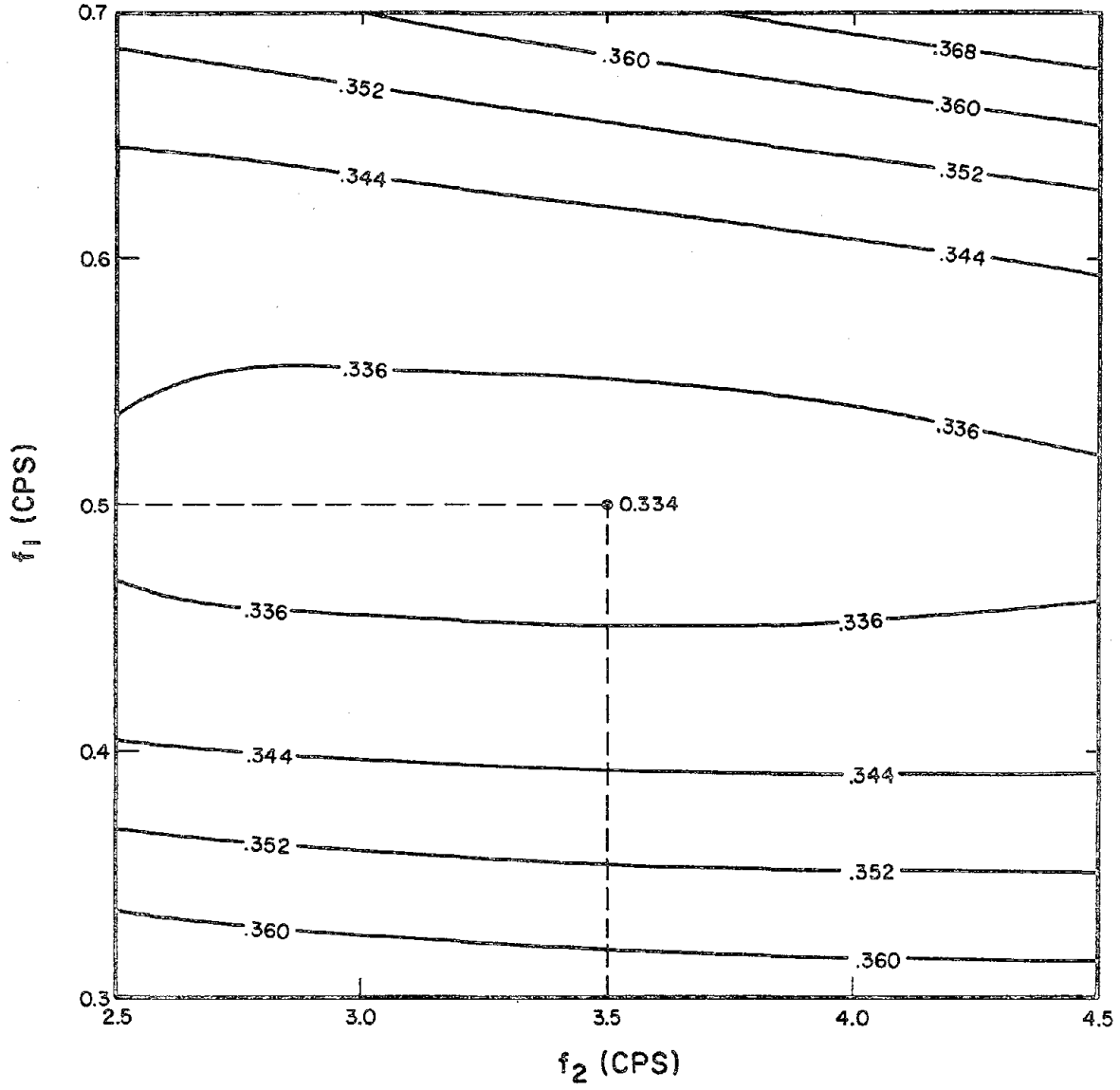

Fig. 5.44 Contours of Average Coefficient of Variation in the Velocity Region for Elastic Spectra with 5% Damping Normalized by 2% Spectrum Intensity between f_1 and f_2

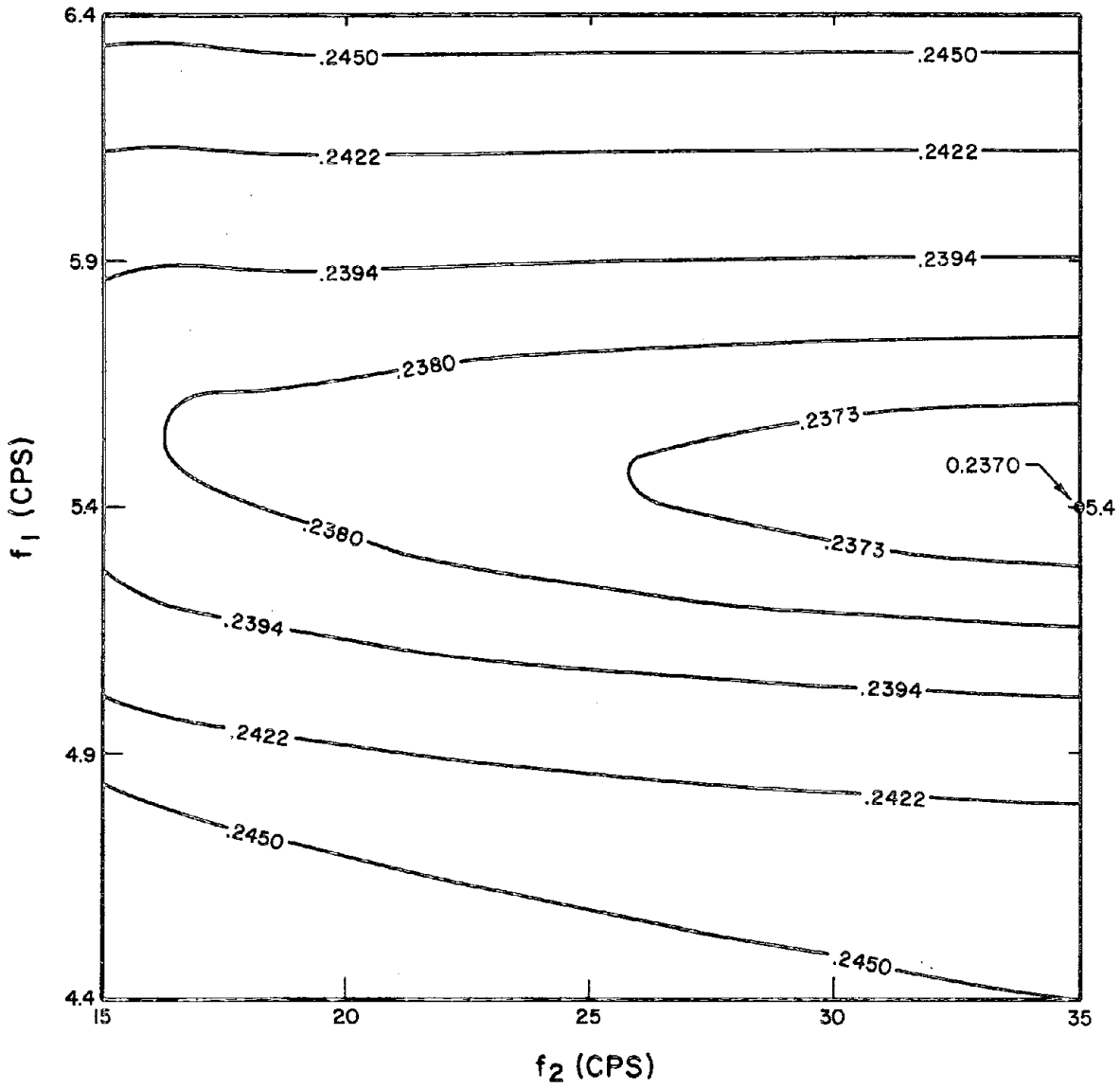

Fig. 5.45 Contours of Average Coefficient of Variation in the Acceleration Region for Elastic Spectra with 5% Damping Normalized by 2% Spectrum Intensity between f_1 and f_2

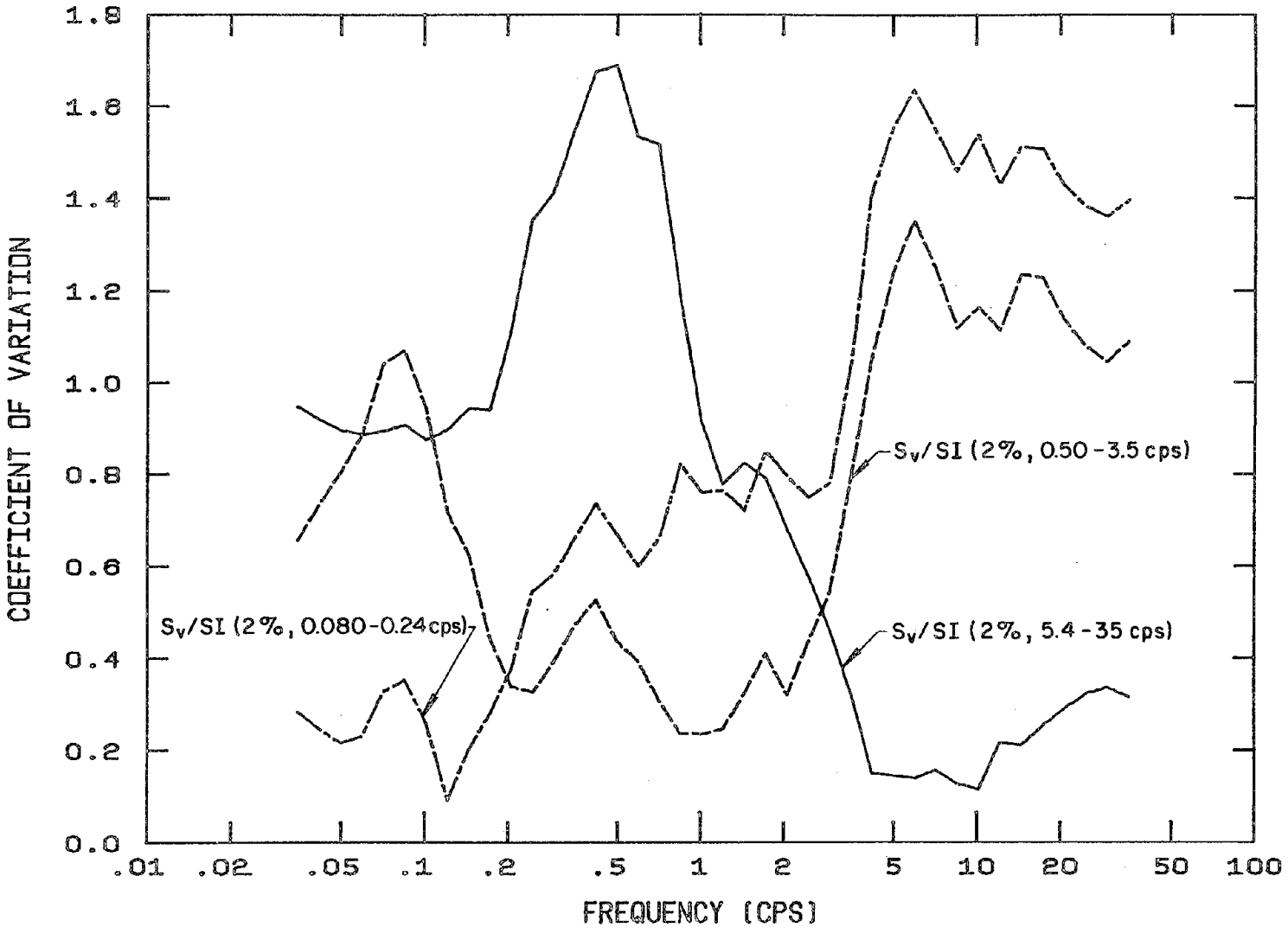

Fig. 5.46 Coefficients of Variation for Elastic Spectra with 5% Damping Normalized by 2% Spectrum Intensities

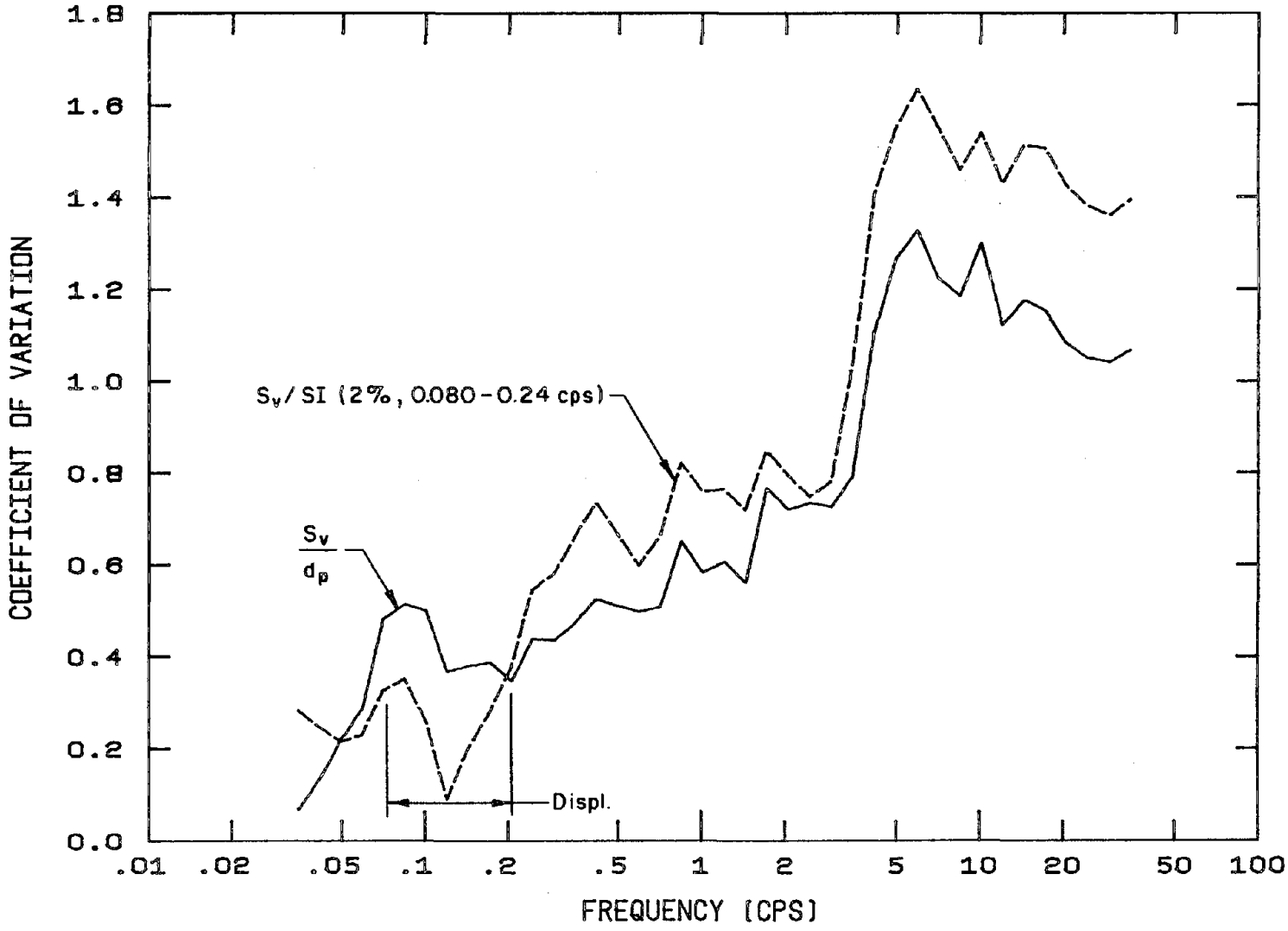

Fig. 5.47 Coefficients of Variation for Elastic Spectra with 5% Damping Normalized by Peak Ground Displacement and 2% Spectrum Intensity between 0.080 and 0.24 cps

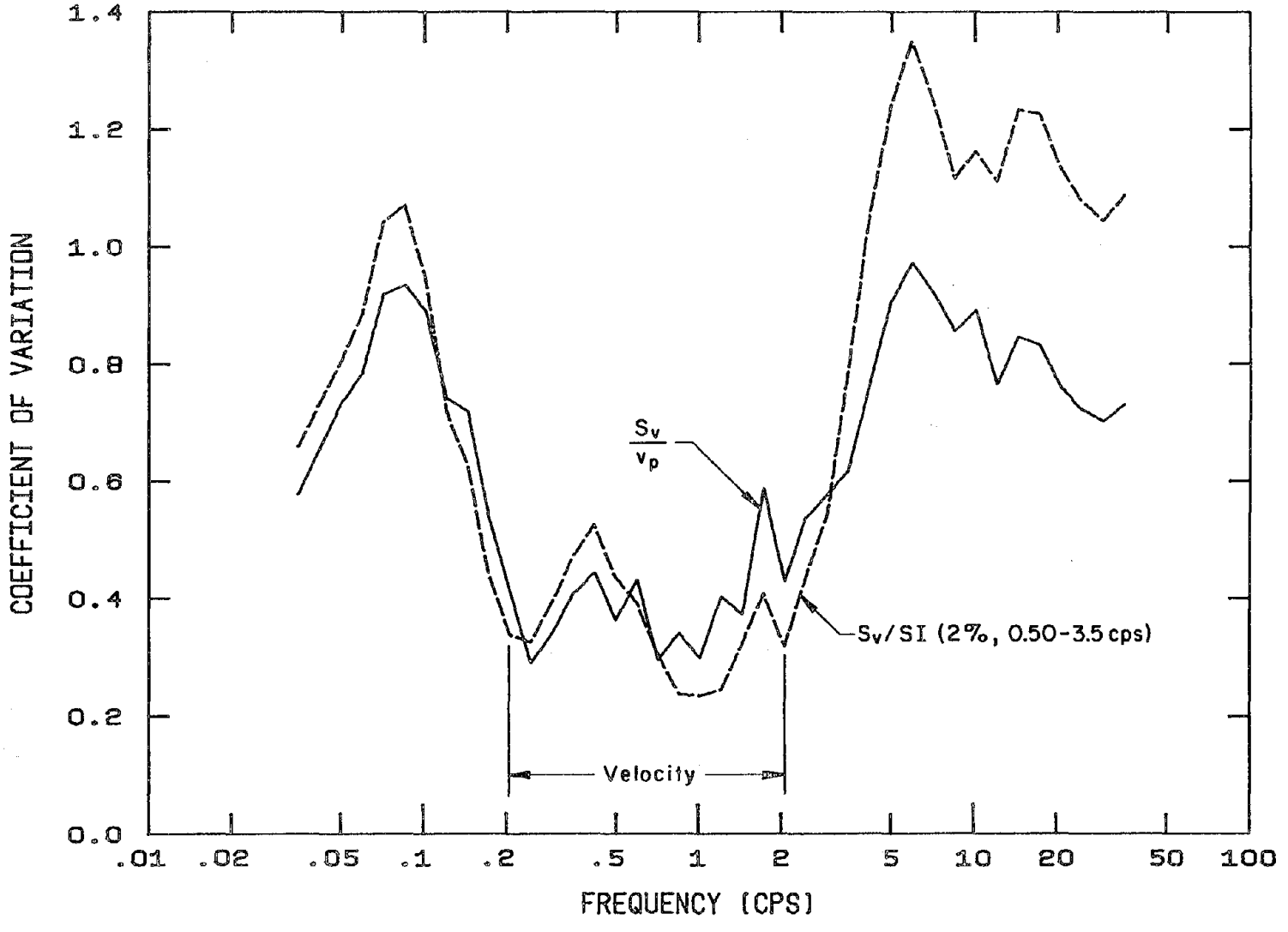

Fig. 5.48 Coefficients of Variation for Elastic Spectra with 5% Damping Normalized by Peak Ground Velocity and 2% Spectrum Intensity between 0.50 and 3.5 cps

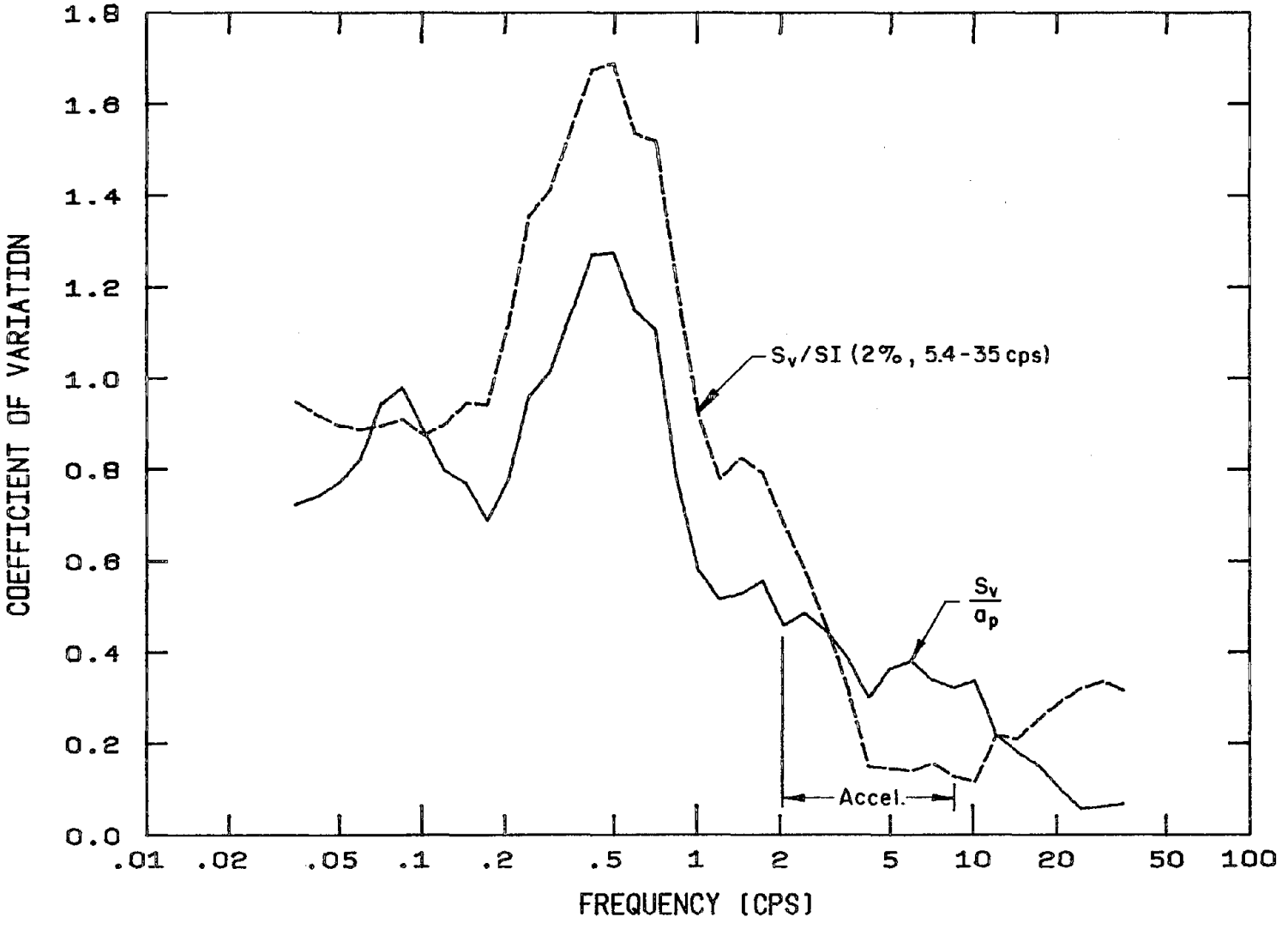

Fig. 5.49 Coefficients of Variation for Elastic Spectra with 5% Damping Normalized by Peak Ground Acceleration and 2% Spectrum Intensity between 5.4 and 35 cps

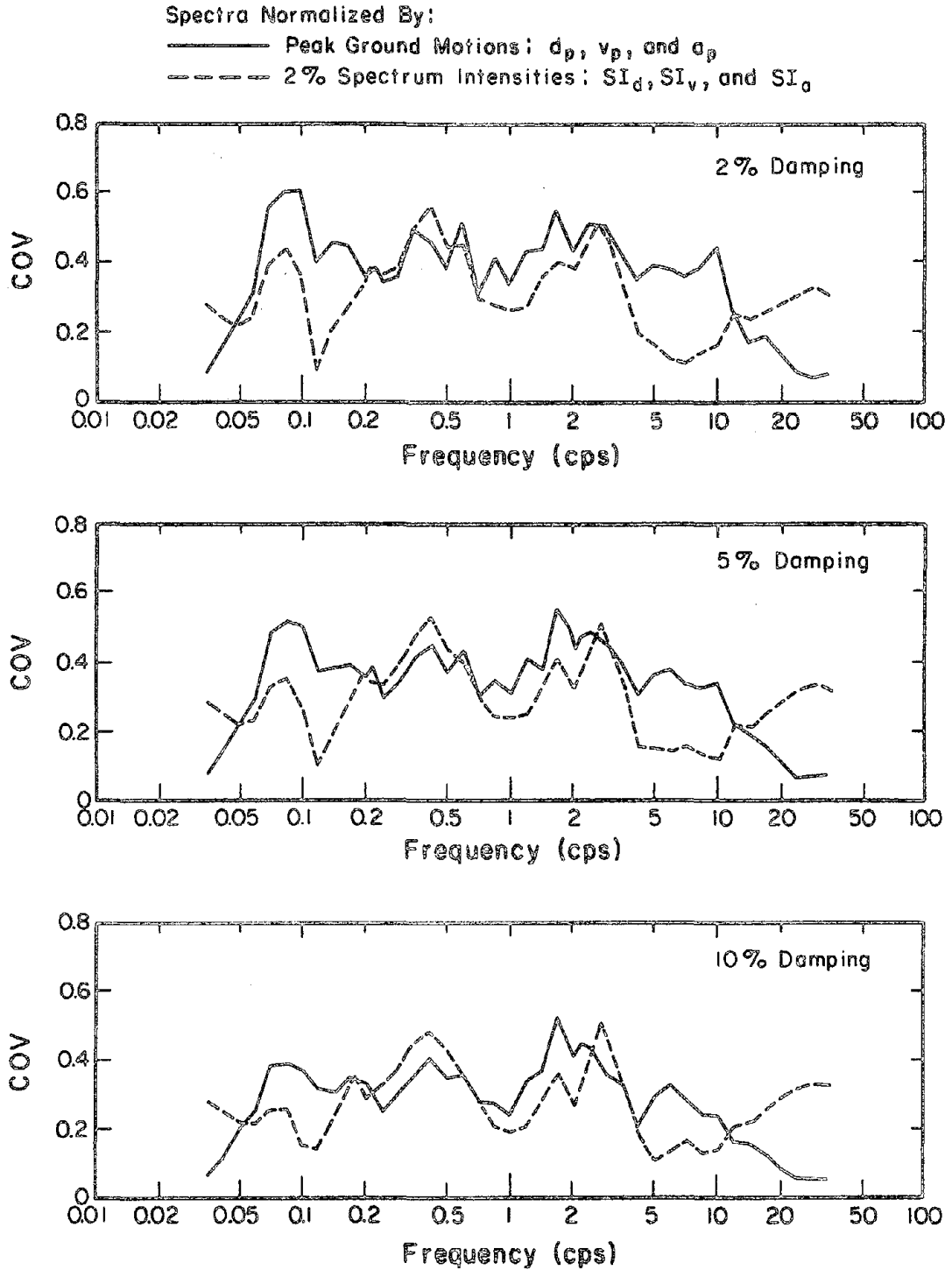

Fig. 5.50 Coefficients of Variation for Elastic Spectra Normalized by Peak Ground Motions and 2% Spectrum Intensities

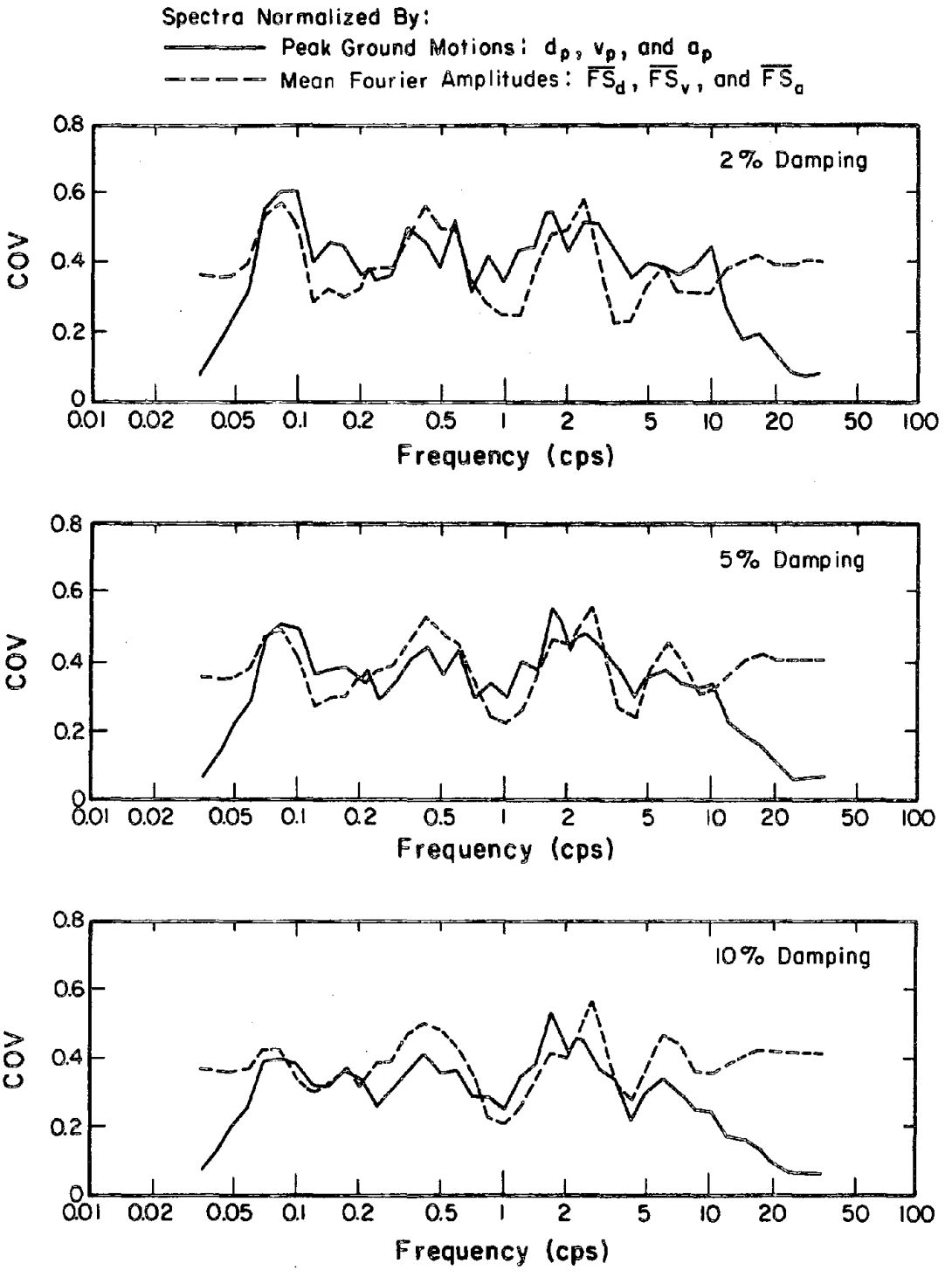

Fig. 5.51 Coefficients of Variation for Elastic Spectra Normalized by Peak Ground Motions and Mean Fourier Amplitudes

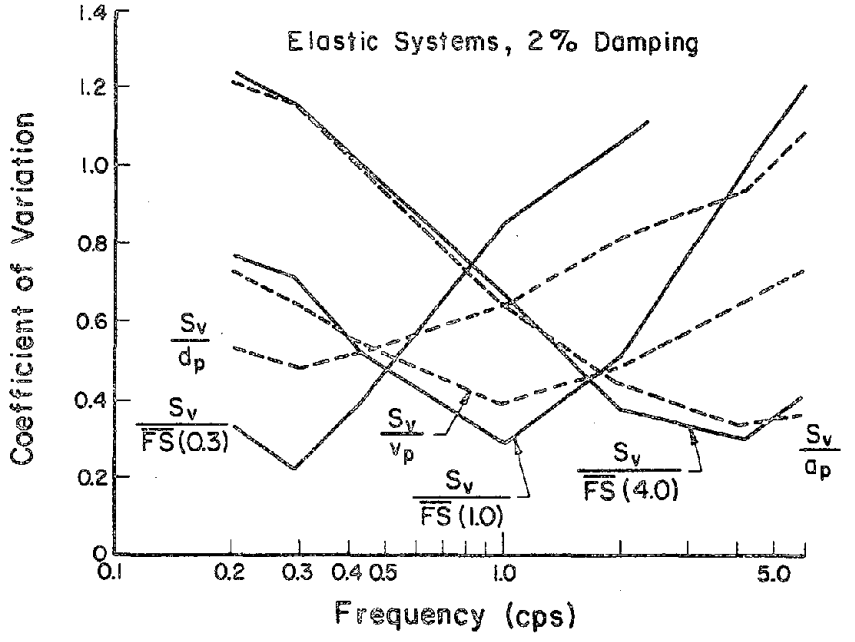

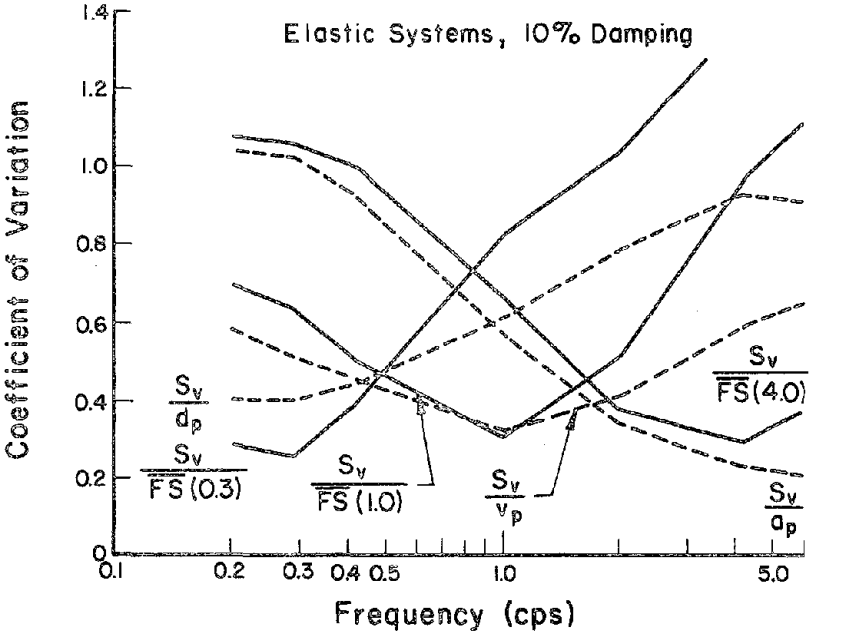

Fig. 5.52 Coefficients of Variation for Elastic Spectra Normalized by Peak Ground Motions and Mean Fourier Amplitudes. After Cornell, Banon, and Shakal (11)

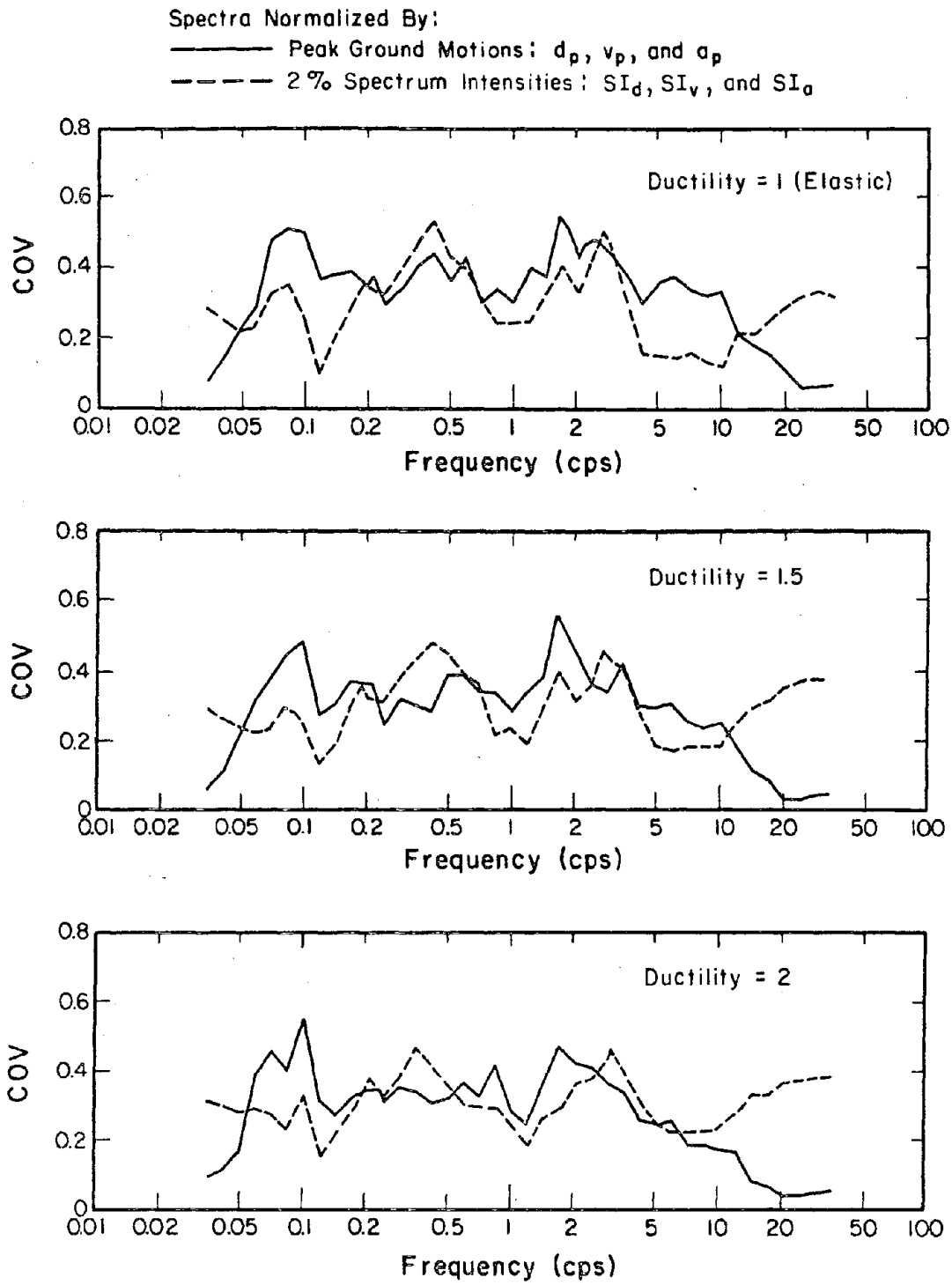

Fig. 5.53 Coefficients of Variation for Elastoplastic Yield Spectra with 5% Damping Normalized by Peak Ground Motions and 2% Spectrum Intensities: Ductilities = 1 (Elastic), 1.5, and 2

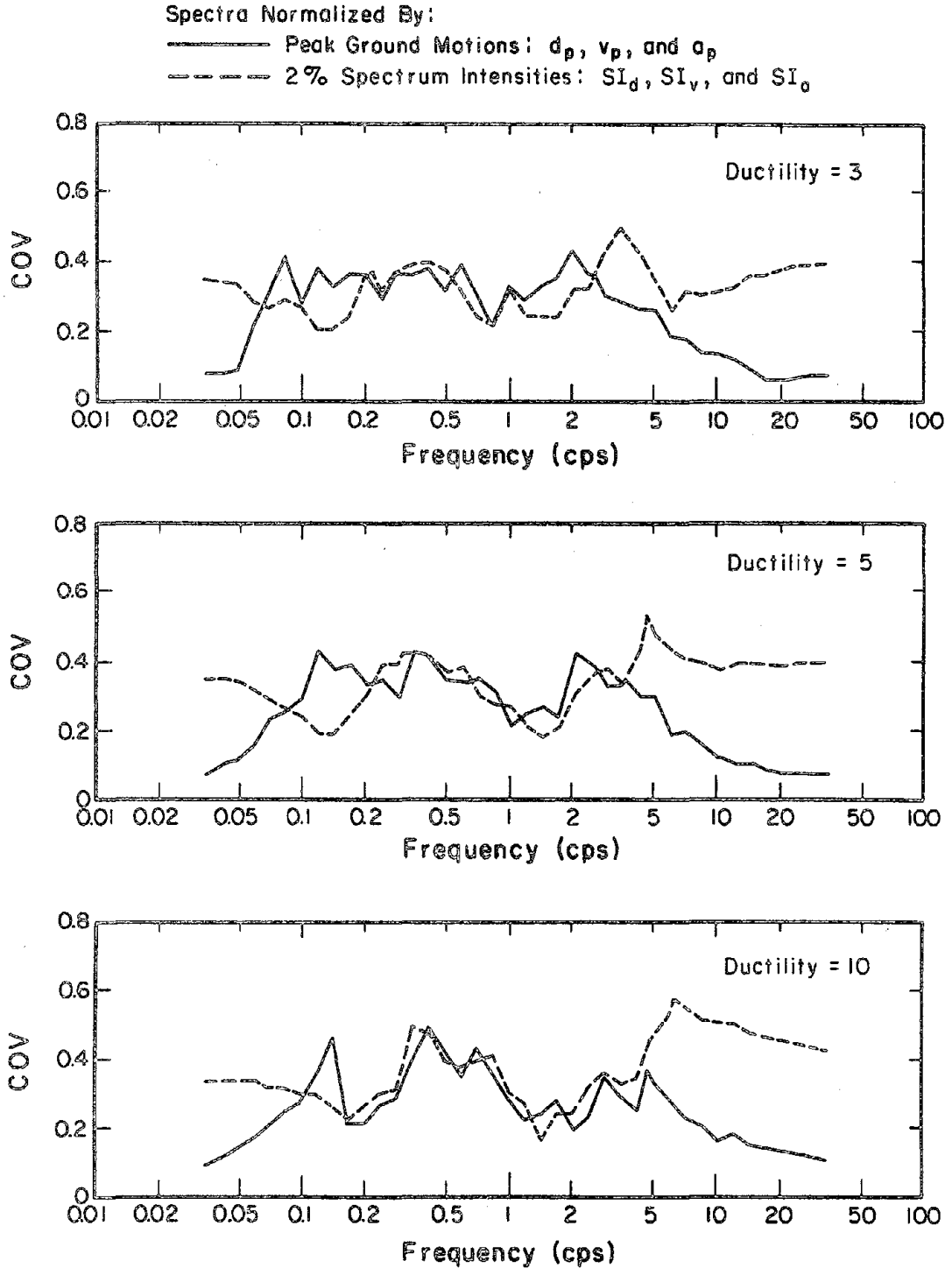

Fig. 5.54 Coefficients of Variation for Elastoplastic Yield Spectra with 5% Damping Normalized by Peak Ground Motions and 2% Spectrum Intensities: Ductilities = 3, 5, and 10

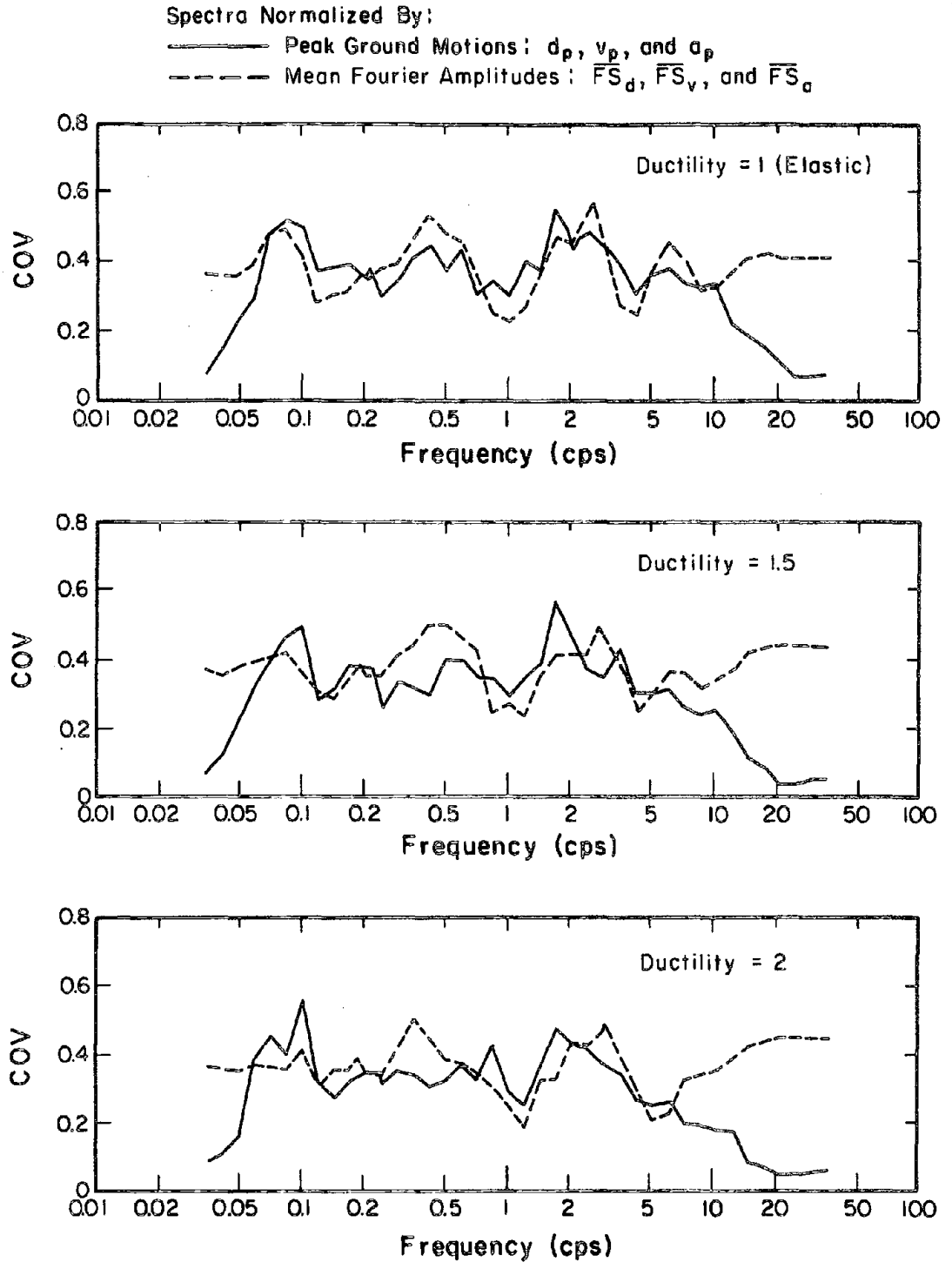

Fig. 5.55 Coefficients of Variation for Elastoplastic Yield Spectra with 5% Damping Normalized by Peak Ground Motions and Mean Fourier Amplitudes: Ductilities = 1 (Elastic), 1.5, and 2

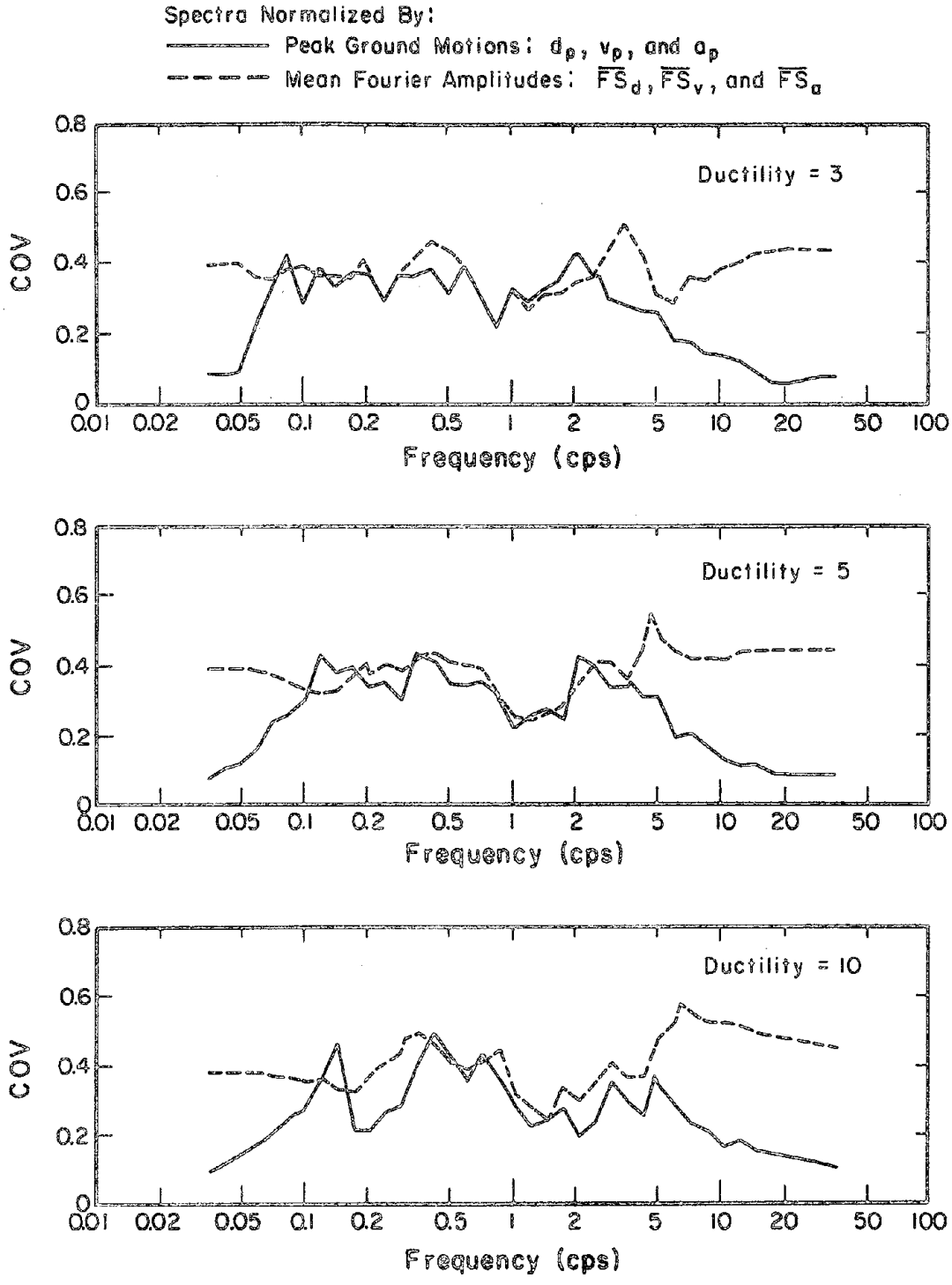

Fig. 5.56 Coefficients of Variation for Elastoplastic Yield Spectra with 5% Damping Normalized by Peak Ground Motions and Mean Fourier Amplitudes: Ductilities = 3, 5, and 10

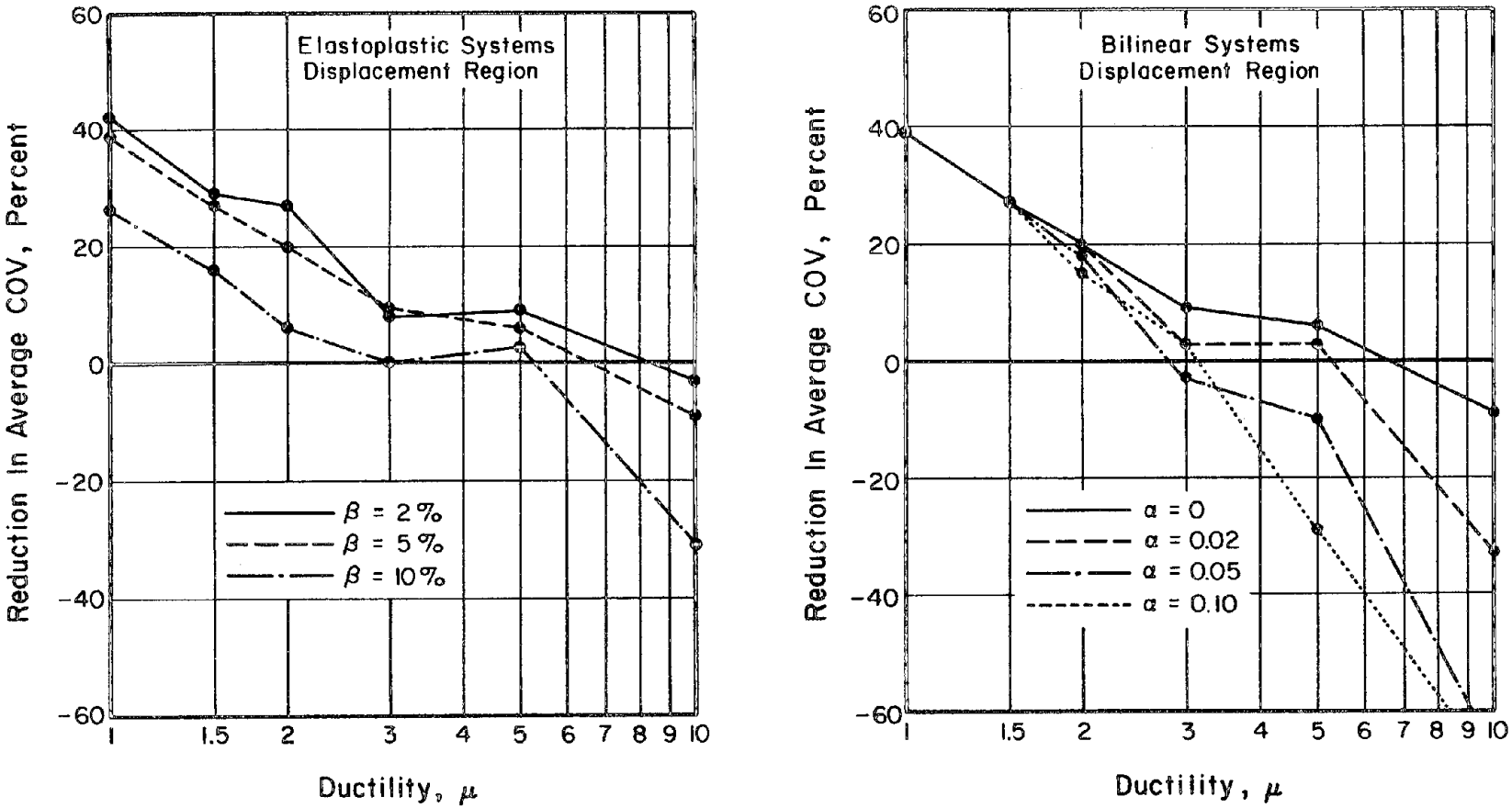

Fig. 5.57 Reduction of Average Coefficient of Variation in the Displacement Region for Inelastic Yield Spectra Normalized by 2% Spectrum Intensity between 0.08 and 0.24 cps

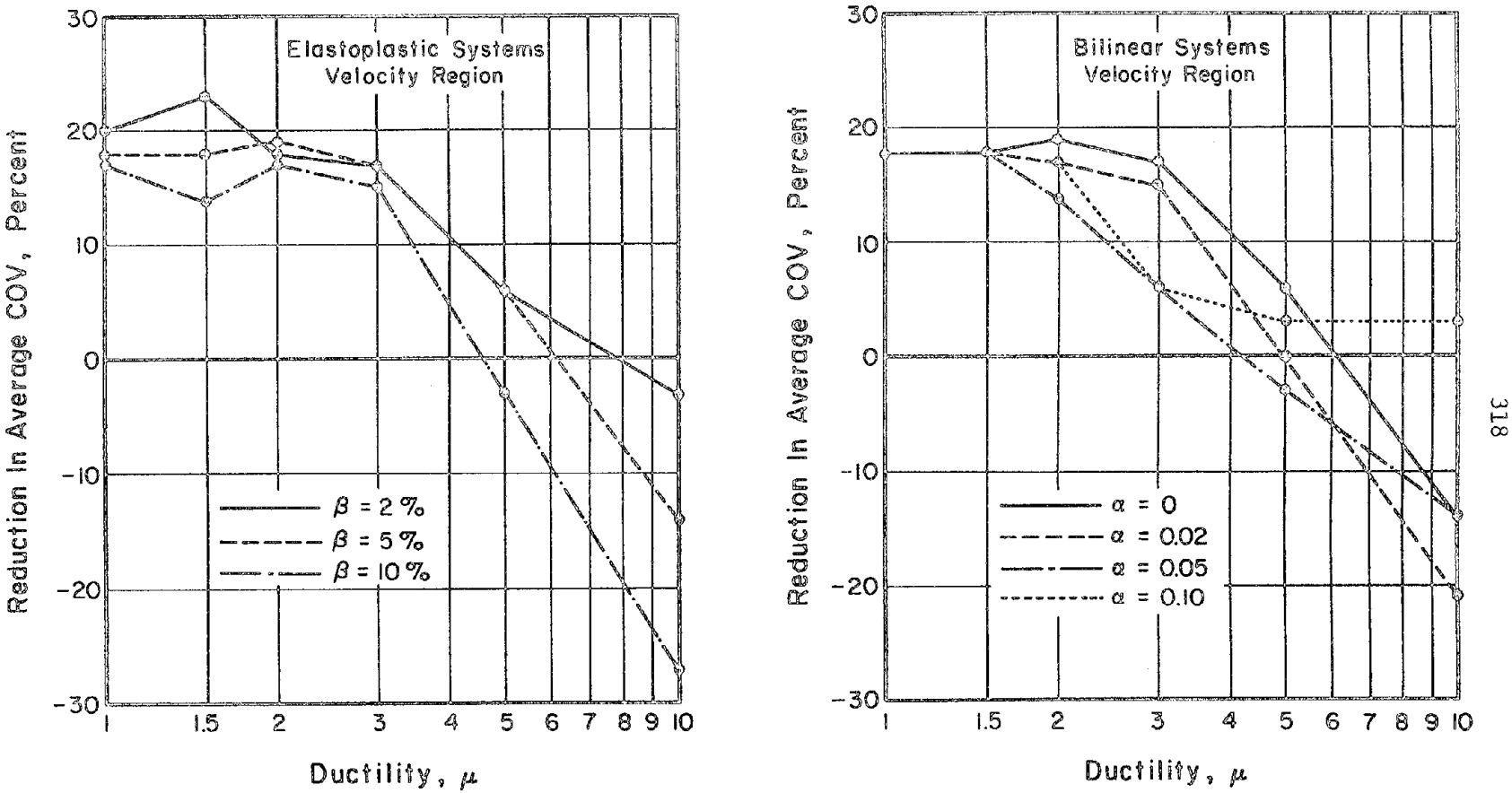

Fig. 5.58 Reduction of Average Coefficient of Variation in the Velocity Region for Inelastic Yield Spectra Normalized by 2% Spectrum Intensity between 0.50 and 3.5 cps

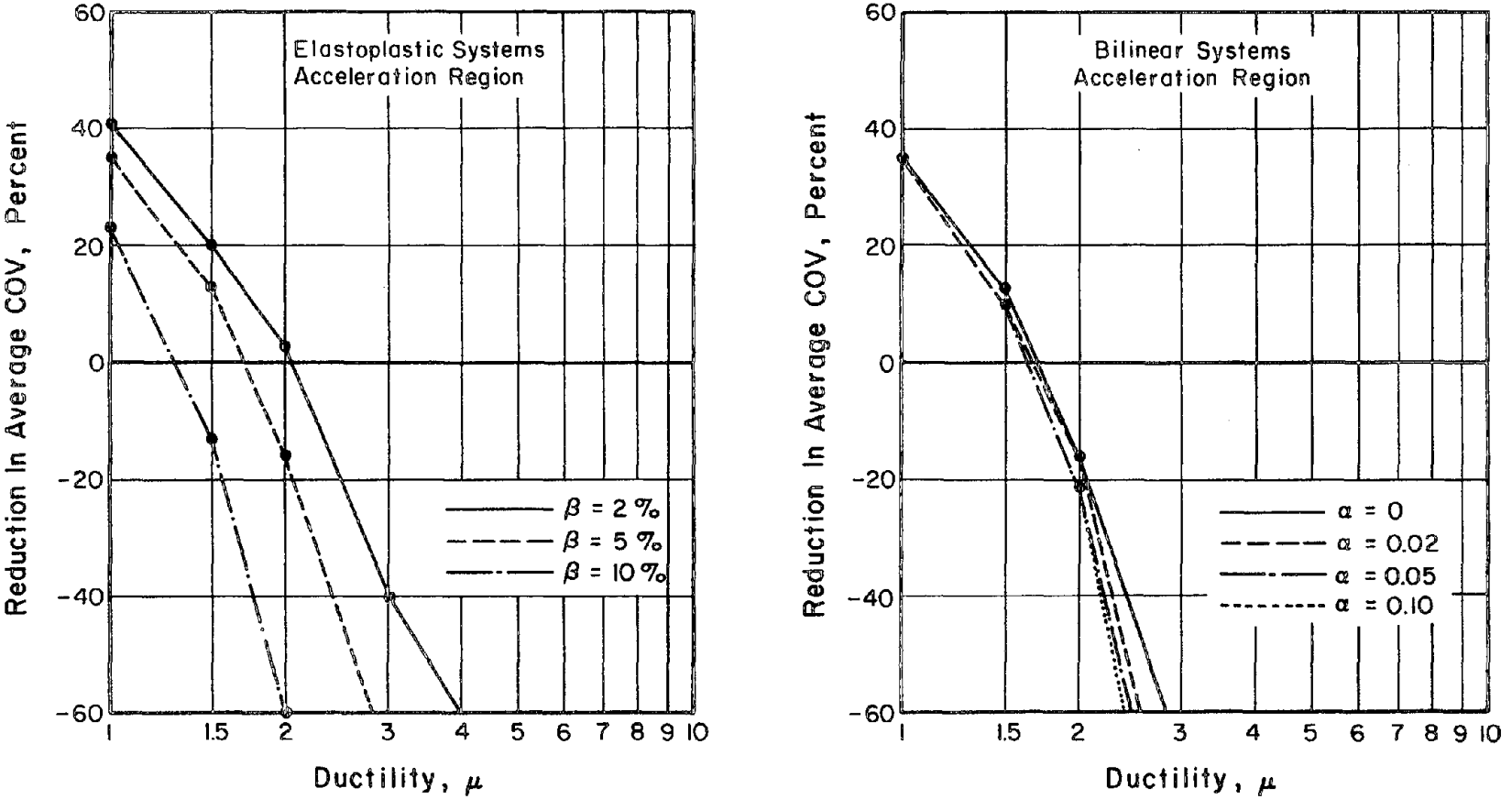

Fig. 5.59 Reduction of Average Coefficient of Variation in the Acceleration Region for Inelastic Yield Spectra Normalized by 2% Spectrum Intensity between 5.4 and 35 cps

LIST OF REFERENCES

1. Anagnostopoulos, S. A., Haviland, R. W., and Biggs, J. M., "Use of Inelastic Response Spectra in Aseismic Design," Journal of the Structural Division, ASCE, Vol. 104, No. ST1, Jan. 1978, pp. 95-109.

2. Arias, A., "A Measure of Earthquake Intensity," in Seismic Design for Nuclear Power Plants, R. J. Hansen, editor, Massachusetts Institute of Technology Press, Cambridge, Mass., 1970, pp. 438-483.

3. Bertero, V. V., "Establishment of Design Earthquakes - Evaluation of Present Methods," Proceedings of the International Symposium on Earthquake Structural Engineering, St. Louis, Mo., Aug. 1976, Vol. I, pp. 551-580.

4. Bertero, V. V., Mahin, S. A., and Herrera, R. A., "Aseismic Design Implications of Near-Fault San Fernando Earthquake Records," Earthquake Engineering and Structural Dynamics, Vol. 6, No. 1, Jan.-Feb. 1978, pp. 31-42.

5. Blume, J. A. and Associates, "Recommendations for Shape of Earthquake Response Spectra," WASH-1254, Directorate of Licensing, U.S. Atomic Energy Commission, Washington, D.C., Feb. 1973.

6. Bolt, B. A., "Duration of Strong Ground Motion," Proceedings of the Fifth World Conference on Earthquake Engineering, Rome, Italy, June 1973, Vol. 1, pp. 1304-1313.

7. Brady, A. G., et al., "Seismic Engineering Data Report, Romanian and Greek Records, 1972-77," Open File Report No. 78-1022, U.S. Geological Survey, Menlo Park, Calif., Sept. 1978.

8. Brady, A. G. and Perez, V., "Seismic Engineering Data Report, 1972 Records, Strong-Motion Earthquake Accelerograms, Digitization and Analysis," Open File Report No. 78-941, U.S. Geological Survey, Menlo Park, Calif., Oct. 1978.

9. Chang, F. K., "State-of-the-Art for Assessing Earthquake Hazards in the United States, Report 9, Catalogue of Strong Motion Earthquake Records, Volume 1, Western United States, 1933-1971," Miscellaneous Paper S-73-1, U.S. Army Engineer Waterways Experiment Station, Vicksburg, Miss., Apr. 1978.

10. Clough, R. W. and Penzien, J., Dynamics of Structures, McGraw-Hill Book Co., Inc., New York, 1975.

11. Cornell, C. A., Banon, H., and Shakal, A. F., "Seismic Motion and Response Prediction Alternatives," Earthquake Engineering and Structural Dynamics, Vol. 7, No. 4, July-Aug. 1979, pp. 295-315.

12. "Damping Values for Seismic Design of Nuclear Power Plants," Regulatory Guide 1.61, Directorate of Regulatory Standards, U.S. Atomic Energy Commission, Washington, D.C., Oct. 1973.

13. "Design Response Spectra for Seismic Design of Nuclear Power Plants," Regulatory Guide 1.60, Directorate of Regulatory Standards, U.S. Atomic Energy Commission, Washington, D.C., Revision 1, Dec. 1973.

14. Dewey, J. W., et al., "The Managua Earthquake of 23 December 1972: Location, Focal Mechanism, Aftershocks, and Relationship to Recent Seismicity of Nicaragua," Proceedings of the Earthquake Engineering Research Institute Conference on the Managua Earthquake of December 23, 1972, San Francisco, Nov. 1973, Vol. I, pp. 66-88.

15. Dobry, R., Idriss, I. M., and Ng, E., "Duration Characteristics of Horizontal Components of Strong-Motion Earthquake Records," Bulletin of the Seismological Society of America, Vol. 68, No. 5, Oct. 1978, pp. 1487-1520.

16. Donovan, N. C., "Earthquake Hazards for Buildings," Building Practices for Disaster Mitigation, Building Science Series No. 46, National Bureau of Standards, Washington, D.C., Feb. 1973, pp. 82-110.

17. Gates, N. C., "The Earthquake Response of Deteriorating Systems," EERL 77-03, Earthquake Engineering Research Laboratory, California Institute of Technology, Pasadena, Calif., Mar. 1977.

18. "Geotechnical and Strong-Motion Earthquake Data from U.S. Accelerograph Stations," Report for the U.S. Nuclear Regulatory Commission, NUREG-0029, Vol. 2, Shannon & Wilson, Inc. and Agbabian Associates, June 1978.

19. Gulkan, P. and Sozen, M. A., "Inelastic Response of Reinforced Concrete Structures to Earthquake Motions," Journal of the American Concrete Institute, Vol. 71, No. 12, Dec. 1974, pp. 604-610.

20. Hall, W. J., Mohraz, B., and Newmark, N. M., "Statistical Studies of Vertical and Horizontal Earthquake Spectra," Report for the U.S. Nuclear Regulatory Commission, NUREG-0003, N. M. Newmark Consulting Engineering Services, Urbana, Ill., Jan. 1976.

21. Hall, W. J. and Newmark, N. M., "Earthquake Resistant Design Considerations," presented at the EERI Seminar on Intra-Plate Earthquakes, Salt Lake City, Utah, May 1980.

22. Hays, W. W., "Procedures for Estimating Earthquake Ground Motions," Professional Paper 1114, U.S. Geological Survey, Washington, D.C., 1980.

23. Housner, G., "Spectrum Intensities of Strong-Motion Earthquakes," Proceedings of the Symposium on Earthquake and Blast Effects on Structures, Earthquake Engineering Research Institute, Los Angeles, Calif., June 1952, pp. 20-36.

24. Housner, G. W., "Behavior of Structures During Earthquakes," Journal of the Engineering Mechanics Division, ASCE, Vol. 85, No. EM4, Oct. 1959, pp. 109-129.

25. Housner, G. W., "Design of Nuclear Power Reactors Against Earthquakes," Proceedings of the Second World Conference on Earthquake Engineering, Tokyo and Kyoto, Japan, July 1960, Vol. I, pp. 133-149.

26. Housner, G. W. and Jennings, P. C., "Generation of Artificial Earthquakes," Journal of the Engineering Mechanics Division, ASCE, Vol. 90, No. EM1, Feb. 1964, pp. 113-150.

27. Housner, G. W., "Strong Ground Motion," Chapter 4 in Earthquake Engineering, R. L. Wiegel, editor, Prentice-Hall, Inc., Englewood Cliffs, N.J., 1970, pp. 75-91.

28. Housner, G. W., "Design Spectrum," Chapter 5 in Earthquake Engineering, R. L. Wiegel, editor, Prentice-Hall, Inc., Englewood Cliffs, N.J., 1970, pp. 93-106.

29. Housner, G. W., "Earthquake Research Needs for Nuclear Power Plants," Journal of the Power Division, ASCE, Vol. 97, No. PO1, Jan. 1971, pp. 77-91.

30. Housner, G. W., "Measures of Severity of Earthquake Ground Shaking," Proceedings of the U.S. National Conference on Earthquake Engineering, Earthquake Engineering Research Institute, Ann Arbor, Mich., June 1975, pp. 25-33.

31. Housner, G. W. and Jennings, P. C., "The Capacity of Extreme Earthquake Motions to Damage Structures," in Structural and Geotechnical Mechanics, W. J. Hall, editor, Prentice-Hall, Inc., Englewood Cliffs, N.J., 1977, pp. 102-116.

32. Hudson, D. E., Reading and Interpreting Strong Motion Accelerograms, Earthquake Engineering Research Institute, Berkeley, Calif., 1979.

33. Husid, R., "Gravity Effects on the Earthquake Response of Yielding Structures," Earthquake Engineering Research Laboratory, California Institute of Technology, Pasadena, Calif., June 1967.

34. Idriss, I. M., "Characteristics of Earthquake Ground Motions," Proceedings of the Specialty Conference on Earthquake Engineering and Soil Dynamics, ASCE, Pasadena, Calif., June 1978, Vol. III, pp. 1151-1265.

35. Iwan, W. D. and Gates, N. C., "The Effective Period and Damping of a Class of Hysteretic Structures," Earthquake Engineering and Structural Dynamics, Vol. 7, No. 3, May-June 1979, pp. 199-211.

36. Iwan, W. D., "Estimating Inelastic Response Spectra from Elastic Spectra," Earthquake Engineering and Structural Dynamics, Vol. 8, No. 4, July-Aug. 1980, pp. 375-388.

37. Lander, J. F., "Seismological Notes - March-April 1973," Bulletin of the Seismological Society of America, Vol. 63, No. 6, Dec. 1973, pp. 2203-2209.

38. Leeds, D. J., editor, "Newsletter," Earthquake Engineering Research Institute, Berkeley, Calif., Vol. 13, No. 6, Nov. 1979.

39. Leeds, D. J., editor, "Reconnaissance Report, Imperial County California Earthquake, October 15, 1979," Earthquake Engineering Research Institute, Berkeley, Calif., Feb. 1980.

40. Mahin, S. A. and Bertero, V. V., "An Evaluation of Inelastic Seismic Design Spectra," Journal of the Structural Division, ASCE, Vol. 107, No. ST9, Sept. 1981, pp. 1777-1795.

41. Miller, I. and Freund, J. E., Probability and Statistics for Engineers, Prentice-Hall, Inc., Englewood Cliffs, N.J., 1965.

42. Montgomery, C. J. and Hall, W. J., "Studies on the Seismic Design of Low-Rise Steel Buildings," Civil Engineering Studies, Structural Research Series No. 442, University of Illinois, Urbana, Ill., July 1977.

43. Morris, L., Smookler, S., and Glover, D., "Catalog of Seismograms and Strong Motion Records," Report SE-6, World Data Center A for Solid Earth Geophysics, NOAA, Boulder, Colo., May 1977.

44. Nelson, I., discussion of "Effect of Initial Base Motion on Response Spectra," Journal of the Engineering Mechanics Division, ASCE, Vol. 105, No. EM2, Apr. 1979, pp. 345-347.

45. Newmark, N. M., "A Method of Computation for Structural Dynamics," Journal of the Engineering Mechanics Division, ASCE, Vol. 85, No. EM3, July 1959, pp. 67-94.

46. Newmark, N. M. and Hall, W. J., "Seismic Design Criteria for Nuclear Reactor Facilities," Proceedings of the Fourth World Conference on Earthquake Engineering, Santiago, Chile, Jan. 1969, Vol. II, Session B-4, pp. 37-50.

47. Newmark, N. M., "Current Trends in the Analysis and Design of High-Rise Structures," Chapter 16 in Earthquake Engineering, R. L. Wiegel, editor, Prentice-Hall, Inc., Englewood Cliffs, N.J., 1970, pp. 403-424.

48. Newmark, N. M. and Rosenblueth, E., Fundamentals of Earthquake Engineering, Prentice-Hall, Inc., Englewood Cliffs, N.J., 1971.

49. Newmark, N. M., "Earthquake Response Analysis of Reactor Structures," Nuclear Engineering and Design, Vol. 20, No. 2, July 1972, pp. 303-322.

50. Newmark, N. M. and Hall, W. J., "Procedures and Criteria for Earthquake Resistant Design," Building Practices for Disaster Mitigation, Building Science Series No. 46, National Bureau of Standards, Washington, D.C., Feb. 1973, pp. 209-236.

51. Newmark, N. M., Consulting Engineering Services, "A Study of Vertical and Horizontal Earthquake Spectra," WASH-1255, Directorate of Licensing, U.S. Atomic Energy Commission, Washington, D.C., Apr. 1973.

52. Newmark, N. M., Blume, J. A., and Kapur, K. K., "Seismic Design Spectra for Nuclear Power Plants," Journal of the Power Division, ASCE, Vol. 99, No. PO2, Nov. 1973, pp. 287-303.

53. Newmark, N. M., "Comments on Conservatism in Earthquake Resistant Design," Urbana, Ill., Sept. 1974.

54. Newmark, N. M., "Seismic Design Criteria for Structures and Facilities, Trans-Alaska Pipeline System," Proceedings of the U.S. National Conference on Earthquake Engineering, Earthquake Engineering Research Institute, Ann Arbor, Mich., June 1975, pp. 94-103.

55. Newmark, N. M., "A Response Spectrum Approach for Inelastic Seismic Design of Nuclear Reactor Facilities," Paper K5/1, Transactions of the 3rd International Conference on Structural Mechanics in Reactor Technology, London, Sept. 1975, Vol. 4, Part K.

56. Newmark, N. M., "A Rationale for Development of Design Spectra for Diablo Canyon Reactor Facility," Report for the U.S. Nuclear Regulatory Commission, N. M. Newmark Consulting Engineering Services, Urbana, Ill., Sept. 1976.

57. Newmark, N. M., Hall, W. J., and Morgan, J. R., "Comparison of Building Response and Free Field Motion in Earthquakes," Proceedings of the Sixth World Conference on Earthquake Engineering, New Delhi, India, Jan. 1977, Vol. II, pp. 972-978.

58. Newmark, N. M., "Inelastic Design of Nuclear Reactor Structures and its Implications on Design of Critical Equipment," Paper K4/1, Transactions of the 4th International Conference on Structural Mechanics in Reactor Technology, San Francisco, Aug. 1977, Vol. K(a).

59. Newmark, N. M. and Hall, W. J., "Development of Criteria for Review of Selected Nuclear Power Plants," Report for the U.S. Nuclear Regulatory Commission, NUREG/CR-0098, N. M. Newmark Consulting Engineering Services, Urbana, Ill., May 1978.

60. Nigam, N. C. and Jennings, P. C., "Digital Calculation of Response Spectra from Strong-Motion Earthquake Records," Earthquake Engineering Research Laboratory, California Institute of Technology, Pasadena, Calif., June 1968.

61. Nigam, N. C. and Jennings, P. C., "Calculation of Response Spectra from Strong Motion Earthquake Records," Bulletin of the Seismological Society of America, Vol. 59, No. 2, Apr. 1969, pp. 909-922.

62. Page, R. A., et al., "Ground Motion Values for Use in the Seismic Design of the Trans-Alaska Pipeline System," Circular 672, U.S. Geological Survey, Washington, D.C., 1972.

63. Pecknold, D. A. and Riddell, R., "Effect of Initial Base Motion on Response Spectra," Journal of the Engineering Mechanics Division, ASCE, Vol. 104, No. EM2, Apr. 1978, pp. 485-491.

64. Pecknold, D. A. and Riddell, R., closure to "Effect of Initial Base Motion on Response Spectra," Journal of the Engineering Mechanics Division, ASCE, Vol. 105, No. EM6, Dec. 1979, pp. 1057-1060.

65. Person, W. J., "Seismological Notes -- September-December 1979," Bulletin of the Seismological Society of America, Vol. 70, No. 6, Dec. 1980, pp. 2317-2325.

66. Porcella, R. L. and Matthiesen, R. B., "Compilation of Strong-Motion Records from the August 6, 1979 Coyote Lake Earthquake," Open File Report 79-385, U.S. Geological Survey, Menlo Park, Calif., Oct. 1979.

67. Riddell, R. and Newmark, N. M., "Statistical Analysis of the Response of Nonlinear Systems Subjected to Earthquakes," Civil Engineering Studies, Structural Research Series No. 468, University of Illinois, Urbana, Ill., Aug. 1979.

68. Riddell, R. and Newmark, N. M., "Force-Deformation Models for Nonlinear Analyses," Journal of the Structural Division, ASCE, Vol. 105, No. ST12, Dec. 1979, pp. 2773-2778.

69. Riddell, R., "Effect of Damping and Type of Material Nonlinearity on Earthquake Response," Proceedings of the Seventh World Conference on Earthquake Engineering, Istanbul, Turkey, Sept. 1980, Vol. 4, Part I, pp. 427-433.

70. "Seismic Engineering Data Report, Strong-Motion Earthquake Accelerograms, Digitization and Analysis, 1971 Records," Open File Report No. 76-609, U.S. Geological Survey, Menlo Park, Calif., July 1976.

71. "Seismic Engineering Program Report, January-April 1977," Circular 762-A, U.S. Geological Survey, Menlo Park, Calif., 1977.

72. "Seismic Engineering Program Report, May-August 1979," Circular 818-B, U.S. Geological Survey, Menlo Park, Calif., 1980.

73. Shibata, A. and Sozen, M. A., "The Substitute-Structure Method for Earthquake-Resistant Design of Reinforced Concrete Frames," Civil Engineering Studies, Structural Research Series No. 412, University of Illinois, Urbana, Ill., Oct. 1974.

74. Shibata, A. and Sozen, M. A., "The Substitute-Structure Method for Seismic Design in R/C," Journal of the Structural Division, ASCE, Vol. 102, No. ST1, Jan. 1976, pp. 1-18.

75. "Strong Motion Earthquake Accelerograms, Digitized and Plotted Data," Vol. II, Corrected Accelerograms and Integrated Ground Velocity and Displacement Curves, Part A, EERL 71-50, Earthquake Engineering Research Laboratory, California Institute of Technology, Pasadena, Calif., Sept. 1971.

76. "Strong Motion Earthquake Accelerograms, Index Volume," Report No. EERL 76-02, Earthquake Engineering Research Laboratory, California Institute of Technology, Pasadena, Calif., Aug. 1976.

77. Tansirikongkol, V. and Pecknold, D. A., "Approximate Modal Analysis of Bilinear MDF Systems Subjected to Earthquake Motions," Civil Engineering Studies, Structural Research Series No. 449, University of Illinois, Urbana, Ill., Aug. 1978.

78. Thomson, W. T., Theory of Vibration with Applications, Prentice-Hall, Inc., Englewood Cliffs, N.J., 1972.

79. Trifunac, M. D., "Low Frequency Digitization Errors and a New Method for Zero Baseline Correction of Strong-Motion Accelerograms," EERL 70-07, Earthquake Engineering Research Laboratory, California Institute of Technology, Pasadena, Calif., Sept. 1970.

80. Trifunac, M. D., Udwadia, F. E., and Brady, A. G., "High Frequency Errors and Instrument Corrections of Strong-Motion Accelerograms," EERL 71-05, Earthquake Engineering Research Laboratory, California Institute of Technology, Pasadena, Calif., July 1971.

81. Trifunac, M. D. and Lee, V., "Routine Computer Processing of Strong-Motion Accelerograms," EERL 73-03, Earthquake Engineering Research Laboratory, California Institute of Technology, Pasadena, Calif., Oct. 1973.

82. Trifunac, M. D. and Brady, A. G., "On the Correlation of Seismic Intensity Scales with the Peaks of Recorded Strong Ground Motion," Bulletin of the Seismological Society of America, Vol. 65, No. 1, Feb. 1975, pp. 139-162.

83. Trifunac, M. D. and Brady, A. G., "A Study on the Duration of Strong Earthquake Ground Motion," Bulletin of the Seismological Society of America, Vol. 65, No. 3, June 1975, pp. 581-626.

84. Valera, J. E., "Soil Conditions and Local Soil Effects During the Managua Earthquake of December 23, 1972, "Proceedings of the Earthquake Engineering Research Institute Conference on the Managua Earthquake of December 23, 1972, San Francisco, Nov. 1973, Vol. I, pp. 232-264.

85. Veletsos, A. S., Newmark, N. M., and Chelapati, C. V., "Deformation Spectra for Elastic and Elastoplastic Systems Subjected to Ground Shock and Earthquake Motions," Proceedings of the Third World Conference on Earthquake Engineering, Aukland and Wellington, New Zealand, Jan.-Feb. 1965, Vol. 2, pp. 663-680.

86. Veletsos, A. S. and Vann, W. P., "Response of Ground-Excited Elastoplastic Systems," Journal of the Structural Division, ASCE, Vol. 97, No. ST4, Apr. 1971, pp. 1257-1281.

87. "Western Hemisphere Strong-Motion Accelerograph Station List - 1980," Open File Report No. 81-664, U.S. Geological Survey, Menlo Park, Calif., Jan. 1981.